

NELC / TD 490

ADA 034486

Technical Document 490

12

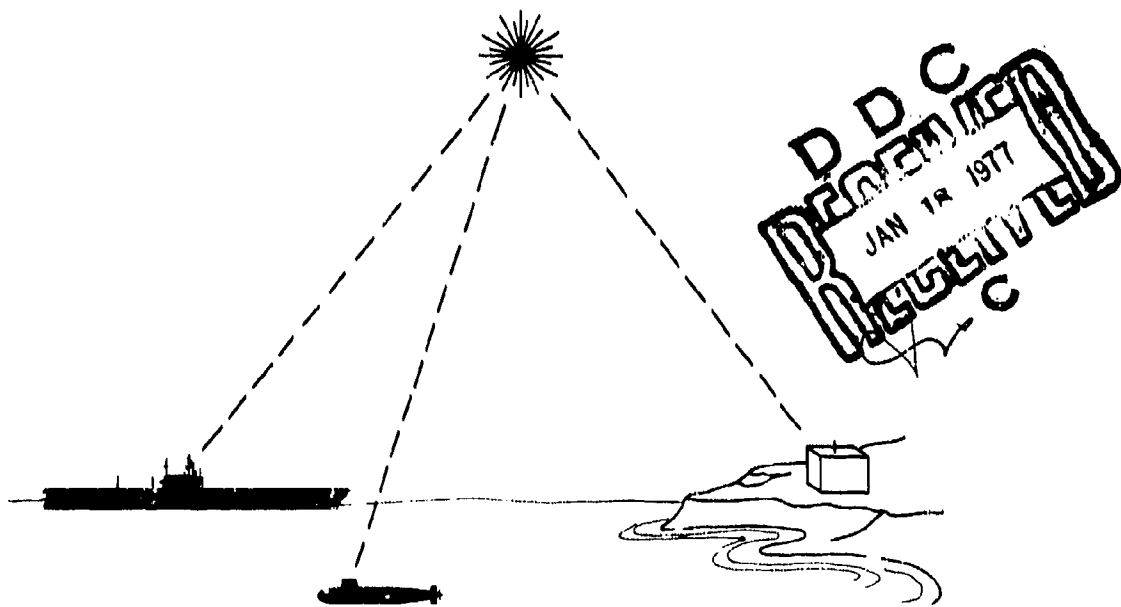
NELC / TD 490

OPSATCOM FIELD MEASUREMENTS

Volume II
Supplemental Information

1 June 76

Research and Development, June through August 1975



APPROVED FOR PUBLIC RELEASE;
DISTRIBUTION IS UNLIMITED

NAVAL ELECTRONICS LABORATORY CENTER

San Diego, California 92152

COPY AVAILABLE TO DDC DOES NOT
PERMIT FULLY LEGIBLE PRODUCTION

UNCLASSIFIED

SECURITY CLASSIFICATION OF THIS PAGE (When Data Entered)

REPORT DOCUMENTATION PAGE		READ INSTRUCTIONS BEFORE COMPLETING FORM
1. REPORT NUMBER NELC Technical Document 490 (TD 490) ✓	2. GOVT ACCESSION NO.	3. RECIPIENT'S CATALOG NUMBER
4. TITLE (and Subtitle) OPSATCOM FIELD MEASUREMENTS Volume II, Supplemental Information. NR	5. TYPE OF REPORT & PERIOD COVERED Research and Development <i>rept.</i> June 1975 Aug 1975 75	
7. AUTHOR(s) R. Anderson, et al	6. PERFORMING ORG. REPORT NUMBER	
9. PERFORMING ORGANIZATION NAME AND ADDRESS Naval Electronics Laboratory Center San Diego, CA 92152		8. CONTRACT OR GRANT NUMBER(s)
11. CONTROLLING OFFICE NAME AND ADDRESS Office of Naval Research Washington, DC	10. PROGRAM ELEMENT, PROJECT, TASK AREA & WORK UNIT NUMBERS 60000N; NRL; NIF (NELC J425)	
14. MONITORING AGENCY NAME & ADDRESS (if different from Controlling Office) <i>(12) 162p.</i>	12. REPORT DATE 1 June 1976	
	13. NUMBER OF PAGES 166	
	15. SECURITY CLASS. (of this report) UNCLASSIFIED	
	18a. DECLASSIFICATION/DOWNGRADING SCHEDULE	
16. DISTRIBUTION STATEMENT (of this Report) Approved for public release; distribution is unlimited.		
17. DISTRIBUTION STATEMENT (of the abstract entered in Block 20, if different from Report)		
18. SUPPLEMENTARY NOTES		
19. KEY WORDS (Continue on reverse side if necessary and identify by block number) Optical Communication-Blue Green Spacecraft Communication-Terminals Mathematical Models-Multiple Scattering Subsurface Communication Terminals Air/Sea Interface		
20. ABSTRACT (Continue on reverse side if necessary and identify by block number) This document reports on the results of a series of experiments performed in June through August 1975 at Santa Catalina Island. The purpose of these experiments was to determine the feasibility of satellite-to-submarine communications. The experiments addressed the propagation aspects of the problem through the water, through the air/sea interface for both the uplink and downlink. Certain aspects of cloud penetration were also considered. The relationship of radiative transfer theory to this problem was also addressed.		

DD FORM 1 JAN 73 1473

EDITION OF 1 NOV 65 IS OBSOLETE
S/N 0102-014-6601

UNCLASSIFIED

SECURITY CLASSIFICATION OF THIS PAGE (When Data Entered)

403 940

PREFACE

Volume II contains supplemental material pertinent to the data, conclusions, and recommendations presented in Volume I. Each section is a separate entity.

In some cases original material was edited and produced for this publication. However, where the technical content was reproduced from existing reports or documents, the contents were not changed or modified. Acknowledgements for all sections are provided below.

Section 1. The OPSATCOM Field Test Laser

Author: John E. Celto

Section 2. Underwater Radiance Scanner

Author: Richard D. Anderson

Section 3. Aircraft Receiver System.

Author: Robert F. Howarth

Section 4. F(θ) Receiver.

Author: Merv Hyde

Section 5. An Instrument for the Measurement of Spectral Attenuation Coefficient and Narrow Angle Volume Scattering Function of Ocean Waters, SIO Ref. 75-25.

Authors: R.W. Austin and T.J. Petzold

Section 6. Surface Support Platform

Author: Lt. Robert J. Giannaris, USN

Section 7. Atmospherical and Optical Background Monitoring System.

Author: Merv Hyde

A tilted document fragment, possibly a checklist or form, is visible in the lower right corner. It features a large handwritten letter 'A' in the bottom left corner. Above it, there are several lines of text, some of which are partially obscured. A checkmark is visible in the top right corner of the fragment. The text on the fragment includes 'WAVE SPECTRUM', 'SUN SPECTRUM', and 'ATMOSPHERIC/BACKGROUND CORRECTIONS'.

ADMINISTRATIVE INFORMATION

The equipment described in Volume II constitutes a complex assemblage of apparatus. The construction, assembly, test, checkout, fielding, and maintenance of this equipment would not have been possible without the able assistance of many dedicated technical people. Among those deserving special mention are:

Mr. Leonard A. Ruth, NELC Code 2520
Mr. Edward Schumacher, NELC Code 2520
Mr. Joe Lopes, Adroit Engineering
Mr. Walt Foley, Megatek, Inc.
Mr. Lou Wuellner, ITT, Ft. Wayne
Mr. Dave Wulfin, NELC Code 2200
Mr. Bill Martin, NELC Code 2200
Mr. Verne Duvall, NELC Code 6540
Mr. Jim Burlesen, NELC Code 6530
ETN2 John Murabeus, NELC Code 2520
ET1 Frank Weges, NELC Code 2520
ETN2 Bruce Wooley, NELC Code 1400
EOSA Paul Webb, Amphibious Construction Battalion 1
Mr. Jim Carter, Catalina Island Co., Comp and Cove Agency
Mr. James Baldwin, NELC Code 1400
Mr. Larry Langin, Santa Catalina Marine Biological Laboratory
Lt. Dennis Guilford, USN, NELC Code 5200

This work was performed by members of the Satellite Systems Program Office, the Propagation Division, and the LOS and Satellite Communications Division of the Naval Electronics Laboratory Center under Program Element 60000N, Project NRL, Task Area NIF, and NELC Work Unit J425 for the Office of Naval Research. This document was approved for publication on 1 June 1976.

TABLE OF CONTENTS

Section	Page
1 THE OPSATCOM FIELD TEST LASER	1-1
Introduction	1-1
Detailed System Description	1-7
Installation, Operation, and Maintenance	1-11
Calibration	1-14
2 UNDERWATER RADIANCE SCANNER	2-1
Background	2-1
Brief Description	2-2
Underwater Radiance Scanner Sensor	2-5
Digital Video Unit	2-11
Digital Equipment	2-14
Operating Programs	2-14
Calibration	2-26
References	2-49
3 AIRCRAFT RECEIVER SYSTEM	3-1
Introduction	3-1
System Configuration	3-1
System Description	3-10
System Specifications	3-17
Calibration	3-18
4 F(θ) RECEIVER	4-1
Introduction	4-1
System Description	4-2
Sensor Assembly	4-2
Positioning Carriage Subassembly (PCS)	4-2
Sensor Head Subassembly (SHS)	4-7
Receiver-Control Panel	4-7
Sync Receiver	4-7
Control Functions	4-10
Calibration	4-10
Absolute Irradiance	4-11
Receiver Response	4-15
Field of View	4-15
Absolute Radiance	4-18
Spectral Filter	4-18

TABLE OF CONTENTS (Cont)

Section		Page
5	AN INSTRUMENT FOR THE MEASUREMENT OF SPECTRAL ATTENUATION COEFFICIENT AND NARROW ANGLE VOLUME SCATTERING FUNCTION OF OCEAN WATERS	5-1
	Abstract	5-1
	Introduction	5-1
	Design Objective and Specifications	5-1
	Optical Design	5-3
	Mechanical Design	5-8
	Electronic Design	5-9
	Data Output	5-11
6	SURFACE SUPPORT PLATFORM	6-1
	Introduction	6-1
	General Description	6-1
	The Barge	6-3
	Vertical Guide and Instrument Platform	6-7
	Barge Equipment	6-11
7	ATMOSPHERICAL AND OPTICAL BACKGROUND MONITORING SYSTEM	7-1
	Background	7-1
	System Description	7-1
	Equipment Description	7-4
	Calibration	7-10

LIST OF ILLUSTRATIONS

Figure

SECTION 1

1.	OPSATCOM dye laser with panel mounted hardware removed from canister	1-2
2.	Top view of laser situated inside canister; cover with optical window removed	1-3
3.	Close-up view of panel front carrying most of the electronics	1-4
4.	Close-up view of panel back, showing dye and cooling water tanks	1-5
5.	Control unit for operating laser via cable at remote stations	1-6
6.	Underwater laser block diagram	1-8
7.	Laser control panel block diagram	1-10

LIST OF ILLUSTRATIONS (Cont)

Figure		Page
8.	Laser output. Each photograph contains 20 pulses	1-17
9.	Laser spectrum (densitometer scan)	1-20
10.	Beam divergence (air)	1-21
11.	Underwater control unit	1-23
12.	Miscellaneous schematics	1-24
13.	Laser control panel	1-26

SECTION 2

1.	Radiance scanner system	2-4
2.	Underwater radiance scanner sensor	2-6
3.	Features and specifications	2-6
4.	Coordinate system	2-6
5.	Optical filter wavelength, angstroms	2-8
6.	Image dissector camera and DVU (front view)	2-10
7.	Image dissector camera and DVU (rear view)	2-10
8.	Computer output format to DVU	2-12
9.	Overall block diagram	2-13
10.	Scan pattern automatic hemispherical scan program	2-15
11.	Underwater radiance scanner - automatic hemispherical scan routine	2-17
12.	Mag tape write subroutine	2-24
13.	Radiance pattern from 50 feet, overcast sky	2-25
14.	Underwater calibration apparatus	2-27
15.	Deflection calibration data points (from table 1)	2-28
16.	Data points and circular fit	2-30
17.	Zenith angle vs. deflection radius	2-30
18.	Calculated and measured X_0 , Y_0	2-31
19.	Deflection in air	2-33
20.	Response of video circuit	2-34
21.	Video response showing offset	2-36
22.	Dwell gain vs. potentiometer turns	2-38
23.	Data point 32 isometric projection	2-40
24.	ΔN_λ values	2-46

SECTION 3

1a.	A/C receiver rear view	3-2
1b.	A/C receiver front view	3-2
2.	Simplified system	3-3
3.	The Consolidated PBY-5A Flying Boat	3-5
4.	A/C receiver installed in PBY	3-6
5.	A/C system; equipment location in PBY-5A	3-7
6.	A/C system console 1	3-8
7.	A/C system console 2	3-9

LIST OF ILLUSTRATIONS (Cont)

Figure		Page
8.	A/C receiver system	3-11
9.	Transmittance characteristic A/C radiance sensor	3-12
10.	Aircraft timing sequence	3-13
11.	A/C system data format	3-14
12.	Aircraft receiver tracking system	3-16
13.	Aircraft receiver calibration	3-18
14.	A/C receiver sensitivity range 1 (no optical attenuation)	3-21
15.	A/C receiver sensitivity range 2 (no optical attenuation)	3-21
16.	Pitch calibration	3-22
17.	Roll calibration	3-22

SECTION 4

1.	F(θ) receiver	4-3
2.	F(θ) receiver block diagram	4-4
3.	Positioning carriage assembly	4-5
4.	PSC installed	4-6
5.	F(θ) sensor head subassembly	4-8
6.	Filter position assembly	4-9
7.	F(θ) receiver calibration	4-12
8A.	F(θ) receiver calibration chart	4-13
8B.	F(θ) receiver calibration chart	4-14
9A.	F(θ) receiver calibration chart	4-16
9B.	F(θ) receiver calibration chart	4-17
10A.	F(θ) receiver underwater radiance calibration	4-19
10B.	F(θ) receiver underwater radiance calibration	4-20
11A.	F(θ) receiver underwater radiance calibration	4-21
11B.	F(θ) receiver underwater radiance calibration	4-22

SECTION 6

1.	Surface platform design concept	6-2
2.	Aerial view of the surface support platform	6-3
3.	Side view of surface support platform showing the horizontal guide track	6-5
4.	Positioning carriage subassembly (end view)	6-5
5.	Positioning carriage subassembly (side view)	6-6
6.	The arrangement of the support pontoons is shown	6-8
7.	The pipe during tow	6-8
8.	The vertical instrument platform is shown	6-10
9.	Replenishing the barge diesel oil supplies	6-12

SECTION 7

1.	Atmospherical and optical background monitoring system	7-2
2.	Sample printout	7-3

LIST OF ILLUSTRATIONS (Cont)

Figure		Page
3.	Spectral response, optical filter	7-5
4.	Solar monitor	7-6
5.	Deck cell	7-6
6.	Spectral response (deck cell)	7-7
7.	Pyrheliometer	7-8
8.	Wind speed and direction sensors	7-8
9.	Interface panel block diagram	7-9
10.	Digital to analog converter	7-11
11.	Solar monitor response linearity	7-13

LIST OF TABLES

Table

SECTION 1

1.	System Specifications	1-7
2.	Laser Output Parameters	1-15
3.	Laser Log Excerpts	1-18
4.	Laser Control Panel Terminal Identification	1-22

SECTION 2

1.	Deflection Calibration Data Points	2-28
2.	Deflection Angle Relationships Prediction	2-33
3.	Polar Deflection Sensitivity	2-34
4.	Azimuthal Deflection Sensitivity (Empirical)	2-35
5.	Signal Ratios Between Gain Settings	2-37
6.	Camera Gain Factors	2-37
7.	Dwell Gain Factor G_d	2-38
8.	Radiometric Response	2-41
9.	Response Diameter and Corresponding Field of View (Averaged Data)	2-42
10.	Peak Signal and Volume (Averaged Data)	2-43
11.	Unit Spectral Radiance Factor	2-46

SECTION 3

1.	Numbered Items	3-4
2.	Magnetic Tape Output Format Legend	3-15

LIST OF TABLES (Cont)

Table	Page
SECTION 4	
1. F(θ) Receiver Features and Specifications	4-1
2. F(θ) Receiver Dynamic Response	4-15
3. Radiance Values	4-18
SECTION 7	
1. Summary of Calibration Results	7-12
2. Multipliers Determined	7-12

SECTION I THE OPSATCOM FIELD TEST LASER

INTRODUCTION

The underwater light source used in the OPSATCOM field tests is a flashlamp-pumped dye laser system that was specifically designed and built for the project at NELC. The system consists of three main parts — the laser proper in a submersible canister (fig. 1-4), a topside control panel (fig. 5), and 250 feet of interconnecting cable. The general system specifications are given in table 1.

The other features of the laser system are:

- Automatic control of pulse amplitude
- Leak-initiated shutdown
- Pressure and temperature interlocks
- Stable pulse rate
- Telemetry sync output
- Rapid dye solution and flashlamp replacement

This report is arranged to present a description of the system electronics; the installation, operation, and maintenance of the laser; and the results of system calibration.

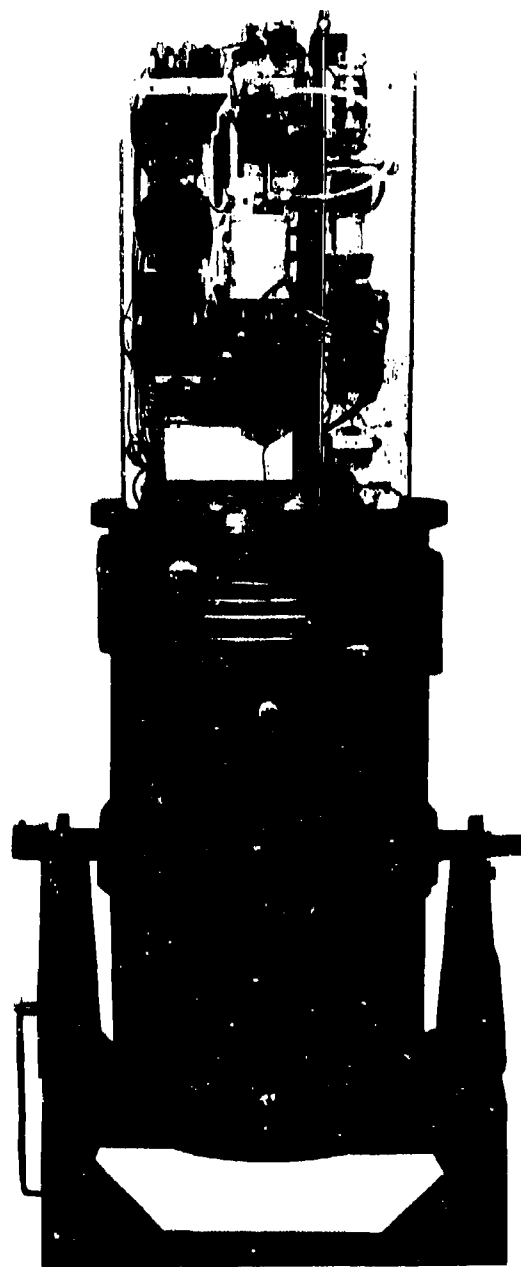


Figure 1. OPSATCOM dye laser with panel mounted hardware removed from canister.

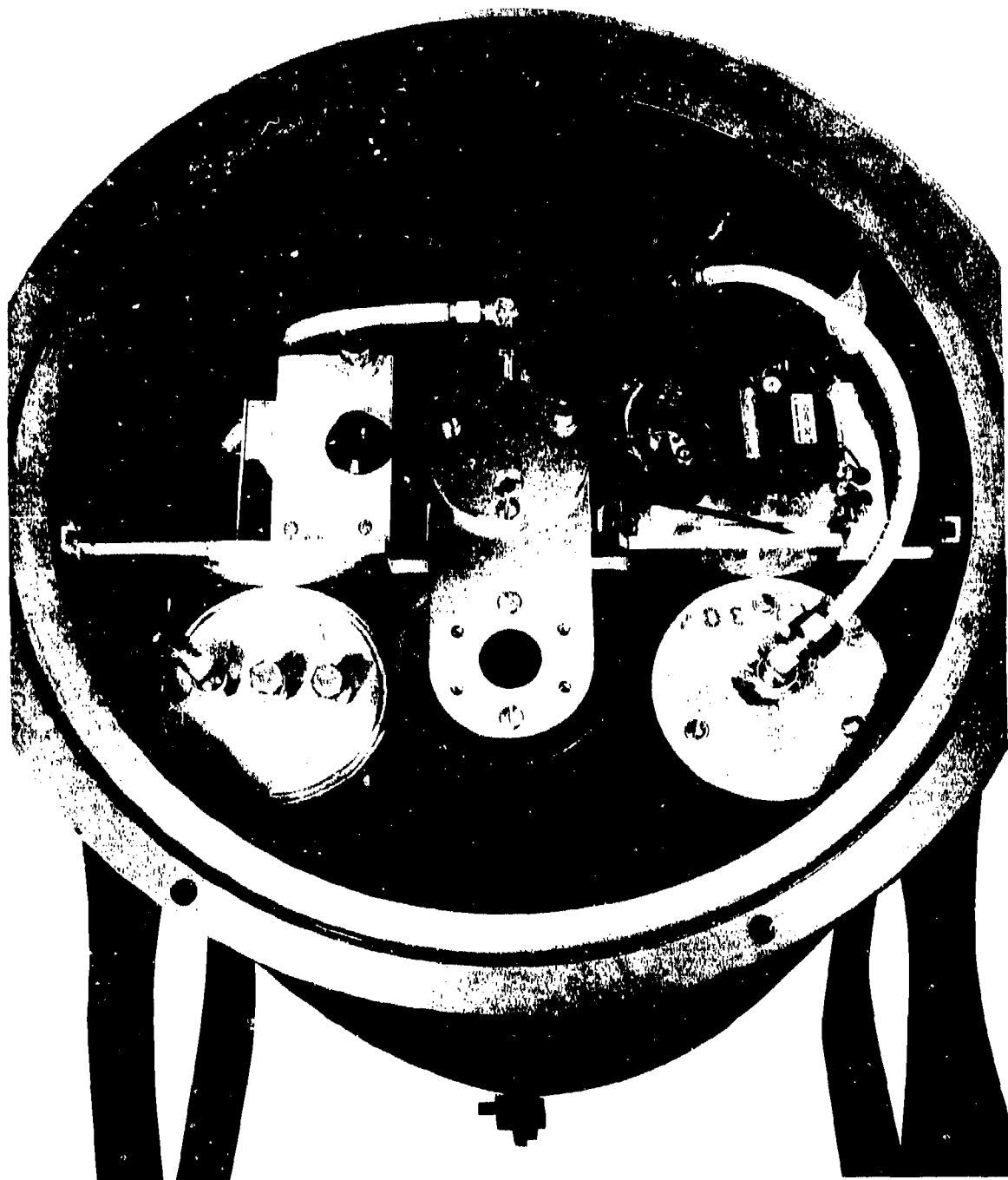


Figure 2. Top view of laser situated inside canister; cover with optical window removed.

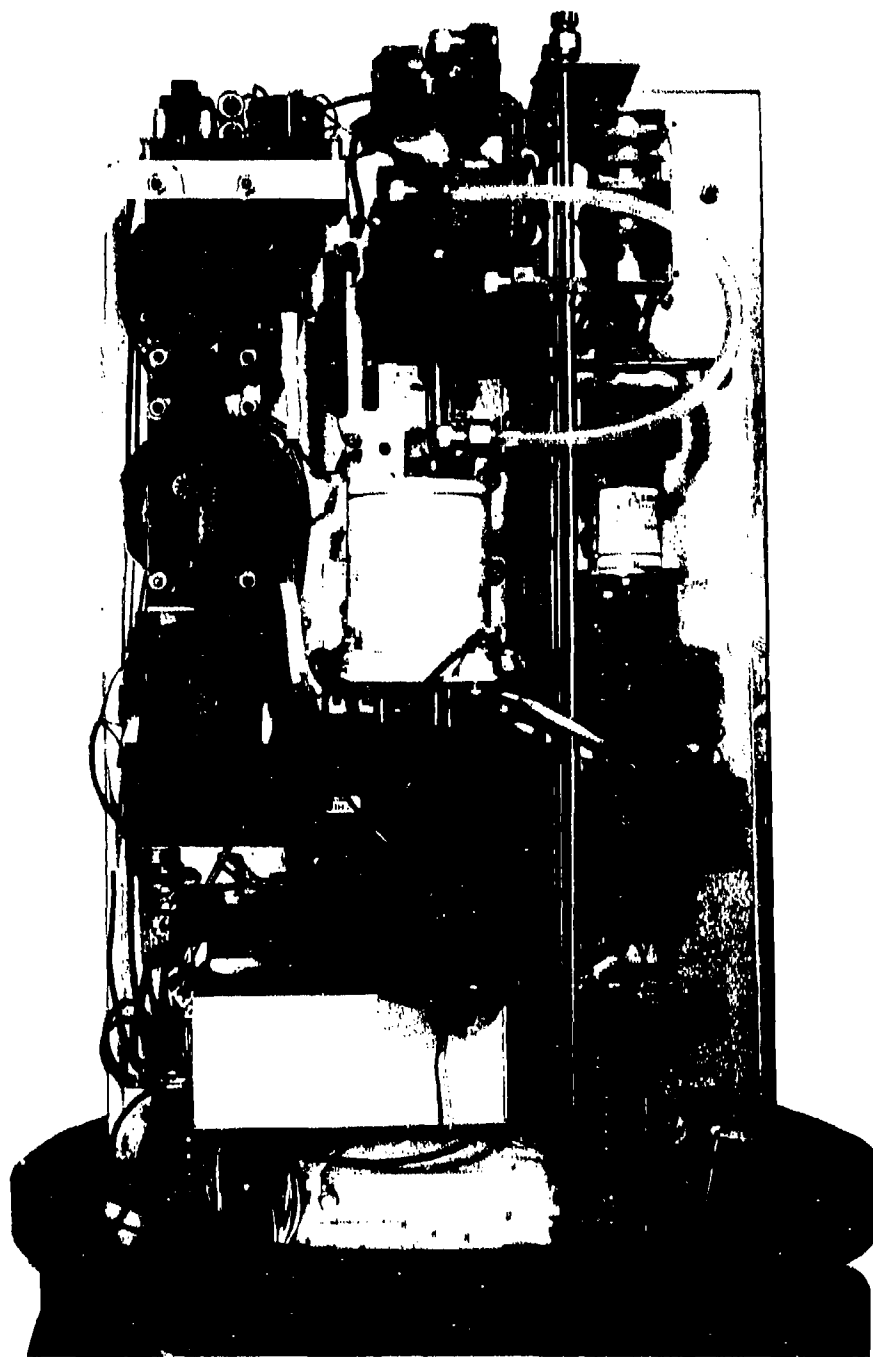


Figure 3. Close-up view of panel front carrying most of the electronics.

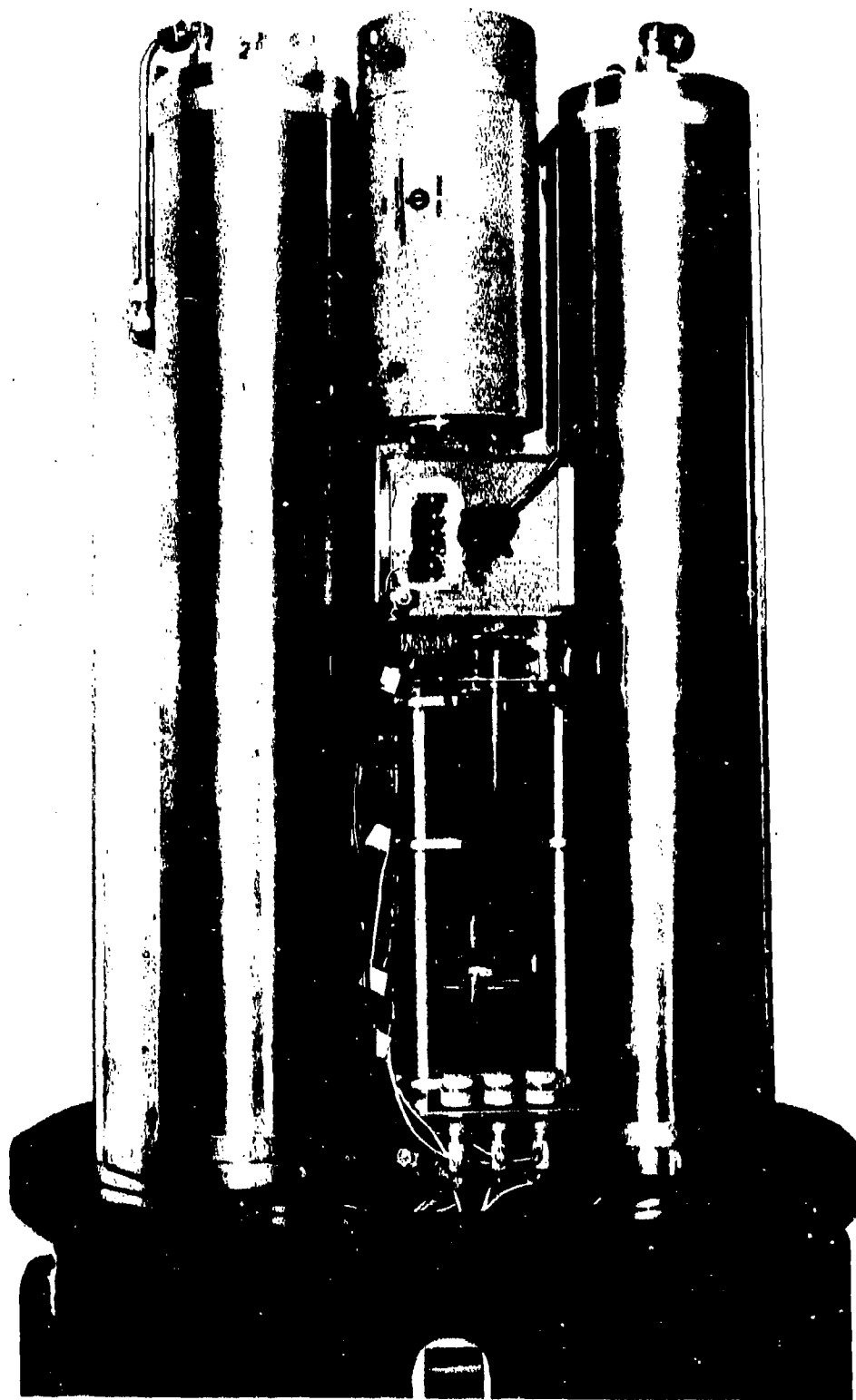


Figure 4. Close-up view of panel back, showing dye and cooling water tanks.

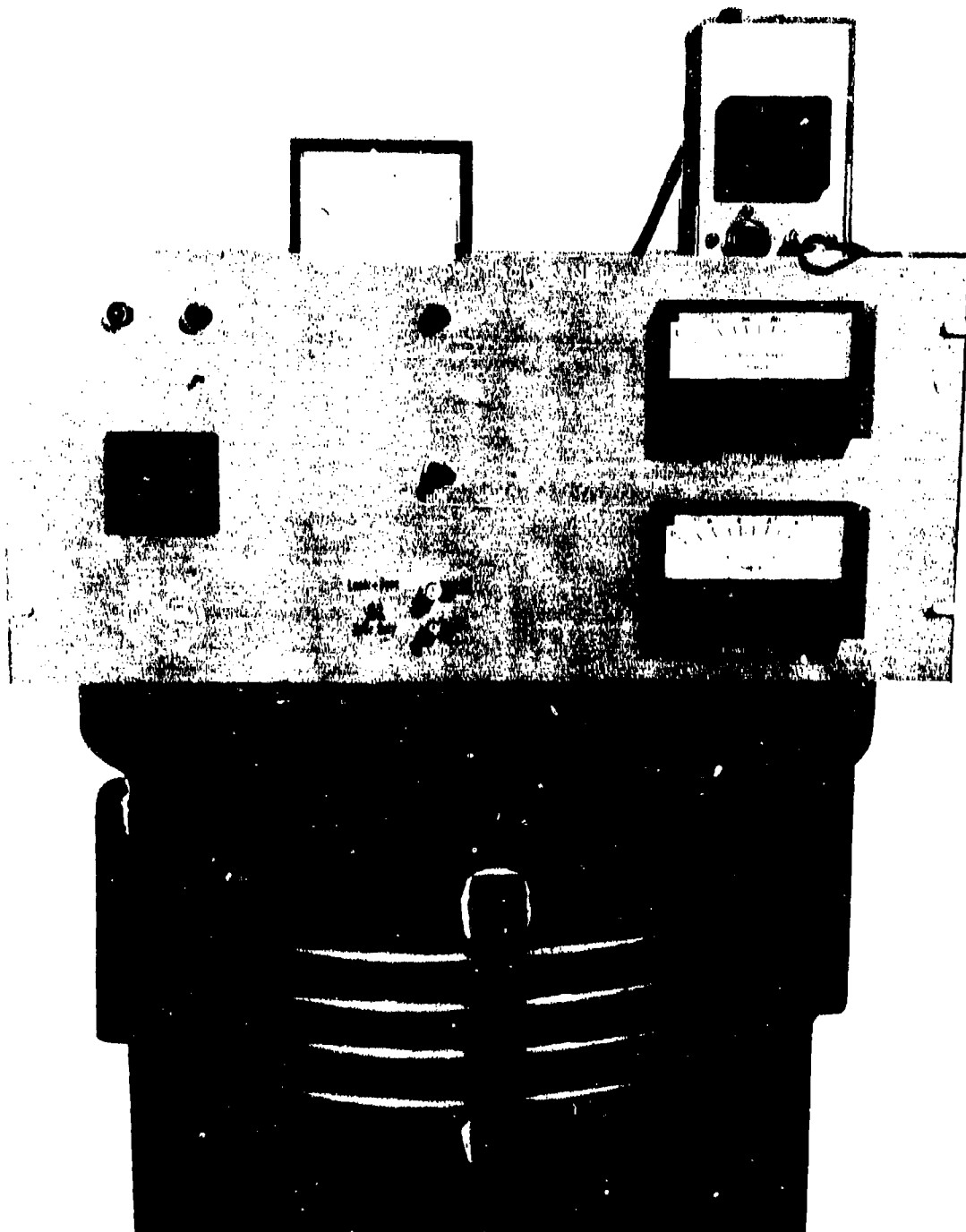


Figure 5. Control unit for operating laser via cable at remote stations.

TABLE 1. SYSTEM SPECIFICATIONS.

Mechanical

Canister size	41-cm dia X 84-cm height (16 X 33 in) 46-cm-dia flange (18 in)
Weight	109 kg (240 lb)
Displacement	114 kg (250 lb)
Depth limit	180 m (600 ft)

Electrical

Input power	1 kW, 3 phase, 400 Hz, Y
Lamp energy	up to 10 joules

Optical

Wavelength	blue-green, depending on dye
Pulse rate	20 p/s (pulses per second)
Pulse energy	up to 5 mJ
Peak power	up to 6.5 kW
Pulse width	0.75 μ s

DETAILED SYSTEM DESCRIPTION

THE LASER

Figure 6 is a block diagram of the underwater portion of the laser system. The laser head, the black rectangular block in top center of figure 3, is shown bounded by dotted lines at the top of the diagram.

The lasing medium in this system is a solution of a fluorescent organic dye in ethanol that circulates through a 3-inch-long quartz capillary tube. Curved mirrors at either end of the tube satisfy the feedback requirements for multimode laser action and a linear xenon flashlamp acts as the laser pump. The flashlamp and parallel capillary lie along the foci of a cylindrical elliptical reflector built into the laser head.

Most of the remaining elements diagrammed in figure 6 are concerned with flashing the flashlamp. They control both the timing and brightness of the pumping light.

The energy required by the flashlamp for any given laser pulse is provided by the energy storage capacitor (ESC) shown just below and to the left of the laser head in figure 6 and at top center in figure 4. Typically, 5 joules of input energy (7 kV in 0.2 μ F) is required for a laser output energy of 5 mJ. Discharge of the ESC into the flashlamp is controlled by the thyatron switches to the right in figure 6 and recharge of the capacitor is managed by

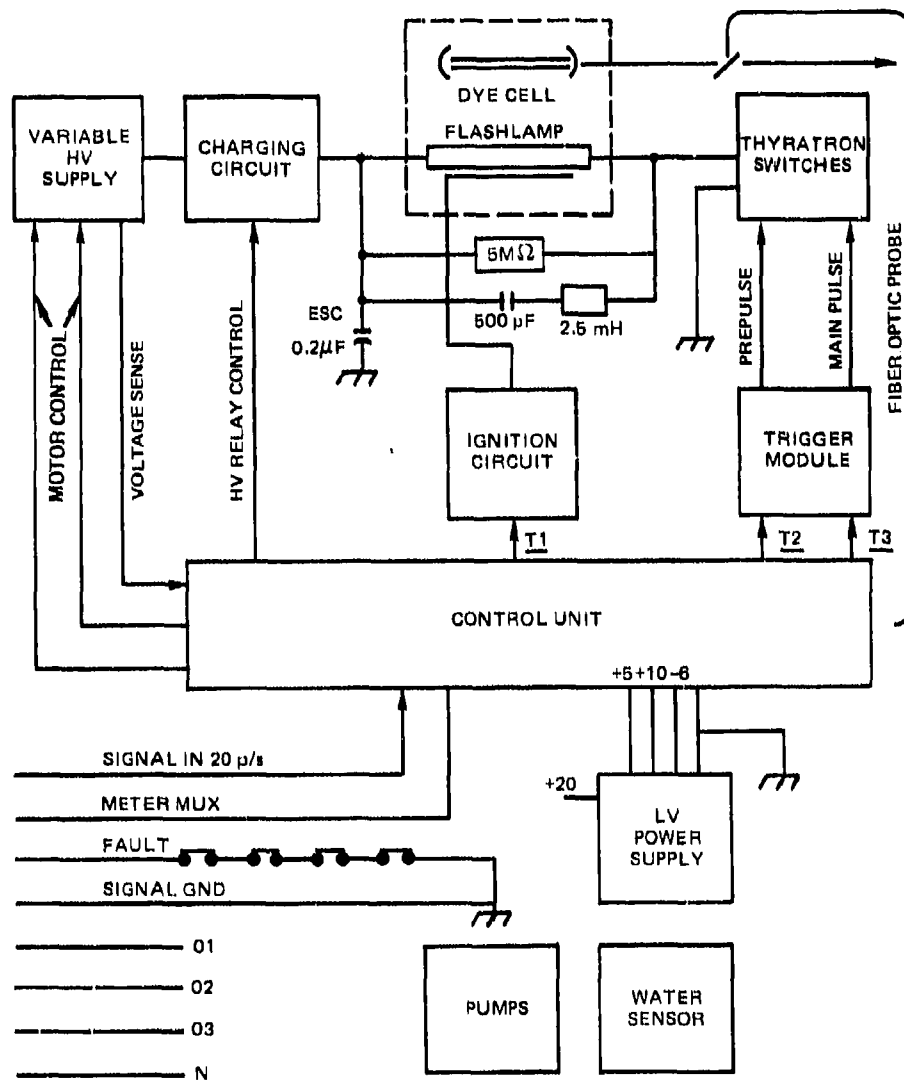


Figure 6. Underwater laser block diagram.

the circuit elements to the left. Assuming that the capacitor starts charged, the discharge and recharge cycle proceeds as follows:

1. A trigger pulse, T1, from the control unit is applied to the ignition circuit which, in turn, applies a 20-kV pulse to a wire wrapped around the flashlamp. A feeble spark is produced within the xenon by displacement currents and the gas is left in a partially ionized state.
2. Fifteen microseconds later, a second pulse, T2, after conversion to a 1.5-kV pulse in the trigger module, turns on the first of two thyratrons in the thyatron switch section. This prepulse thyatron causes roughly 2% of the stored energy to be dissipated in the flashlamp, producing a larger spark and a much higher level of ionization.
3. A 1.5-kV pulse generated by the T3 signal appears 10 μ s later, turns on the main pulse thyatron, and dumps the remaining stored charge into the flashlamp. The intense flash produced pumps the laser more efficiently than a flash produced without a prepulse and more reliably than a flash produced without an ignition pulse.
4. Recharge of the ESC begins immediately through the charging circuit, an inductor/diode arrangement that effectively doubles the voltage provided by the high-voltage supply. The charge cycle takes approximately 2 ms and the ESC "coasts" for the 48 ms preceding the next pulse. During the time that the system is on but not being triggered from the surface, a vacuum relay in the charging circuit disconnects the ESC from the high voltage to prevent corrosion of the water-cooled flashlamp terminals.

Associated with the flashlamp is a parallel resistor of 5 M Ω that is required to bias the thyatron anodes and a series circuit consisting of a 2.5-mH choke and a 500-pF capacitor. This LC network aids in reliable thyatron turnoff.

The laser output level is stabilized in this system by a feedback loop that includes a beamsplitter and fiber optic probe, detector, filter, and relay circuits within the control unit, and a motor-driven Variac in the high-voltage supply. This loop compensates for decreases in output caused by flashlamp and dye solution aging processes. Some 8 hours of operation can be expected between lamp and dye changes.

Also represented as blocks in figure 6 are the dye and cooling water circulating pumps and a water sensor circuit. The latter shuts the system down if salt water invades the canister. Additionally, four normally closed switches are shown in the fault line. These switches sense pressure and temperature in the dye and water circuits and prevent triggering of the flashlamp if the liquids overheat or stop circulating. A meter MUX line carries multiplexed signals representing high-voltage input to the lamp and the laser output to the surface for display on the control panel.

Detailed diagrams of the blocks in figure 6 are given in figures 11 through 13.

THE LASER CONTROL PANEL

The laser control panel of figure 7 controls the prime power to the laser canister, provides a 20-Hz signal to "run" the laser, displays two important laser operating parameters, and provides a signal for an FM sync transmitter.

The prime power control is straightforward. A 5-ampere circuit breaker turns the control panel on and off and simultaneously powers the laser through four of the interconnecting wires. A phase reversal switch is included in two of the lines to reverse the direction of rotation of the pumps if required.

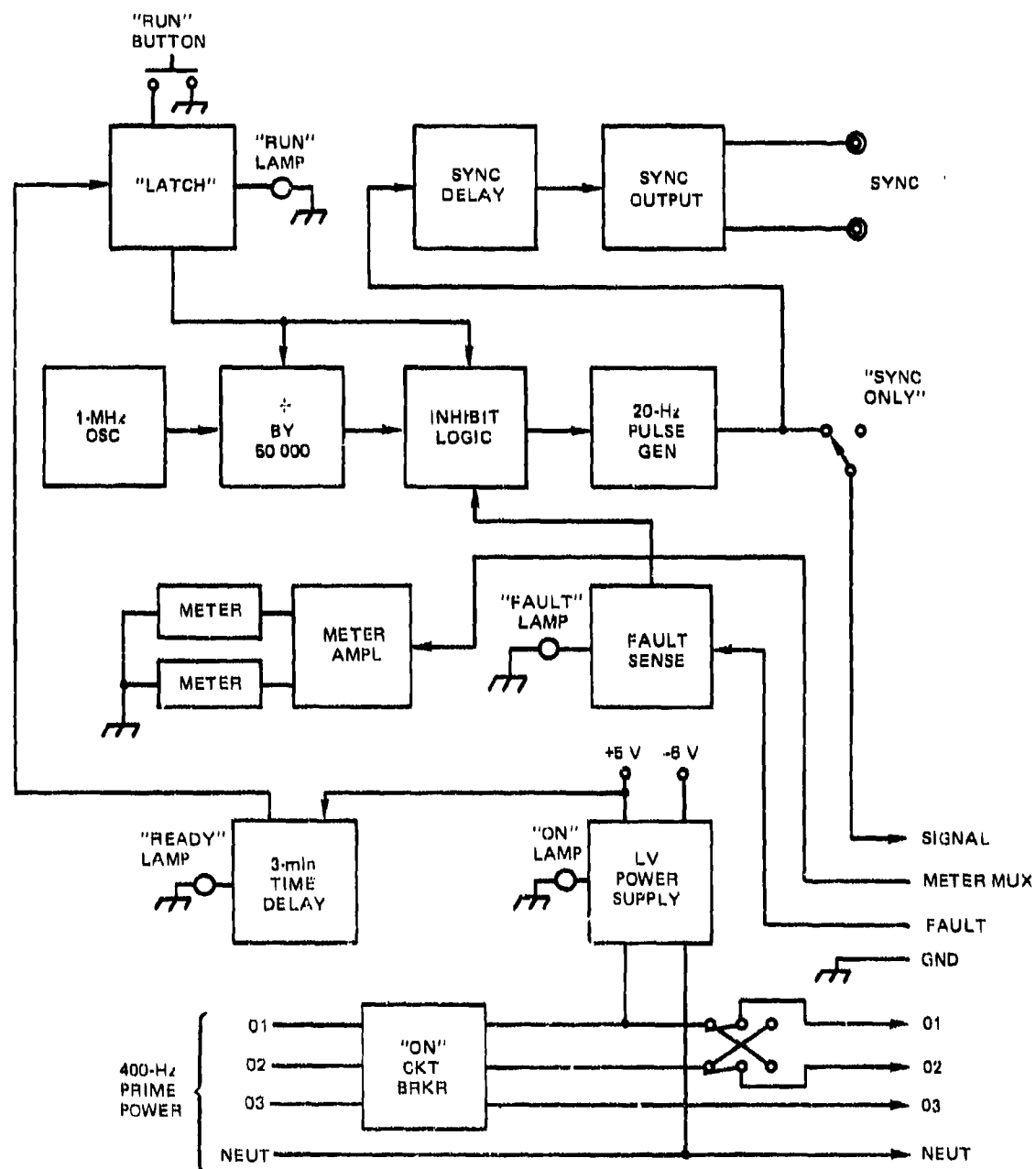


Figure 7. Laser control panel block diagram.

The 20-Hz laser trigger signal is derived from a 1-MHz crystal oscillator by dividing by 50 000. Whether or not the signal is sent to the laser is determined by the state of the thyatron warm-up time delay, the run button, the FAULT SENSE, and the SYNC ONLY switch as shown in the diagram.

The multiplexed meter signal is received and decoded by a circuit in the control panel and a measure of flashlamp high-voltage input and laser output is displayed for the operator's use. The readings on these meters determine when a flashlamp change is required.

There is a nominal 25- μ s delay between the time a signal is sent to the laser and the time the laser output pulse appears. The OPSATCOM sync transmitter requires a 5- μ s lead; or, relative to the signal sent, a 20- μ s delay. This function is handled by the elements shown in the upper right of figure 7.

While in the field, a pulse counter and line voltage monitor were added to the control panel as shown in figure 5.

(Detailed control panel circuitry is shown in fig 13.)

INSTALLATION, OPERATION, AND MAINTENANCE

SYSTEM INSTALLATION AND CHECKOUT

**CAUTION: DO NOT RUN THE LASER
WITHOUT FIRST PURGING WITH NITROGEN!**

1. Connect 3-phase, 4-wire, Y, 400-Hz power to the top four terminals of the barrier strip on the side of the control panel case as shown in table 4. The voltage should be 120 volts line-to-neutral.
2. Connect the eight-conductor laser interconnecting cable terminations to terminals 5 through 12 on the barrier strip. (See table 4.)
3. Connect the cable to the laser canister.
4. Turn on the system. If the FAULT lamp lights and stays lit, turn off the system and reverse the position of the switch on the side of the control panel case. If the FAULT lamp does not light, go to 6.
5. Turn on the system. The FAULT lamp should go out, indicating the pumps are running in the right direction.
6. Observe that the lower meter reads upscale, the upper meter reads zero.
7. Observe that after a 3-minute delay, the green READY lamp lights.
8. Tapping the RUN button with the Laser + Sync/Sync Only switch in the Laser + Sync position should light the button and produce an upscale reading on the upper meter. A slight decrease in the lower meter reading is normal. In the Sync Only position, the RUN button should light without an upscale reading.
9. To complete the installation, connect a BNC cable between the TTL sync output and the sync transmitter input. Secure the system.

SYSTEM OPERATION

**CAUTION: DO NOT RUN THE LASER
WITHOUT FIRST PURGING WITH NITROGEN!**

1. With the proper 400-Hz power applied and the laser canister interconnected and submerged, push the control panel circuit breaker to ON.
2. Allow 3 minutes for warm-up. The green READY light should come on. This is the normal laser standby condition.
3. If sync transmission is desired whether the laser is running or not, place the Laser + Sync/Sync Only switch in the Sync Only position and tap the RUN button. Control the laser by switching between Sync Only and Laser + Sync with the RUN button lit.
4. If sync transmission is desired only when the laser is running, switch to Laser + Sync and control the laser with the RUN button, tapping it to start or stop.
5. Each time the laser is activated, the upper meter should return to the same reading. Failure to read a constant value indicates that the output level regulation system is out of regulation.
6. If the upper meter reading begins to decrease with the lower meter reading near 8, the flashlamp needs replacement. If the flashlamp is replaced and the lower meter reading does not decrease to a value near 6, the dye may need replacement.

FLASHLAMP REPLACEMENT PROCEDURE

1. Turn off the power to the system and remove the canister cover. Inspect the interior for water leakage. Remedy the problem if necessary.
2. Remove the protective cover from the anode assembly and discharge the anode assembly to the chassis with an insulated-handle screwdriver.
3. Remove the three screws securing the circular flange to the anode assembly.
4. Slowly lift the flange and lamp straight up until clear of the anode assembly. Avoid splashing or dripping water into the beamsplitter recess. Should the lamp separate from the flange and remain in the water jacket, remove the lamp with a pair of pliers.
5. Remove the old lamp from the flange ferrule and replace it with a new one. The end of the lamp marked + must be within the ferrule and the slit on the trigger wire sleeve should face the light exit hole in the flange.
6. Wait long enough for the water level in the lamp jacket to recede and carefully reinsert the lamp. Avoid overflowing water into the beamsplitter recess.
7. Secure the flange to the anode assembly with the three screws. Make sure the beamsplitter is clean and dry and add the plastic protective cover. The system may be operated briefly to check output and regulation. Turn off before proceeding.
8. Inspect the cover sealing surfaces and add silicone grease if necessary. Install the cover and start two bolts.
9. Prop the cover open on one side with a matchbook or equivalent and connect a tank nitrogen line to the purge fitting on the side of the canister.

10. Purge with nitrogen. Allow for a 100-psi (1 psi = 6894.7 Pa) pressure decrease in a standard size tank. Turn off the gas.

11. Secure the cover, remove the nitrogen line, and cap the purge fitting.

DYE REPLACEMENT PROCEDURE

1. Secure the system, remove the canister cover, and discharge the anode assembly to chassis.

2. Uncap the drain line above the drain valve knob and connect a plastic drain line. Route the drain line to an empty container.

3. Remove one of the caps on the dye tank and connect a line to a source of nitrogen gas at 10 psi.

4. Turn the drain valve to the DRAIN LASER position. Keep the valve in that position until the drain line blows dry (approx 1 min).

5. Turn the drain valve through RUN to DRAIN TANK. Keep the valve in that position until the drain line blows dry (approx 4 min).

6. Disconnect the pressure line and return the valve to RUN. Cap the drain line.

7. Remove the second cap on the dye tank. Affix the valve cap assembly to a container of new dye. Close the valve.

8. Invert the dye container and secure the valve to one of the uncapped dye tank fittings.

9. Open the valve to the dye container and squeeze the dye into the tank. When empty, close the valve and remove dye container.

10. Cap off the dye tank fittings and make sure the dye drain valve is in the RUN position.

11. Cover and purge the canister as in FLASHLAMP REPLACEMENT PROCEDURE.

OUTPUT PEAK POWER ADJUSTMENT

1. Open the canister, disconnect the water lines, and raise the vertical chassis until the holes in the edge of the plate are just above the tops of the guide channels. Secure in this position with 1/4-inch-diameter pins.

2. Interconnect the chassis plug and the jack in the base of the canister with the extension cord and replace the water lines with the longer lines provided.

3. Connect the control panel to canister cable and energize the 400-Hz power line.

4. Attach an EG&G model 580-00-11 narrow-beam adapter to a model 580-25-A detector head and secure both to a model 585-00-15 tripod. Interconnect the head and a model 580-11A meter unit.

5. Set the controls on the detector head as follows:

Negative bias voltage to INT

External viewing multiplier to X100

Aperture multiplier to X10

Anode to INT

Signal to ANODE

6. Set the controls on the meter unit as follows:

Ampere multiplier to 10-7

Current/Charge to Current

Hold/Integrate/Reset to Reset

7. Position the detector head 12 inches above the laser output aperture with the face of the adapter pointing downward, parallel to the floor. Turn on the meter unit and zero the meter.

8. Connect water and drain lines to the laser heat exchanger coil and turn on the water.

9. Operate the laser and reposition the detector, if necessary, to locate the spot in the center of the diffuser plate. Turn off the laser beam.

10. Connect a coaxial cable from the signal output of the detector head to the vertical input of an accurate oscilloscope. Set the vertical gain for 0.2 volt/division and the sweep speed for 0.5 μ s/division. Turn on the laser at the control panel and adjust the scope sync for a stationary pulse pattern.

11. The calibration for NELC Code 2500's radiometer is 1.625-V/kW with the external viewing multiplier in the X100 position. With the aperture multiplier in the X10 position, 0.1625 V represents 1 kW. For 5-kW peak power, 0.8125 V is required. If the peak amplitude on the scope differs from that, the level setting adjustment can be changed to correct the reading.

12. The control is located on the outboard face of the control module located on the lower left center of the chassis. It is the screwdriver adjustment closest to the chassis plate in the lower left corner. Turning the screw clockwise will increase the laser output. The system tends to stabilize from the top down, and it is advisable to cycle the laser on and off a number of times while making this adjustment.

13. Secure the equipment and restore the laser to its normal operating configuration. Purge with nitrogen.

CALIBRATION

The purpose of the OPSATCOM laser calibration was to provide, for data reduction purposes, a complete and accurate list of laser output parameters. A summary of that list is presented in table 2, and the following paragraphs describe briefly the measurement procedures.

TABLE 2. LASER OUTPUT PARAMETERS.

Pulse repetition rate	20 p/s (pulses per second)
Peak pulse amplitude	5 kW ($\pm 6\%$ rel, $\pm 10\%$ abs)
Pulse width	0.75 μ s
Pulse energy	4 mJ/p (nom)
Center wavelength	521.4 nm
Bandwidth	4.65 nm
Beamwidth (in water)	21.4 mrad (FWHM)

THE LASER CALIBRATION REFERENCE

The local standard used for setting the laser output to the 5-kW peak power level used for the field tests is an EG&G radiometer unit of the 580 series. The equipment is factory calibrated against an NBS certified thermopile and is supplied with a complete set of sensitivity vs wavelength tables. It is one of the most accurate radiometric equipments available.

EG&G gives an absolute accuracy specification of $\pm 8\%$, a precision specification of $\pm 1\%$, and an NBS uncertainty specification of approximately 3%. Presumably, the precision and uncertainty together with other calibration tolerances make up the overall accuracy specification.

The calibration constant that applies to the OPSATCOM laser is 1.625 V/kW. Five times that level is established during laser setup while viewing the output pulse on a calibrated oscilloscope.

The radiometer can also be used to measure pulse energy. The nominal output pulse energy corresponding to 5-kW peak power is 4 mJ. This number varies slightly depending on mirror alignment and was not specifically recorded during the field tests.

PULSE AMPLITUDE STABILITY

Once the laser has been set up to provide a specified peak output level, then the short- and long-term stability of the output becomes a factor to consider.

Short-term (pulse to pulse) stability is determined by the flash-to-flash uniformity in brightness and position of the arc in the flashlamp. For a given input energy, a small variation in output pulse amplitude is to be expected. Long-term stability is determined by how well the output control system compensates for changes in the output of the flashlamp and in the efficiency of the dye solution as the lamp and dye age.

As part of the post-field-test calibration effort, quantitative measurements of these factors were made. Before the results are presented, a laser design flaw that bears upon them will be described.

It was necessary, when designing the amplitude control system, to build a delay into the circuitry to allow the voltage that represents the output level enough time to rise to its true value. The delay was designed to lock out the motor drive to the Variac to keep the system from increasing lamp input energy at the start of each run cycle. As it turned out, the delay persists after the run cycle ends, and the Variac is driven upward -- out of the

regulator dead zone, anyway. In short, every time the laser is switched to RUN, the output starts slightly high and restabilizes to the set value. This cycle affects the first 5 seconds or so of laser output and may not be an altogether detrimental flaw. It also has the effect of narrowing the dead zone by starting at the upper edge each and every time the laser is operated.

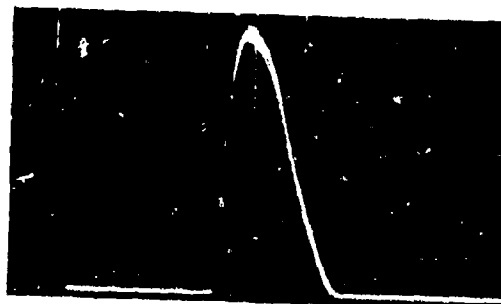
Figure 8 shows the laser output at the indicated times during four separate run cycles. Each photograph is a 1-second exposure and contains 20 individual pulses. The gain of the scope was adjusted so that one small division equals 4% of set amplitude and the sweep speed is 0.5 μ s/cm.

As can be seen in the photographs, the amplitude starts high, about 7%, and within 5 seconds stabilizes at the set value. Once stabilized, the pulse-to-pulse stability together with the reset error amounts to a nominal $\pm 5\%$. These samples are representative of both the short- and long-term stability of the system.

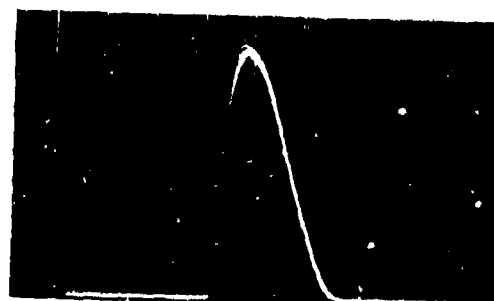
The stability of the control system over longer periods of time is also evidenced by the data given in table 3. These are excerpts of the log kept on laser operation during those parts of the field tests when actual measurements were made. Although intended for gross monitoring purposes only, the meter readings indicate that the system was regulating and that the output was stable during these intervals. The difference in upper meter readings (output) between the two series of dates does not include actual differences in output level but rather a difference in the position of the fiber optic probe in its drilled passage at the beamsplitter.** In both series, the operating peak power level was 5 kW.

For error analysis purposes, a stability of $\pm 5\%$ in peak power amplitude will be used.

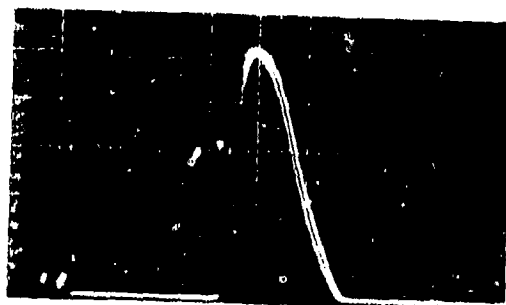
** Between these dates, the laser was reworked at NLLC to solve a problem with unexpected shutdown and the disassembly/reassembly operation resulted in a different probe position. The probe does not move during operation.



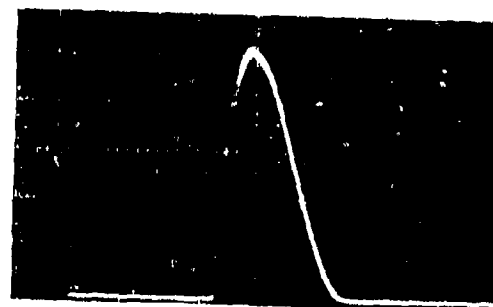
FIRST SECOND: +10 TO +3%



FIFTH SECOND: +5 TO -3%



TENTH SECOND: +3 TO -2%



TWENTIETH SECOND: +4 TO -3%

Figure 8. Laser output. Each photograph contains 20 pulses.

TABLE 3. LASER LOG EXCERPTS.

Date	Count	Lower Meter	Upper Meter	Comments
6/18	22	7.1	1.0	Photos (U-W)
6/19	27	6.9	1.0	Display
6/19	28	6.9	1.0	Display
6/19	35	6.8	1.0	A/C pass
6/19	39	6.6	1.05	Same
6/25	70	6.8	1.05	f(Θ) meas
6/25	89	7.0	1.05	A/C pass
6/26	102	6.2	1.05	filming
6/27	102	6.2	1.05	A/C pass
....				
7/16	93		1.5	Calibration
7/17	126	6.4	1.4	A/C pass
7/19	133	6.4	1.4	A/C pass
7/19	170	6.4	1.4	A/C pass
7/21	201	6.4	1.4	A/C pass
7/22	245	6.4	1.5-1.4	A/C pass
7/23	305	6.4	1.4	f(Θ)
7/24	348	6.2	1.5	A/C pass

LASER WAVELENGTH AND BANDWIDTH

The laser cavity used in the OPSATCOM laser is an untuned cavity; that is, prisms or gratings are not used to peak the cavity gain at any particular wavelength. The dielectric coatings used for mirrors are spectrally flat throughout the blue-green and a large number of dye/solvent combinations can be made to lase in this cavity.

The dye/solvent combination used for OPSATCOM has, in common with all other dye/solvent mixtures, a fluorescence spectrum that is several tens of nanometers wide and could be made to lase in a tuned cavity at wavelengths ranging from the yellow through the blue-green. When this dye is used in an untuned cavity, the requirements for laser action are simultaneously satisfied for a number of colors and, in fact, the system lases over a band of wavelengths that corresponds to the peak in the dye/solvent fluorescence spectrum. Measurements made before the field tests with a small prism spectrometer indicated a center wavelength of 522 nm and a bandwidth of 5 nm.

As part of the calibration procedure, the output spectrum of the laser was more accurately measured with a Jarrell-Ash 1-meter spectrometer. A densitometer scan of the laser spectrum together with a pair of reference lines is shown in figure 9. The lower curves were taken with one-half and one-fourth the exposure of the upper curve and serve to define the half-intensity points.

The measured bandwidth is 4.65 nm and the center wavelength is 521.4 nm. These measurements were made with the same dye solution used in the field tests. There is no evidence of the green shift that accompanies dye exhaustion.

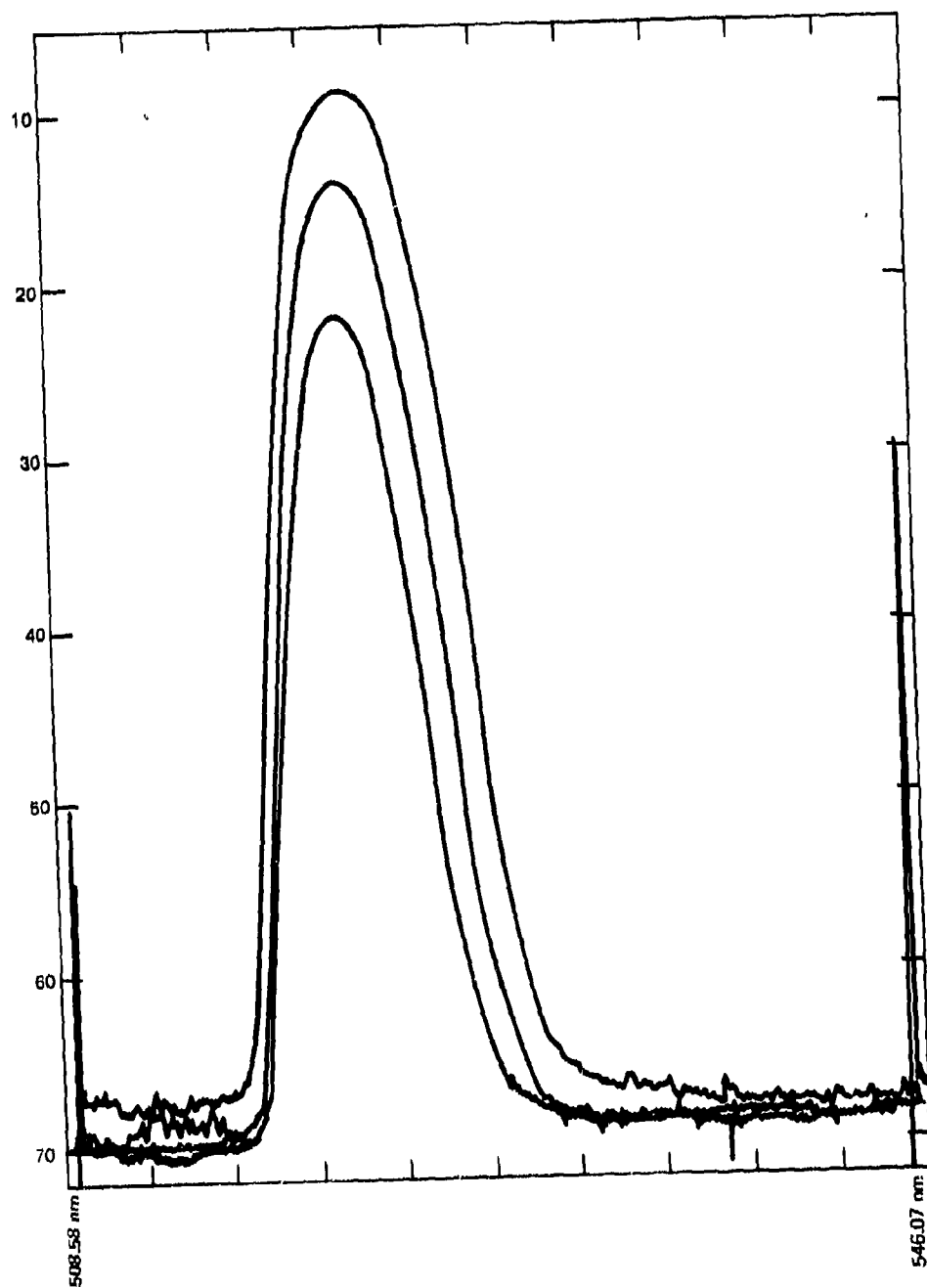


Figure 9. Laser spectrum (densitometer scan).

LASER BEAM DIVERGENCE

An exact measurement of the shape and divergence of the laser beam has also been made. A plot of the data taken is shown in figure 10. The measured beamwidth in air and the calculated beamwidth in water are given below.

Amplitude	Air	Water
0.5	28.4 mrad	21.4 mrad
$1/e$	30.1 mrad	22.6 mrad
$1/e^2$	33.0 mrad	24.8 mrad

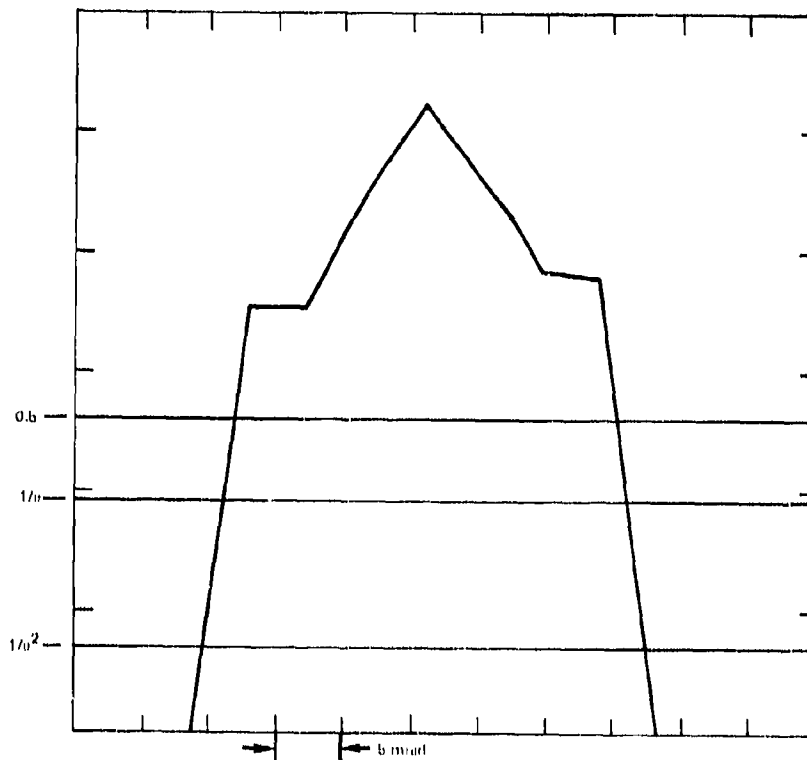


Figure 10. Beam divergence (air).

ERROR ANALYSIS

The beamwidth, center wavelength, and bandwidth of the output of the OPSATCOM laser are, for all practical purposes, invariant quantities. The actual value of the peak pulse amplitude and the stability of that value, on the other hand, are affected by the factors mentioned earlier in the sections covering the calibration reference and pulse amplitude stability. The seemingly largest source of uncertainty is the $\pm 8\%$ accuracy specification associated with the EG&G radiometer unit. In fact, this source of error is not always as important as it appears to be.

Most of the radiometer error consists of a fixed offset in an absolute sense; that is, the instrument would read consistently high or low (or exactly for that matter) when used to measure a precisely known intensity of light at 521.4 nm. Its reproducibility of measurement is less than 1% according to the manufacturer, so, although it may be reading wrong, the error involved in reproducing the wrong reading is small.

If this instrument is used to calibrate the laser and then to calibrate a receiving apparatus, the offset, if there is one, becomes a part of the calibration of both instruments in the same direction. If the laser and receiver are separated and the received signal intensities are expressed in normalized form, such as "dB of path loss" or " $\mu\text{W}/\text{cm}^2$ for a 5-kW laser pulse," then the offset cancels out. The only place the offset shows up is in expressing quantities in absolute units; one cannot compare the receiver calibration data with receiver noise and say that the receiver SNR is 0 dB at $1 \text{ nW}/\text{cm}^2$, for example, without considering the possibility of an offset. For relative measurements the $\pm 1\%$ specification should be used, and for absolute measurements the $\pm 8\%$ specification.

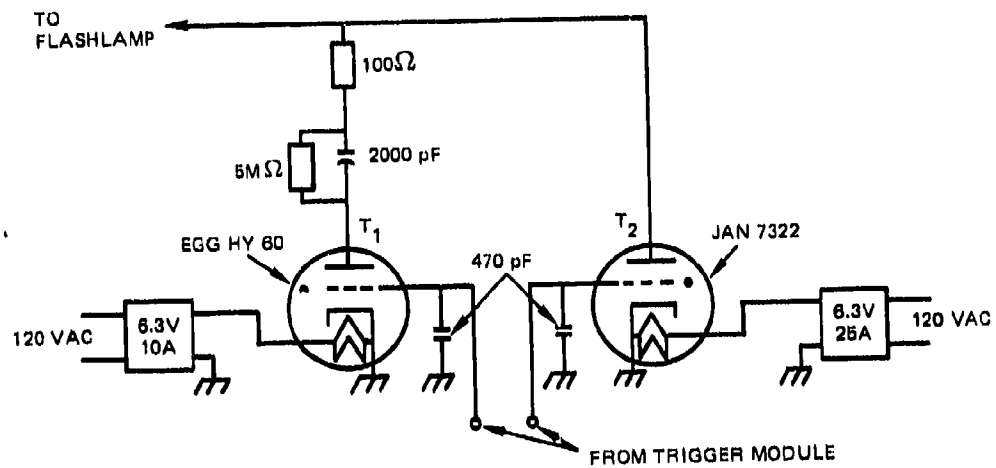
The largest source of error for most purposes, then, is the pulse-to-pulse amplitude stability. This has been shown to be of the order of $\pm 5\%$ in the steady state (after 5 seconds of operation). If another $\pm 2\%$ is allowed twice for oscilloscope error (once when setting up the laser and once when calibrating the receiver), then the limits for relative measurements would be $(1^2 + 2^2 + 2^2 + 5^2)^{1/2} = 6\%$. Absolute measurements, by the same reasoning, could be in error by no more than $\pm 10\%$.

These error limits, $\pm 6\%$ rel and $\pm 10\%$ abs, represent only those factors described above and do not include errors associated with reading or recording data at the receiver.

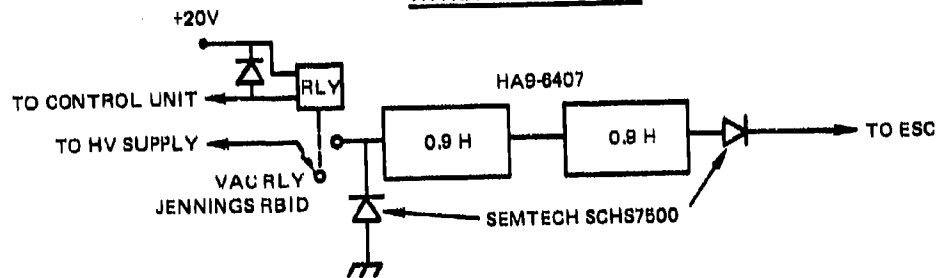
Detailed system information is provided in table 4 and figures 11-13.

TABLE 4. LASER CONTROL PANEL TERMINAL IDENTIFICATION.

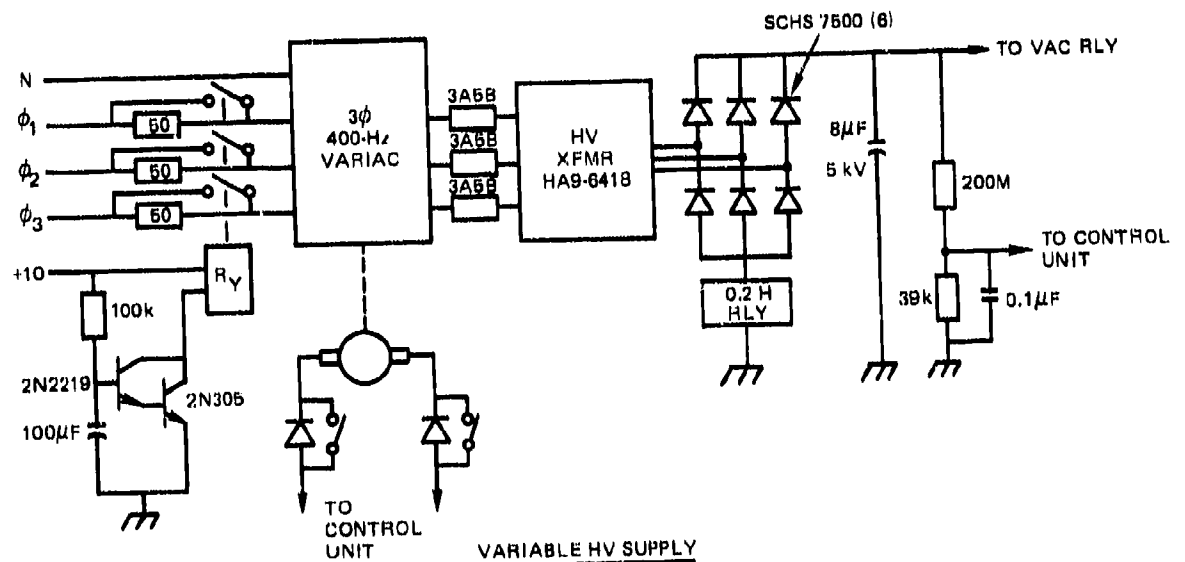
1. Neutral
2. Phase 1 input
3. Phase 2 input
4. Phase 3 input
5. Neutral down (black)
6. Phase 1 down (orange)
7. Phase 2 down (red)
8. Phase 3 down (white/black)
9. 20-Hz signal down (green)
10. Meter MUX up (red/black)
11. Fault up (white)
12. Signal ground (blue)



THYRATRON SWITCHES

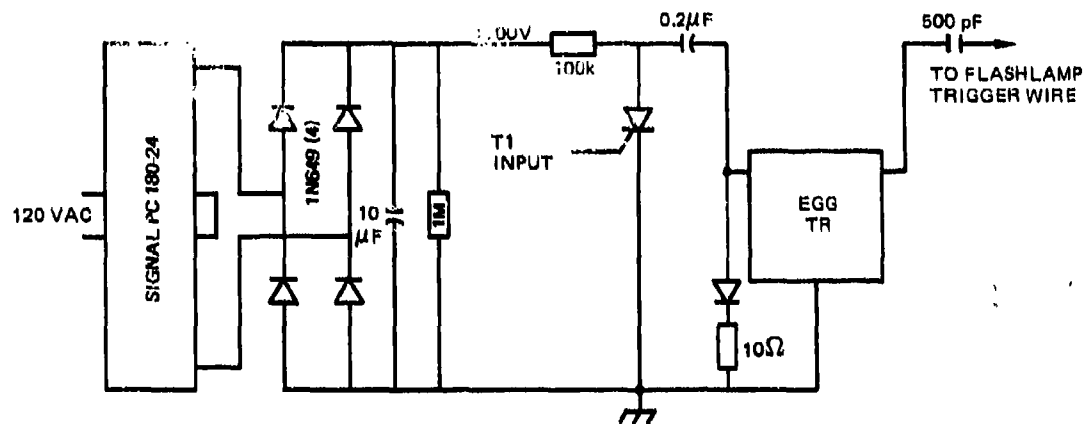


CHARGING CIRCUIT

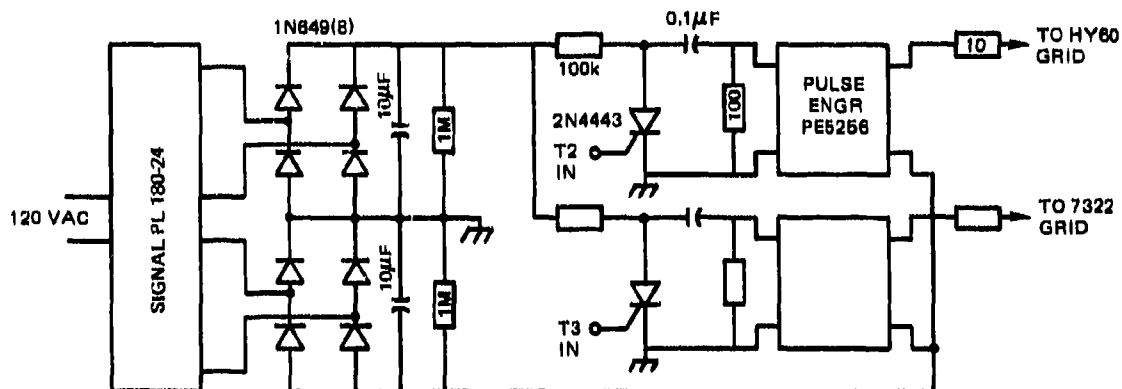


VARIABLE HV SUPPLY

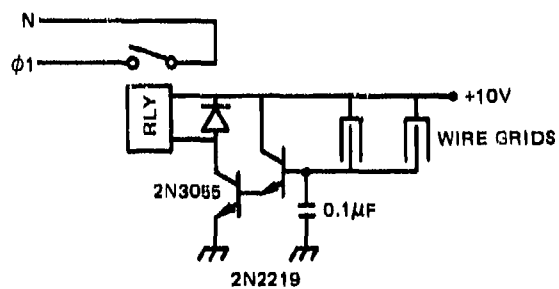
Figure 12. Miscellaneous schematics.



IGNITION CIRCUIT

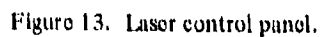


TRIGGER MODULE



WATER SENSOR

Figure 12. (Continued).



SECTION 2 UNDERWATER RADIANCE SCANNER

BACKGROUND

The Underwater Radiance Scanner was developed to measure radiance distributions of natural light fields underwater. It was deployed in a series of experiments designed to validate a model describing propagation of optical energy from a satellite to an underwater terminal.¹ In addition to measuring radiance distribution, the instrument is required to rapidly sample the solar energy distributions found just below the surface at an adequate rate to define the sea surface wave slope statistics.

Radiance is the radiant power incident on a unit surface area per unit solid angle from a defined direction. Radiance distributions are the collections of numbers which describe the radiance values at a point in space from all directions.² Hence, the radiance L may be defined by

$$L = \frac{d^2F}{dA \cos \xi d\Omega} \quad \text{W/cm}^2 \cdot \text{sr} \quad (1)$$

where F is the incident flux density on an area dA at an angle of incidence ξ from a field of $d\Omega$.³

Physical oceanography has recognized radiance distributions as a function of depth as significant measures of the inherent optical properties of water masses.^{4, 5} Early workers devised photometric instruments to obtain radiance distributions in the sea. The resolving power of these instruments, however, was poor; the volume of data which had to be handled was large; and the instruments themselves were awkward, limiting the quality and quantity of the data acquired.

A very complete set of radiance distributions as a function of depth was obtained by Tyler in Lake Pend Oreille in northern Idaho.⁶ Tyler's instrument was a mechanically scanning Gershun tube photometer and was not suitable for work in the open ocean.

The importance of the radiance distribution with depth in water masses as a means of describing inherent optical properties was first recognized by Duntley in 1949. Theoretical work exploring the nature of underwater radiance distributions was accomplished by Duntley⁷ and Preisendorfer⁸ with Tyler⁴ showing that the greatest yield of information from experimental sources on the optical properties of natural waters is provided by the measurement of radiance distribution with depth.

-
1. Karp, S, "Optical Communications Between Underwater and above Surface (Satellite) Terminals" IEEE Tran Comm, COM-24, 66-81 (1976)
 2. Smith, RC, et al, "An Oceanographic Radiance Distribution Camera System," Applied Optics 9, 2015-2022 (1970)
 3. Jerlov, NG, "Optical Oceanography," Elsevier 1968
 4. Tyler, JE, "A Survey of Experimental Hydrologic Optics," J Quant Spectrosc Radn Transfer, 8, 339-354 (1968)
 5. Nygard, K, "Radiance Distribution below the Sea Surface," AGARD lecture Series 61, Optics of the Sea
 6. Tyler, JE, "Radiance Distribution as a Function of Depth in an Underwater Environment," Bull Scripps Inst of Oceanography 7 363-411 (1960)
 7. Duntley, SQ, "The Visibility of Submerged Objects," Visibility Laboratory Report 1952
 8. Preisendorfer, RW, "Model for Radiance Distribution in Natural Hydrosols," JOSA 47 1046 (1957)

In an effort to avoid the many experimental difficulties encountered in acquiring radiance distributions in the sea, Smith designed a Radiance Camera system around the Nikkor fisheye lens, which has a nominal field of 180 degrees.⁹ Since an entire hemisphere is projected onto a photographic film in the focal plane of the fisheye lens, it became practicable for the first time to acquire data of high resolution rapidly. Two such cameras were mounted together, one covering the upper hemisphere, the other the lower, to obtain complete radiance distributions.²

The usual problems of using film to make photometric measurements are encountered in the radiance camera. It is necessary to take two frames at differing exposure values to accommodate the dynamic range of the scene.* Data reduction is accomplished after careful film processing using an automatic scanning microdensitometer coupled to a computer.

BRIEF DESCRIPTION

The Underwater Radiance Scanner uses Smith's radiance camera concept² but eliminates the intermediate and troublesome film process. An improved fisheye lens is utilized to image the upper hemisphere onto an image dissector camera system.

The result is a unique instrument for real-time measurement, recording, and display of underwater radiance distributions. It provides high resolution of fine details in the angular structure of radiance distributions. It is also capable of rapidly acquiring data and can record the complex radiance distributions found near the surface which are due to refraction and reflection effects at the air-sea interface. A complete hemisphere or any portion of a hemisphere may be scanned without mechanical motion of any kind.

The sensory unit of the radiance scanner consists of an image dissector camera system and an 8-mm, f/2.8 fisheye lens system in a submersible pressure vessel. The camera system is a random-access image digitizer and operates under program control from a digital computer through an associated digital video unit. The sensory unit contains electronic circuitry for adjusting the video gain of the camera (by changing the electron multiplier voltage), setting the aperture stop, and performing as many as three additional functions all under the control of the central processor. An optical coupler interfaces the sensory unit to a long underwater cable. A serial-to-parallel receiver is used to drive camera logic circuits and the 12-bit commands to the X- and Y-axis deflection circuits.

Connecting the radiance scanner sensory (underwater) unit to the surface equipment is an interconnecting cable which may be in excess of 110 meters in length. This cable contains three shielded and twisted pairs and three conductors. Power is supplied at nominally ± 20 volts on two of the conductors (the third being the return) to power supplies in the underwater unit. The first twisted pair is used for serial digitized control data transmission down to the scanner; the second supplies the clock pulses; the third transmits the analog video to the surface.

Interface with the computer is achieved by use of a digital video unit which accepts the 16-bit computer output data format and serially transmits these data to the camera. Twelve bits of each word are deflection address commands and four bits are used for control functions. The return video is digitized and provided to the computer in 10-bit positive logic format. Four I/O control signals are employed in interfacing with the computer. This digital video unit also allows manual setting of the three control functions—the lens aperture

9. Miyamoto, K, "Fish Eye Lens," JOSA 54, 1060-1061 (1964)

* Smith, RC, private communication, 23 October 1974

stop, signal dwell (integration) time, and the camera gain functions. Control of the signal dwell time from 40 microseconds to 6.5 milliseconds is possible. The total time required to obtain a single radiance sample ranges from 240 microseconds to 5.2 milliseconds, depending on the integration period. This allows time-varying radiance distributions found near the surface to be sampled rapidly, with each frame being completed in a period which is short compared to scene dynamics.

Digital control of the radiance scanner by a small computer provides a high degree of versatility in the system. A program library has been developed to accommodate a variety of requirements. Peripherals allow program control, display, and recording and can simultaneously service other related experimental equipment and handle data.

A schematic diagram of the entire radiance scanner control system used in the experiment is shown in figure 1.

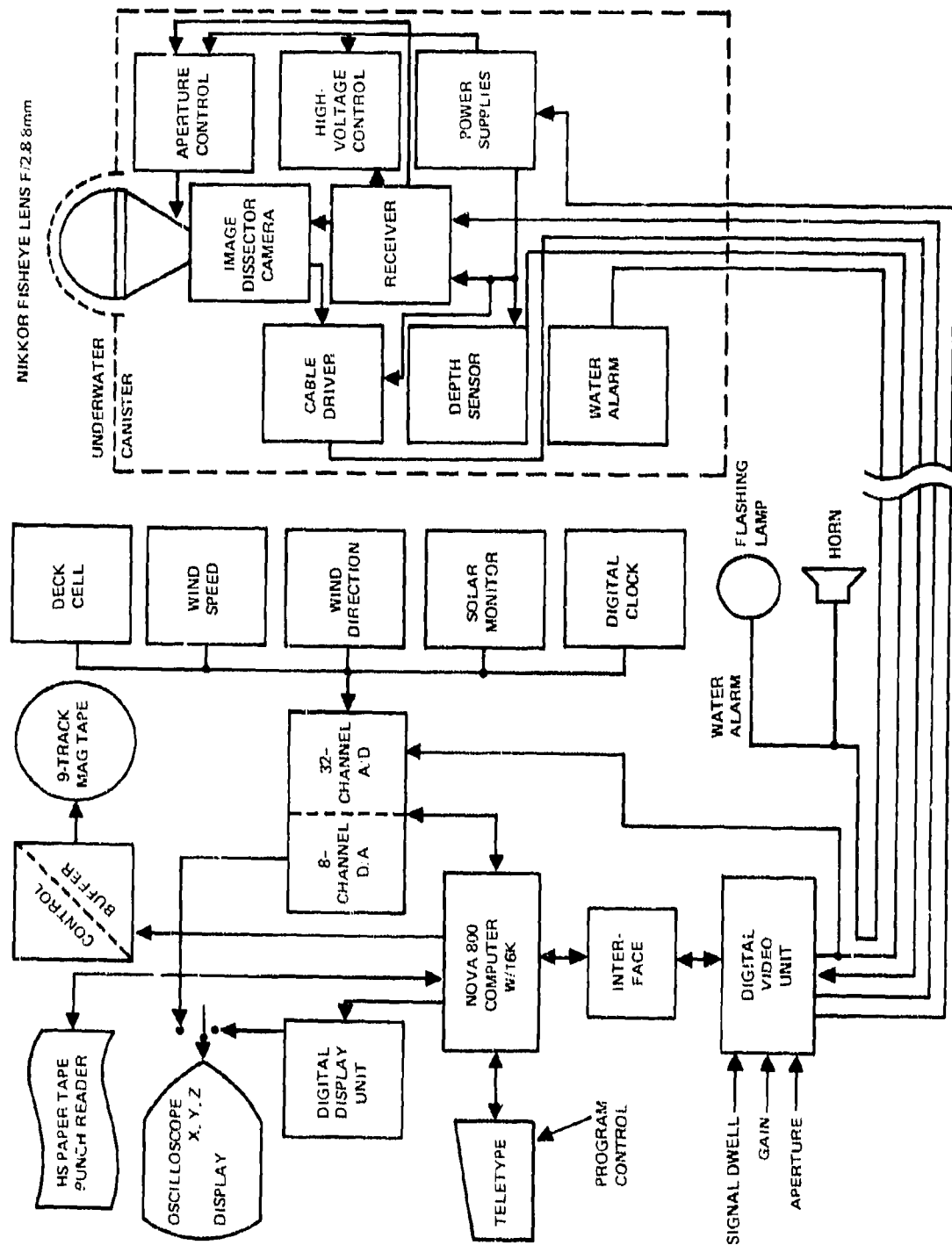


Figure 1. Radiance scanner system.

UNDERWATER RADIANCE SCANNER SENSOR

The sensor element of the underwater radiance scanner mounts in a submersible pressure vessel, as shown in figure 2. Major elements of the sensor operating system are the optics, the image dissector camera, and associated components.

OPTICS

At the heart of the optical system is the 10-element Nikkor 8-mm, f/2.8 fisheye lens described in figure 3. This lens, while similar to the lens used in the radiance camera system,² is faster and appeared to exhibit much less flare around the perimeter of the image due to bright objects in the field.*

All fisheye-type lenses exhibit inherent distortion, which is the result of mapping a hemisphere onto a plane surface and should not be confused with optical aberrations. In this lens, that mapping function is the equidistant projection formula in which the zenith angle ϕ of any point recorded in the image plane is proportional to the distance from the center of the image r ,^{9, 10}

$$r = f\phi \quad (2)$$

where f is the focal length of the lens = 8 millimeters. Such a lens is ideal for photogrammetric purposes and was designed for scientific applications such as measuring the zenith or azimuth of astronomical bodies or recording the distribution of clouds over the entire sky.¹⁰

Consider figure 4 in which the camera entrance and exit pupils are assumed to be at the origin of the coordinate system. An element of the field dA is imaged as ds . The solid angle $d\Omega$ projected by dA at range R and zenith angle ϕ is

$$d\Omega = \frac{dA}{R^2} = \sin \phi \, d\phi \, d\theta \quad (3)$$

and the incremental focal plane area

$$ds = r \, d\theta \, dr \quad (4)$$

Differentiating (2), we obtain

$$dr = f \, d\phi \quad (5)$$

If from (2) we then let

$$r \, d\theta = f \left(\frac{\phi}{\sin \phi} \right) \sin \phi \, d\phi \quad (6)$$

* Smith, RC, private communication, 23 October 1974

10. "Fisheye-Nikkor Lens," instruction manual, Nippon Kogaku KK 1973

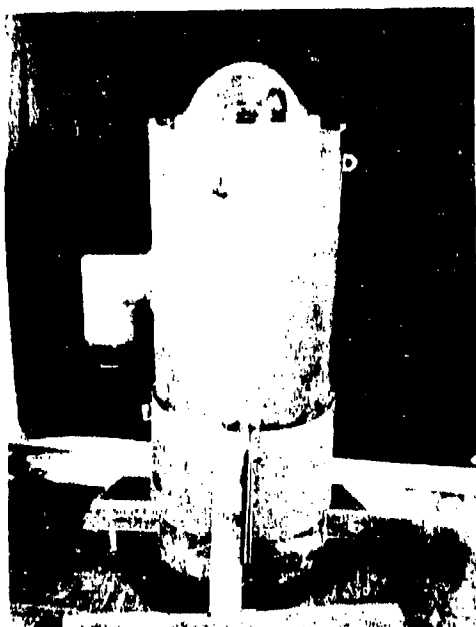


Figure 2. Underwater radlance scanner sensor.

FOCAL LENGTH	APERTURE	8 mm f 2.8
PICTURE ANGLE		180
EFFECTIVE PICTURE FIELD		23 mm ϕ ON FILM
LENS CONSTRUCTION		10 ELEMENTS IN 8 GROUPS
PROJECTION FORMULA		EQUIDISTANT
DIAPHRAGM		AUTOMATIC, STOPS DOWN TO f 22
FOCUSING RANGE		INFINITY (∞) TO 1 FT (0.3 m)
DISTANCE SCALE		GRADUATED IN BOTH FEET AND METERS
MOUNT		NIKON F BAYONET MOUNT
DIMENSIONS		123 mm ϕ X 140 mm
WEIGHT		APPROX 1 kg

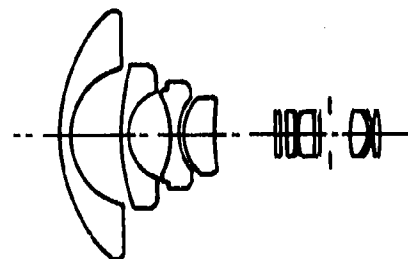


Figure 3. Features and specifications.

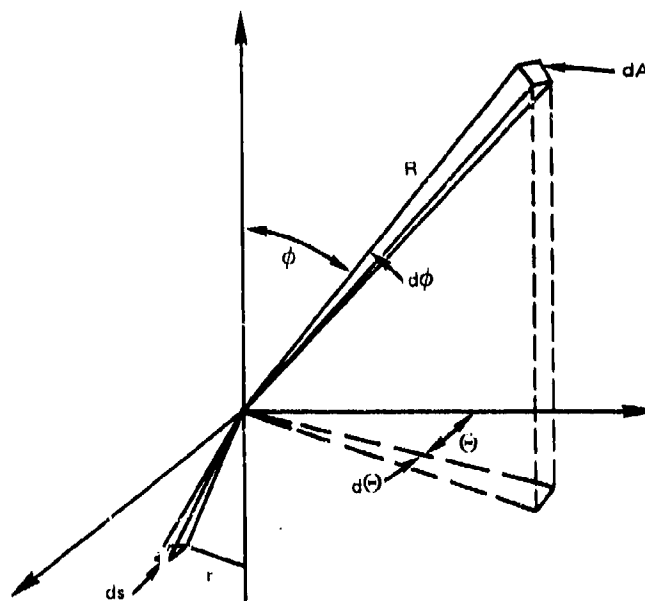


Figure 4. Coordinate system.

combining (3), (4), (5), and (6) yields

$$ds = r d\theta dr = f^2 \left(\frac{\phi}{\sin \phi} \right) d\Omega.$$

The focal plane resolution ds is determined by the area of the aperture which is built into the image dissector tube and is a constant throughout the image plane; hence,

$$d\Omega = \frac{1}{f^2} \left(\frac{\sin \phi}{\phi} \right) ds \quad (7)$$

and the resolution is seen to improve from the zenith ($\phi = 0$) to the equatorial plane ($\phi = \pi/2$) by a factor $\pi/2$, or 1.57.

The camera tube aperture was 0.127 mm in diameter (0.005 in); hence,

$$ds = 1.267 \times 10^{-2} \text{ mm}^2 \quad (8)$$

and

$$\begin{aligned} d\Omega &= 1.98 \times 10^{-4} \text{ steradian at } \phi = 0 \text{ degree} \\ &= 1.89 \times 10^{-4} \text{ steradian at } \phi = 30 \text{ degrees} \\ &= 1.78 \times 10^{-4} \text{ steradian at } \phi = 45 \text{ degrees} \\ &= 1.64 \times 10^{-4} \text{ steradian at } \phi = 60 \text{ degrees} \\ &= 1.26 \times 10^{-4} \text{ steradian at } \phi = 90 \text{ degrees} \end{aligned} \quad (9)$$

are the expected values of resolution.

Other optical elements which must be considered are the dome pressure window and the optical interference filter. The filter is mounted in the back focal length of the lens immediately after the last element. The spectral characteristics of this filter (fig 5) are a peak transmission of 57% and a FWHM optical passband of 93 angstroms.

The acrylic plastic pressure window is a dome of 8.9-cm radius. When submerged, this dome constitutes a negative lens element of approximately -28-cm focal length. Focusing effects are partially compensated by setting the focus ring on the lens to 1 foot when the camera is assembled into the pressure vessel. Wide-angle lenses are very sensitive to optical tolerances at large field angles, and the performance of the lens may be degraded when operated underwater.

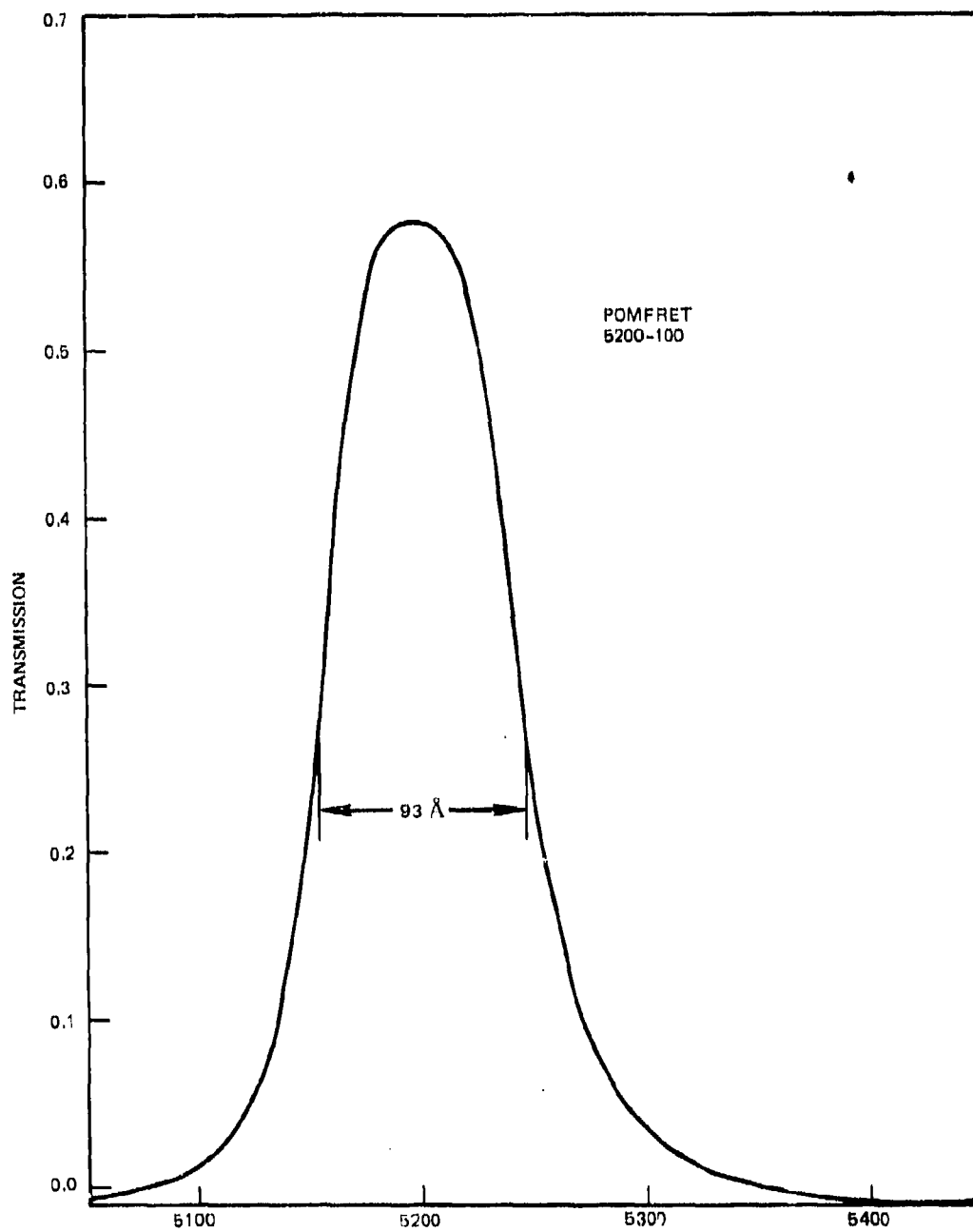


Figure 5. Optical filter wavelength, angstroms.

IMAGE DISSECTOR CAMERA

The image dissector tube is a standard ITT type F4011RP 3.8-cm (1½ in) diameter tube with a remotely processed S-20 photocathode. The responsivity of the photocathode was measured at 0.039 A/W for a quantum efficiency of approximately 9% at 522 nanometers. As stated previously, the fixed aperture was 0.127 mm in diameter.

A modified ITT model 5005 camera head which provides magnetic focusing and deflection coil assemblies is used. Photographs of the image dissector camera assembly are shown in figures 6 and 7. The camera unit also contains:

- Voltage divider
- Video preamplifier
- Focus current regulator
- Deflection amplifiers
- High-voltage power supply
- Voltage regulator

In addition to the camera head there is an electronics box, an underwater power unit, and an electrical motor to drive the aperture stop setting.

The electronics box contains three circuit cards necessary for interfacing with the digital equipment on the surface through more than 110 meters of underwater electrical cable:

1. A serial-to-parallel receiver which accepts data transmitted to the camera in serial format. It is connected to the cable through an optical coupler for isolation. This circuit also receives the clock pulses and performs logical functions such as parity checks.
2. An X, Y register and D/A converter which receives the parallel data and provides an analog drive signal to the deflection amplifiers.
3. The control register and video driver card which receive control bits and retain them until the next transmission. The control register provides five open-collector TTL circuits to operate equipment in the underwater canister. Two control signals are used to operate four relays, one at a time, through a two-to-four-line multiplexer. These relays connect potentiometers which in turn control the high-voltage regulator in the camera, providing four levels of photomultiplier gain in the image dissector tube. Each gain change provides approximately a 5 to 1 change in gain.

The video driver is specially designed to drive more than 110 meters of twisted-pair video cable to the surface signal integrator and digitizer.

The underwater power unit provides ± 15 and +5 volts to the underwater system and provides signal connections to the underwater cable.

A dc gear head motor operating on the +5-volt power supply drives the aperture controlling ring on the lens using miniature chain and sprocket assemblies. The stall torque of the motor is too low to damage the lens when the aperture is driven to either limit, f2.8 or f22. Two control functions are used to operate the motor — one to apply the 5-volt power, the other to reverse polarity.

Other ancillary equipment in the underwater canister includes a depth pressure sensor and a liquid water alarm sensor which operate independently of the camera system.

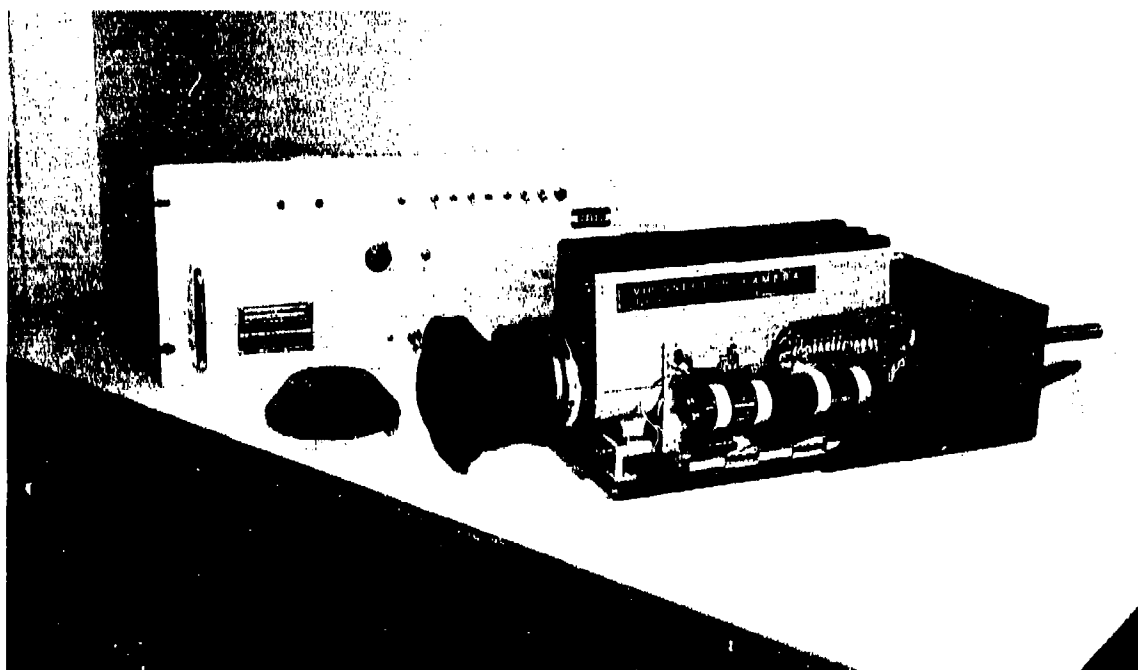


Figure 6. Image dissector camera and DVU (front view).

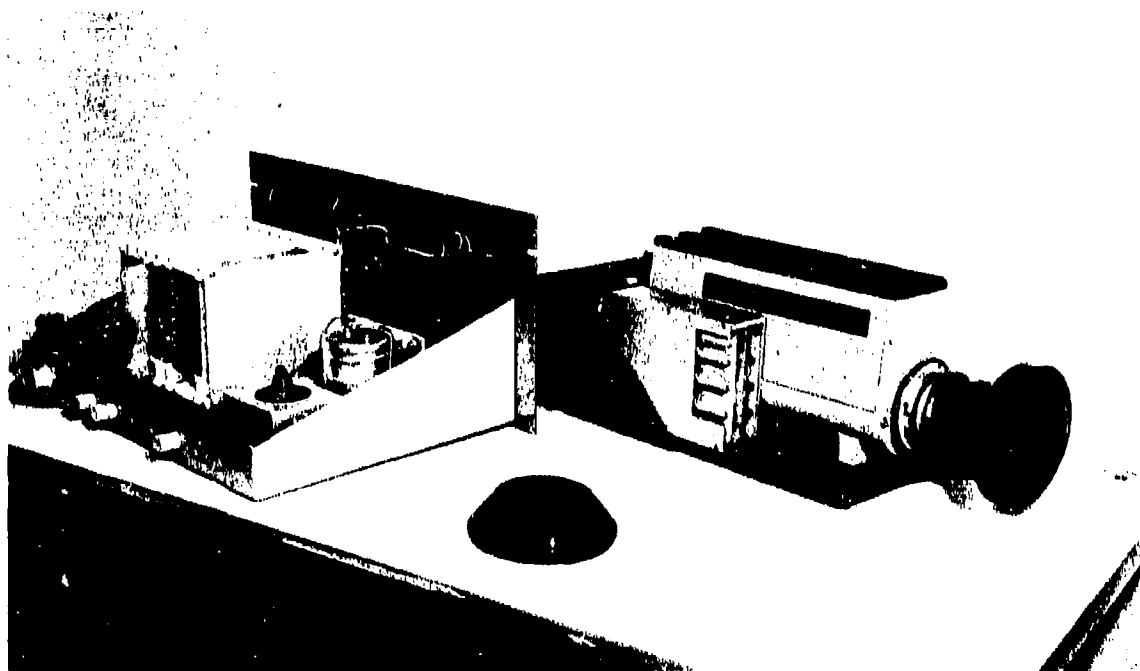


Figure 7. Image dissector camera and DVU (rear view).

DIGITAL VIDEO UNIT

The radiance scanner underwater sensor is controlled from the surface by the digital video unit (DVU), which operates as a peripheral input device for a digital computer. The DVU contains the computer interface, power supplies, and controls for operation of the radiance scanner.

The DVU accepts digital data from the computer and transmits the appropriate command and control signals to the underwater sensor. Provisions are also made for manually entering the control signals by means of panel switches on the DVU.

The video processor in the DVU accepts the analog video signal from the underwater camera and converts it to a 10-bit positive logic video output to the computer. The video processor circuitry consists of a squelched integrator, a sample-and-hold amplifier, and an analog-to-digital converter. The signal integration period, or dwell time, can only be adjusted manually by means of a 10-turn potentiometer control on the DVU control panel.

Two ungrounded, adjustable power supplies are provided, and set to compensate for cable losses to provide a minimum ± 20 volts under full load to the power circuits in the underwater canister.

To interface with the digital computer, the following signals are used:

Computer output data	16 bits, positive logic (4 bits control + 12 bits address)
Computer input data	10 bits straight binary
I/O control signals	OR - DVU requests output data IR - DVU requests video input IA - Computer acknowledges input INIT - Initializes DVU, raises OR

The DVU provides LED panel indicators for the following information signals, not used as logical signals in the operation:

BUSY	High during transmission to camera and deflection settle and dwell time
XMIT	High during transmission of data from camera

The system is designed to operate under computer control; that is, the computer directs the camera to a specified point in the field of view. The camera system measures the brightness of the point and transmits this video signal to the computer.

In addition, the system includes provisions for adjusting video gain (four settings) and operating up to five external system controls by computer or front panel controls.

The sequence of operation is as follows:¹¹

1. The DVU accepts position data from the computer - X and Y data plus a GO signal.
2. The data are transmitted to the camera (approx 150 μ s).
3. The camera deflection moves to the directed point (approx 40 μ s).

11. Wuellner, LE, "Technical Manual Vidisector Camera System for Underwater Photometry," ITT Report Proj 64225, 28 April 1975

4. The video signal is measured (50 μ s to 5 ms by front panel signal dwell time control).

5. The video data are transferred to the computer.

Total time per element, therefore, ranges from 240 μ s to 5.2 ms.

The data format required by the DVU from the computer is shown in figure 8. An overall block diagram of the DVU, underwater cable, and underwater radiance scanner sensor is shown in figure 9.

CONTROL BITS				DATA BITS													
MSB															LSB		
15	14	13	12	11	10	9	8	7	6	5	4	3	2	1	0	FUNCTION	
0	0	0	1	12 bits, 2's complement													X Position
0	0	1	0	12 bits, 2's complement													Y Position
0	1	0	1	12 bits, 2's complement													X Position and Go
0	1	1	0	12 bits, 2's complement													Y Position and Go
0	1	0	0	New data disregarded													Go again
0	1	1	1	12 bits, 2's complement													X=Y and Go
0	0	0	0	New data disregarded													No operation
1	0	0	0	11-7 disregarded						0	0	0	0	0	0	0	Set gain 00, $\approx 1 \times 10^4$
1	0	0	0	11-7 disregarded						0	0	0	0	0	0	1	Set gain 01, $\approx 5 \times 10^4$
1	0	0	0	11-7 disregarded						0	0	0	0	0	1	0	Set gain 10, $\approx 2.5 \times 10^5$
1	0	0	0	11-7 disregarded						0	0	0	0	0	1	1	Set gain 11, $\approx 1.25 \times 10^6$
1	0	0	0	11-7 disregarded						0	0	0	0	1	0	0	Opens aperture to f/2.8
1	0	0	0	11-7 disregarded						0	0	0	1	1	0	0	Closes aperture to f/22

Figure 8. Computer output format to DVU.

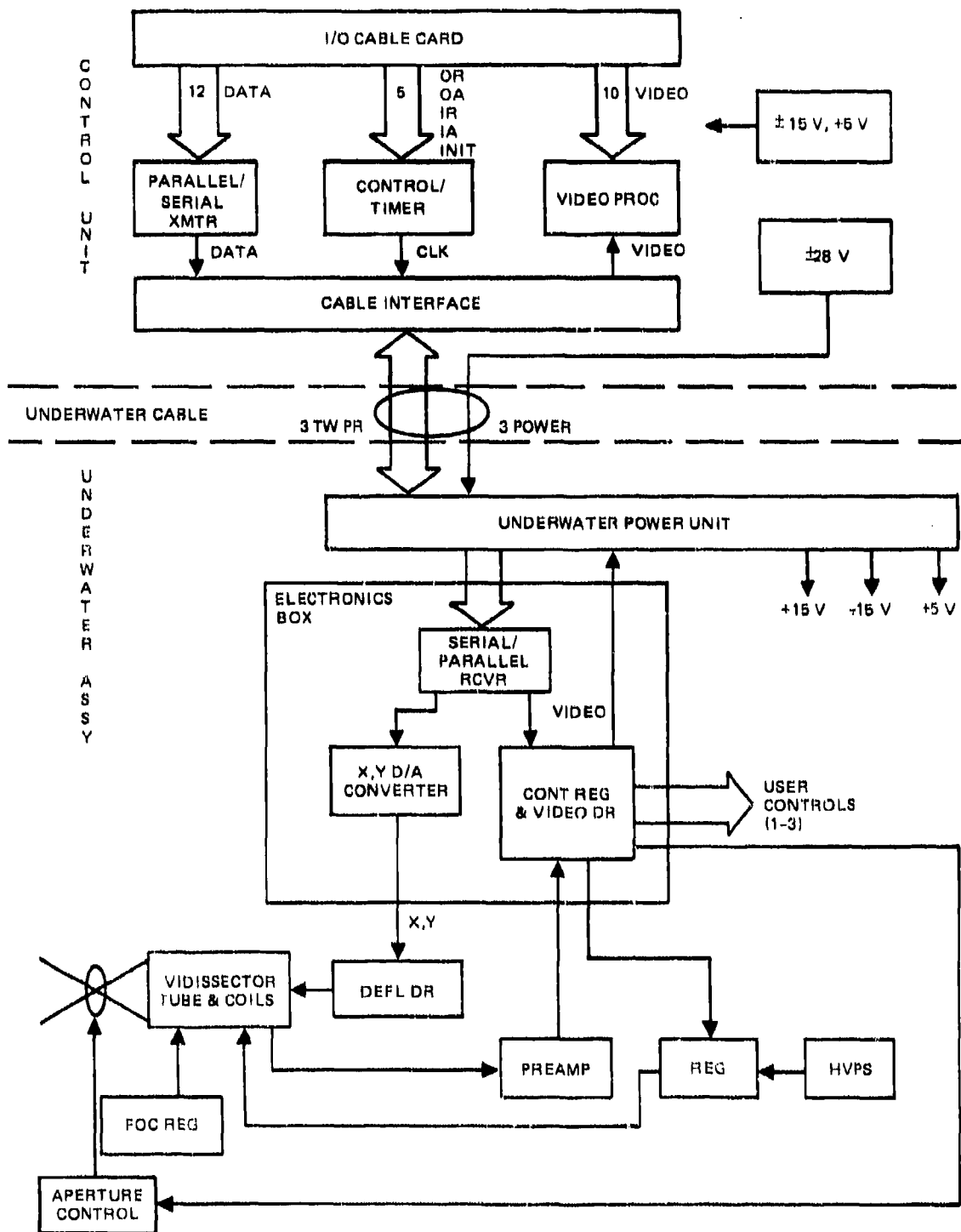


Figure 9. Overall block diagram.

DIGITAL EQUIPMENT

The underwater scanner requires a general-purpose digital computer which can provide program control and handle the return video data. Peripheral equipment of various types may be provided to best suit the user's needs.

For the experiment, the equipment was chosen principally on the basis of ready availability within the laboratory. As a central processor, a Nova 800 computer was utilized having 16k of core memory (16 384 sixteen-bit words). The other equipment, as shown in figure 1, included:

- Megatek PB-721A-08 graphics interface having 256 data point memory with refresh
- Datatron clock and MDB Systems interface board to provide day and time of day to 10 milliseconds
- ASR-33 TTY with a Remex I/O board controller
- Nine-track Wangco magnetic tape deck with Decision controller
- Remex high-speed paper tape reader/punch and controller
- Analogic 32-channel A/D and 8-channel D/A converter with interface
- Tektronix RM-503 oscilloscope

SOFTWARE

For maximum versatility and ease of operation the operating program language was single-user BASIC, as provided by Data General Corporation, but modified to accept subroutine calls to assembly language programs stored in core. These assembly language subroutines operate all the peripheral equipment except the TTY, including the radiance scanner. The transfer of data from BASIC to core storage and to peripheral equipment is also controlled by assembly language subroutines.

Core storage of the NOVA was configured to contain, starting from the highest address, the binary loader or bootstrap. The next 4095 words were dimensioned for the magnetic tape buffer. The assembly language subroutines (drivers) occupy approximately the next 3k of storage followed by the dimensioned arrays. The lowest 4k of core contains the BASIC Interpreter with operating program storage in the space between the BASIC Interpreter and the arrays.

The high-speed paper tape reader was used to duplicate paper tapes and to load the computer. Operating programs, however, could only be entered via the teletype, either by typing in the program or using prepared tapes on the teletype tape reader.

OPERATING PROGRAMS

The virtue of using BASIC in the operating programs is the ability to write or modify programs easily to perform a variety of functions, such as reading the environmental sensors, reducing recorded data, or displaying real-time imagery for examination. A large number of programs were developed during the field tests and during equipment calibration efforts. Two programs, however, were used in various forms to acquire most of the underwater radiance data. These are the Automatic Hemispherical Scan program and the Snapshot program.

AUTOMATIC HEMISPHERICAL SCAN PROGRAM

The Automatic Hemispherical Scan program scans the entire upper hemisphere using three preset resolution values. The data points generated by the deflection program are shown in figure 10. The innermost square contains the zenith and circumscribes zenith angles of up to nominally 30 degrees. Highest resolution is used in this central zone as sky features of interest to the experiment (the sun) will appear in it. The inner-zone resolution is 20 digital deflection units, or approximately 1 degree.

The resolution of the next-larger square is half that used for the inner scan, about 2 degrees. This square circumscribes the Snell circle, a circle of approximately 50 degrees from the zenith within which is refracted the entire hemisphere of light above the water. The outer region uses a resolution of 4 degrees and is circularly configured to match the image format of the fisheye lens.

At the start of each data run, the operator enters a starting electron multiplier gain for the first scan in each zone. The operator must manually set the signal dwell or integration period and the aperture opening. The first operation performed by the program is to read the day and time-of-day clock and then the environmental monitors. These data are stored in the magnetic tape buffer and written onto the tape later.

The program scans the inner area first, using the initial camera gain setting that is entered at the start of the program. The aperture of the camera is positioned at $X = -600$, $Y = -600$ and scans inward towards the zenith. The positioning is performed in the Camera X,Y deflection coordinate system. Readings are taken at (X,Y) , $(X,-Y)$, $(-X,-Y)$, and $(-X,Y)$. The X coordinate is then increased by 1 degree (20 deflection units), and another set of four readings is taken. The X coordinate is increased and readings are taken until its value is 0, then X is reset at -600 again and Y is increased to -580 . Readings are taken in this manner until the aperture is positioned at the zenith.

A check is made while scanning the inner area to determine whether the threshold of the camera (maximum video signal of 1023) has been exceeded. If it has, scanning will be switched to the Snell area of the viewing field. If not, the gain setting on the camera is checked to determine whether the highest gain setting on the camera has been used for scanning. If not, the gain is increased and the aperture is reset at $X = Y = -600$ and scanning

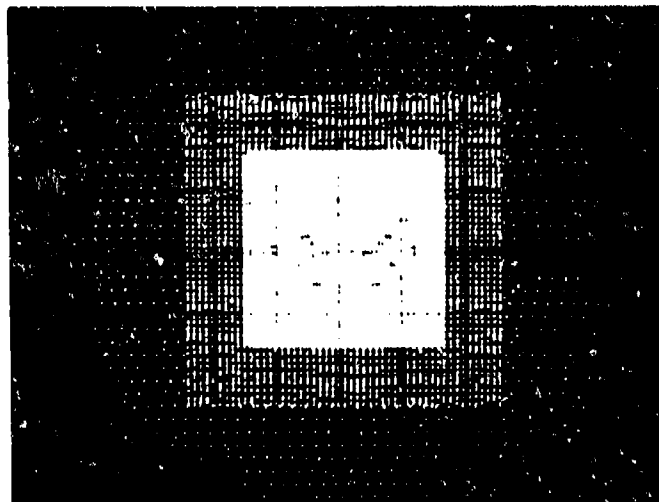


Figure 10. Scan pattern automatic hemispherical program.

of the inner area is made again. The scanning is switched to the Snell zone if the highest gain was used. The Snell and outer area scans are made in the same manner.

When the aperture of the camera has been positioned at a data point, the camera sends back a signal to the analog-to-digital converter. The A/D converter changes the signal to a number from 0 to 1023, with 1023 being the threshold. This number is stored in the computer buffer area along with the X and Y coordinates of the aperture position. When the buffer is full, its contents are written onto magnetic tape as a record.

The program stores the highest signal read in each area, the coordinates of the position, and the camera gain setting. The program also keeps a counter of the number of times the signal exceeds the camera threshold. These data are printed by the teletypewriter along with a completion message when the program has been executed. Flow charts of the Automatic Hemispherical Scan program are shown in figures 11 and 12.

A variation of this program drives the digital-to-analog converters with the X,Y deflection and the return video. An oscilloscope monitor can provide a real-time image of the scene for preview and monitoring. Unfortunately, the oscilloscope available to this project responded poorly to Z-axis modulation. Figure 13 is a photograph of the radiance distribution made from the oscilloscope monitor. The depth was 15.24 meters in the morning of 12 June 1975, during a heavily overcast condition. In the photograph North is up, but West is found toward the right. The shadow beginning in the lower right-hand corner and disappearing toward the zenith is the 8-inch vertical pipe support for the instrument platform.

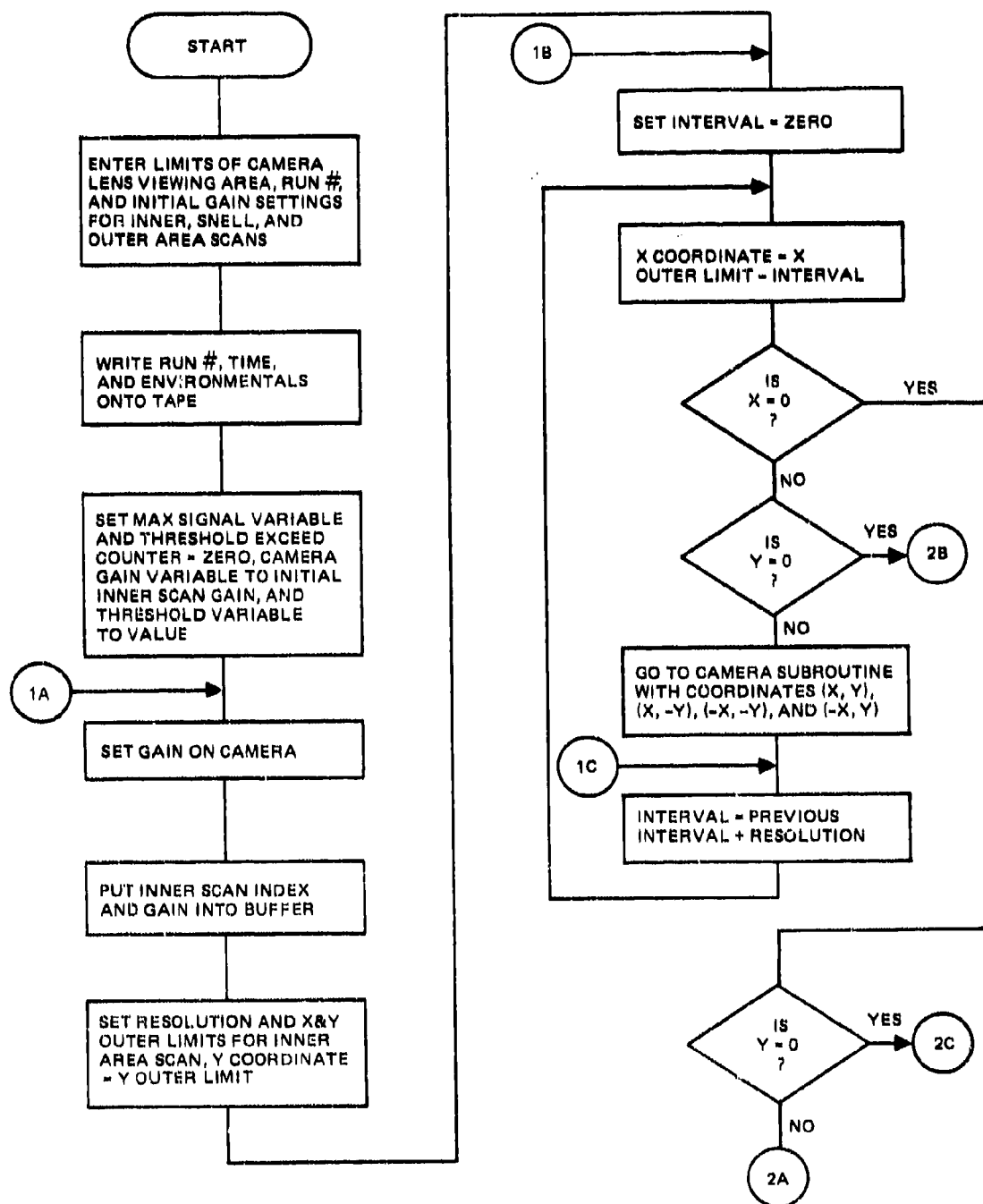


Figure 11. Underwater radiance scanner automatic hemispherical scan routine.

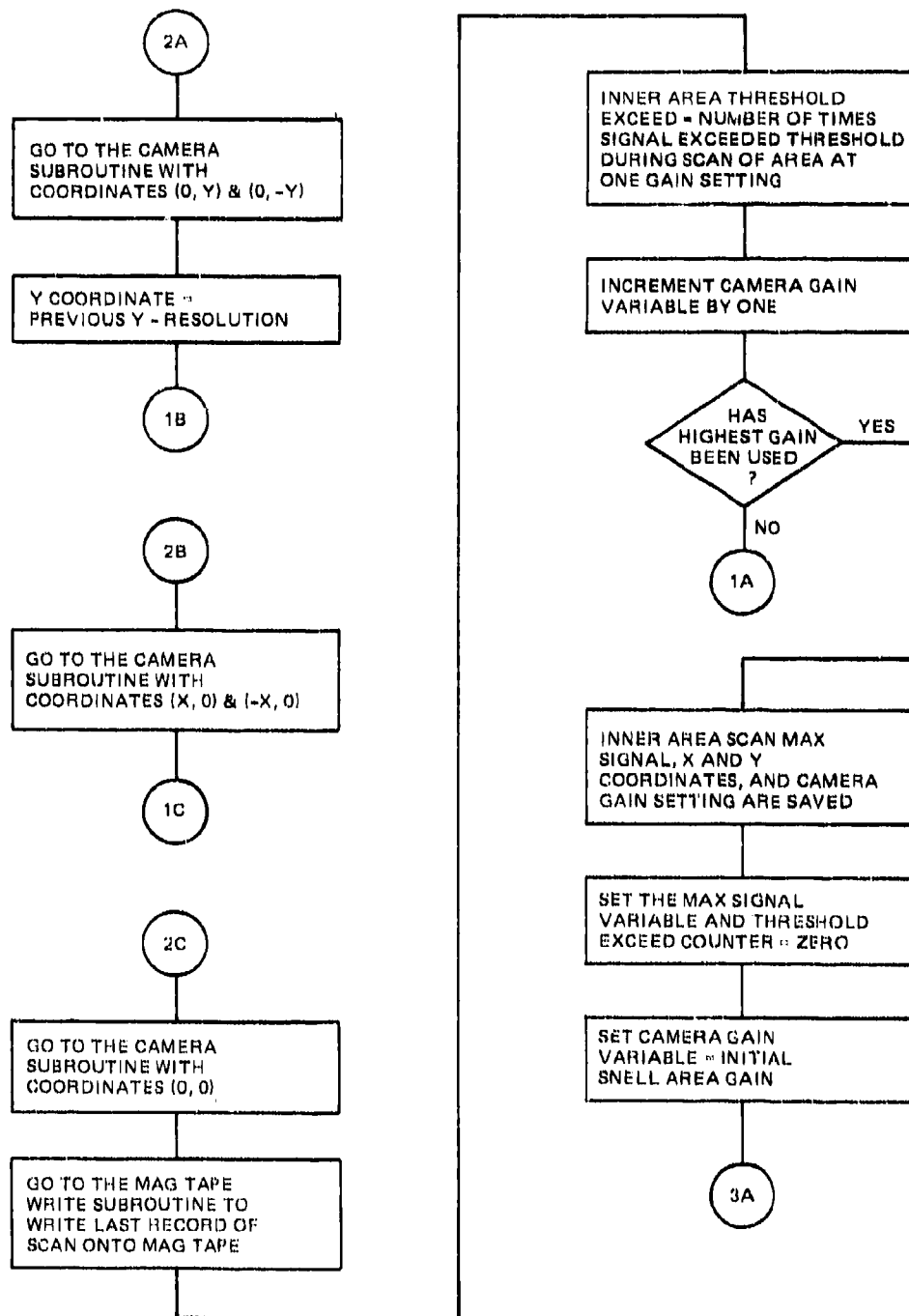


Figure 11. (Continued).

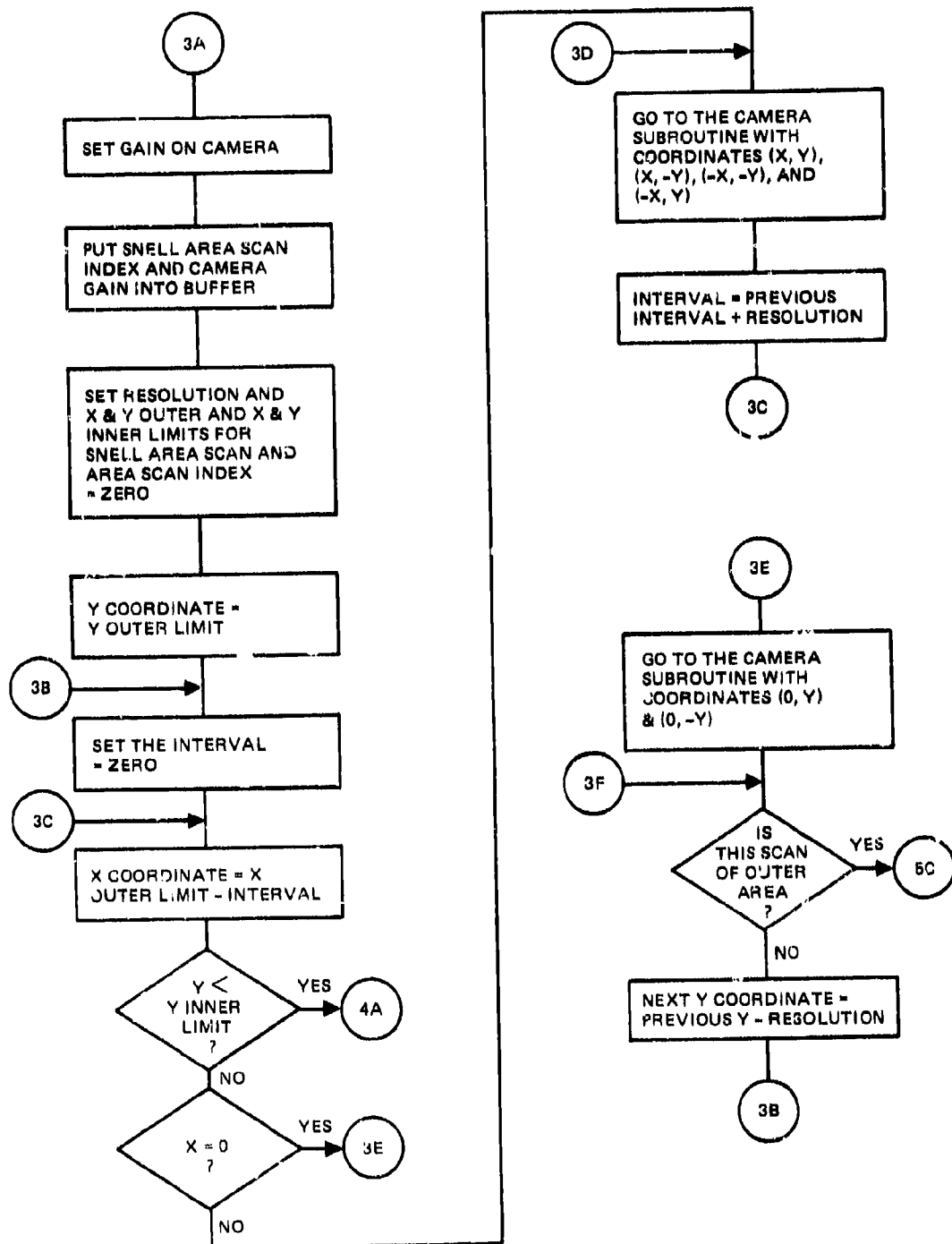


Figure 11. (Continued).

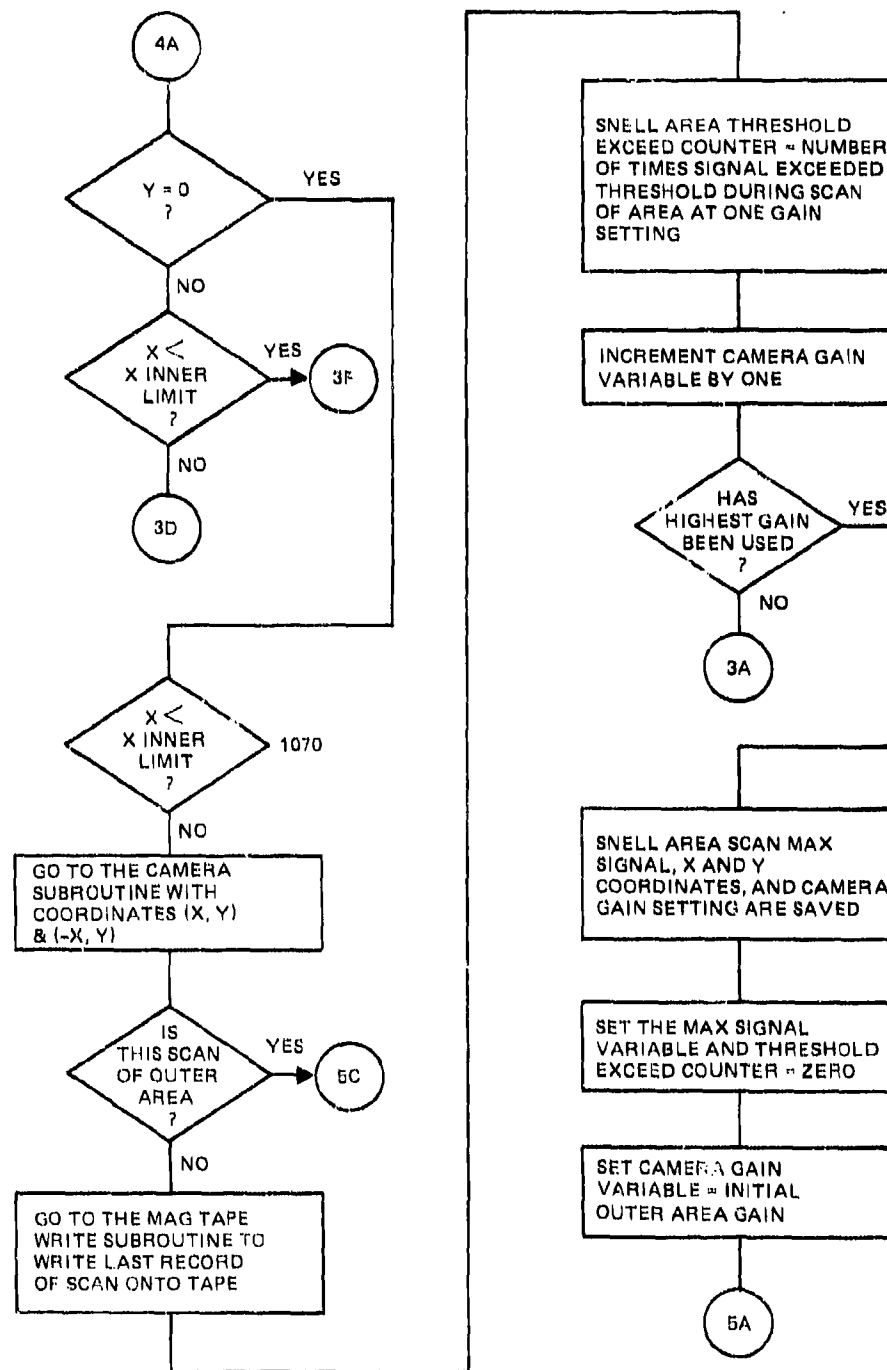


Figure 11. (Continued).

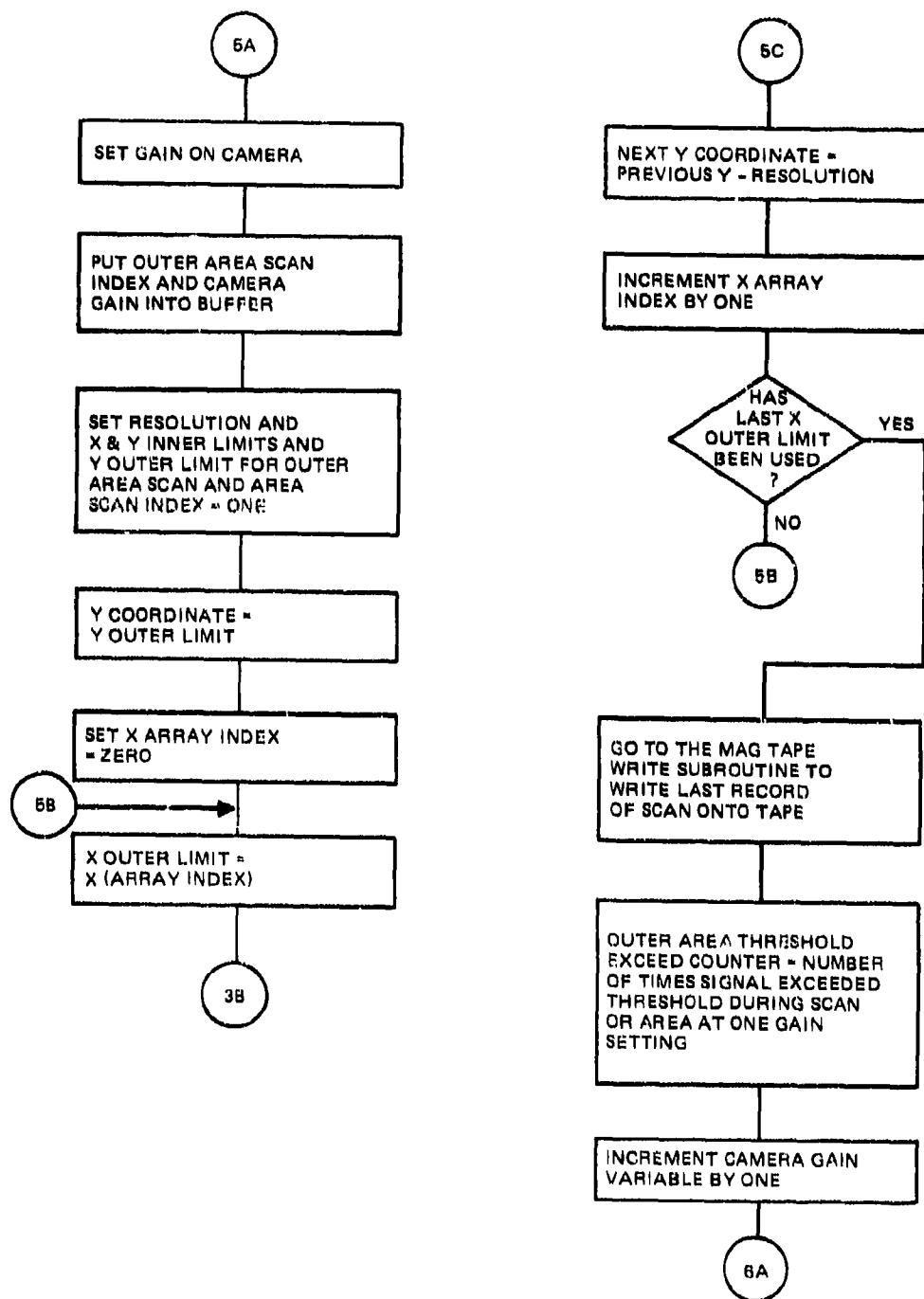


Figure 11. (Continued).

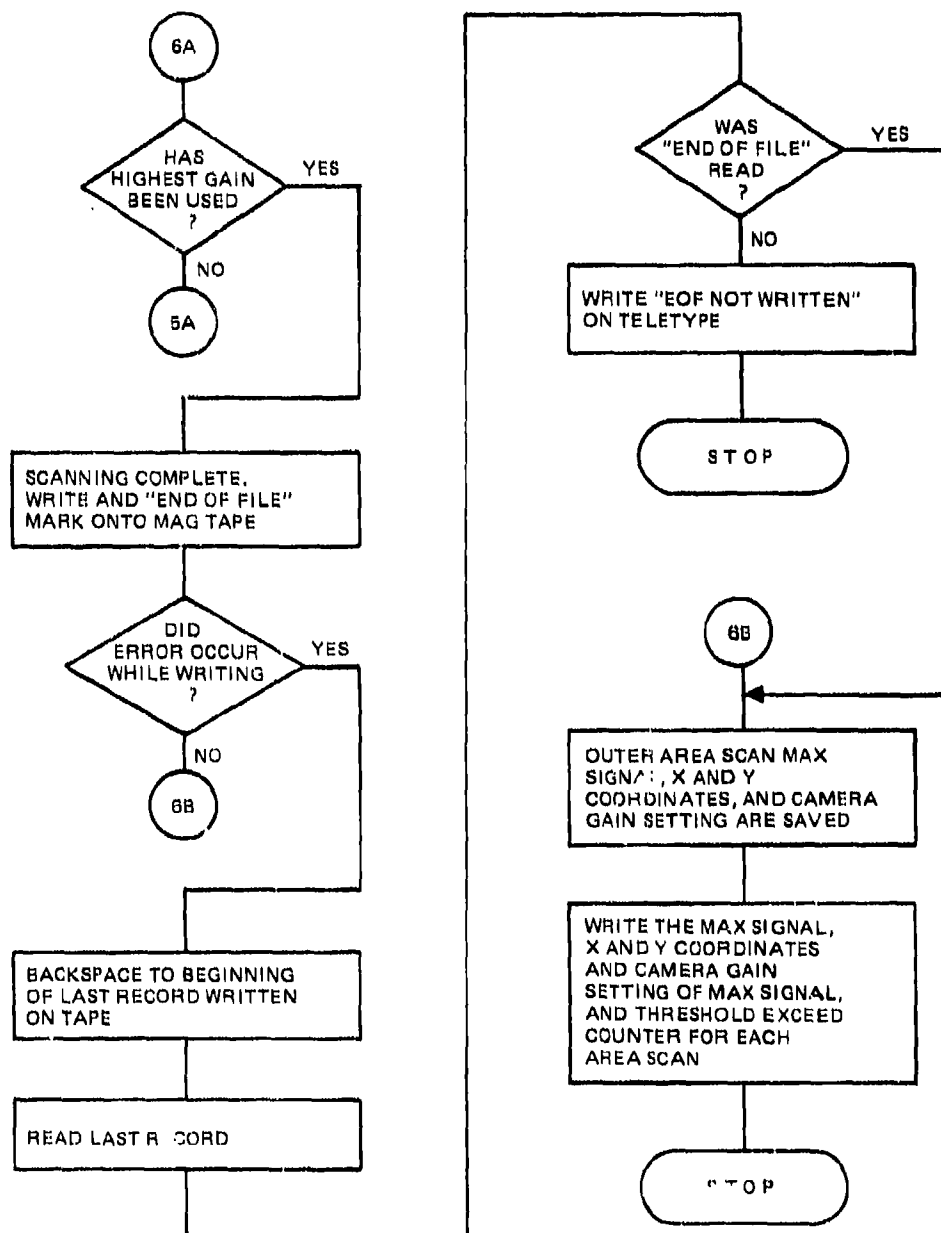


Figure 11. (Continued).

CAMERA POSITIONING SUBROUTINE

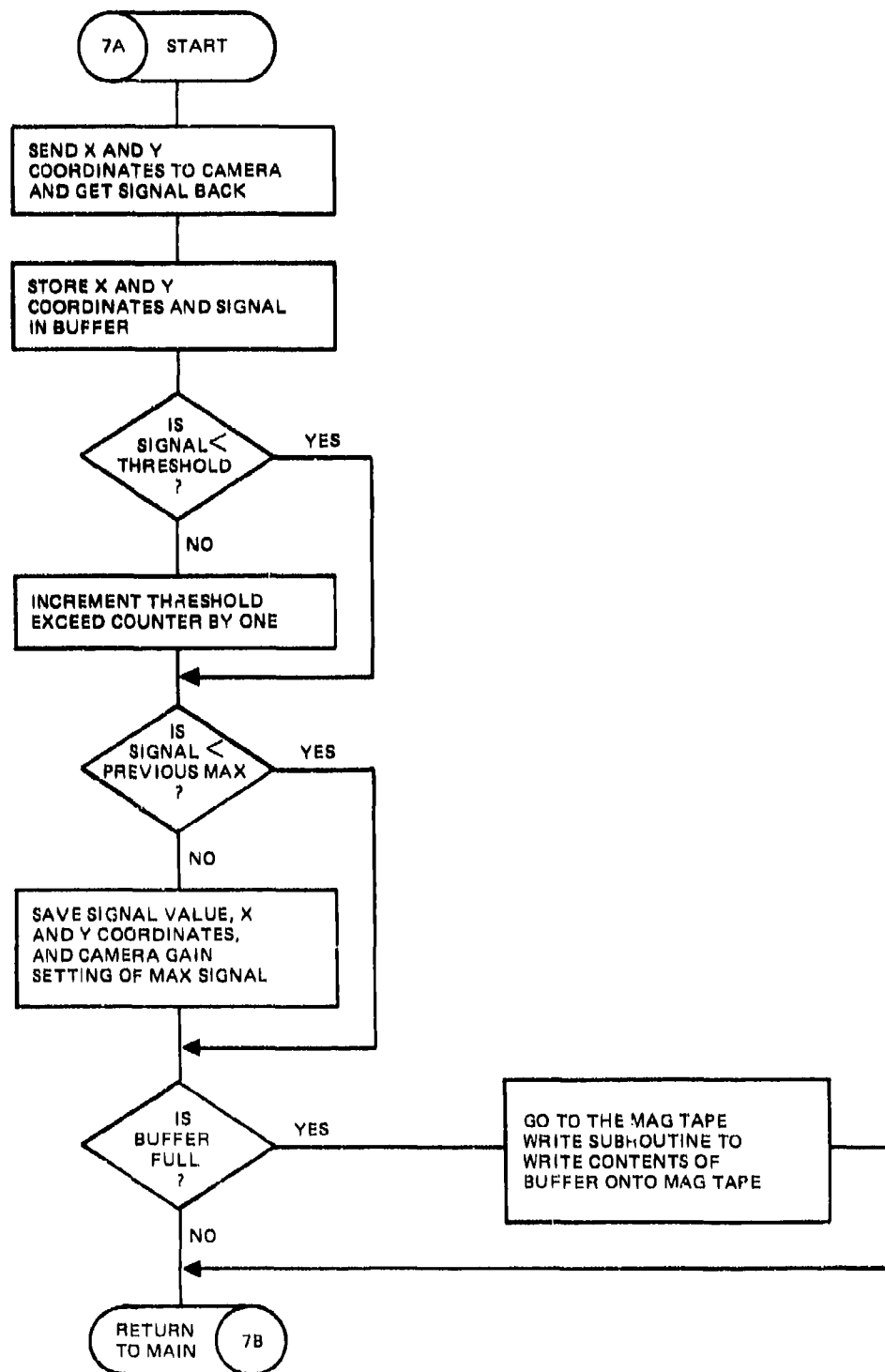


Figure 11. (Continued).

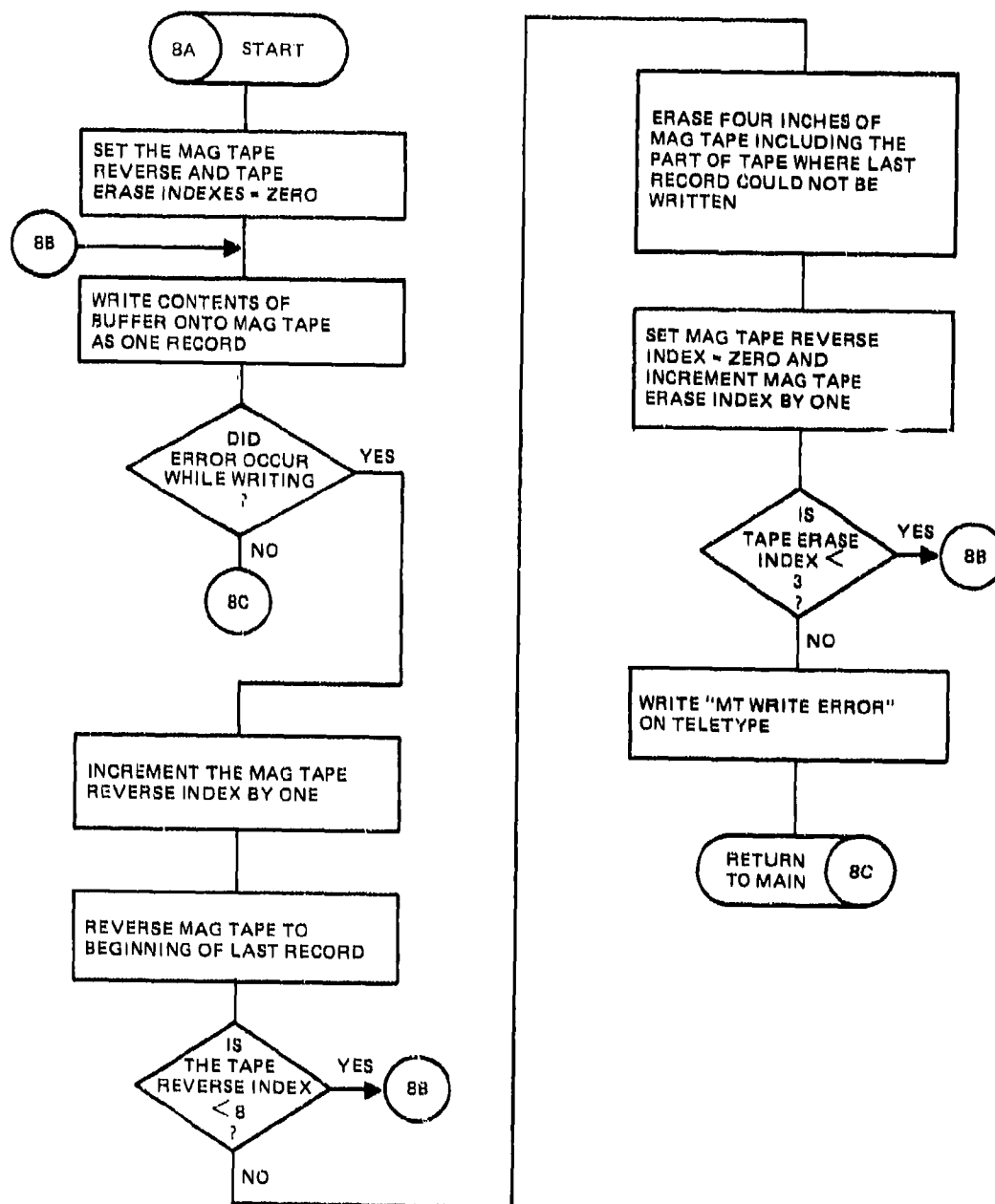


Figure 12. Mag tape write subroutine.

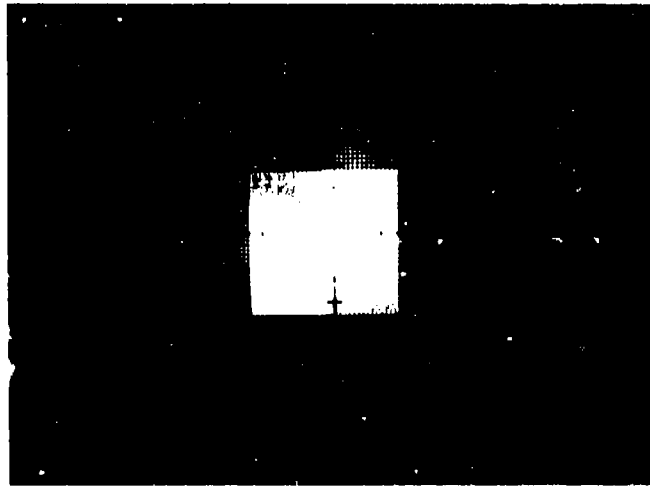


Figure 13. Radiance pattern from 50 feet, overcast sky.

SNAPSHOT PROGRAM

The Snapshot program was developed to acquire a large volume of data in the shortest possible time. The operating program begins by reading the day and time-of-day clocks and the environmental sensors as before. But the program then goes to an assembly language subroutine which operates the camera in a nonautomatic open-loop mode. The operator must manually enter the electron multiplier gain, the signal dwell, and the aperture stop before initiating program RUN.

The program requests a center X,Y coordinate location, a resolution, and the number of scans desired. The assembly language subroutine drives the camera deflection circuits to develop a 60 X 60 square array of 3600 data points. The center coordinates are found in the 30th row and column of this array. Data are stored directly in the magnetic tape buffer. It is the size of this buffer, 4096 words, which limits the array to 60 X 60. The time to scan this array is 860 milliseconds with the signal dwell set in its lowest position. Recording the data on magnetic tape requires less than 1/2 second so that repetitive scans can be made every 1.3 seconds. Dynamic events such as wave action have been studied by making records of more than 200 consecutive frames.

The solid angle or field covered by the Snapshot program depends on the operator-specified resolution, since adjacent data points are separated by this resolution. If a resolution of 20 is specified (deflection units), then the array will be approximately ± 30 degrees (± 600 deflection units) in X and Y around the specified center coordinates. An unused feature of the program allows the X-axis resolution to be different from the Y-axis resolution.

A later development of the Snapshot program gives operator control over the size of the array as well, allowing smaller frames to be taken more rapidly.

CALIBRATION

The purpose of calibrating the radiance scanner is to quantify its performance characteristics and to provide an analytical means of interpreting the response of the scanner in terms of the incident energy.

Calibration of the radiance scanner was performed twice, before and after fielding the instrument to acquire data.

The initial calibration effort was directed toward verifying the instrument functions, performing necessary adjustments, and developing confidence in the hardware. During this effort accessibility to the camera was essential, and it was not installed in the watertight pressure canister. Radiometric measurements of camera sensitivity and resolution were made as well as camera field-of-view deflection sensitivity. These data compared camera performance with predicted values and provided numbers which would be useful in the initial interpretation of the data. The radiometric calibration is reproduced later in this section for use whenever the camera is operated above the water to calibrate the scene.

It was recognized; however, that operation of the camera underwater in the canister would be characterized by somewhat different calibration levels due to the additional lens element formed by the submerged dome. Setting of the wide-angle fisheye lens focus ring from infinite (∞) object distance to 1 foot provided a correctly focused image. The entrance pupil, stops, and projection formula of the lens, however, could not be simply corrected, and an underwater calibration was recognized as essential.

At conclusion of the field tests the radiance scanner was returned to the laboratory for calibration. It was determined that calibration should be accomplished with minimal risk of altering the condition or configuration of the instrument. Therefore, no electronic adjustments were allowed and the underwater canister was not opened or disturbed in any way.

To accomplish the underwater calibration, a fixture was designed and constructed to fit over the dome on the underwater canister. This fixture, itself a hemispherical dome of 40.6-cm (16 in) diameter, was fitted with five flat 5-cm (2 in) diameter windows on a great circle through the center (zenith) of the dome. These windows were cemented into openings drilled at the zenith (0 degree) and at 30, 45, 60, and 85 degrees from the zenith. The entire dome fixture was painted black except for the windows.

The camera was positioned vertically by leveling the cover plate, using a Starrett square bubble levelhead, and shimming the support stand. The dome was then placed over the top of the camera and filled with tap water. During the calibration procedure it was necessary to remove and reposition the dome on the camera a number of times. A Starrett machinist protractor head with bubble level was used to determine the angle of each window from the vertical several times, always measuring in the plane of the great circle. As a result, it was determined that the windows were positioned at zenith angles of 0 degree and 29, 61, and 85 degrees $\pm 1/2$ degree.

A 1000-watt, short-arc, high-pressure xenon lamp was used as a light source. An adjustable, filtered dc power supply operated the lamp and allowed control of its intensity. The lamp was mounted in a lighttight aluminum housing which provided an aperture of 0.635-cm (1/4 in) diameter. The aperture of the lamp was positioned 132 cm from the calibration fixture. A diagram of the calibration apparatus is shown in figure 14. The total length of the optical path from the aperture to the camera entrance pupil (taken to the center of the camera dome) was 149.4 cm. At this range the calibration light source subtended an angle of 0.23 degree, or 4.25 milliradians.

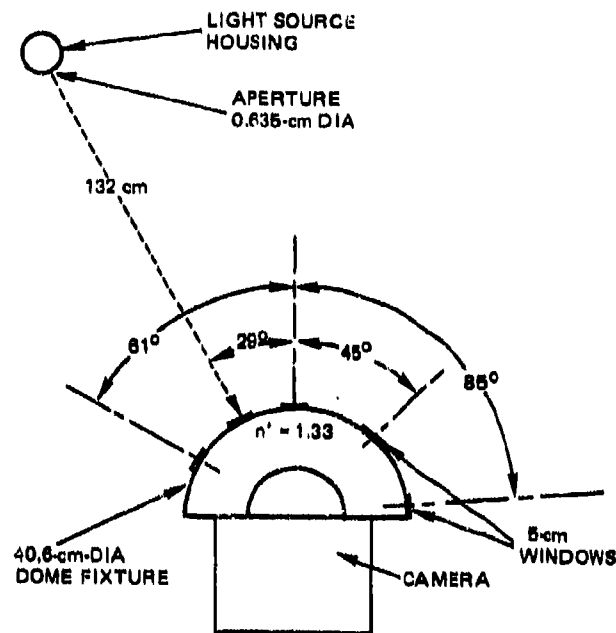


Figure 14. Underwater calibration apparatus.

The experimental configuration shown was arranged to illuminate each of the windows in turn. A small 3-cm mirror was utilized to autocollimate the light source zenith angle position perpendicular to the windows. Irradiance from the light source was monitored by a UDT-21A power meter appropriately filtered to respond to the energy in the passband of the radiance scanner. The power meter head was placed temporarily over the illuminated window at a distance of 130 cm from the source to determine the flux level at that distance. Correcting for window reflection losses and the additional optical path to the camera entrance pupil, the effective flux level is 0.73 that incident on the monitor meter. After the flux level at the window had been measured, the calibrated irradiance meter head was moved to a location adjacent to the window. The window was thus unobscured, and the meter served to monitor the relative light level for unexpected changes in the radiant intensity of the source.

Data were acquired through each window on the radiance scanner sensitivity, the X,Y deflection address, resolution, and effects of gain and dwell settings. After data had been obtained through each window, the dome fixture was removed and rotated 180 degrees to complete the data set for a given great circle, or camera axis when referred to the focal plane. Four such axes were used, nominally the X axis, the Y axis, and the 45° axes ($X = Y$) and ($X = -Y$). The 45-degree axes were chosen to test the deflection system for pincushion distortion. It was not possible to accurately align the data axes with the camera body inside the canister since it was inaccessible. A list of the X Y addresses of peak response is given in table 1, and they are plotted in figure 15 on the X,Y plane of the digital command address.

TABLE 1. DEFLECTION CALIBRATION DATA POINTS.

No.	ϕ	Address		No.	ϕ	Address	
1.	0 degree	63,	-207	20.	45 degrees	-637,	-868
2.	0 degree	71,	-210	21.	45 degrees	-585,	460
3.	0 degree	87,	-201	22.	45 degrees	-10,	730
4.	0 degree	71,	-197	23.	61 degrees	-1169,	-220
5.	0 degree	70,	-205	24.	61 degrees	-68,	1068
6.	0 degree	50,	-132	25.	61 degrees	1341,	-149
7.	0 degree	62,	-216	26.	61 degrees	983,	-1089
8.	29 degrees	82,	494	27.	61 degrees	-824,	666
9.	29 degrees	173,	-829	28.	61 degrees	-830,	-1108
10.	29 degrees	522,	219	29.	61 degrees	994,	706
11.	29 degrees	-554,	-184	30.	61 degrees	260,	-1460
12.	29 degrees	691,	-193	31.	85 degrees	8,	-1910
13.	29 degrees	486,	-650	32.	85 degrees	1757,	-176
14.	29 degrees	-379,	229	33.	85 degrees	-1623,	-188
15.	29 degrees	-376,	-646	34.	85 degrees	-1117,	1006
16.	45 degrees	1010,	-199	35.	85 degrees	1246,	-1405
17.	45 degrees	-881,	-202	36.	85 degrees	1332,	974
18.	45 degrees	721,	-873	37.	85 degrees	-1179,	-1346
19.	45 degrees	768,	453	38.	85 degrees	-133,	1484

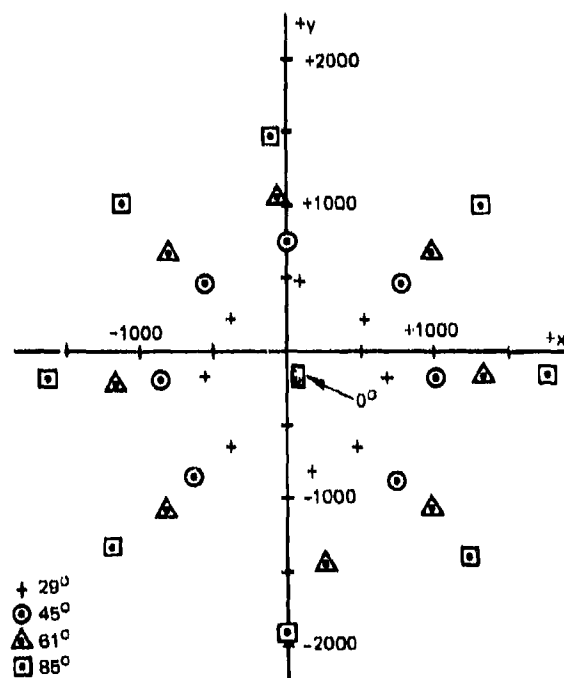


Figure 15. Deflection calibration data points (from table 1).

The zenith (0 degree) data point was measured only three times to establish an approximate center for reference.

There are generally eight data points for each zenith angle. From the basic lens projection formula, these are expected to lie on a circle in the focal plane, the radius of this circle to be proportional to the zenith angle.

The data points for each zenith angle were taken in all combinations of three (56 combinations for eight data points) and the sets of simultaneous equations:

$$\begin{aligned} (X_j - X_0)^2 + (Y_j - Y_0)^2 &= r^2 \quad j, k, l = 1 \text{ to } 8 \\ (X_k - X_0)^2 + (Y_k - Y_0)^2 &= r^2 \\ (X_l - X_0)^2 + (Y_l - Y_0)^2 &= r^2 \end{aligned} \quad (10)$$

solved for the radius r of the circle and the coordinates of the center of the circle X_0, Y_0 . The solutions to the 56 combinations were then averaged to an arithmetic mean. The resulting curves (circles) were found to fit the data rather well. Only data point 8 had to be discarded because of its effect on the results. This technique can only be used where the data points are well behaved. Data points and the circles which fit to the data are shown in figure 16. Radii in digital deflection units for each zenith angle ϕ are:

$\frac{\phi}{0^\circ}$	$\frac{r}{0}$
29°	623
45°	948
61°	1270
85°	1698

These are plotted in figure 17.

Figure 18 shows the calculated X_0, Y_0 pairs as well as the three measured centers, data points 5 through 7. Except for data point 6, the results are clustered closely. The point 72, -204 near the geometric center was chosen as the center, or zenith point, of the radiance scanner.

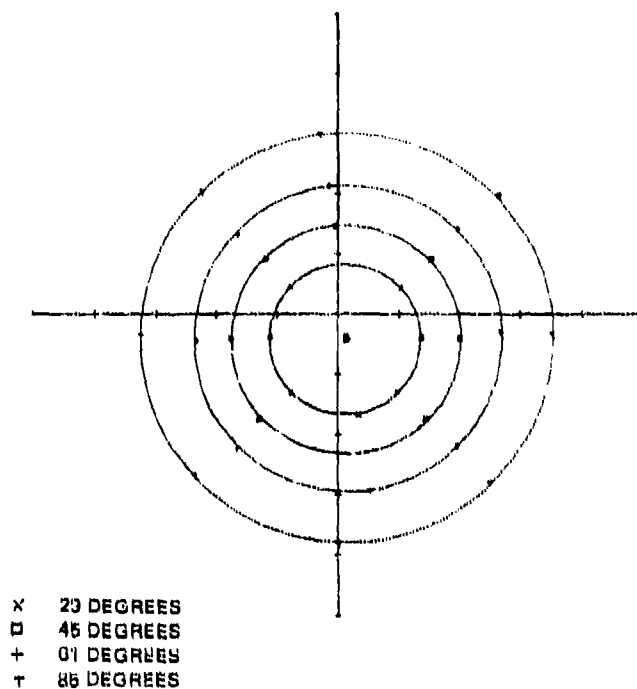


Figure 16. Data points and circular fit.

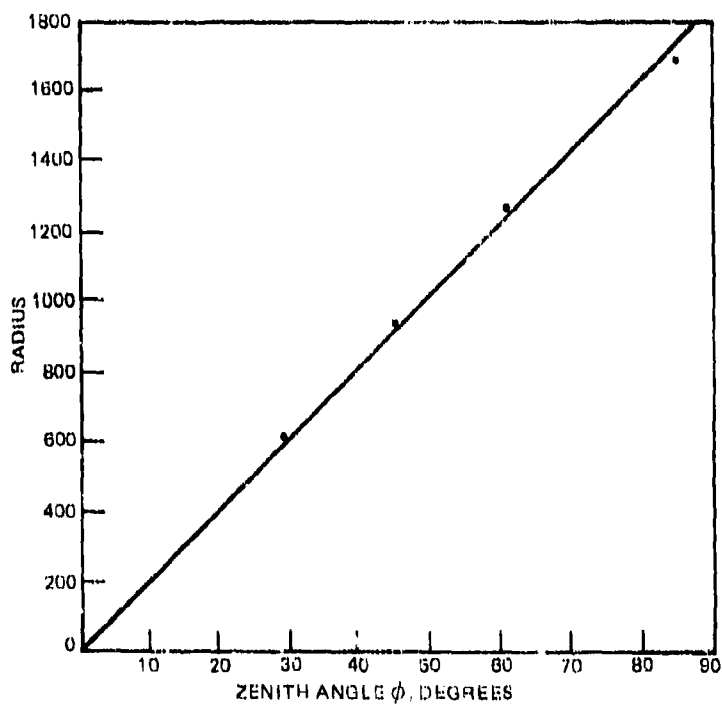


Figure 17. Zenith angle versus deflection radius.

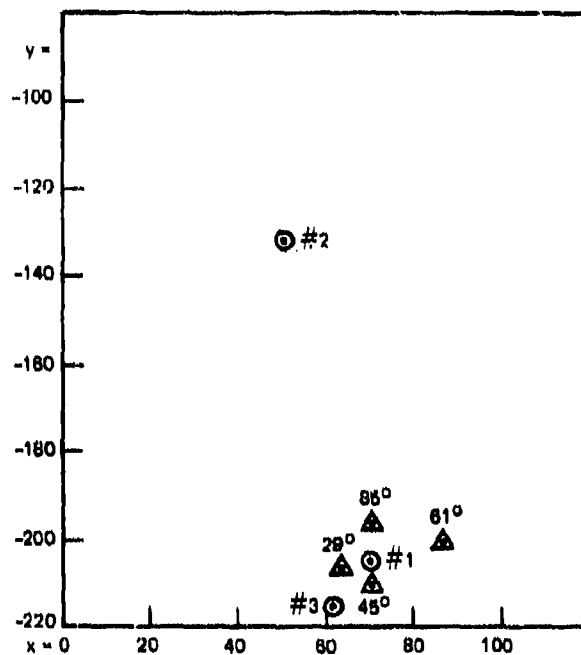


Figure 18. Calculated and measured X_0, Y_0 .

DEFLECTION

By referring to figure 17 it can be seen that the zenith angle projection onto the photocathode departs from the expected linear relationship at some angle greater than 61 degrees. This lens behavior is probably a result of the focusing of the lens for a finite object distance (1 foot), the water-covered dome optics, or both. Four analytical expressions were derived to fit the curve of figure 17. The expressions are:

1. Linear. This relationship is the straight line drawn on figure 17.

$$\frac{[(X - 72)^2 + (Y + 204)^2]^{1/2}}{20.55} = \phi = \frac{r}{20.55} \quad (11)$$

2. Empirical. This relationship attempts to correct for the nonlinearity at large angles.

$$\frac{[(X - 72)^2 + (Y + 204)^2]^{0.53}}{31.61} = \phi = \frac{r^{1.06}}{31.61} \quad (12)$$

3. Polynomial of second degree. Chebyshev polynomials of second and third degree were fitted to the data by a least-squares method. The second-degree relationship is:

$$[(X - 72)^2 + (Y + 204)^2]^{1/2} = -0.01414\phi^2 + 21.747\phi - 1.981 = r. \quad (13)$$

4. Polynomial of third degree. This relationship has not been tested:

$$\left[(X - 72)^2 + (Y + 204)^2 \right]^{1/2} = 0.0001\phi^3 - 0.0263\phi^2 + 22.087\phi - 2.277 = r, \quad (14)$$

Three of these expressions were tested by using the data in table 1 with the exception of data points 6 and 8. Table 2 shows the zenith angles predicted by expressions 1, 2, and 3 from the data of table 1.

The linear relationship is easier to handle analytically and can be made to fit the data rather well (± 1 degree, or $\pm 2.9\%$) for zenith angles of less than 60 degrees. A better fit is provided by the empirical relationship, equation 12, which is $\pm 1.5\%$ over the entire range, and use of this expression is recommended.

Since the radiance scanner was occasionally operated above water to record the angular location of the sun for rotational or azimuthal alignment, the deflection characteristics in air were also measured. Deflection as a function of the radius of the command is shown in figure 19. The center coordinates were unchanged from the underwater case.

TABLE 2. DEFLECTION ANGLE RELATIONSHIPS PREDICTION.

Data Set	Linear (11)	Error	Std Devn	Empirical (12)	Error	Std Devn	Polynomial Degree 2 (13)	Error	Std Devn
0°	0.45	0.45	0.26	0.34	0.34	0.20	0.52	0.52	0.25
29°	30.29	1.29	0.40	28.93	0.07	0.40	29.27	0.27	0.39
45°	46.04	1.04	0.71	45.15	0.15	0.74	44.91	0.09	0.71
61°	61.75	0.75	0.84	61.64	0.64	0.89	60.89	0.11	0.87
85°	82.63	2.37	0.68	83.92	1.08	0.73	82.60	2.40	0.72

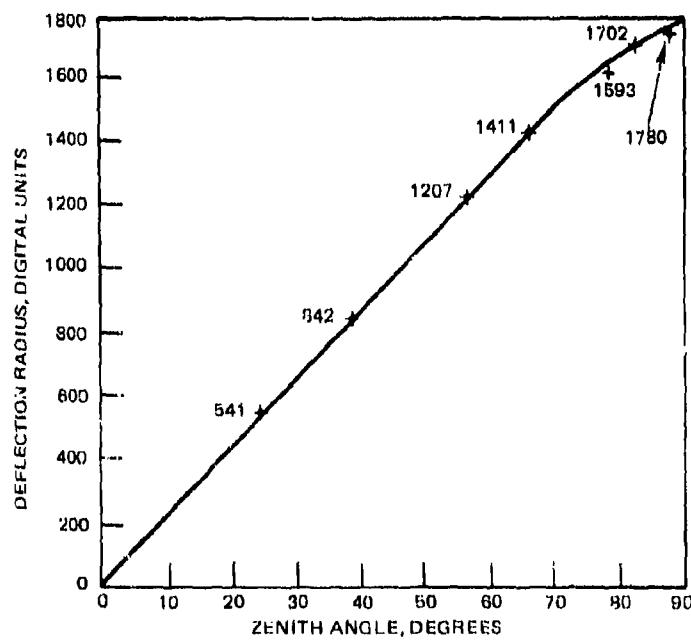


Figure 19. Deflection in air.

DEFLECTION SENSITIVITY

The deflection sensitivity of the radiance scanner is a significant parameter in determining the angular resolution of the instrument. For polar deflections or deflections in planes containing the zenith vector, the relationships derived for polar angle can be differentiated to give:

1. Linear:

$$\frac{d\phi}{dr} = 0.04866 \text{ degree/digit of deflection.} \quad (11')$$

2. Empirical:

$$\frac{d\phi}{dr} = \frac{1.06}{31.61} r^{0.06} \text{ degree/digit of deflection.} \quad (12')$$

3. Polynomial of second degree:

$$\frac{d\phi}{dr} = \frac{0.045983}{1-0.0013\phi} \text{ degree/digit of deflection.} \quad (13')$$

Since the data show that the linear approximation has limited validity while the camera is submerged, it may be necessary to use a nonlinear deflection characteristic, particularly at large zenith angles, for accuracy. The empirical relationship equation 12 offers some convenience and is recommended. Table 3 lists the deflection sensitivities at the zenith angles used in calibration.

TABLE 3. POLAR DEFLECTION SENSITIVITY.

Zenith Angle	Linear		Empirical		2nd Degree Polynomial	
	$\frac{d\phi}{dr}$	$\frac{dr}{d\phi}$	$\frac{d\phi}{dr}$	$\frac{dr}{d\phi}$	$\frac{d\phi}{dr}$	$\frac{dr}{d\phi}$
0°	0.04866	20.55	0.031636*	31.61*	0.045983	21.75
29°	constant		0.04933	20.27	0.047784	20.927
45°	constant		0.05059	19.767	0.048840	20.475
61°	constant		0.05149	19.421	0.049944	20.023
85°	constant		0.05239	19.088	0.051695	19.344

* The derivative of the empirical expression is changing rapidly at 0 degree. The value from the linear relationship is recommended at 0 degree.

If the deflection properties of the camera had been linear, then the deflection sensitivity in the azimuthal direction at various points in the field would also be a constant and equal to the polar deflection sensitivity $d\phi/dr$. However, the azimuthal deflection sensitivity is a function of the zenith angle, or r . The values in table 4 are found by using the empirical relationship.

TABLE 4. AZIMUTHAL DEFLECTION SENSITIVITY
(EMPIRICAL).

	$\frac{d\Theta}{dr}$	$\frac{dr}{d\Theta}$
0°	—	—
29°	0.04655	21.482
45°	0.04747	21.066
61°	0.04803	20.820
85°	0.05006	19.976

VIDEO SIGNAL LEVELS

A subroutine of the computer program commanded the camera to repetitively sample a selected data point and display the digitized value on the teletypewriter terminal. This subroutine was exercised at or near the peak video response obtained for each data point. During the repetitive sampling provided by this procedure the camera gain controls, the signal dwell time, and the camera aperture were stepped over their usable ranges. The resultant changes in video output were printed on the teletypewriter, allowing repeated comparisons between gain setting, dwell setting, and aperture position.

The signal levels at two gain settings were compared to determine the relative gain provided at each of the preset gains (multiplier high voltages). Examination of the data in this manner provided inconsistent results, with the gain ratios apparently signal level dependent.

One possible explanation of this behavior could be an incorrectly set zero level on the sample-and-hold circuit in the video processor with the result that small signals were recorded as zero-level signals.

A 1-volt power supply was arranged to supply small-current signals directly to the image dissector tube anode. A series resistance box of 1% accuracy was used to set the signal levels. Resistance values between 50 kilohms and 3.5 megohms were employed. Figure 20 shows the basically linear response of the video circuit and processor. Figure 21 details the response at the small-signal end of the range. The results were found to be independent of the high voltage, or tube gain setting. It is apparent that a zero offset of approximately 14 digital units is present. When 14 units were added to each data point, the gain setting data were much better behaved.

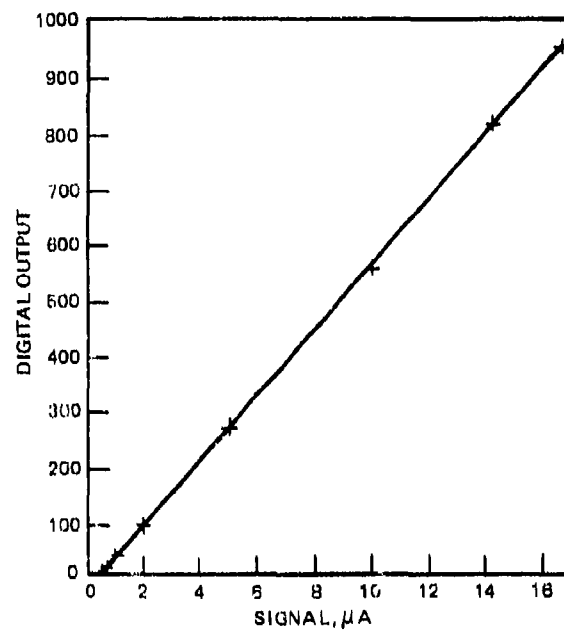


Figure 20. Response of video circuit.

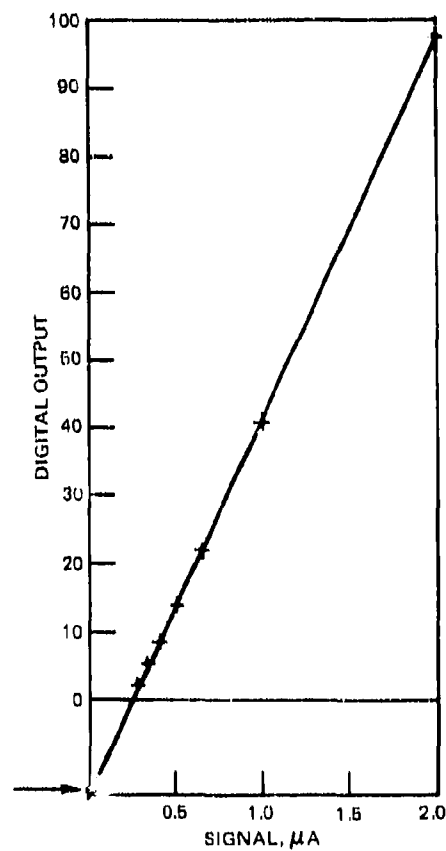


Figure 21. Video response showing offset.

GAIN SETTINGS

From the corrected data, the ratios of the signal levels at any two gain settings can be determined. Using the binary representation of the gains (00, 01, 10, 11), the signal ratios are shown in table 5.

If we define a gain factor G to be used with a camera calibration normalized for gain 10 (2), the values in table 6 can be derived from table 5.

TABLE 5. SIGNAL RATIOS BETWEEN GAIN SETTINGS.

Gains	Ratio	Std Devn	Samples
$\frac{00}{01}$	0.163	0.006 (3.5%)	18
$\frac{01}{10}$	0.228	0.007 (2.0%)	30
$\frac{10}{11}$	0.326	0.02 (6.2%)	8

TABLE 6. CAMERA GAIN FACTORS.

Gain	Factor G
00	0.037
01	0.228
10	1.000
11	3.067

DWELL SIGNAL GAIN

During the repetitive sampling subroutine, the 10-turn potentiometer which controls the signal integration period was calibrated by taking readings at various settings. The signal gain provided by increasing the signal integration time was measured by recording the signal levels at each setting.

Due to the dynamic range provided by the signal integration period, or dwell, the data had to be developed in three segments and joined at 0.5 turn and 5 turns of the potentiometer. The dwell gain factor G_d is defined relative to a gain of 1 at 0 potentiometer turn. Dwell gain factors G_d are shown in table 7 and graphed in figure 22.

The dwell potentiometer was expected to provide a linear control over the signal integration time and hence the signal level, or gain. If control were linear, the equation describing G_d would be

$$G_d = 1 + 12.2D, \quad (15)$$

TABLE 7. DWELL GAIN FACTOR G_d .

Potentiometer Turns	Measured Gain G_d	Std Devn	(%)	Samples	$G_d = 1 + 11.23D^{1.036}$
0	1			0	1
0.1	2.04			1	2.034
0.25	3.66	0.10	3%	17	3.67
0.50	6.47	0.17	3%	19	6.477
0.75	9.12	0.39	4%	5	9.33
1.0	12.23	0.65	5%	31	12.23
2.0	23.81	0.78	3%	23	24.03
3.0	35.59	1.23	3%	20	36.05
4.0	47.68	1.75	4%	19	48.22
5.0	59.27	1.75	3%	11	60.50
6.0	72.31	2.37	3%	9	72.87
7.0	84.76	2.37	3%	3	85.31
8.0	97.20	2.40	2%	2	97.82
9.0	110.83			1	110.39
10.0	123.3			2	123.01

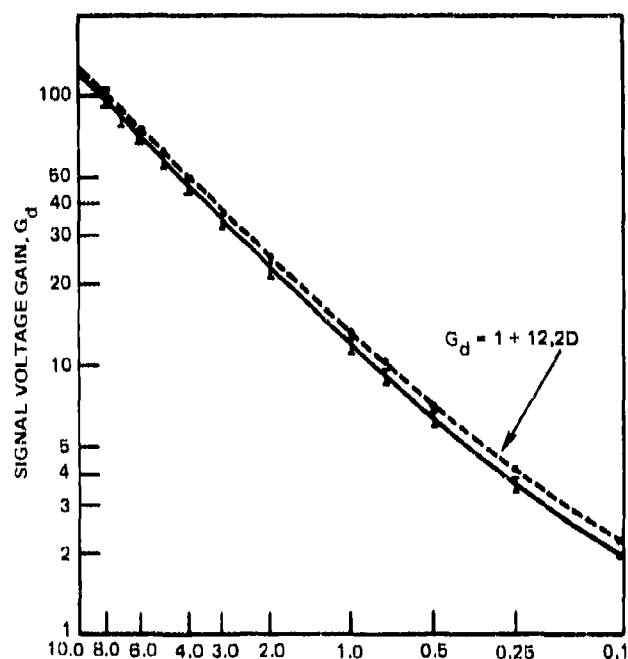


Figure 22. Dwell gain vs potentiometer turns.

where D is the number of turns of the dwell potentiometer. This relationship, shown in figure 22, is not seen to accurately represent the measured data. The empirical relationship

$$G_d = 1 + 11.23D^{1.036} \quad (16)$$

was derived, and values shown in table 7 indicate good agreement with the measured data. This equation is recommended as a convenient analytical tool during data reduction.

APERTURE SETTING

During calibration, attempts were made to compare signal levels obtained with the aperture stop at f2.8 with results at f22. In general, these efforts were not successful; the values found ranged from 47.5 to 8836. In the preexperimental calibration period, the attenuation provided by going from f2.8 to f22 compared favorably with the expected factor of 64.

Apparently, the optical dome underwater has sufficiently perturbed the optical path that the diaphragm is no longer located in the entrance pupil. The result is that aperture function is no longer predictable and will vary over the focal plane.

Fortunately, no quantitative data were acquired with the aperture in the f22 position. The only use of the stopped-down camera in the field was in making sun shots with the camera above the water.

SPECTRAL BANDWIDTH

An interference filter is placed behind the fisheye lens assembly to limit the spectral bandwidth of the radiance scanner.

Spectral characteristics of this filter are shown in figure 5. Additionally, the filter sideband blocking is 10^{-4} or better from the ultraviolet to beyond $1 \mu\text{m}$ in the near infrared.

The back focal length of the lens is greater than 40 millimeters while the maximum radial point in the focal plane is 11 millimeters from the optic axis. Therefore, the maximum angle of incidence at the filter is of the order of 15 degrees. The wavelength characteristic of the filter when used at 15 degrees will shift approximately 65 \AA toward shorter wavelengths, but the passband shape will be unchanged. This shift is less than the effective filter bandwidth and will be inconsequential in viewing natural sunlight fields.

The filter bandwidth at half the peak transmission is measured at $93 \text{ \AA} \pm 3 \text{ \AA}$.

$$\Delta\lambda = 93 \text{ \AA} . \quad (17)$$

RADIOMETRIC SENSITIVITY

To measure the radiance scanner optical response, the known flux density and experimental arrangement shown in figure 14 were used. The camera design resolution was approximately 1 degree (17 milliradians), and since the light source subtense was 0.23 degree (4.5 milliradians), it effectively measured the peak response of the camera field. To mechanize this technique, a modification of the Snapshot program was used to drive the

radiance scanner. This program sampled camera response over a 60×60 X,Y array for a total of 3600 data points. Spacing between elements of the array was reduced to 1 digital address for maximum resolution. The data were recorded on magnetic tape for later reduction. A playback option in the program allowed for the display of the array, characterized by a single digit (0-9) for each element, on the teletypewriter.

Figure 23 is an isometric contour plot of the 60×60 array for data point 32. This solid has as its base area the X,Y plane represented in digital deflection units and as its height the video response at each corresponding address. The volume $V(X,Y)$ of this solid represents the total camera response to the irradiance from the test light source. The shape, or distribution, of the volume describes the spatial resolution of the radiance scanner.

Limited though these data may be, they required considerable time and effort to acquire. The 14 digits of signal offset were discovered after the basic radiometric response data were obtained. Even if these measurements could be repeated, the camera alignment has been disturbed by disassembly sufficiently to invalidate the results.

Subsequently it was determined that the data could be utilized by adding 14 to each nonzero signal level. This introduces a small error since signal levels below 14 were reported by the camera as zero signals and these data points cannot be corrected as they cannot be discerned from genuine zero-level signals.

The solid volume $V(X,Y)$ of the camera response was computed for each data point and the value of the peak signal response $S(X,Y)$ recorded after adding 14 units to each nonzero value. Additionally, the diameter of a right circular cylinder whose height is equal to the peak signal and whose volume is identically the camera response was calculated. This diameter is related to the effective camera resolution. These values are presented in table 8. The data in the "corrected" columns are normalized to a flux input of 2.92×10^{-7} W/cm², a gain setting of 10 (2), and a signal dwell setting of 0 turn.

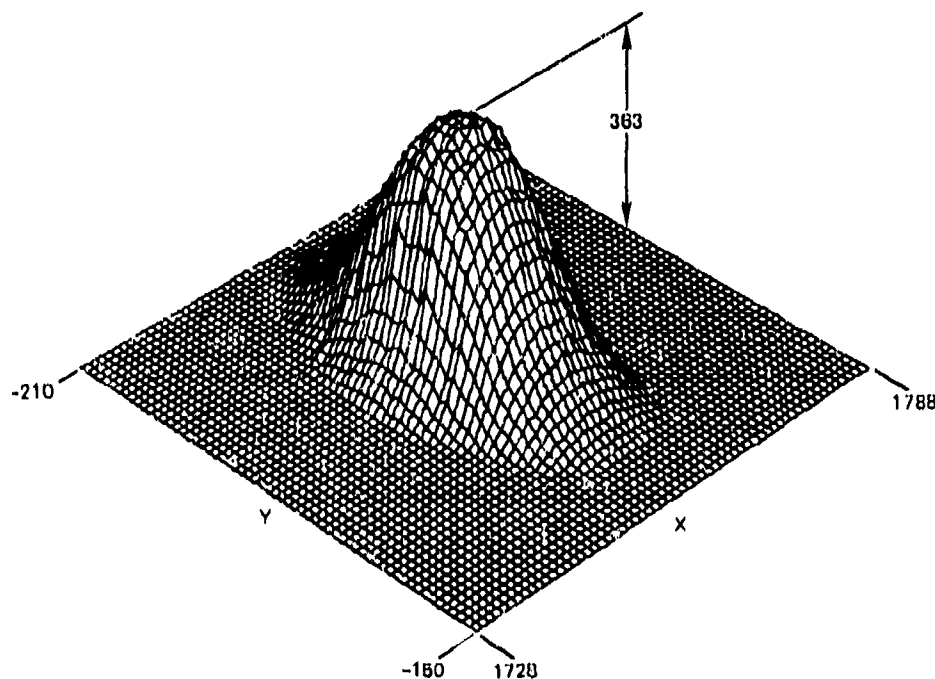


Figure 23. Data point 32 isometric projection.

TABLE 8. RADIOMETRIC RESPONSE.

Data	Tape	File	ϕ	Coordinates	Equiv Dia d	Corrected		p(X,Y)	Normalize to p(X,Y) = 600		$\Delta\Omega \times 10^{-4}$	$\Delta N_{\lambda} \times 10^8$
						Peak S	Volume V		Peak S	Volume V		
6	1	2	0	50	20.67	635	2.14×10^5	614	621	2.09×10^5	2.420	2.089
7	3	6	0	62	18.85	470	1.31×10^5	658	429	1.19×10^5	2.013	3.636
8	1	7	29	82	23.81	489	2.18×10^5	561	523	2.33×10^5	3.115	1.927
9	6	6	29	173	19.52	582	1.72×10^5	679	514	1.52×10^5	2.093	2.919
10	6	0	29	522	19.02	640	1.82×10^5	586	655	1.86×10^5	1.987	2.412
11	2	5	29	554	18.73	497	1.37×10^5	642	464	1.28×10^5	1.927	3.512
12	3	5	29	691	20.66	624	2.09×10^5	676	554	1.86×10^5	2.345	2.417
13	4	6	29	486	18.91	650	1.83×10^5	666	586	1.65×10^5	1.965	2.727
14	4	13	29	-379	19.33	538	1.58×10^5	507	637	1.87×10^5	2.053	2.401
15	5	2	29	-376	18.88	544	1.52×10^5	586	557	1.56×10^5	1.958	2.879
16	3	2	45	1010	19.20	626	1.81×10^5	690	544	1.57×10^5	2.118	2.725
17	3	7	45	-881	18.92	482	1.35×10^5	458	631	1.77×10^5	2.057	2.419
18	4	11	45	721	19.13	618	1.78×10^5	688	539	1.55×10^5	2.103	2.770
19	5	4	45	768	19.01	606	1.72×10^5	593	613	1.74×10^5	2.076	2.467
20	6	1	45	-637	18.81	462	1.28×10^5	548	506	1.40×10^5	2.033	3.052
21	4	5	45	-585	18.91	432	1.21×10^5	482	538	1.51×10^5	2.055	2.840
22	6	7	45	-10	18.88	574	1.61×10^5	483	713	2.00×10^5	2.048	2.150
23	2	12	61	-1169	18.89	376	1.05×10^5	431	523	1.46×10^5	2.111	2.844
25	3	4	61	1341	22.85	94	3.86×10^4	696	81	3.33×10^4	3.089	12.55
26	4	7	61	983	19.84	405	1.25×10^5	752	323	9.97×10^4	2.329	4.174
27	4	14	61	-824	19.29	394	1.15×10^5	424	558	1.63×10^5	2.202	2.555
28	5	0	61	-830	19.46	488	1.45×10^5	540	542	1.61×10^5	2.241	2.585
29	5	8	61	994	23.19	81	3.4×10^4	630	77	3.27×10^4	3.182	12.81
30	6	5	61	260	19.86	540	1.67×10^5	705	460	1.42×10^5	2.334	2.924
31	0	27	85	8	20.70	328	1.10×10^5	700	281	9.43×10^4	2.689	4.155
32	3	3	85	1757	21.40	374	1.34×10^5	732	307	1.10×10^5	2.874	3.559
33	4	0	85	-1623	19.35	235	6.91×10^4	406	347	1.02×10^5	2.349	3.852
34	4	3	85	-1117	20.95	309	1.06×10^5	394	471	1.61×10^5	2.754	2.421
35	4	9	85	1246	20.99	362	1.25×10^5	780	278	9.62×10^4	2.764	4.086
36	5	5	85	1332	20.48	413	1.36×10^5	613	404	1.33×10^5	2.632	2.953
37	6	3	85	-1179	19.63	252	7.63×10^4	492	307	9.30×10^4	2.418	4.230
38	6	8	85	-133	19.97	326	1.02×10^5	421	465	1.45×10^5	2.502	2.699

Radiance scanner sensitivity is expected to be a function of zenith angle ϕ from equation 7. The solid volume and peak response numbers for each zenith angle data set were examined. Data points 25 and 29 are obviously deficient and were not used. The standard deviations for each data set of peak signals and volumes are disappointingly large at 11% to 23%.

The equivalent diameter d of each data set was also examined. The results are shown in table 9.

The diameter d data show much less variance in general, and deviations in the peak signal S and the volume V data are correlated since

$$d^2 = \frac{4V}{\pi S} \quad (18)$$

In an attempt to explain the variance in the camera response data, the canister was opened and the lens removed from the radiance scanner to measure the uniformity of the photocathode surface. A speck of dirt on the face of the photocathode of the image dissector tube was immediately obvious. Closer inspection disclosed a number of smaller white particles. The presence of this contamination in the image plane could explain the poor response logged for data points 25 and 29. Xylene and dry air were used to carefully clean the face of the tube.

A carefully baffled light source was used to illuminate the face of the tube through a 522-nm filter of 10-nm bandwidth. The flux density was monitored by a 0.38-mm-diameter optical fiber probe connected to a UDT-21A power meter. Flux density over the surface was uniform to $\pm 5\%$.

The camera was commanded to sample the photocathode response with 10 digital units between samples from $-1800 \leq X, Y \leq 1790$. The resulting 360×360 array map of the photocathode is compatible with the "look up" table capabilities of available computational equipment.

Examination of this photocathode uniformity data shows approximately a 3 to 1 change in responsivity over the useful area, the lower response zone lying generally in the $-X, +Y$ extremity of the field and the higher in the $+X, -Y$ corner. This sensitivity surface appears reasonably uniform with the variations, better described as a "wedge" or smooth slope across the face of the tube.

TABLE 9. RESPONSE DIAMETER AND CORRESPONDING FIELD OF VIEW (AVERAGED DATA).

Data Set	Digital Diameter d	Std Devn	(%)	Field of View	
				Measured (steradian)	Theoretical $\Delta\Omega$
0 degree	19.76			2.21×10^{-4}	1.98×10^{-4}
29 degrees	19.86	1.71	8.6	2.16×10^{-4}	1.89×10^{-4}
45 degrees	18.98	0.14	0.7	2.07×10^{-4}	1.78×10^{-4}
61 degrees	19.47	0.4	2.1	2.24×10^{-4}	1.64×10^{-4}
85 degrees	20.43	0.72	3.5	2.62×10^{-4}	1.26×10^{-4}

The uniformity array contains relative values of the photocathode response p expressed as 129 600 three-digit entries. The value of $p(X,Y)$ for the nearest array element can be taken from the array and used in normalizing the camera response. It appears feasible to develop an analytic expression for a surface which closely approximates the $p(X,Y)$ array values. In either approach, the error is expected to be less than $\pm 5\%$.

Values of $p(X,Y)$ are shown in table 8 for each calibration data point. The signal S and volume V values normalized to $p(X,Y) = 600$ by

$$\bar{S}(X,Y) = \frac{S p(X,Y)}{600 G G_d} \quad (19)$$

are shown in table 8.

These normalized values did not display significant improvements in the standard deviations of the results as shown in table 10.

It is recommended, however, that a photocathode uniformity factor be incorporated in the data reduction formulae in view of the known variations which may affect the data more dramatically than the limited sample of calibration points.

TABLE 10. PEAK SIGNAL AND VOLUME
(AVERAGED DATA).

	Not Normalized		Normalized to $p=600$	
	S	V	\bar{S}	\bar{V}
29°	571	1.76×10^5	561	1.74×10^5
std	63.2	0.277	63.7	0.315
dev	11%	15.7%	11%	18%
45°	543	1.54×10^5	583	1.65×10^5
std	81.7	.252	72.5	0.2
dev	15%	16%	12%	12%
61°	441	1.31×10^5	481	1.42×10^5
std	70.2	0.248	96	0.255
dev	16%	19%	20%	18%
85°	325	1.07×10^5	358	1.17×10^5
std	60	0.248	79.3	0.26
dev	18.5%	23%	22%	22%

FIELD OF VIEW

The instantaneous field of view of the radiance scanner was calculated by using the deflection sensitivity values developed for the empirical deflection equation and the equivalent diameters (in digital deflection units) of camera response. For present experimental purposes, the shape of the instantaneous field is not of primary importance, only the solid angle $\Delta\Omega$.

Therefore, the polar and azimuthal deflection sensitivities $d\phi/dr$ and $d\theta/dr$, tables 3 and 4, were used to calculate the incremental, or instantaneous, field: shown in table 9.

$$\Delta\Omega = \frac{\pi^3 d^2}{1.296 \times 10^5} \frac{d\phi}{dr} \frac{d\theta}{dr} \quad (20)$$

It may be noted that the change in field with polar angle follows the theoretical function out to 45 degrees and then reverses due undoubtedly to the critical effect of the extra optical element, the dome, at large field angles.

$\Delta\Omega$ for each data point is presented in table 8.

RADIANCE CALIBRATION

From the data developed, we may now express the sensitivity of the radiance scanner. It should be noted that the volume V of the signal solid is the total camera response to the input flux density. To calibrate for radiance measurements, this camera response is normalized to the instantaneous field of view $\Delta\Omega$. The field has been shown (equation 20) as the product of a constant and the square of the digital diameter, d , or

$$C d^2 = \Delta\Omega \quad (21)$$

Since the radiance scanner only measures directly the response S , the quantity $S\Delta\Omega$ is equivalent to V with the appropriate constants.

During the calibration procedure (fig 14) camera response was measured for each data point X_c, Y_c for a given flux density $H(X_c, Y_c)$. The response of the camera $S(X_c, Y_c)$ has been normalized and corrected for camera conditions by

$$\bar{S}(X_c, Y_c) = \frac{[S(X_c, Y_c) + 14] p(X_c, Y_c)}{600 G G_d} \quad (22)$$

Calibration data were obtained at a set of N calibration points $X_c, Y_c, c = 1, 2, \dots, N$ where N consists of 32 useful data points.

The sensitivity of the radiance scanner can be characterized by a unit spectral radiance ΔN_λ ($\text{W cm}^{-2} \text{ sr}^{-1} \text{ \AA}^{-1} \text{ digit}^{-1}$) defined in calibration by the set of N equations

$$\Delta N_\lambda = \frac{H(X_c, Y_c)}{\bar{S}(X_c, Y_c) \Delta\Omega(X_c, Y_c) \Delta\lambda} \quad (23)$$

The value of ΔN_λ from each data point is shown in the last column of table 8. Table 11 lists the average values for each angle data set.

These averaged values are plotted in figure 24. Also shown in figure 24 are two linear relationships, joined at $\theta = 45$ degrees, which together fit the table 11 values to within $\pm 2\%$, except for $\theta = 0$. This suggests a convenient analytic approach by letting

$$\begin{aligned} \Delta N_\lambda &= 2.68 \times 10^{-8}, & r^2 &\leq 898704 \\ \Delta N_\lambda &= 2.68 \times 10^{-8} + 2 \times 10^{-10} \left(\frac{r^{1.06}}{31.61} - 45 \right), & r^2 &< 898704. \end{aligned} \quad (24)$$

To determine the spectral radiance value $N_\lambda(X,Y)$ associated with a camera response of $S(X,Y)$ measured with a camera gain of G (from table 6) and a dwell gain of G_d (from table 7 or equation 16), first normalize the output by

$$\bar{S}(X,Y) = \frac{[S(X,Y) + 14] p(X,Y)}{600 G G_d}, \quad (25)$$

where $p(X,Y)$ is the photocathode array element nearest X,Y .

Next calculate

$$r^2 = (X - 72)^2 + (Y + 204)^2. \quad (26)$$

Finally obtain the spectral radiance by using the expression

$$N_\lambda(X,Y) = \Delta N_\lambda(r) \bar{S}(X,Y). \quad (27)$$

During the period before the experiment, a calibration was performed which may be useful in calibrating sky scene radiance with the radiance scanner above water.

The procedure outlined above using equations 25 through 27 may be used with the following values for ΔN_λ :

$$\begin{aligned} \Delta N_\lambda &= 3.68 \times 10^{-8}; & r^2 &\leq 1.5 \times 10^6 \\ \Delta N_\lambda &= 3.68 \times 10^{-8} \left[1 + 0.74 \frac{r^2}{1.5 \times 10^6} \right]; & r^2 &> 1.5 \times 10^6. \end{aligned} \quad (24')$$

TABLE 11. UNIT SPECTRAL RADIANCE FACTOR.
 $\text{W cm}^{-2} \text{ sr}^{-1} \text{ \AA}^{-1} \text{ digit}^{-1}$

Data Set	ΔN_{λ}	Std Devn	%
0°	2.863×10^{-8}		
29°	2.649×10^{-8}	0.474×10^{-8}	17.9
45°	2.632×10^{-8}	0.303×10^{-8}	11.5
61°	3.016×10^{-8}	0.667×10^{-8}	22.1
85°	3.494×10^{-8}	0.711×10^{-8}	20.3

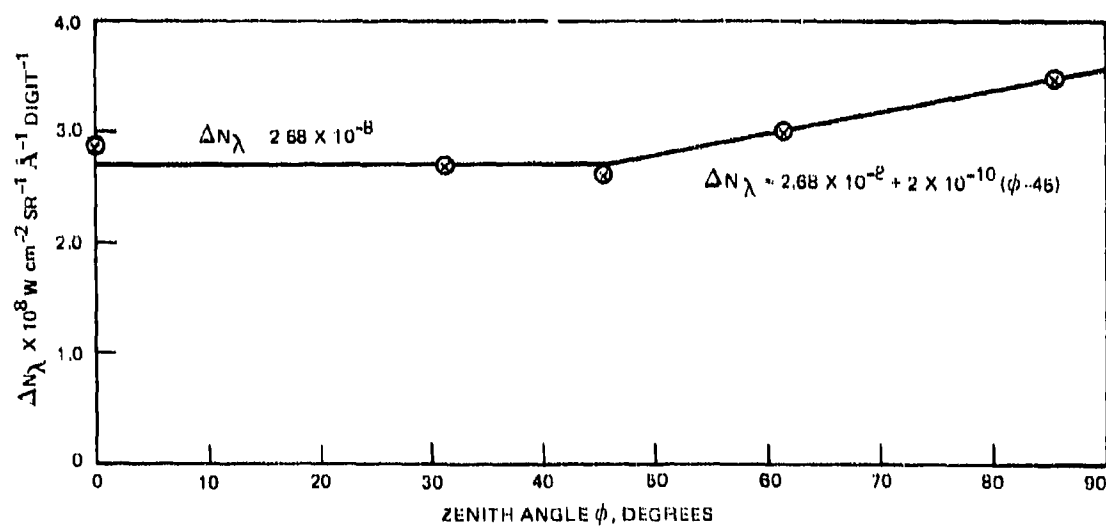


Figure 24. ΔN_{λ} values.

CALIBRATION ACCURACY

The uncertainty in the spectral radiance factor, from table 11, is approximately $\pm 20\%$ based on observed variations in the calibration data. These variations are not completely explainable from consideration of the uncertainties associated with the procedure.

Random variations may arise from several sources. The first of these is the source geometry shown in figure 14 where the radiant flux F at the camera aperture is determined basically by measurement of a flux value F_m outside the window at a range R' from the source. The entrance pupil is assumed at some effective range R . The ranges R' and R can vary together between measurements by $\pm 1/2$ cm.

Use $R' = 130$ cm, $R = 150$ cm, $dR' = dR = 1.0$ cm.

$$F = F_m \left(\frac{R'}{R} \right)^2, \quad (28)$$

$$dF = 2 F_m \frac{R dR' - R' dR}{R^2}, \quad (29)$$

and

$$\frac{dF}{F} = \frac{R dR' - R' dR}{R^2} = 0.12\%, \quad (30)$$

Another source of random error occurs during the data scan. By referring to figure 23 it can be seen that the base of the solid volume nearly fills the 60×60 array. On some data points, a portion of the volume falls outside the array and was not recorded. This error will show up in the determination of $d\Omega$, since the volume and not the peak signal is affected. Referring to table 9, we can average the standard deviations to find

$$\frac{dV}{V} = 3.7\% \quad (31)$$

and

$$\frac{d\Omega}{\Omega} = 2 \left(\frac{dV}{V} \right) = 7.4\% \quad (32)$$

Other random variations can occur due to the experimental setup and the small aperture of the camera, such as water drops, window imperfections, and particles in the water. Because of the possibility that waterborne materials might obscure the aperture, at least three complete scans were made of each data point. The variation between these scans is typically on the order of 0.1% , indicating good reproducibility. The most significant variable must be the distribution of the small species of contaminant found on the photocathode.

Systematic variations, as opposed to random variations, can enter from several sources. The most obvious source of systematic error is the calibration standard used throughout these measurements, the UDT-21A irradiance meter, serial 70086. This

instrument was delivered with a $\pm 5\%$ calibration accuracy claimed by the manufacturer. To test the meter at the wavelengths used here, a spectral irradiance standard as described by Stair was used.¹² Commercial units made by Electro-Optics Associates models L101 and P101 were employed, which provide a $\pm 5\%$ absolute spectral irradiance. The filter was carefully measured and reinstalled in the UDT-21A meter. Response of the UDT-21A with the expected value from the calibration standard was 2.1% high. It is concluded that the UDT-21A was within its specified $\pm 5\%$ absolute accuracy.

Another systematic error could arise due to thermal effects in the camera during calibration. In the closed canister without the efficient cooling provided by the ocean, the camera can be expected to operate at higher temperatures, with the temperature increasing with operating time. Examination of the data does now show effects related to the period of time the camera had been operating.

The last systematic error to be considered is due to the 14-bit offset found in the data after calibration data taking had been completed. These 14 bits, to the extent that they cannot be corrected, affect the center of gravity of the solid volume, figure 23. The lost volume is a triangularly shaped cross-sectional ring around the base of the solid. For the solid in figure 23, that perimeter has a length of about 120 deflection units. The half-height of the cross section is seven digital units. If the missing ring is 10 deflection units wide, then a volume of about 8×10^5 is missing. The measured volume of data point 32 is 1.34×10^5 ; the missing volume would add 6.3%. The effect on the field of view would be an increase of 3.1%.

In summary, an uncertainty of 20% in the absolute calibration of the radiance scanner must be assumed, although this variation cannot be explained from known variations in the procedure.

In future work, if the unknown source of photocathode contamination can be eliminated and the photocathode kept clean, the calibration uncertainty can be limited to

$$\left[(0.12)^2 + (7.4)^2 + (5)^2 + (3.1)^2 \right]^{1/2} = 9.5\%, \quad (33)$$

A field calibration fixture to perform periodic calibrations in the field would be a desirable development. Such a fixture was used by Smith with the radiance camera* and can increase confidence in experimental results.

12. Stair, R. et al, "A New Standard of Spectral Irradiance," *Appl Optics* 2 1151 (1963)

* Smith, RC, private communication, 23 October 1974

REFERENCES

1. Karp, S, "Optical Communications Between Underwater and above Surface (Satellite) Terminals," IEEE Tran Comm, COM-24, 66-81 (1976)
2. Smith, RC, et al, "An Oceanographic Radiance Distribution Camera System," Applied Optics 9, 2015-2022 (1970)
3. Jerlov, NG, "Optical Oceanography," Elsevier 1968
4. Tyler, JE, "A Survey of Experimental Hydrologic Optics," J Quant Spectrosc Radn Transfer, 8 339-354 (1968)
5. Nygard, K, "Radiance Distribution below the Sea Surface," AGARD lecture Series 61, Optics of the Sea
6. Tyler, JE, "Radiance Distribution as a Function of Depth in an Underwater Environment," Bull Scripps Inst of Oceanography 7 363-411 (1960)
7. Duntley, SQ, "The Visibility of Submerged Objects," Visibility Laboratory Report 1952
8. Preisendorfer, RW, "Model for Radiance Distribution in Natural Hydrosols," JOSA 47 1046 (1957)
9. Miyamoto, K, "Fish Eye Lens," JOSA 54 1060-1061 (1964)
10. "Fisheye-Nikkor Lens," instruction manual, Nippon Kogaku KK 1973
11. Wuellner, LE, "Technical Manual. Vidisector Camera System for Underwater Photometry," IIT Report Proj 64225, 28 April 1975
12. Stair, R, et al, "A New Standard of Spectral Irradiance," Appl Optics 2 1151 (1963)

SECTION 3

AIRCRAFT RECEIVER SYSTEM

INTRODUCTION

The Aircraft Receiver System was designed and built to measure the radiance distribution profile emanating from the OPSATCOM Field Test Laser which was operated underwater at required depths. Measurements were made while the receiver passed overhead in its aircraft platform and tracked the laser. Acquisition of signal and initiation of track were performed by the receiver operator pointing the receiver while viewing the area of interest through the receiver's optical system see Fig. 1. After acquisition of signal the receiver automatically tracked the laser signal and recorded on magnetic tape the signal intensity, and the receiver's pitch and roll angles. From these data and the calibration constants of the Aircraft Receiver System one can plot the desired distribution profiles (cuts). Changing laser depth and repeating the above procedure yields a family of profiles as a function of depth.

SYSTEM CONFIGURATION

A simplified system diagram illustrating the signal flow from optical input to digital tape recorded output is shown in Figure 2. Table 1 provides a brief description of each of the numbered items.

The system was configured to fit into a Consolidated PBY-5A amphibian flying boat. Figure 3 shows the platform. Figure 4 shows the installation. The APU was mounted in the blister compartment in order to reduce audible noise and exhaust gas effects on personnel. All other parts of the system were mounted in Compartment 2. Figure 5 shows the platform layout. The "front view" of Figure 5 shows the receiver operator in position viewing the diffuse screen and controlling the sensor assembly field of view with the pitch-roll joystick. Figure 6 shows the panel layout of Console 1, Figure 7 shows Console 2. The Midwestern analog recorder and the Tektronix R2601 units were used briefly during hardware checkout, but were not used during the data acquisition portion of the program.

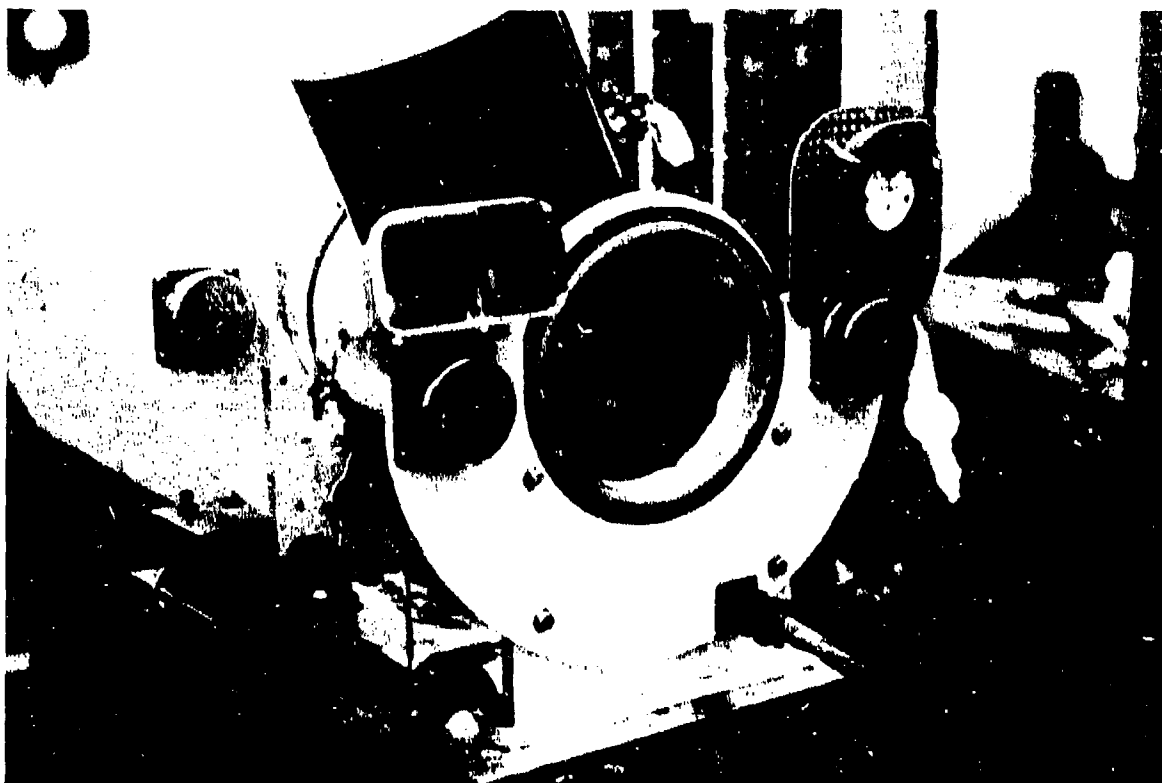


Figure 1a. A/C Receiver Rear View.

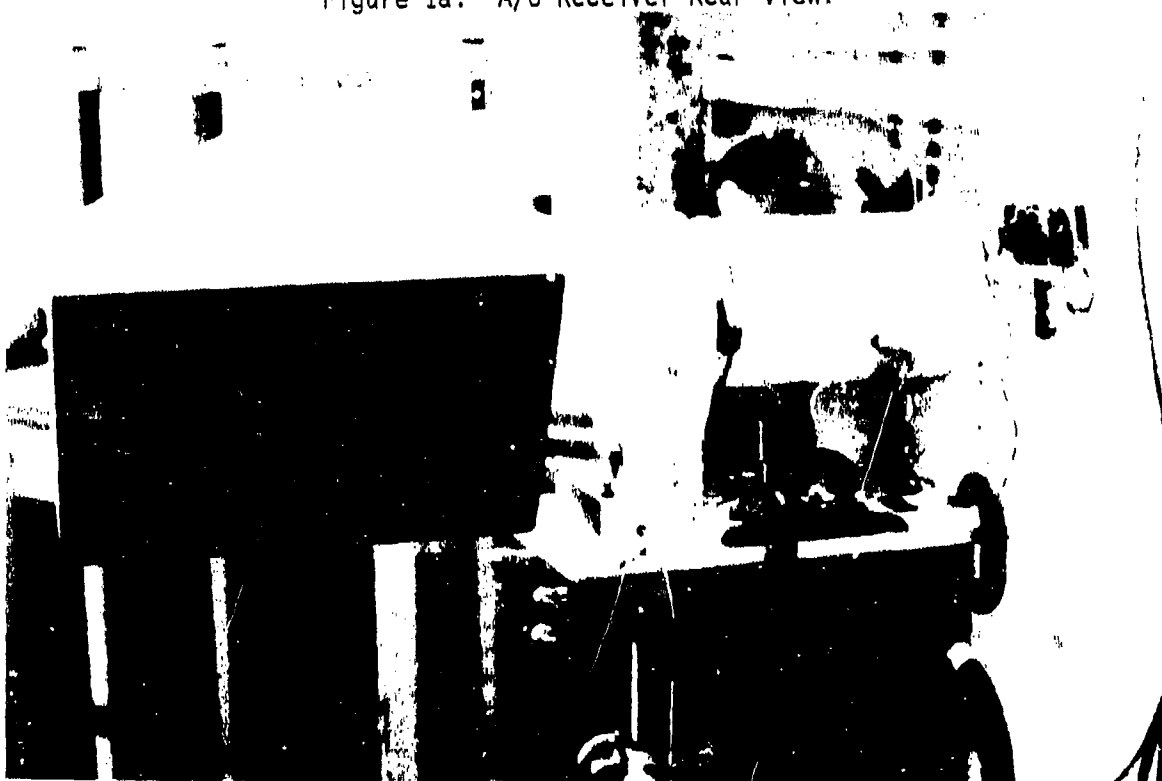


Figure 1b. A/C Receiver Front View.

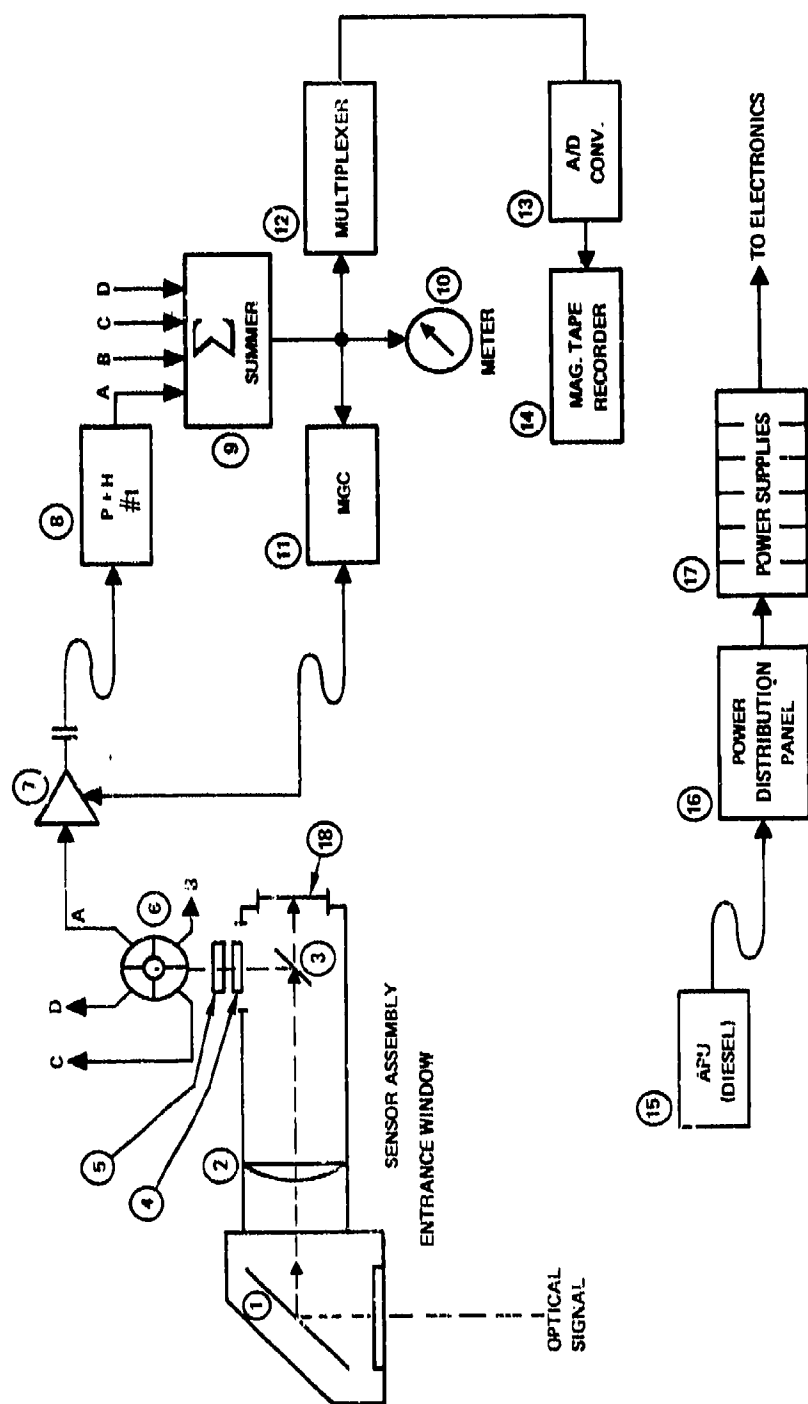


Figure 2. Simplified System.

Table 1.

Item

1. Roll Mirror
2. Objective Lens
3. Dichroic Mirror
4. Neutral Density Attenuating Filter
5. Spectral Filter
6. Quadrant Detector
7. Transimpedance Amplifier
8. Peak and Hold for Quadrant 1
9. Summing Unit for The 4 Peak and Holds
10. Signal Strength Panel Meter
11. Manual Gain Control Switch Unit
12. Signal Multiplexer
13. Analog to Digital Converter
14. Signal Recorder, Magnetic Tape Unit
15. Auxiliary Power Unit, Prime Power Source
16. Power Distribution Panel
17. Power Supply Complement
18. Diffuse Viewing Screen

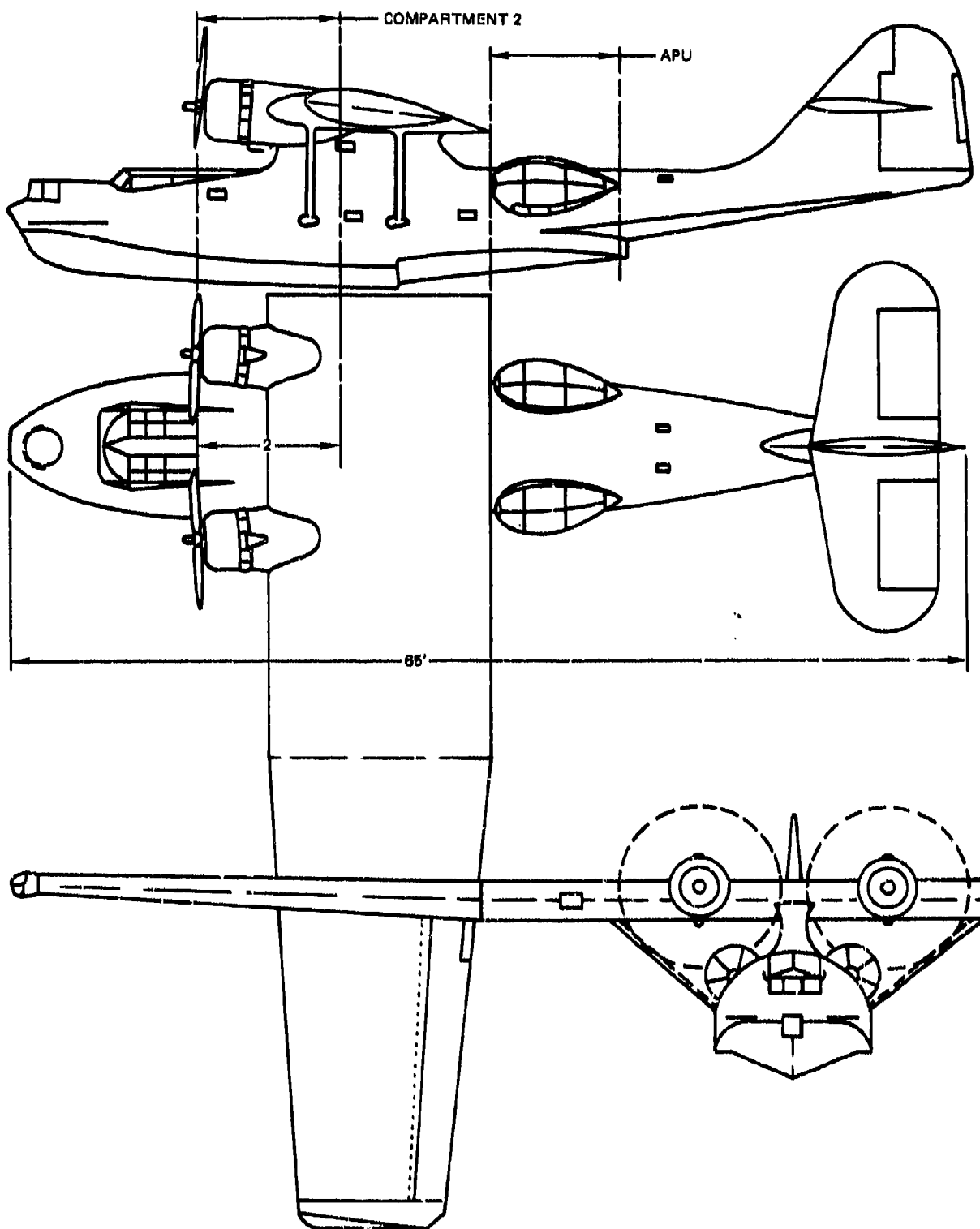


Figure 3. The Consolidated PBV-5A Flying Boat.



Figure 4. A/C Receiver Installed in PBY.

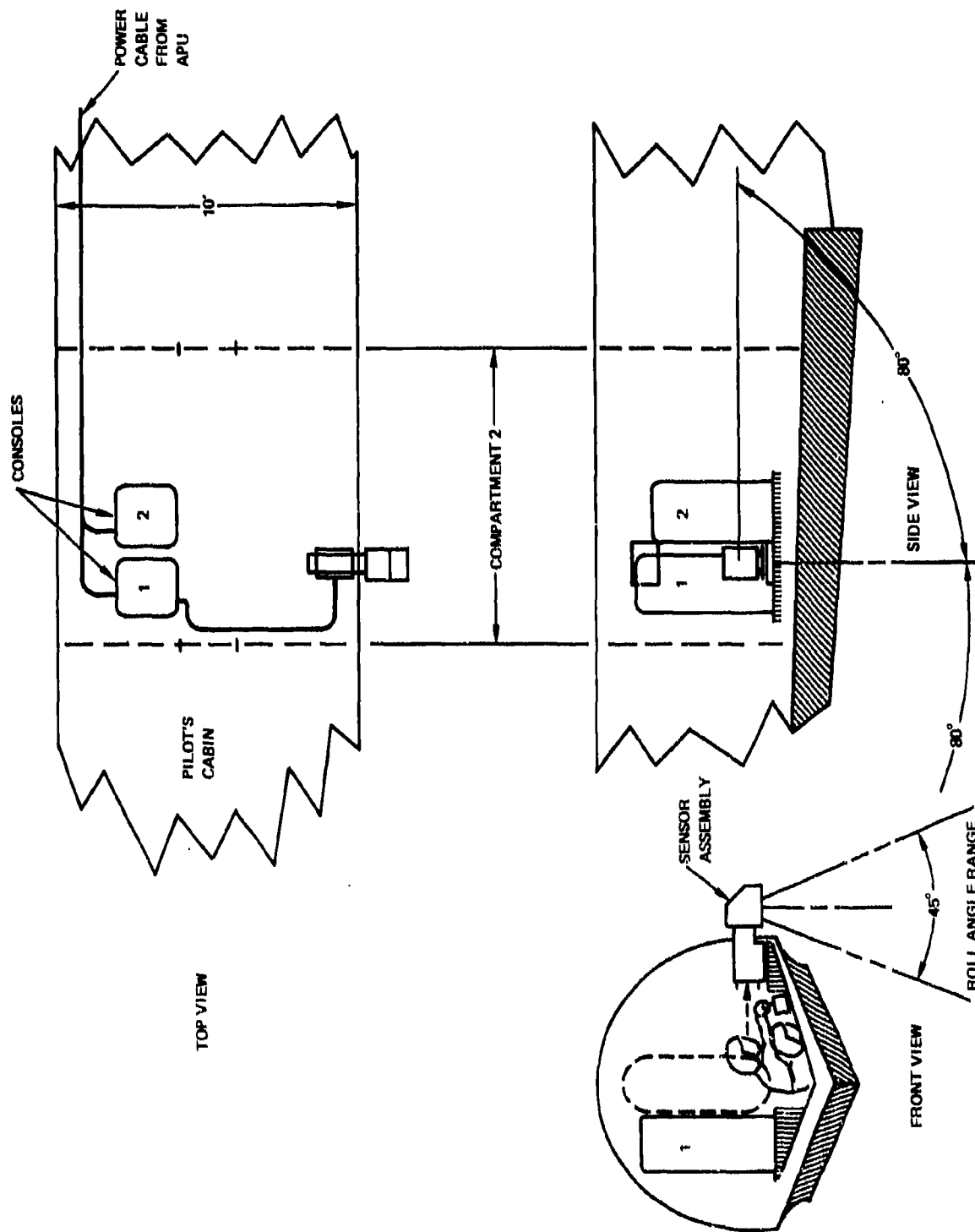


Figure 5. A/C System; Equipment Location in PBV-5A.

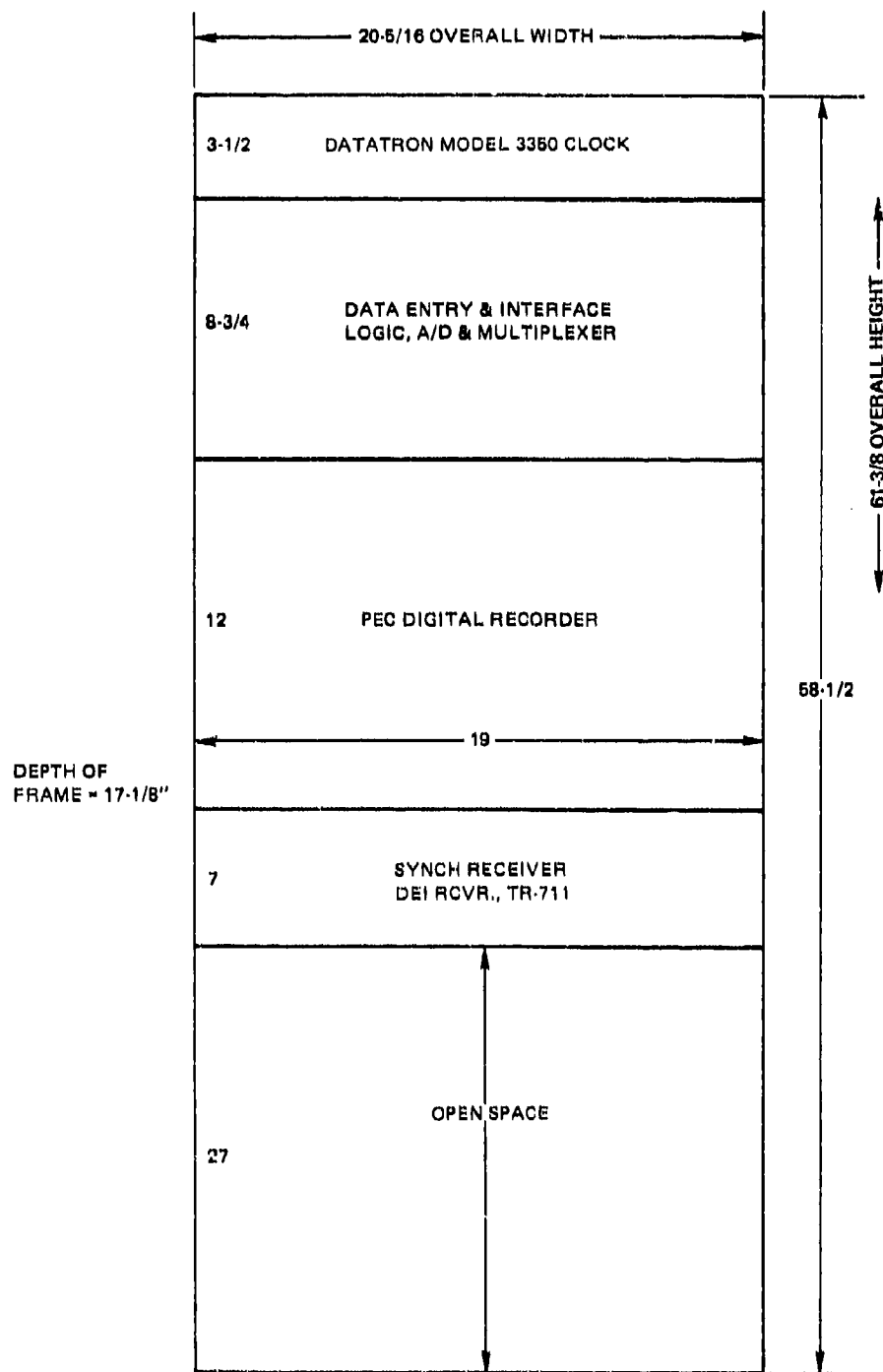


Figure 6. A/C System Console 1.

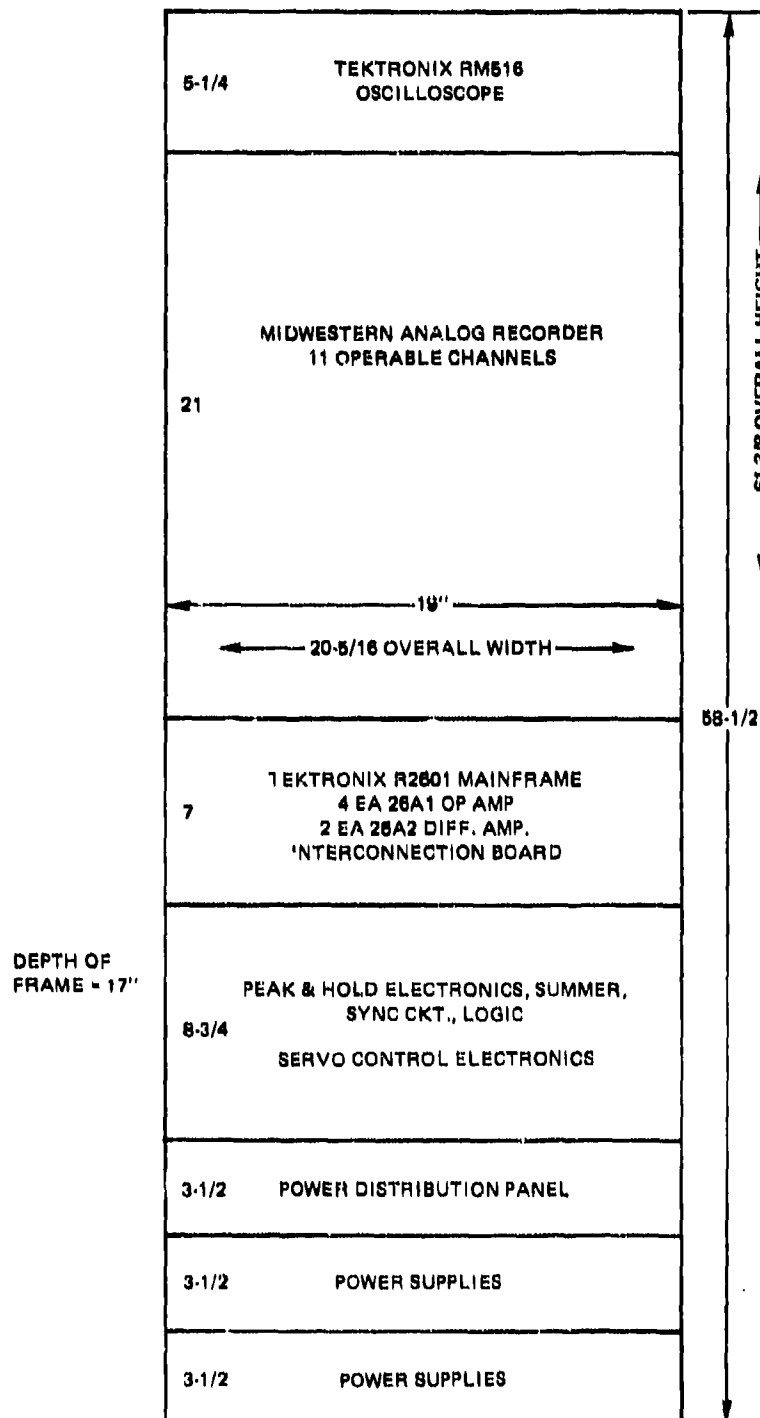


Figure 7. A/C System Console 2.

SYSTEM DESCRIPTION

A simplified diagram showing signal flow from optical input to digital output recorded on magnetic tape was previously cited as Figure 2. A more detailed diagram is shown in Figure 8.

Laser optical radiation passes through the entrance window of the sensor assembly, is reflected by the roll mirror, collected by the 6-inch objective lens and imaged in its focal plane on the quadrant photodiode. Some spectral prefiltering is effected by the beamsplitting dichroic mirror. Spectral pass band filtering at $5200 \pm 50 \text{ \AA}$ is done by the spectral filter mounted in front of the quadrant detector; Figure 9 shows the resultant filter. The visual field of view (approx. 15°) is imaged on the 5-inch diameter diffuse viewing screen; the center 1 inch of the viewing screen is minus green in spectral content due to the color separation function of the dichroic mirror.

The synchronizing signal receiver shown in Figure 8 receives an FM carrier frequency at 227.7 MHz transmitted from the laser control electronics. This 227.7 MHz carrier is modulated at a 20 Hz rate by the laser trigger pulse. After demodulation by the synch receiver and sharpening by a pulse shaping circuit the synch pulse is utilized to enable the "hold" function of the peak and hold circuitry (see Figure 10). Also shown in Figure 10 are the time relationships between the 20 Hz clock source (at the laser control console), the laser pulse and the record command "sync to recorder" which enables the record function at the required 20 Hz rate.

During track the laser optical signal is equally distributed on the four detector quadrants. Each quadrant's output is amplified and buffered by a transimpedance amplifier (item 7, Figure 2) and applied to a peak and hold amplifier (P+H) as shown in Figure 8. The outputs of the four P&H units are summed and connected to a multiplexer, then to an analog to digital converter, and then finally to the magnetic tape digital recorder for storage. The summer output is also displayed on a panel meter indicator. If the summed signal exceeds the 10 V full scale of the meter (and of the PEC recorder), the operator must reduce amplifier gains by adjusting the gain switch on the manual gain control unit (MGC).

The Datatron clock shown in Figure 8 provides time of day information to the recorder to be stored on command at the 20 Hz rate. This data is shown in the left column set of Figure 11, a typical section of the magnetic tape data record printout. Table 2 provides a legend for the data printout format.

The tracking capability of the Aircraft Receiver System is effected by moving the roll mirror such that the source image is positioned symmetrically on the quadrant detector and held there as long as the source is within the data field of view. The outputs of opposite quadrants of the detector, at the peak and hold outputs are applied to a difference amplifier (see Figure 12). An imbalance generates an error signal which is amplified and applied to one of the servo motors to drive the error signal to zero. Both the pitch and roll axes are controlled in

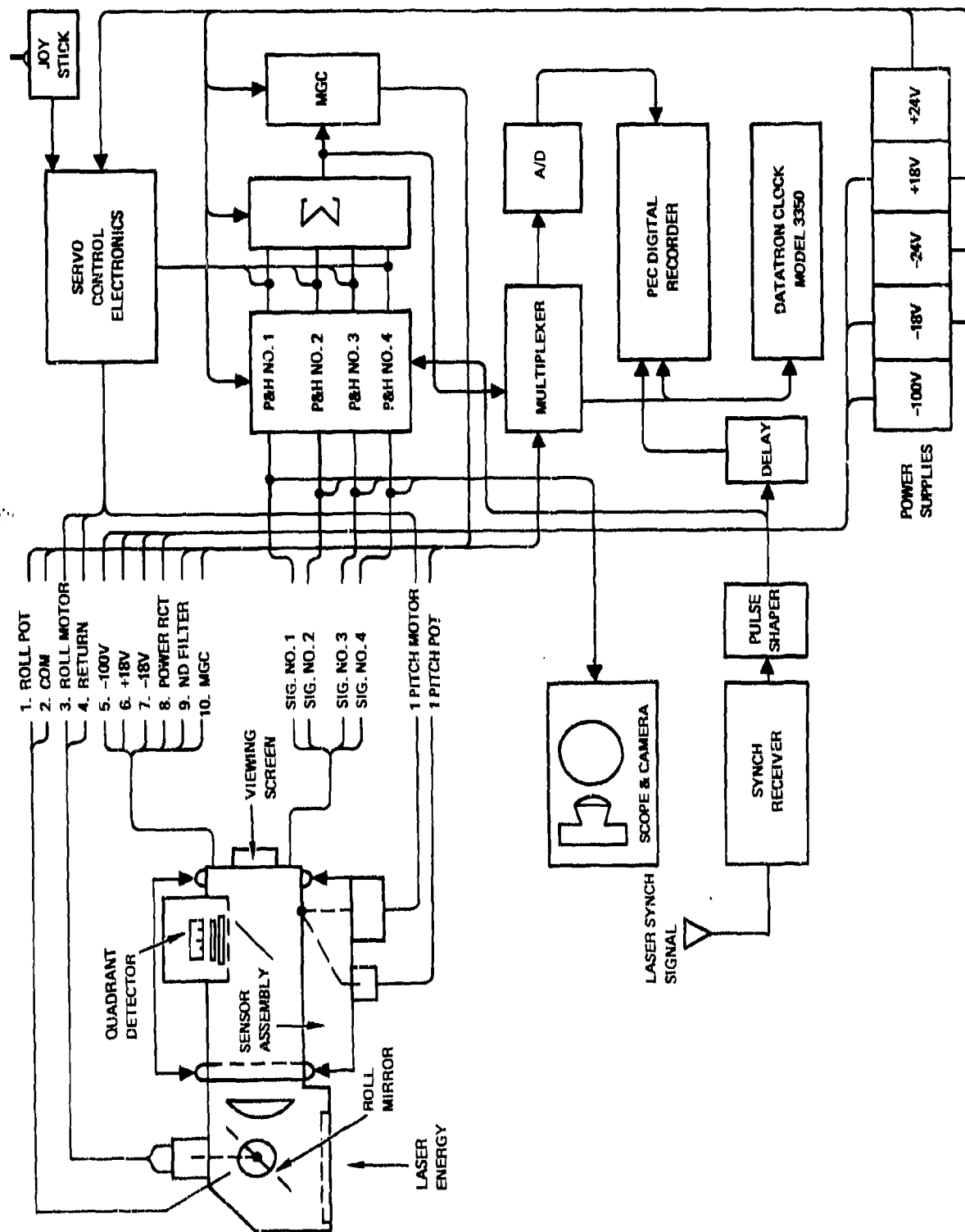


Figure 8. A/C Receiver System.

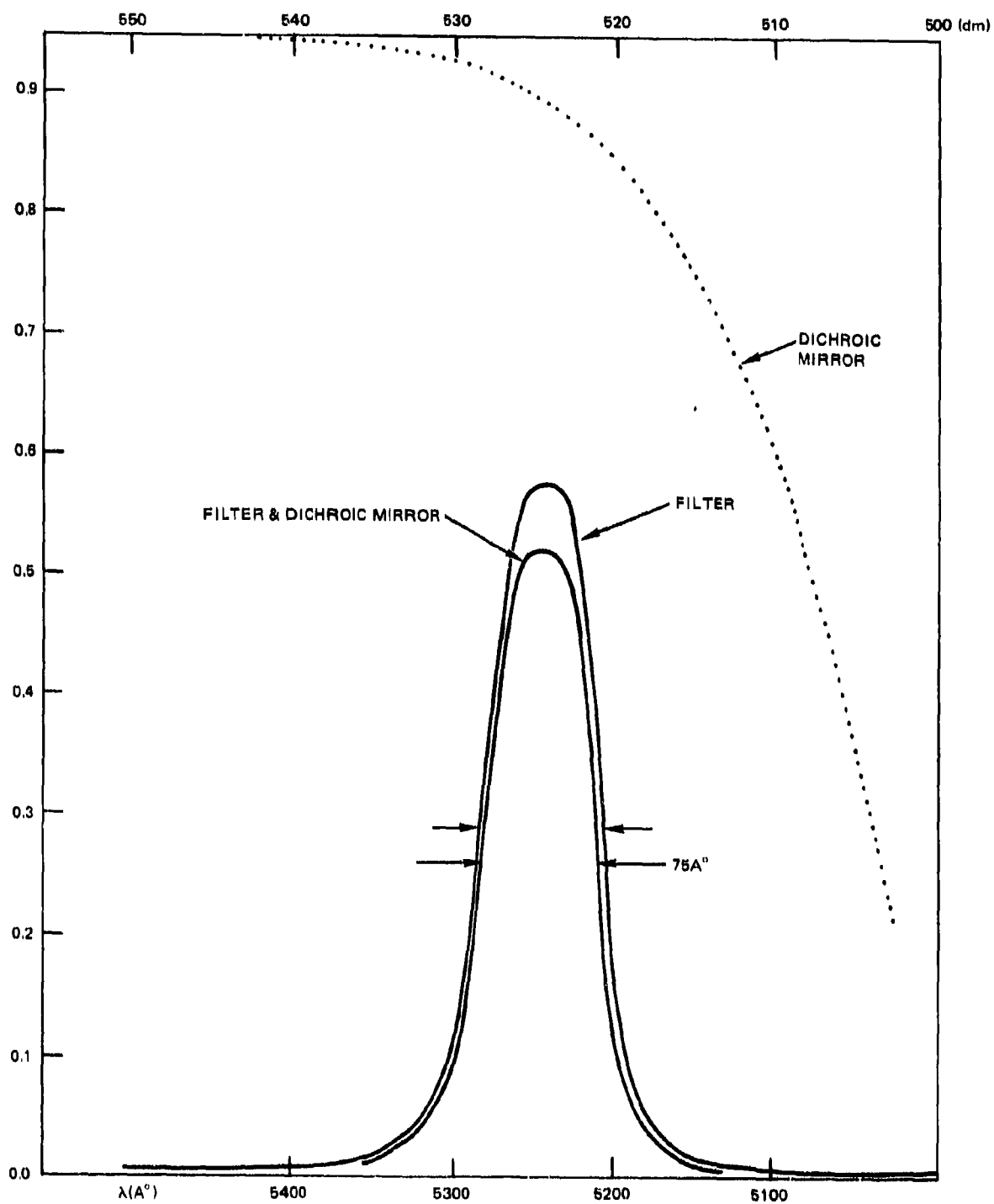


Figure 9. Transmittance Characteristic A/C Radiance Sensor.

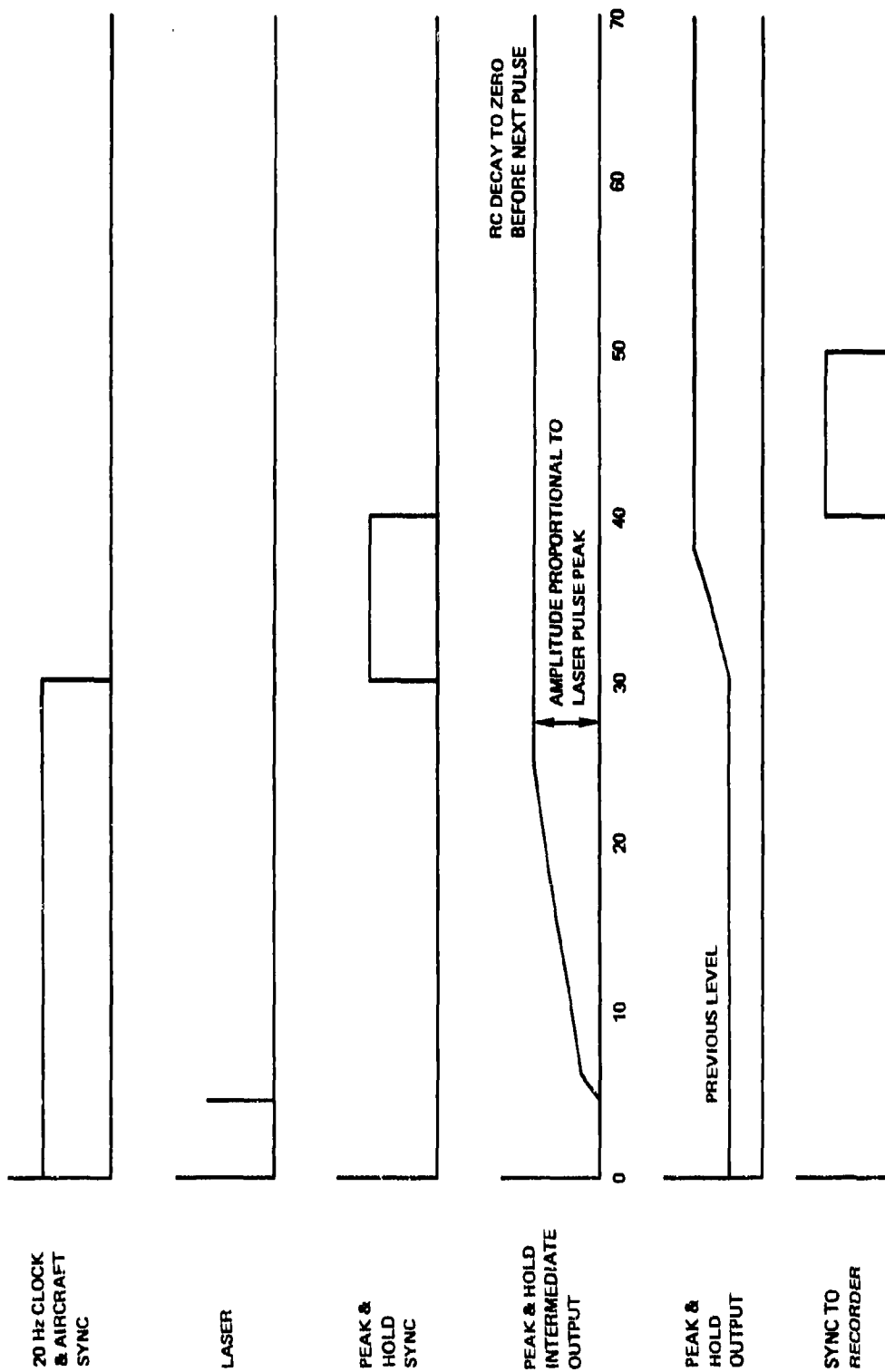


Figure 10. Aircraft Timing Sequence.

Table 2.

Legend: Magnetic Tape Output Format

COLUMNS 1 → 11 Time in hours, minutes, seconds and hundredths of seconds.

SWITCHES 12 → 6 Binary pass number manually set by operator. Least significant bit in 12 column, most significant bit in 6 column.

SWITCH 5 A zero in this column indicates an attenuating filter in the detector optics of N.D. = 2 (1% transmission) a true (1) indicates no filter.

SWITCH 4 A zero in this column indicates an attenuating filter in the detector optics of N.D. = 1 (10% transmission) a true (1) indicates no filter.

SWITCH 3 When this entry is 0 the system is in the operate mode. A true or 1 in this column indicates internal calibration of the system.

SWITCH 2 If the receiver is operating within its dynamic range this column will be true, show a 1.

SWITCH 1 When the sum signal (see below) is sufficient to sustain automatic tracking, this column indicates a 0 digit. During low signal conditions this bit goes true indicating that the receiver cannot be tracking.

CH 1 The numerical entry in CH 1 is proportional to the summation of the optical signal on each of the four quadrants. The correspondence of this numerical value to the signal strength meter reading on the control panel is 0 to -9.999 is 0 to 99.99 meter deflection where a meter deflection of 100 is full scale.

CH 2 Entries in this column will assume one of three nominal values, +5, 0, or -5. A -5 indicates that the receiver sensitivity is on range 1, the most sensitive scale. A value near 0 indicates the receiver sensitivity is on range 2. The least sensitive position, +5, was not used.

CH 3 Indicates a voltage proportional to the pitch angle of the receiver. A zero reading indicates that the receiver pitch axis was oriented vertically downward. Positive entries indicate the pitch axis of the receiver was pointed forward along the aircraft flight path, while negative entries indicate an aft orientation.

CH 4 Indicates a voltage proportional to the receiver roll angle. A zero reading is obtained when the receiver roll axis is oriented nominally vertically downward. Positive entries indicate the receiver roll axis deflected toward the port side of the aircraft while negative entries indicate a starboard deflection.

CH 5 and CH 6 not used.

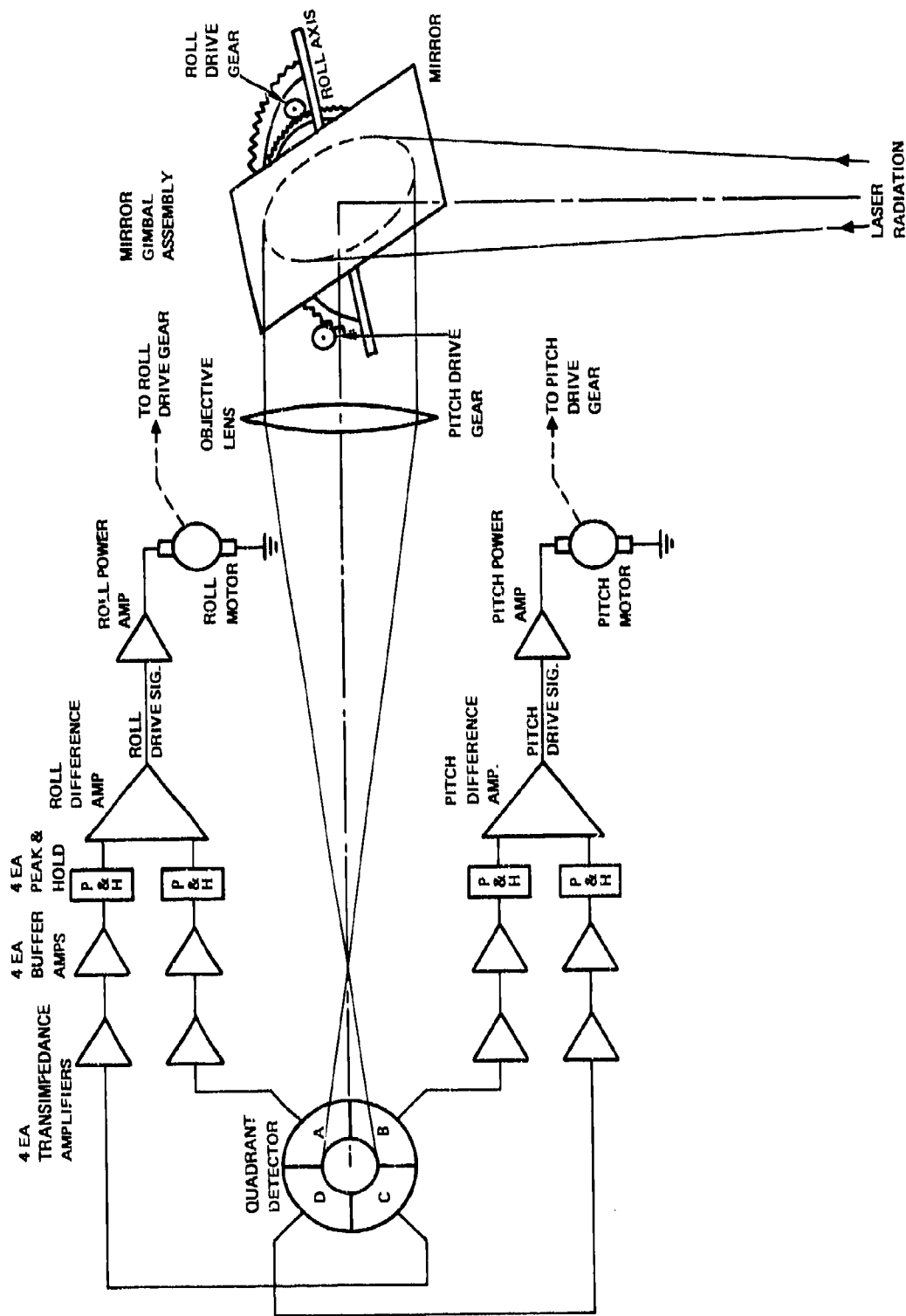


Figure 12. Aircraft Receiver Tracking System.

this manner. The roll axis correction is done by driving the roll mirror directly. The pitch axis correction is effected by turning the entire sensor assembly housing on its support ball bearings. As indicated in Figure 12 the spot imaged on the quadrant detector is defocused, that is, the plane of the quadrant detector was positioned somewhat beyond the focal point of the objective lens. This was intentionally done to optimize the response of the tracking system and to reduce the maximum power density at the photodetector.

SYSTEM SPECIFICATIONS

The following tabulation describes the operational characteristics of the Aircraft Receiver System:

Sensor Assembly

Sensitivity (10% of full scale)	4.7×10^{-9} W CM ⁻²
F/#	3
Lens Diameter	6"
Spectral Bandpass	5240 ± 38 Å
Data FOV	1.4° (25 mr)
Visual FOV	15°
Allowable Roll Angle	$\pm 22.5^\circ$
Allowable Pitch Angle	$\pm 90^\circ$

Detector-Preamplifier

Detector	EG&G SGD-444-4
Preamplifier	Optical Electronics Inc. 9730
Combination Bandwidth	D.C. to 2.5 MHz

Tracking System

Deadband	$< \pm .14^\circ$ (2.5 mr)
Roll Rate Correction	$> 5^\circ \text{ Sec}^{-1}$
Pitch Rate Correction	$> 5^\circ \text{ Sec}^{-1}$
Joy Stick Slew Rate (both axes)	$> 15^\circ \text{ Sec}^{-1}$

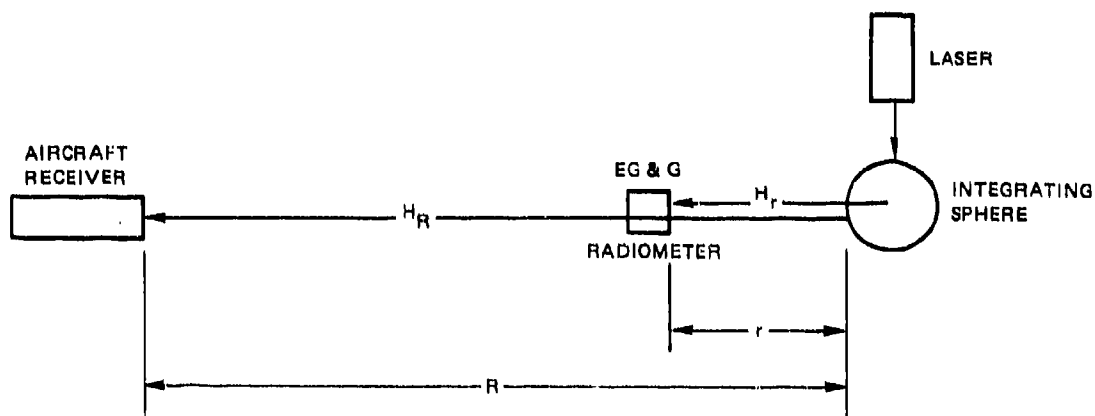
CALIBRATION

The aircraft receiver produces a voltage at its output in response to the received optical power density. The determination of this response in absolute irradiance units is the purpose of this calibration.

The approach taken is to first establish a single absolute irradiance response value. Next, a curve is plotted depicting the receiver's response at the maximum gain setting. The absolute irradiance value then becomes a point on this calibration chart relating all the remaining points in absolute terms.

The aircraft receiver and the field experiment dye laser form a source-detector pair in the field, hence the dye laser is a natural choice for the optical calibration source. As shown in fig 13, the laser beam is injected into an integrating sphere transforming the beam into a Lambertian source which at a "large" distance approaches a point source. The minimum distance required for this condition to be satisfied to an accuracy of 1% is one hundred times (100X) the radius of the sphere's exit aperture, or 6.25 feet.

To establish an absolute irradiance response value it is necessary to fix a value of incident irradiance at the receiver (H_R). However, direct measurement with available laboratory equipment (EG&G 480 spectroradiometer) is not possible in most cases due to insufficient sensitivity of the spectroradiometer. Since the calibration source has been configured to provide a point source, the emerging power density (H)



$$H_R = H_r \left[\frac{r}{R} \right]^2$$

Figure 13. Aircraft Receiver Calibration.

obeys an inverse square law. Thus, we may measure irradiance directly at a point closer to the source (H_r) where values exist within the spectroradiometer's range. The inverse square law is then used to compute incident irradiance at the receiver (fig 13).

Having thus found a value for H_r , the resulting voltage at the output of the receiver is plotted. The remainder of the response data is obtained by attenuating the incident irradiance in known increments with neutral density filters.

ABSOLUTE IRRADIANCE

Referring again to fig 11, the EG&G 480 was located 9.77 feet from the integrating sphere while the aircraft receiver was located 98 feet from the sphere. The calibration was conducted in a long windowless hallway and the apparatus baffled to control extraneous light.

During the course of the calibration, periodic measurements of the source's flux density were taken with no detectable variation indicating the pulse-to-pulse variation in the laser did not exceed the 10% absolute accuracy of the spectroradiometer. The measured value of the irradiance at the monitor (H_r) was $2.42 \times 10^{-4} \text{ W-cm}^{-2}$. This yields an irradiance at the receiver (H_p) of

$$2.42 \times 10^{-4} \text{ W-cm}^{-2} \left[\frac{9.77}{98.0} \right]^2 = 2.4 \times 10^{-6} \text{ W-cm}^{-2}$$

The error inherent in this measurement arises primarily from pulse-to-pulse variation in the laser and the accuracy of the EG&G 480. Both are specified at $\pm 10\%$. A third component of this error budget is introduced in the output voltage measurement. This is oscilloscope reading error generally accepted at $\pm 5\%$. The fourth component of error arises from the transmittance accuracy of the neutral density attenuator ($\pm 5\%$). Taking the rms value of these four error contributions yields an overall accuracy of

$$\% \text{ accuracy} = [(10)^2 + (10)^2 + (5)^2 + (5)^2]^{1/2} = \pm 16\%$$

Data was taken with the receiver in the Hi Gain position (Range 1) and the 1.0% (Density 2.0) transmission Attenuator filter in the optical path. The measurement was repeated twice with the following results:

Measurement	Irrad. at Receiver	Receiver Output	Meter Reading	Noise
1	$2.4 \times 10^{-6} \text{ W-cm}^{-2}$	4.8 volts	48	4
2	2.4×10^{-6}	4.8 volts	48	4

The noise reading of 4 was observed with the receiver's objective lens occluded. From previous successful attempts to minimize this noise it was found to be due primarily to electrical coupling between cabling

and circuit components. Insertion of extra shielding and some cable rerouting was done in the time available. This reduced the noise but did not entirely eliminate its effects.

Interpreting the noise reading as a 4% of full scale uncertainty, the value for full scale sensitivity for range 1 is found to be

$$\text{F.S.} = \frac{2.4 \times 10^{-6} \times 10^{-2} \times 10^2}{48} = 5 \times 10^{-8} \text{ Wcm}^{-2}$$

with an accuracy of $\pm(16+4) = \pm 20\%$.

Fig 14 shows the calibration characteristic.

Similarly for range 2 the following was measured:

Measurement	Irrad. at Receiver	Receiver Output	Meter Reading	Noise
1	$2.4 \times 10^{-6} \text{ Wcm}^{-2}$	4.2 volts	42	4
2	$2.4 \times 10^{-6} \text{ Wcm}^{-2}$	4.2 volts	42	4
3	$2.4 \times 10^{-6} \text{ Wcm}^{-2}$	3.9 volts	39	3.5

Then for range 2

$$\text{F.S.} = \frac{2.4 \times 10^{-6} \times 10^2}{41} = 5.8 \times 10^{-6} \text{ Wcm}^{-2}$$

with an accuracy of $\pm(15 + 4) = \pm 19\%$.

Figure 15 shows the calibration characteristic.

PITCH AND ROLL CALIBRATION:

In both the pitch and roll axes a precision potentiometer was coupled to the respective axis and an output voltage proportional to angle was recorded on the magnetic tape at a 20 Hz rate. The pitch pot is a Beckman SA 3845 unit, 10 turns, with a $\pm 0.25\%$ linearity; its resistance is 1.0 K ohm. The measured voltage at 0° was less than the least count of the recording system, $5 \times 10^{-3} \text{ V}$. The roll pot is a PIC DA-43 unit of $\pm 1.0\%$ linearity and a resistance of 2.0 K ohms. Measured voltage at 0° was less than $5 \times 10^{-3} \text{ V}$.

The voltages applied to both pot circuits are regulated to $\pm 0.25\%$, hence the accuracy of the pitch and roll voltage to the A/C System recorder is better than $\pm 1.25\%$. Figure 16 shows the pitch pot calibration, figure 17 the roll pot calibration.

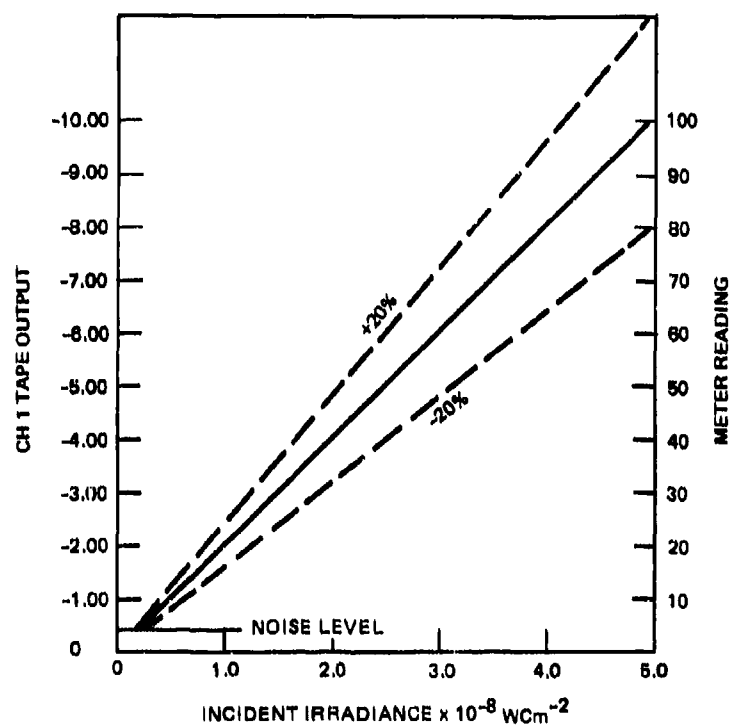


Figure 14. A/C Receiver Sensitivity Range 1 (no optical attenuation).

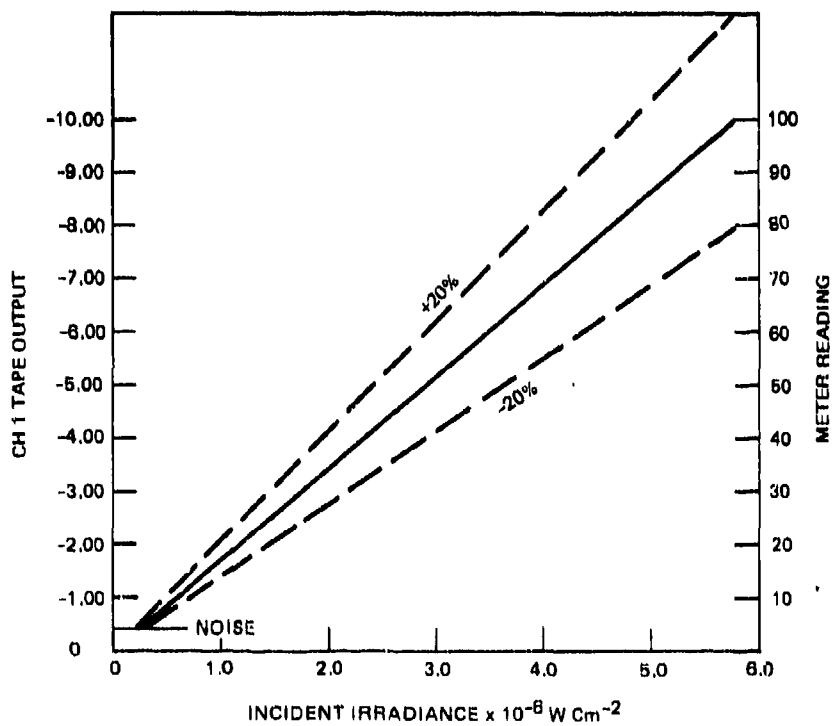


Figure 15. A/C Receiver Sensitivity Range 2 (no optical attenuation).

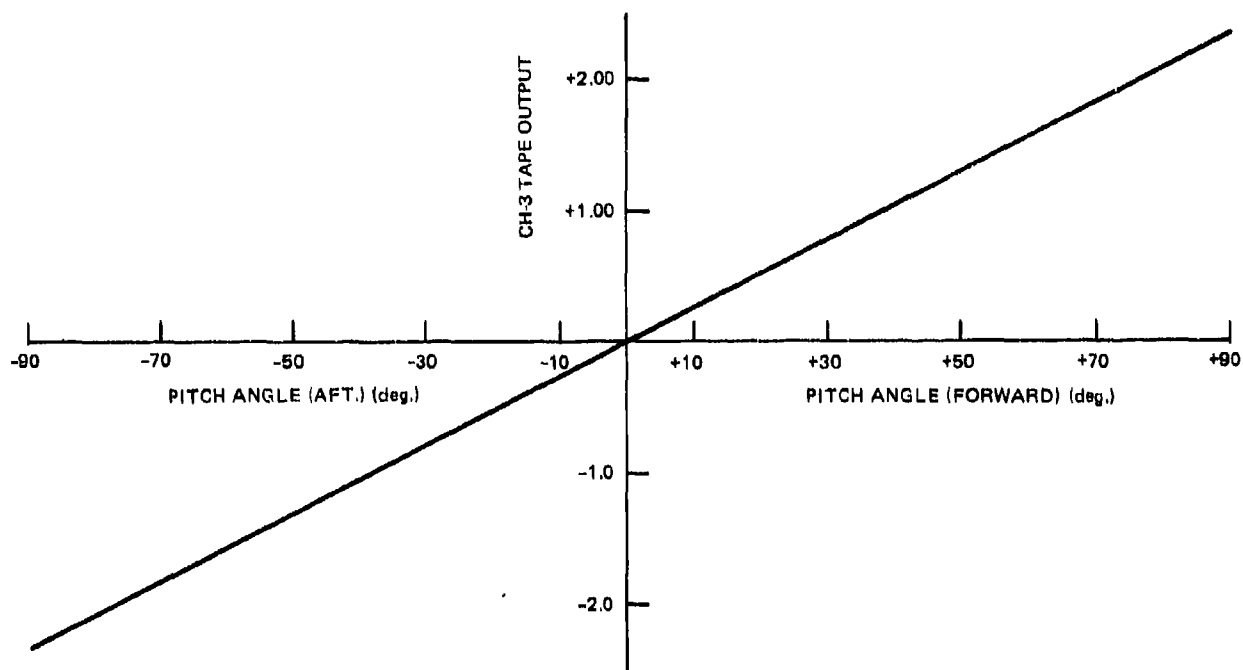


Figure 16. Pitch Calibration.

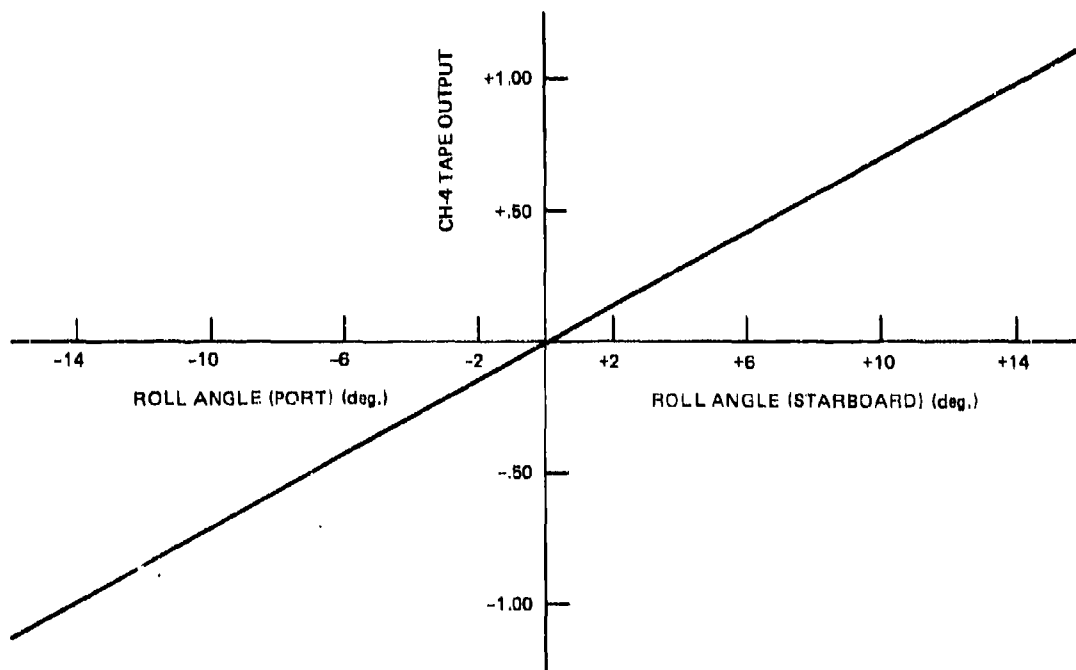


Figure 17. Roll Calibration.

SECTION 4

F(θ) RECEIVER

INTRODUCTION

A multiple scattering medium, such as ocean water, is characterized by the volume scattering function $F(\theta)$ defined as the secondary radiation pattern created by a plane wave traversing a volume sufficiently small that only single scattering occurs. The validity of the link models, ref (1), rests on the scattering model assumed which relates the radiance in the field of a submerged light source as a function of range to the light source, distance off axis, water scattering properties and other optical parameters of the medium and the source itself. The need for quantitative information concerning $F(\theta)$ and the underlying assumption in the model provided the design impetus for this instrument, named for the relation it measures.

The $F(\theta)$ receiver is an underwater synchronous, optical pulse amplitude reading, radiometer. It is positioned relative to the optical axis of a pulsed dye laser, either on axis or at some angle relative to that axis and measures that component of the initially collimated laser output that is scattered into the receiver's field of view.

Some of the equipment's features and specifications are shown in table 1.

Ref (1) Karp, S., "Optical Communications Between Underwater and Above Surface (Satellite) Terminals," IEEE Trans on Comm, COM-24, 66-81 (1976)

TABLE 1

Aperture	3" diameter, f/1.3
Field of view	46 milliradians (in water)
Minimum detectable signal	3.5×10^{-10} w/cm ²
Maximum detectable signal (attenuator in optical path)	7×10^{-3} w/cm ²
Optical bandwidth	100 Å centered at 5240 Å
Detector	RCA PF1023 2" diameter, 10 stage photomultiplier
Detector electrical bandwidth	10 MHz
Output	0-10 V pulse to oscilloscope 0-10 Vdc time averaged peak value to DVM

SYSTEM DESCRIPTION

The $F(\theta)$ receiver shown in figure 1 is composed of two major subsystems, the sensor assembly and the receiver-control panel. They are connected by 150 feet of multiconductor underwater cable. Since both of these subsystems are discussed in detail later in this report, the focus here is on their functions as a unit.

Signal flow and major components are shown in the block diagram in figure 2. Incident light pulses of 75 μ sec width from the experimental dye laser pass through a spectral filter at a rate of 20 per second and are brought to a focus on the faceplate of a photomultiplier by a $f/1.3$, 3-inch-diameter objective lens. A neutral density filter is normally in the optical path immediately preceding the photomultiplier to prevent tube damage and to provide over-range protection. This filter, which has a transmission of 0.1% (density 3), may be switched out of the optical path remotely via the filter position control unit located on the receiver-control panel.

From the photomultiplier, the output pulse passes through a line driver that feeds the shielded coaxial cable connecting the sensor assembly and the receiver control panel. From out of the cable, the pulse is amplified and supplied to an oscilloscope for direct measurement of the instantaneous pulse amplitude.

The same signal available to the scope is routed to the sample-and-hold circuit which outputs a DC voltage proportional to the instantaneous peak value of the input. Following the sample-and-hold, a statistical averaging circuit smooths the pulse-to-pulse fluctuations for monitoring by a digital voltmeter.

To enhance the signal-to-noise ratio, a clock pulse is initiated in the laser circuitry whose leading edge is synchronized with the transmission of the dye laser pulse. The receiver is thus informed as to the location of a possible pulse prior to its arrival. Thus, with the proper delay, the receiver may be switched into the sample mode in time to receive a signal which is optimum relative to the ambient noise. The clock output is also used as a scope sync for viewing the output of the video amp.

SENSOR ASSEMBLY

As mentioned in the previous section, the $F(\theta)$ receiver consists of two major subassemblies, the sensor and the receiver-control. The sensor assembly is, itself, divided into the sensor head and positioning carriage subassemblies.

POSITIONING CARRIAGE SUBASSEMBLY (PCS)

This device shown in figure 3 supports the sensor head underwater and allows it to be positioned relative to the vertically directed beam of the submerged dye laser. The carriage is a 3 foot long section of 7 inch steel channel to which nylon rollers are attached via stainless steel shafts. The track upon which the carriage rides is a 60 foot length of 6 X 6 inches wide flange steel H beam. One end of the beam is located directly over the laser so the receiver may be positioned directly on axis or up to 60 feet off axis.

The sensor head is suspended beneath the track underwater and can be rotated $\pm 80^\circ$ from the vertical in 5° increments. A large protractor is fastened to the carriage in order to indicate the sensor's pointing angle and to provide a convenient clamping mechanism to secure the sensor once it is pointed.

Figure 4 shows the PCS installation.



Figure 1. $F(\theta)$ receiver.

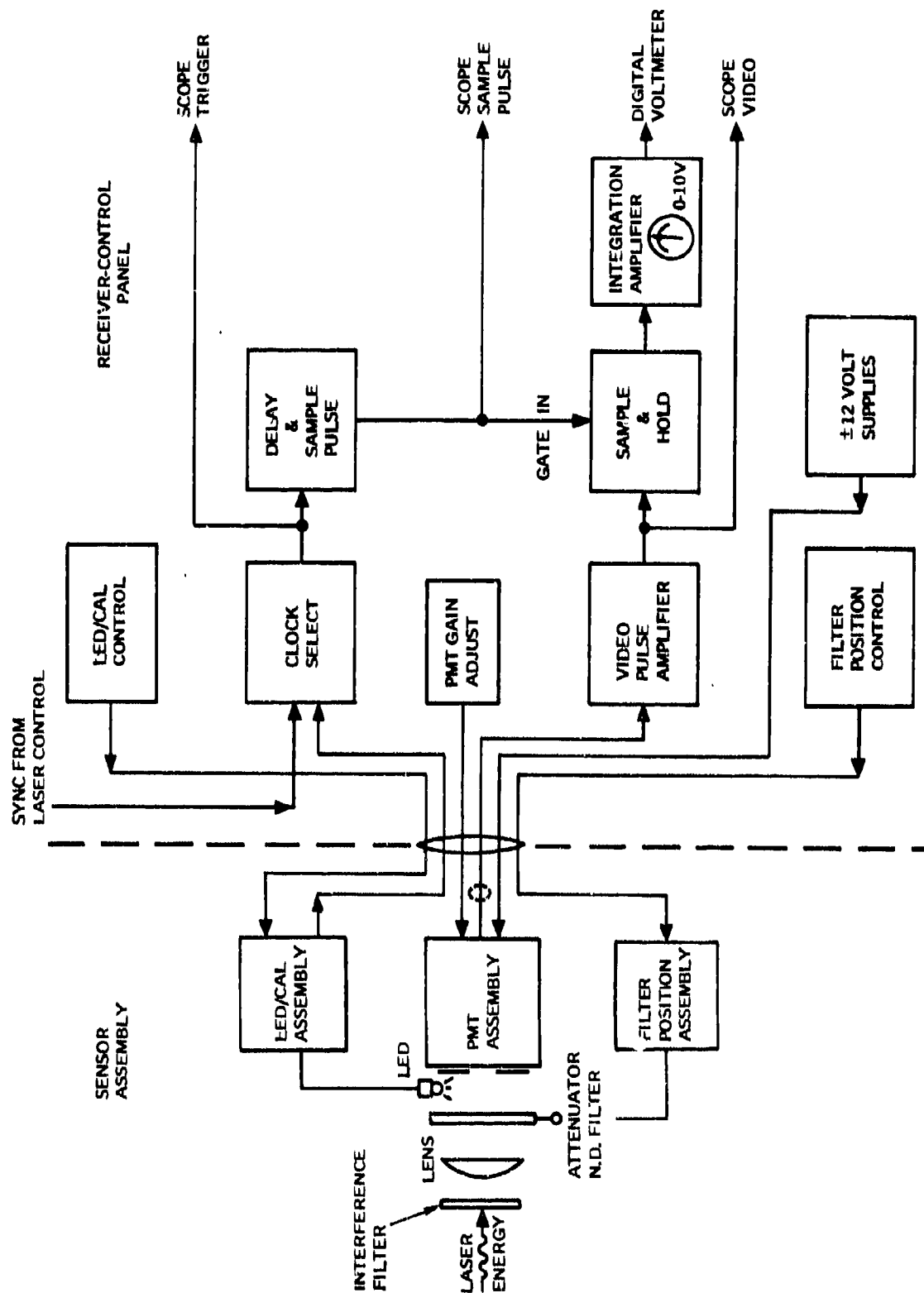


Figure 2. $F(\theta)$ receiver block diagram.

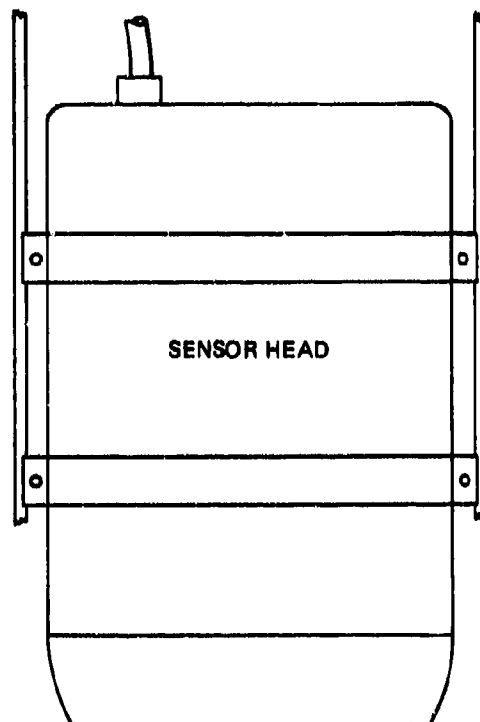
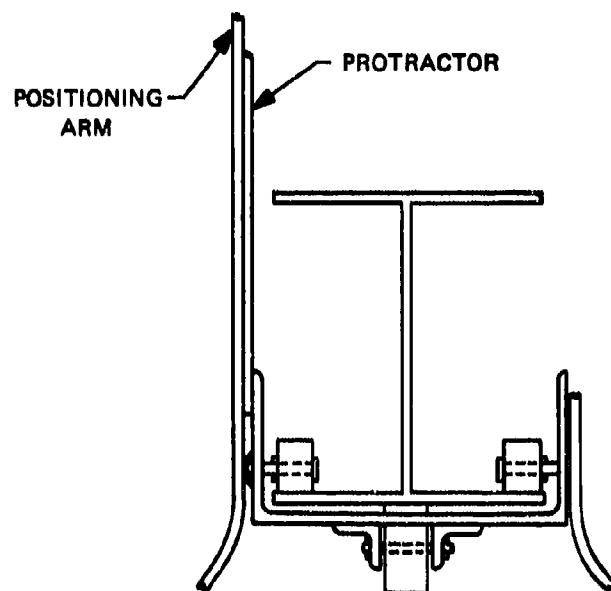


Figure 3. Positioning carriage assembly.



Figure 4. PSC installed.

SENSOR HEAD SUBASSEMBLY (SHS)

The SHS, shown removed from its waterproof canister in figure 5, consists of the collection optics, the photomultiplier assembly, a remote control filter actuator, and a reference light source for system self-check and adjustment.

Light incident on the SHS passes through the canister faceplate and strikes, in turn, a narrowband (100 Å) interference filter, a 3-inch-diameter, f/1.3 objective lens, a removable N.D. filter, a field stop, and the photomultiplier. The photomultiplier is part of an integrated photodetection unit (RCA PF 1023) which contains a 10-stage photomultiplier tube, high voltage power supply, and output pulse amplifier in a single, ruggedized, sealed package. The tube's gain is varied by an external potentiometer and the required input power is ± 12 Vdc, thus removing the need to supply high voltage through a considerable length of cable underwater. The photocathode is an ERMA II which has a peak response at 5000 Å.

Insertion or removal of the neutral density filter (attenuator) from the optical path is accomplished by rotating the filter holder as shown in figure 6. Space requirements precluded the conventional motor-driven filter wheel normally used for this purpose. Instead, a linear actuator of the type used in radio-control model airplanes was adapted to position the filter. A 5-volt pulse initiated by the operator at the control panel drives the actuator to either extreme. Limit switches at the position extremes light LED position indicators on the control panel so that the filter status (i.e., in or out) is available to the operator.

Also located in the SHS is the reference source, an LED which is activated and pulsed from the control panel. This feature permits a known amount of pulsed radiation to be received by the instrument for checking system gain and verifying general system performance when the sensor is underwater or otherwise inaccessible.

Construction of the SHS is simple and rugged, consisting of four Micarda discs, fastened together with three 1/4-20 threaded rods. This assembly is press fit into a cast aluminum underwater strobe canister which is penetrated by a packing gland for passage of the multiconductor interconnection cable. The cable contains ten No. 22 AWG conductors and two 75 ohm shielded coax for signal. The entire assembly is 20 inches long, 9-1/2 inches in diameter and weighs approximately 35 pounds.

RECEIVER-CONTROL PANEL

This unit contains the synchronous receiver circuits, the instrument control electronics and system power supplies. All routine commands to the sensor assembly originate here, as well as the monitoring of all phases of the F(0) experiment operation.

SYNC RECEIVER

Operation of the synchronous receiver is initiated by a signal generated in the dye laser control electronics, indicating the laser is about to be fired. This signal triggers a monostable multivibrator whose time constant is approximately 5 microseconds. This delay pulse allows the laser pulse to be sensed by the photomultiplier, sent up the cable, and amplified by the video pulse amplifier before the receiver is gated on. The trailing edge of the delay pulse fires a second monostable which generates an 11 microsecond "sample" pulse. This pulse switches a .01-mfd capacitor into the output of an operational amplifier driven by the peak value of the received laser pulse. The capacitor-op amp combination is in the sample-and-hold circuit

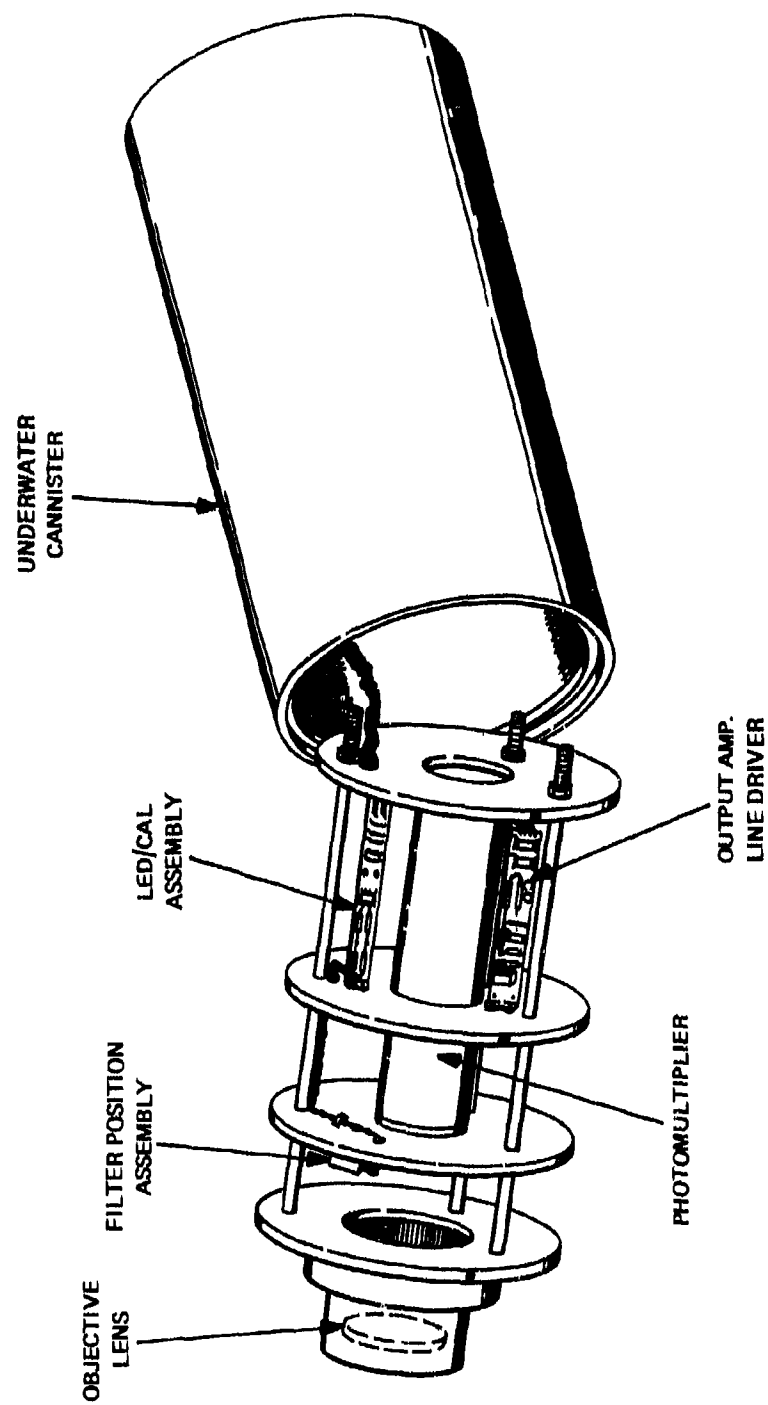


Figure 5. $F(\theta)$ sensor head subassembly.

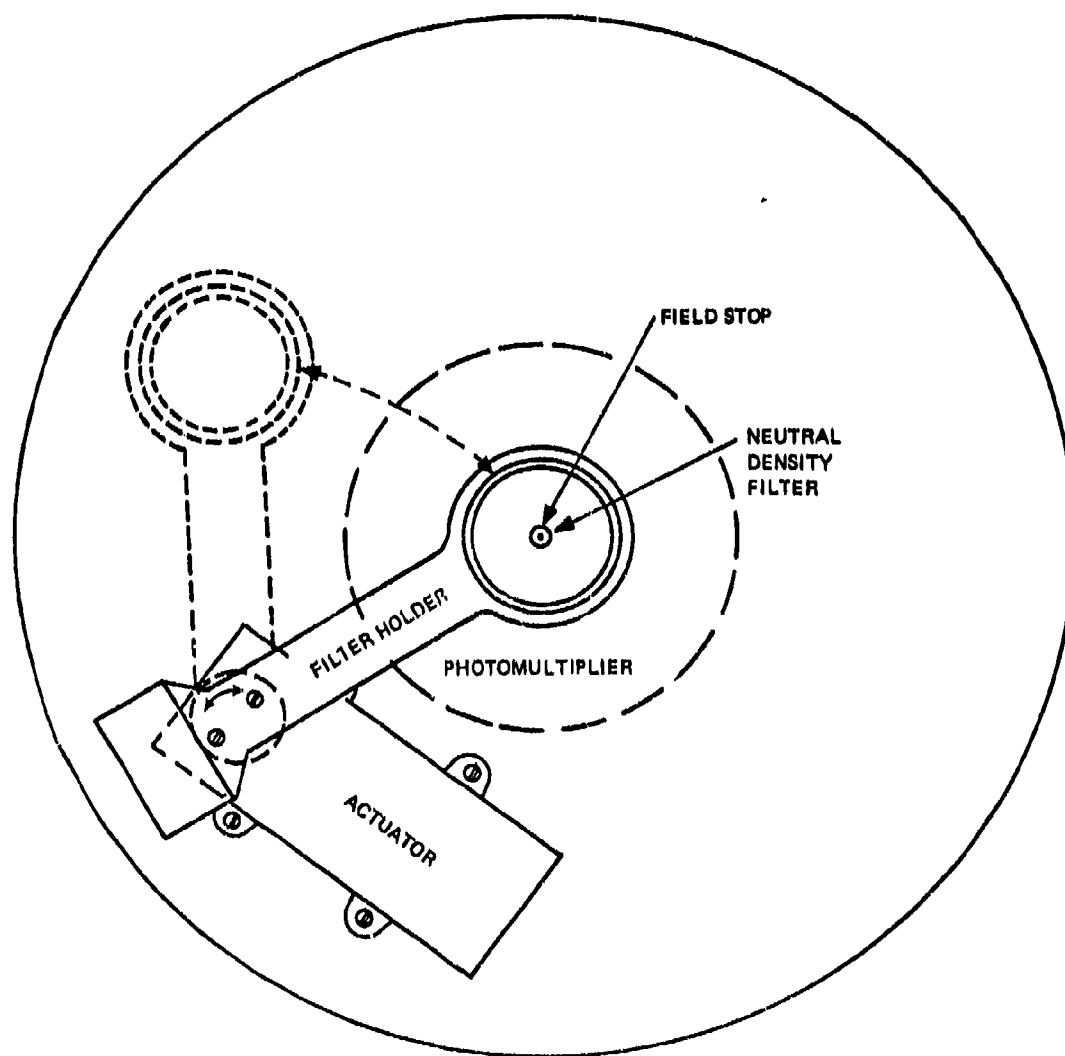


Figure 6. Filter position assembly.

whose output is switched to the integration amplifier by the trailing edge of the sample pulse. The integration amp has a long time constant (5 seconds), enabling the average of approximately 100 laser pulse peaks to drive a meter movement on the panel or a digital voltmeter.

CONTROL FUNCTIONS

The functions controlled by the Receiver-Control Panel include photomultiplier gain and input power, attenuator filter position and the calibration LED.

The photomultiplier is powered by positive and negative 12 volts. According to RCA, these voltages must be applied simultaneously or possible damage to the unit may occur. Accordingly, a voltage sensor/protection circuit employing an "and" gate and a capacitive delay assures that both voltages are present for at least 3 seconds before application to the photomultiplier via relay. If either supply fails, the output of the "and" gate will be insufficient to keep the relay energized and power will be removed from the detector.

A feature of the photomultiplier assembly is its remote gain programming capability. A lead is brought out of the assembly and connected to ground through a resistor in the range 0 to 10K with the gain inversely proportional to the resistance. In the receiver-control panel this lead is connected to one of three (lo, med, hi) resistors via the GAIN SELECT switch.

As indicated in the description of the sensor assembly, the filter position assembly is controlled from the filter position control unit in the receiver control panel. The control unit supplies power (4.4 Vdc) to the filter actuator as well as a 5-volt, 2-millisecond pulse that drives the actuator from one extreme to the other. Also included in the filter position control unit are the status indicators that inform the operator whether the filter is in or out of the optical path. These indicators are LEDs connected to micro switches located at the extremes of the filter holder's travel.

The final control function performed at the receiver-control panel is the operation of the internal calibration and self-check LED located in the sensor head. By switching into the calibrate mode, power (+5 Vdc) is applied to the LED driver circuit and to the "clock select" relay (+15 Vdc). The LED driver consists of free-running oscillator operating at 3 KHz, a monostable multivibrator and several voltage followers. The oscillator sets the pulse repetition rate and provides the sync for the receiver through the "clock select" relay. Pulse width is determined by the monostable multivibrator and is set at 1 microsecond to simulate the laser pulse. To further enhance the simulation of the laser pulse, the monostable output is routed to a voltage follower which provides a gaussian pulse shape at its output. This pulse becomes the driver for the calibration LED whose output is detected by the photomultiplier and fed back into the receiver for operator monitoring.

CALIBRATION

The $F(\theta)$ receiver produces a voltage at its output in response to the received optical power density which in turn can be related to source radiance. The determination of this response in absolute radiance and irradiance units is the purpose of this calibration.

The approach taken in this work is to first establish a single absolute irradiance response value. Next, a family of curves is plotted depicting the receiver's response at all gain settings. The absolute irradiance value then becomes a point on this calibration chart relating all the remaining points in absolute terms. Finally, from data developed in the calibration the absolute radiance is calculated and entered on the calibration chart.

Since the $F(\theta)$ receiver and the field experiment dye laser form a source-detector pair in the field, the dye laser is a natural choice for the optical calibration source. As shown in figure 7, the laser beam is injected into an integrating sphere transforming the beam into a Lambertian source which at a "large" distance approaches a point source. The minimum distance required for this condition to be satisfied is taken to be one hundred times (100X) the radius of the integrating aperture, or 6-1/4 feet.

To establish an absolute irradiance response value it is necessary to fix a value of incident irradiance at the receiver (H_R). However, direct measurement with available laboratory equipment (EG&G 480 spectroradiometer) is not possible in most cases due to insufficient sensitivity of the spectroradiometer. Since the calibration source has been configured to provide a point source, the emerging power density (H) obeys an inverse square law. Thus, we may measure irradiance directly at a point closer to the source (H_P) where values exist within the spectroradiometer's range. The inverse square fall-off is then exploited to compute incident irradiance at the receiver.

Having thus found a value for H_R , the resulting voltage at the output of the receiver is plotted. The remainder of the response data is obtained by attenuating the incident irradiance in known increments with neutral density filters. This procedure is repeated for each gain setting.

Assuming a point source, the radiation of that source can be computed by dividing the irradiance received by the acceptance solid angle of the receiver. The computation of this scale on the calibration chart, figures 8a and 8b, completes the calibration.

ABSOLUTE IRRADIANCE

Referring again to figure 7, the EG&G 480 was located 9.77 feet from the sphere. The calibration was conducted in a long windowless hallway and the apparatus baffled to control extraneous light.

During the course of the calibration, periodic measurements of the source's flux density were taken with no detectable variation indicating the pulse-to-pulse variation in the laser did not exceed the 10% absolute accuracy of the spectroradiometer. The measured value of the irradiance at the receiver (H_R) was

$$2.42 \times 10^{-4} \text{ W-cm}^{-2} \left[\frac{9.77}{98.0} \right]^2 = 2.4 \times 10^{-6} \text{ W-cm}^{-2} \quad (1)$$

The uncertainty inherent in this measurement arises primarily from pulse-to-pulse variation in the laser and the accuracy of the EG&G 480. Both are specified at $\pm 10\%$. The third component of this error budget is introduced in the output voltage measurement. This is the uncertainty in reading the oscilloscope, generally accepted at $\pm 5\%$. Taking the rms value of these three contributions yields an overall uncertainty of

$$\left[(10)^2 + (10)^2 + (5)^2 \right]^{1/2} = \pm 15\% \quad (2)$$

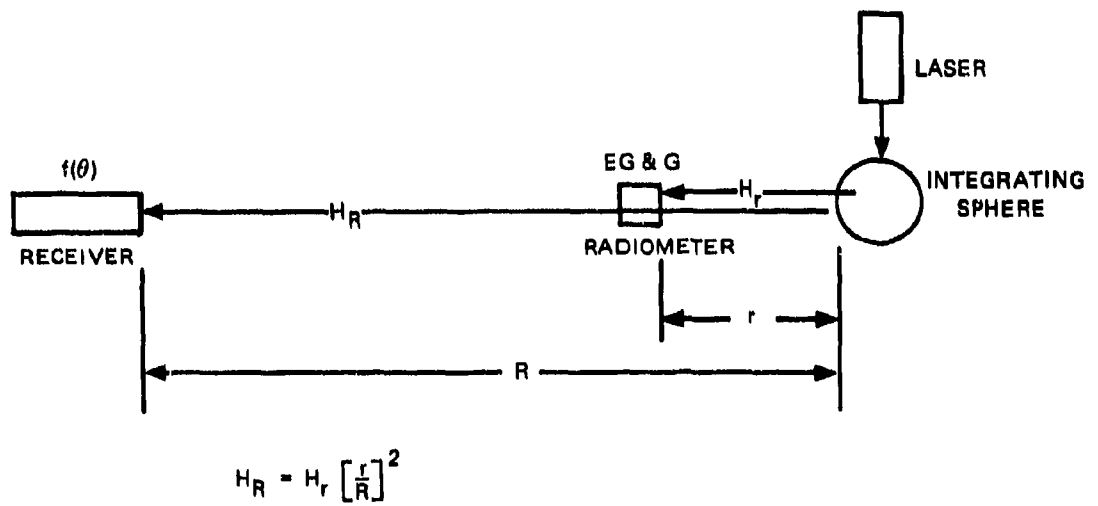


Figure 7. $F(\theta)$ receiver calibration.

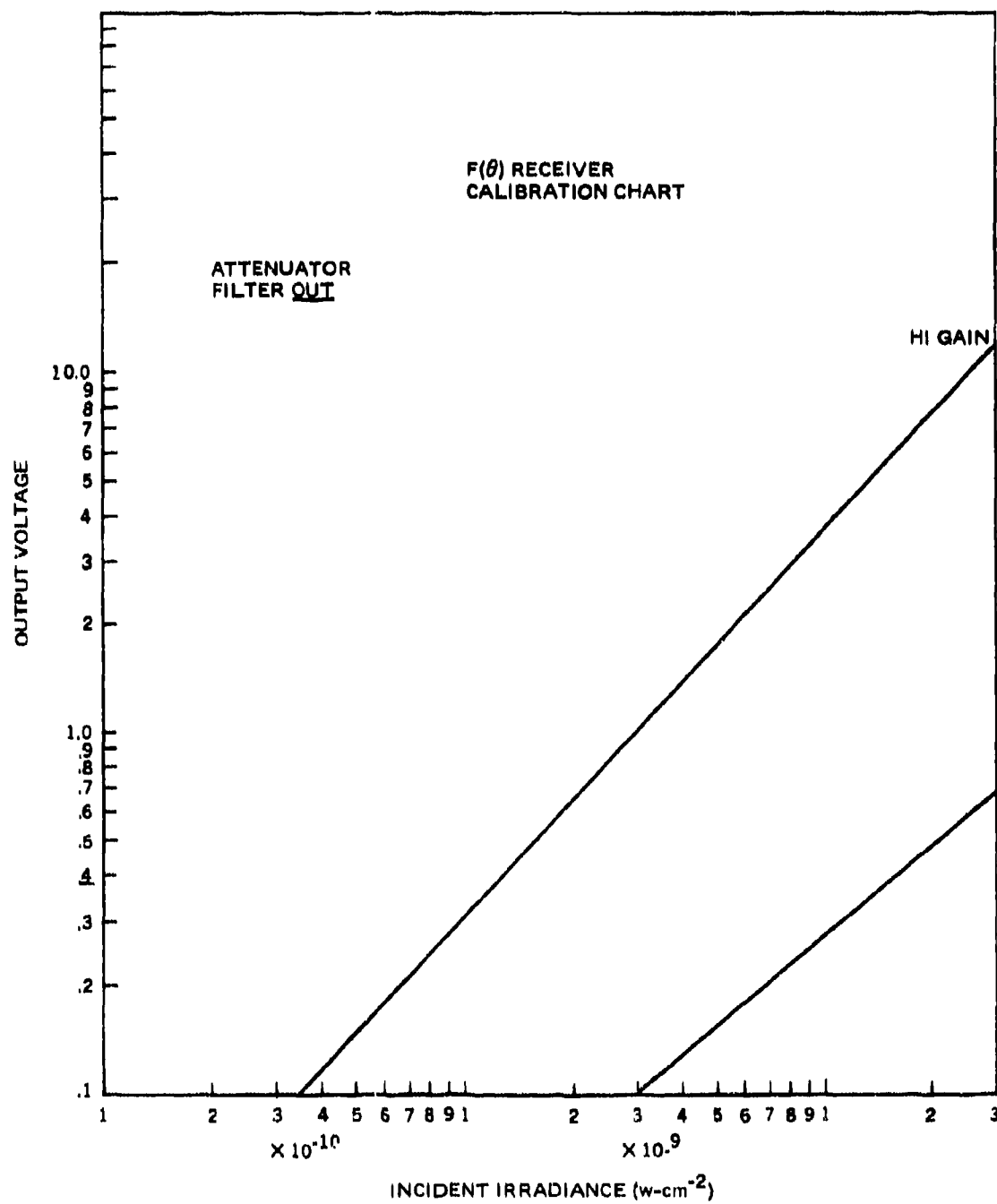


Figure 8A. F(θ) receiver calibration chart.

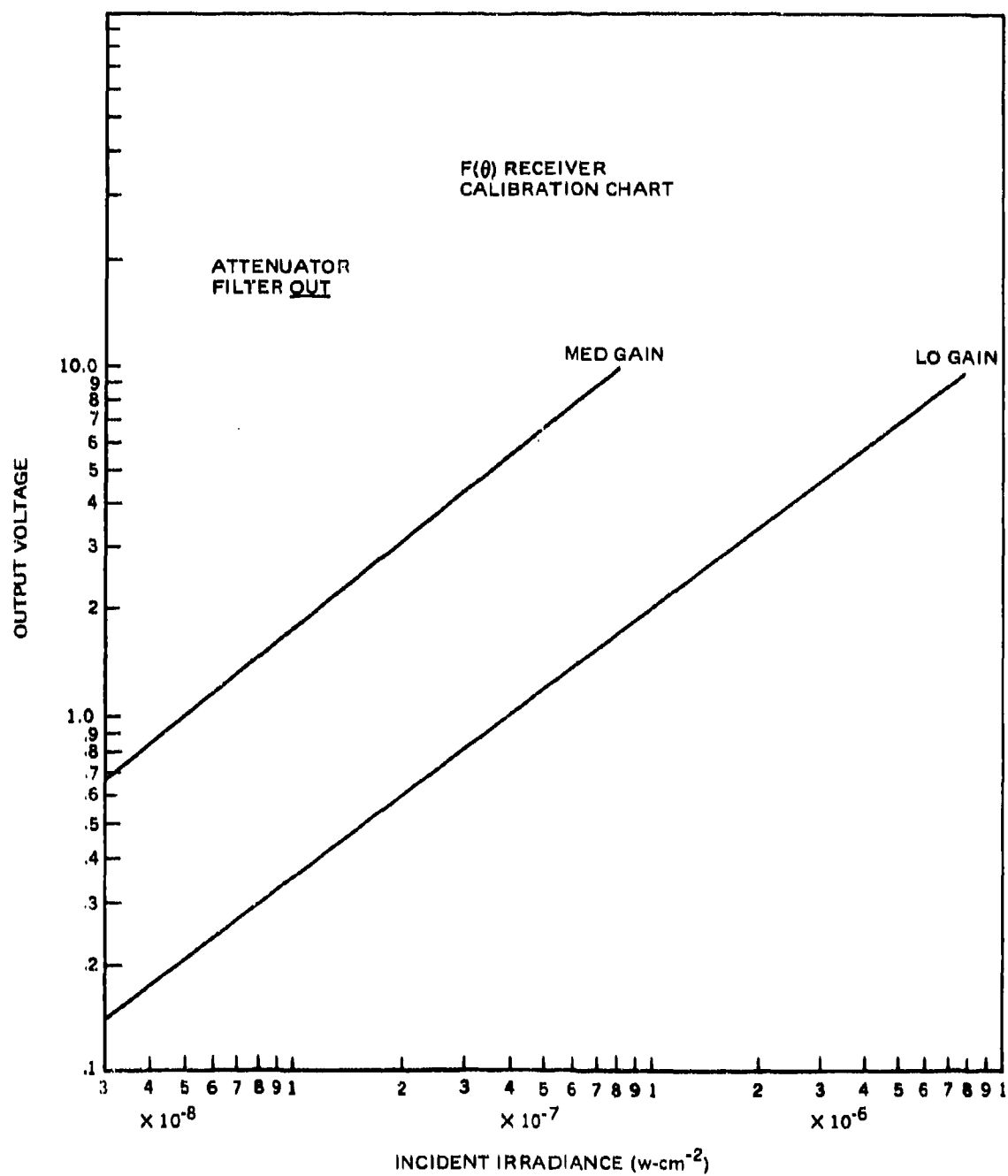


Figure 8B. F(θ) receiver calibration chart.

Data was taken with the receiver in the Lo Gain position and the 0.1% (Density 5.0) transmission Attenuator filter out of the optical path. The measurement was repeated twice with the following results:

Irrad. at receiver	receiver output	accuracy
$2.4 \times 10^{-6} \text{ W-cm}^{-2}$	4 volts	$\pm 15\%$

RECEIVER RESPONSE

The dynamic response of the $F(\theta)$ receiver was investigated by allowing successively weaker irradiance values to illuminate the receiver and charting the resulting output voltages. Data was taken on several gain settings for the same irradiance wherever possible.

The irradiance was controlled by inserting neutral density (attenuating) filters in the optical path near the source. The data was normalized to a receiver output of 4 volts and displayed in table 2.

TABLE 2. $F(\theta)$ RECEIVER DYNAMIC RESPONSE

Filter Density	Rel. Irrad.	Irrad.	Output Voltage		
			Lo Gain	Mod Gain	Hi Gain
	1.0	$2.4 \times 10^{-6} \text{ W-cm}^{-2}$	4 volts		
.3	0.5	1.2×10^{-6}	2.5		
1.0	0.1	2.4×10^{-7}	0.7	4	
1.3	5×10^{-2}	1.2×10^{-7}	0.4	2	
2.0	1×10^{-2}	2.4×10^{-8}	0.12	0.6	10
2.3	5×10^{-3}	1.2×10^{-8}		0.3	4.4
3.0	1×10^{-3}	2.4×10^{-9}			0.74
3.3	5×10^{-4}	1.2×10^{-9}			0.4

Density 3 Attenuator filter out

When the density 3 Attenuator noted above is rotated to the in position, all irradiance values are multiplied by 10^3 . This situation is shown in figures 9a and 9b.

FIELD OF VIEW

The $F(\theta)$ receiver contains a circular field stop located immediately in front of the multiplier phototube that determines the field of view of the instrument. If the field stop has diameter d and the receiver a focal length f , the FOV in air is given by

$$\text{FOV} = d/f = .14/4.0 = .035 = 35 \text{ milliradians} \quad (3)$$

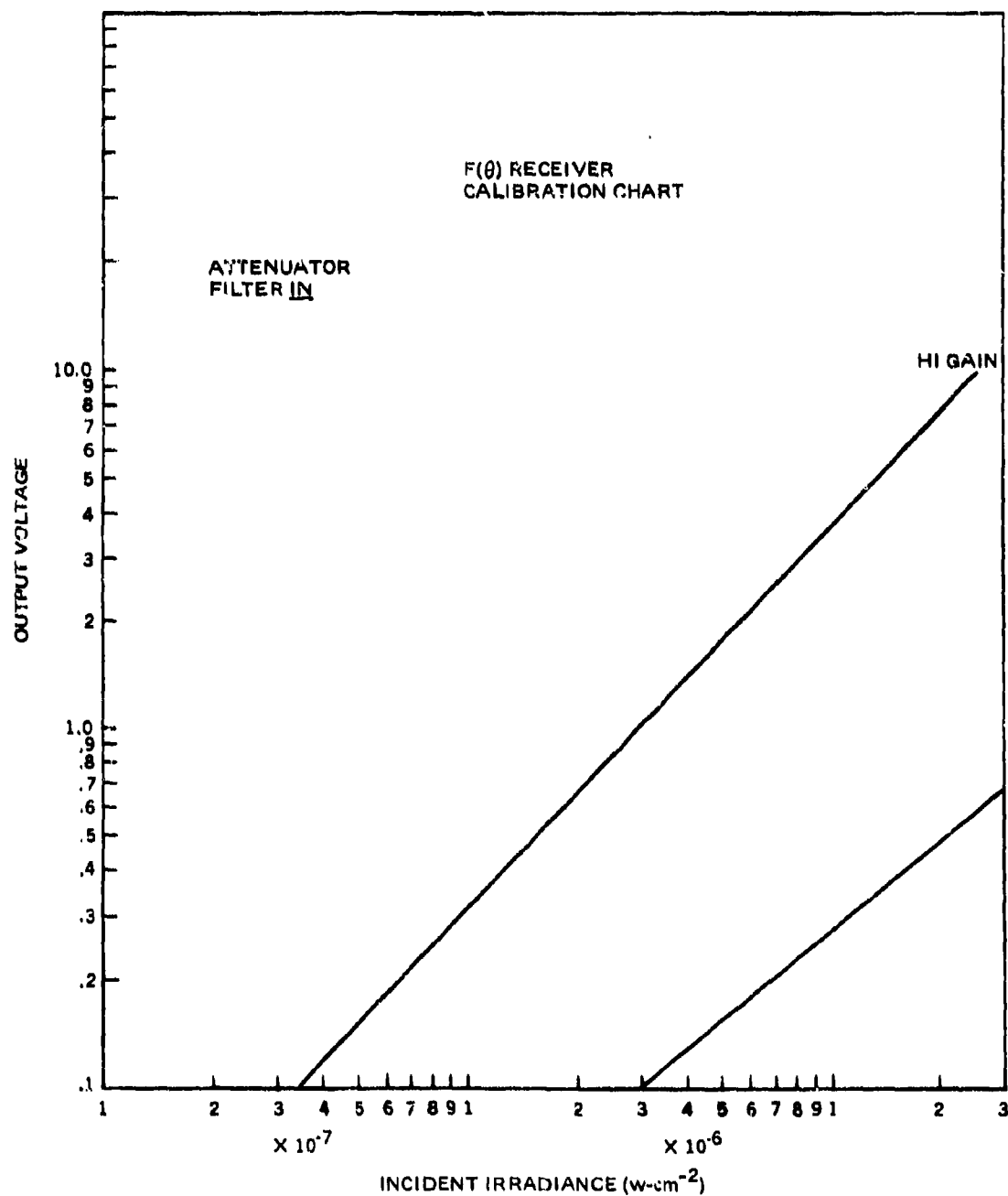


Figure 9A. F(θ) receiver calibration chart.

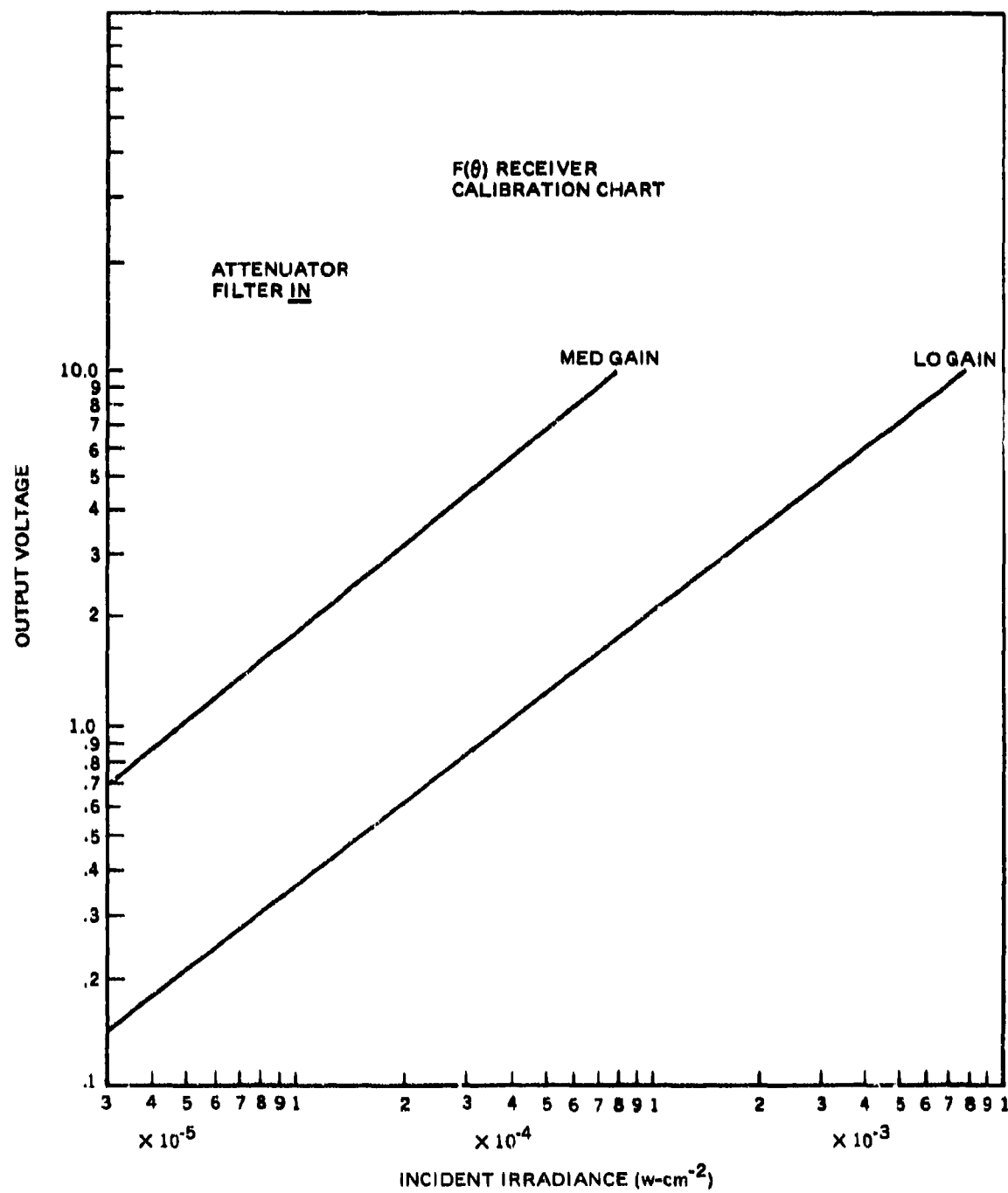


Figure 9B. F(θ) receiver calibration chart.

In water, the FOV is modified by the water's index of refraction or 1.33 the value of air. Thus, in water we have

$$\text{FOV}_{\text{water}} = 1.33 (35 \text{ mr}) = 46 \text{ mr} \quad (4)$$

In both cases, the FOV is circular.

ABSOLUTE RADIANCE

From the absolute irradiance data determined in this calibration and the calculated FOV, absolute radiance response can be determined. As the $F(\theta)$ receiver was used to map the radiance distribution of a submerged source, the $\text{FOV}_{\text{water}}$ is used.

From the FOV we obtain the solid acceptance angle as

$$\Omega_{\text{water}} = \frac{\pi[\text{FOV}]^2}{4} = 1.66 \times 10^{-3} \text{ sr} \quad (5)$$

Now radiance values are obtained by dividing the irradiance data by Ω_{water} . The results are shown in table 3, figures 10a, 10b, 11a, and 11b.

TABLE 3

irrad. (W/cm^2)	$\Omega(10^{-3} \text{ sr})$	Attenuator out rad. ($\text{W}\text{-cm}^{-2}\text{sr}^{-1}$)	Attenuator in rad. ($\text{W}\text{-cm}^{-2}\text{sr}^{-1}$)
2.4×10^{-6}		1.4×10^{-3}	1.4
1.2×10^{-6}		7.2×10^{-4}	.72
2.4×10^{-7}		1.4×10^{-4}	.14
1.2×10^{-7}		7.2×10^{-5}	7.2×10^{-2}
2.4×10^{-8}		1.4×10^{-5}	1.4×10^{-2}
1.2×10^{-8}		7.2×10^{-6}	7.2×10^{-3}
2.4×10^{-9}		1.4×10^{-6}	1.4×10^{-3}
1.2×10^{-9}		7.2×10^{-7}	7.2×10^{-4}

SPECTRAL FILTER

The $F(\theta)$ receiver is equipped with a spectral filter to reduce background radiation. It has no effect on the calibration, however, since its bandwidth is larger than the calibration source and all measurements are referenced to a plane in front of the filter, i.e., incident radiation.

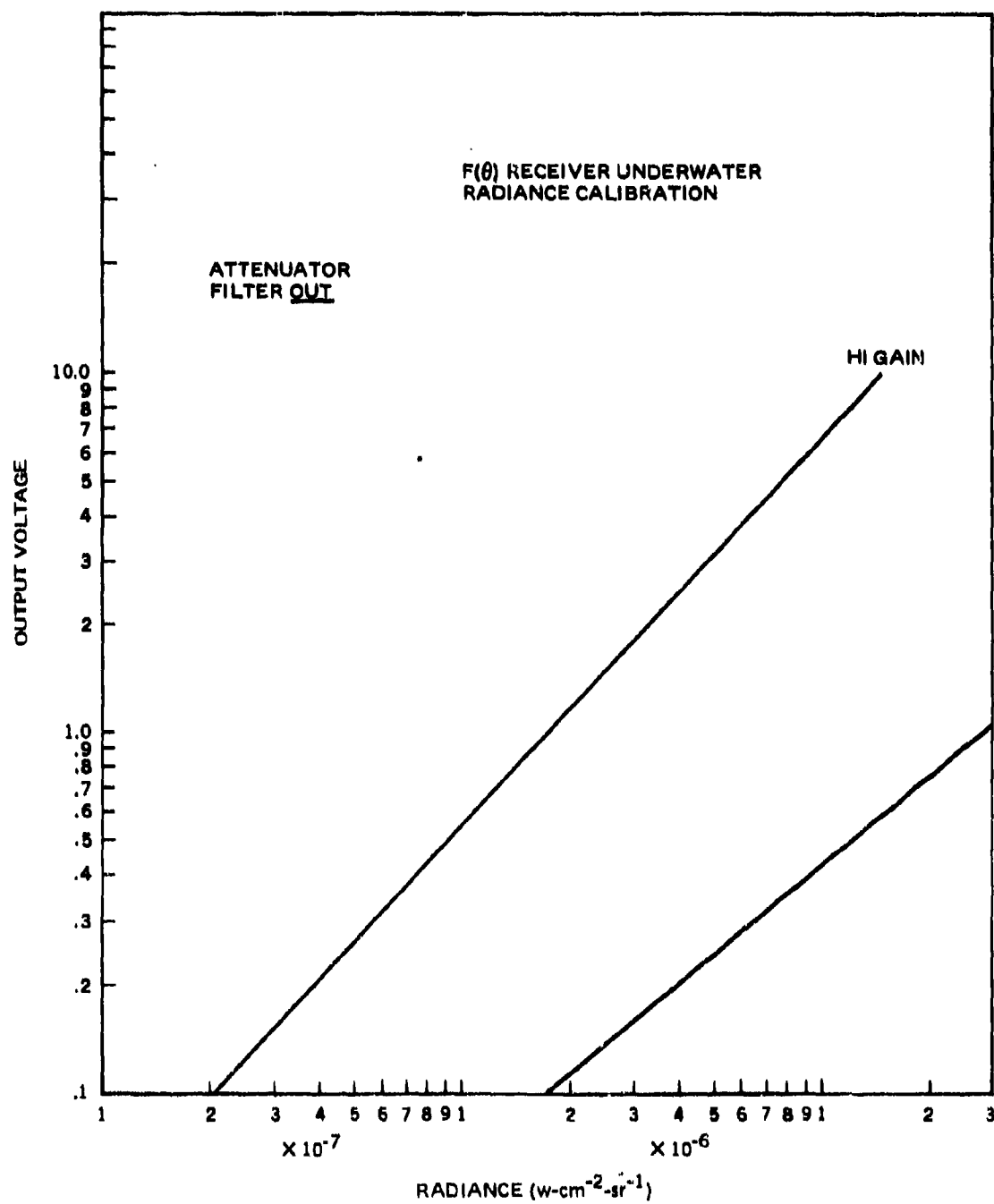


Figure 10A. F(θ) receiver underwater radiance calibration.

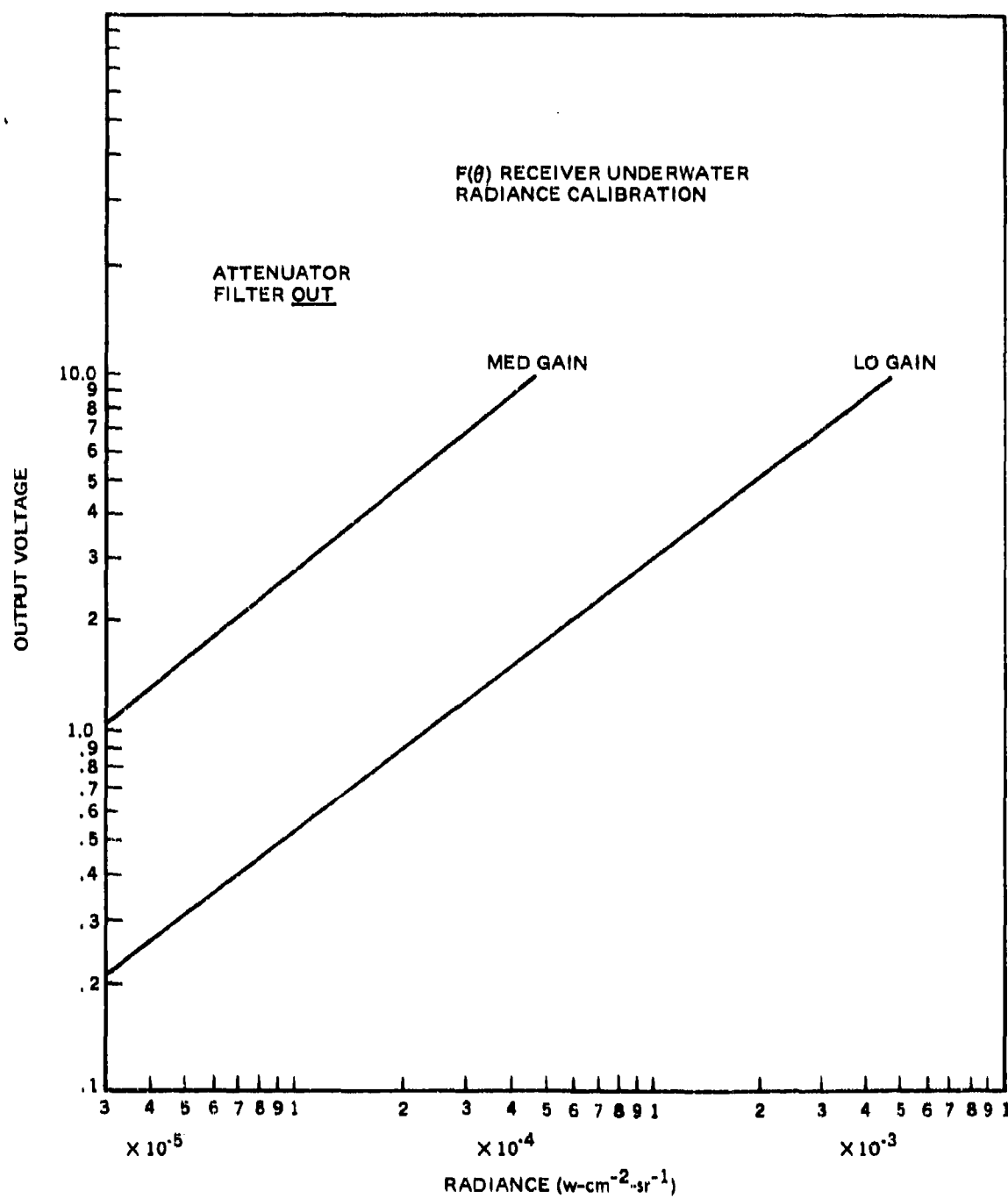


Figure 10B. F(θ) receiver underwater radiance calibration.

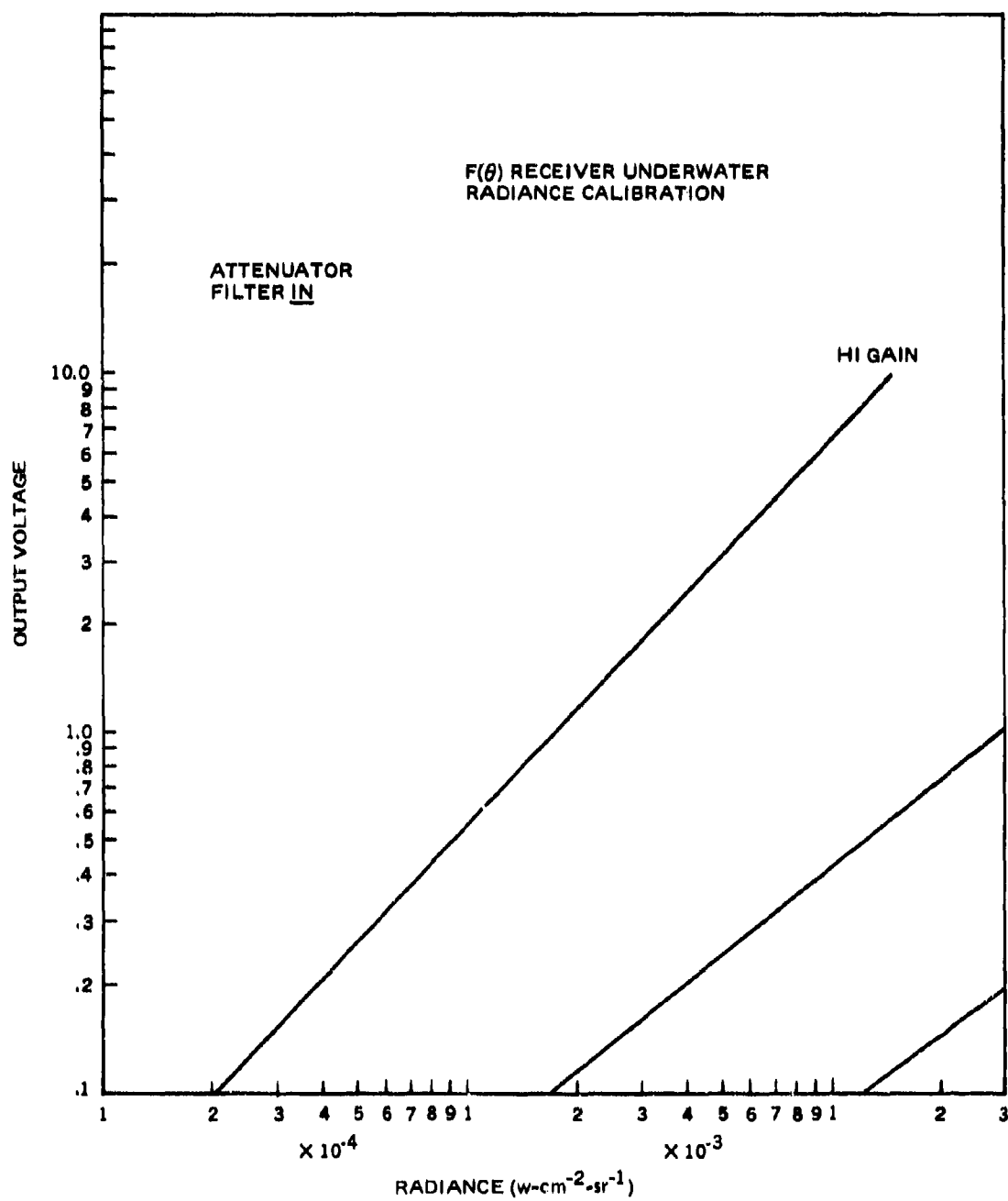


Figure 11A. F(θ) receiver underwater radiance calibration.

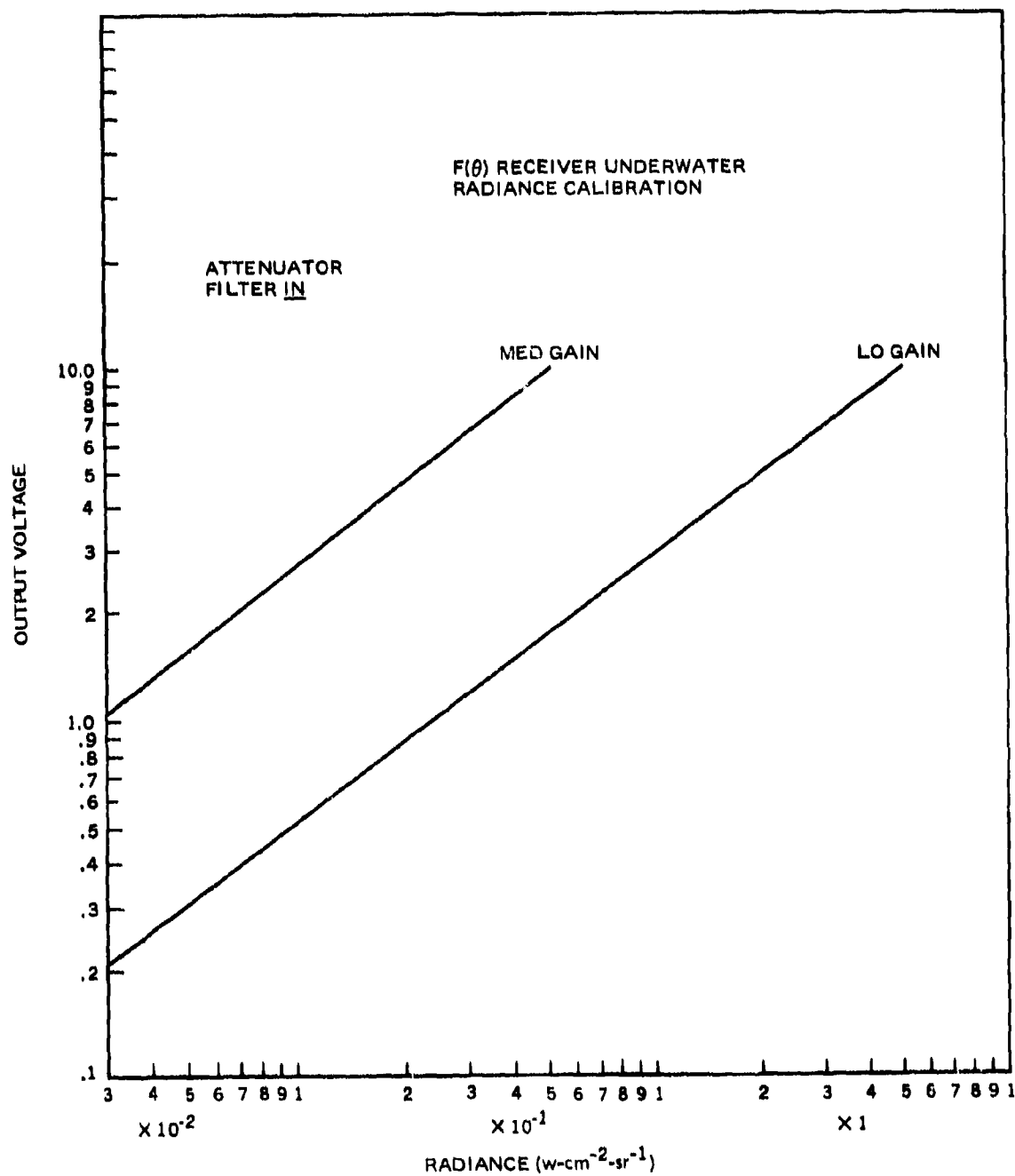


Figure 11B. F(θ) receiver underwater radiance calibration.

SECTION 5

AN INSTRUMENT FOR THE MEASUREMENT OF SPECTRAL ATTENUATION COEFFICIENT AND NARROW ANGLE VOLUME SCATTERING FUNCTION OF OCEAN WATERS

Abstract

A new instrument has been developed for the study of those optical properties of ocean water that affect the transmission of image-forming light. The instrument performs simultaneous measurements of the volume attenuation coefficient and the volume scattering function at three angles. Any of ten wavelengths covering the spectral range from 400 to 670 nanometers may be used. A depth capability of 500 meters permits the examination of water below the euphotic zone and of the bottom waters on the continental shelf. The considerations leading to the design of the instrument, its capabilities and the unique features it incorporates are discussed. Some examples of the data obtained with the instrument are presented.

Introduction

The study and solution of visibility and image transmission problems requires information regarding the optical properties of ocean water for various geographical areas and water depths. The present state of our knowledge of these properties has been severely restricted by the type and capability of the instrumentation that has been available. Visibility and image transmission through water is affected by the optical processes of absorption and scattering. Therefore, measurements of the medium are required from which the significant factors of the absorption and scattering properties can be derived. Generally, both vary with the wavelength of the radiation involved, with geographical location, with depth, and with time. It is essential, therefore, that the measurements be obtained rapidly over the spectral region of interest and over the volume of water of concern in order that a complete and quasi-instantaneous assessment of these properties can be obtained.

Recent studies of near-surface data from stable, well-documented water confirm that a reasonably precise estimate of the total scattering coefficient, s , can be obtained if the volume scattering function (VSF), $\sigma(\theta)$, is known at a suitably small angle from the direction of propagation. As a result of this, the absorption coefficient, a , may be determined from a knowledge of the volume attenuation coefficient, α , and the VSF $\sigma(\theta)$ since $\alpha = s + a$. Thus a single instrument capable of measuring α and $\sigma(\theta)$ at a number of wavelengths in rapid succession would satisfy the requirement for simultaneous spectral data on the absorption and scattering properties of ocean waters of interest. The validity of the correlation between $\sigma(\theta)$ and s for near-bottom waters, where the scattering material may differ in important respects from that found in surface waters, has not yet been verified. We expect from theoretical considerations and from our evaluation of the nature of the near bottom scattering material that a satisfactory relationship between $\sigma(\theta)$ and s will be found to exist.

On this premise, the Visibility Laboratory has developed an instrument to perform the simultaneous measurement of the beam transmittance, T , (from which a may be obtained) and the VSF at three small angles. This instrument when used in conjunction with the Visibility Laboratory general angle scatter meter** capable of measuring the VSF from 10° to 170° can obtain values of $\sigma(\theta)$ over a range of angles large enough to allow the computation of s directly from the relationship,

$$s = 2\pi \int_0^\pi \sigma(\theta) \sin\theta \, d\theta \quad (1)$$

If the expected correlation between $\sigma(\theta)$ and s is found in bottom water below the euphotic zone, we may proceed with confidence to utilize this single instrument, measuring Alpha and volume SCATtering function (hence the acronym ALSCAT), for the evaluation of those optical properties of near-bottom water which are important for the assessment of the operation of underwater viewing systems.

Design Objective and Specifications

This section will provide a brief description of the important functional specifications of the instrument. It will also serve as an introduction to the instrument and some of the concepts used in its design. Additional background and details will be provided in later paragraphs.

General Description

The instrument system consists of four components:

1. An underwater unit measuring beam transmittance, volume scattering function, water temperature, and instrument depth.
2. A special cable with strain member (two lengths, 400 foot and 2000 foot, the latter for use on an existing winch).

* The work described was performed with support provided by the Defense Advanced Research Projects Agency under ARPA Order 2431.

** Developed with support provided by the Naval Air Development Center under Contract N62289-71-C-0076.

3. A deck unit for topside digital signal conditioning, data display, and functional control of underwater unit.
4. A data recording unit with a 21-column digital data printer, an incremental magnetic tape data recorder and an x, y, z plotter.*

The maximum design operating depth is 500 meters (1640 feet). The cable strength is adequate to support the instrument and 2000 feet of cable in water with normal acceleration forces.

Vertical profiles of transmittance, volume attenuation coefficient, volume scattering function, and water temperature may be obtained at a rate of about 30 meters per minute or 14 minutes for a 500-meter profile (neglecting wire angle effects). Faster payout and retrieval may be possible depending upon the gradients of the variables, the system time constants, and the desired accuracy.

Optical Measurements

All optical measurements may be made at any of 10 wavelengths selectable by command from the surface. The wavelength is determined by interference filters having half power bandwidths of 12.3 nanometers or less and nominal center wavelengths of 400, 430, 460, 490, 520, 550, 580, 610, 640, and 670 nanometers.

The water path length may be changed from 1/2 meter to 2 meters in 1/2-meter increments by means of spacers installed between the projector and receiver.

Collimated projector and receiver optical systems are used. The projector uses a 15-watt tungsten lamp generating a beam 9.33 millimeters in diameter having a divergence of 0.5 milliradians (half angle in water). The lenses in the projector and receiver are plano-convex achromats specially fabricated for this instrument.

A portion of the flux from the lamp is carried directly to the receiver by a fiber optic light pipe. This flux, which is unaffected by the characteristics of the water path, serves as a continual reference signal to enable the system to compensate for fluctuations in the lamp output and/or receiver sensitivity.

The receiver acceptance half angle is 1.5 milliradians in water for the transmittance measurement. The receiver aperture stop for transmittance is 20 millimeters in diameter. The receiver field of view and aperture stop diameter are changed for the three volume scattering function (VSF) measurements. The nominal measurement angles (in water) over which the VSF is measured are 3, 6, and 12 milliradians. For path lengths 1 meter and shorter all three VSF measurements can be made. With a water path length of 1.5 or 2 meters, only the 3 and 6 milliradian measurements can be made due to restrictions created by the 50 millimeter maximum receiver aperture diameter.

Pressure/Depth Measurement

Instrument depth is determined by a bonded strain gage pressure transducer having a range of 0-750 psia and a terminal linearity of ± 0.15 percent of full scale output. The transducer will withstand pressures of 150 percent of full scale without affecting performance characteristics and in excess of 250 percent of full scale before bursting.

The transducer output is amplified to obtain a scale factor of 1 volt per 100 meters of instrument depth (i.e., 5 volts for maximum depth of 500 meters). The digital data transmission link has a resolution of 0.01 volts, corresponding to an effective depth resolution of 1 meter. The transducer linearity limits the direct loading accuracy to ± 0.8 meters. An alternate range of 0-200 meters may be selected from the control panel. This selection increases the gain in the underwater instrument by a factor of 10 with a resultant depth resolution of 0.1 meters. As the accuracy in this case is limited by the basic transducer, no improvement in absolute accuracy is realized.

Temperature Measurement

Water temperature at the depth of the instrument is sensed by a precision platinum resistance thermometer. The sensor resistance changes approximately 1.8 ohms per degree Celsius with a repeatability of $\pm 0.03^\circ\text{C}$. The sensor time constant in agitated water is 1.6 seconds or less.

The temperature response of the sensor system is 1 volt per 10°C on the topside temperature display and recording. The range of temperatures which the sensor system can handle exceeds the requirements for ocean measurements. The time constant of the thermometer probe requires that the rate of instrument lowering or retrieval be reduced for those portions of the water column where there is a marked thermocline if the full temperature accuracy is to be achieved.

Digital Data and Command Transmission System (DIDACTS)

This system provides for the transmission of digital addresses and commands from the surface control unit to the various underwater sensors (downlink) and for the transmission of digital data from the underwater sensors to the surface for display and recording (uplink).

The underwater portion of DIDACTS will handle up to eight analog input channels (± 10 volts full scale). As any of these channels is addressed by the surface unit, its analog voltage is multiplexed into a bi-polar analog-to-digital converter. The digital data along with the status and address of the channel are sent to the surface via the twisted pair data transmission line in the underwater cable. Upon receipt of the digital information, the surface unit stores and displays the data and status information. It then initiates

* The data logger was constructed with funds provided by another contract, but it is compatible with the recording requirements of ALSCAT and it will be used with this instrument.

the cycle for another channel by sending down to the underwater unit the appropriate address and any digital command for a change in status of the underwater unit. The time required to complete the interrogation of a channel is 7.83 milliseconds. As seven channels are currently being used, each channel is sampled 18.21 times per second. This data rate is in excess of that required to accurately record any of the variables.

The capability is provided to address any one or any combination of the eight data channels in sequence. Only those so addressed will be interrogated.

A 4-bit command word is associated with each channel. These digital commands are transmitted to the underwater unit with each cycle of the DIDACTS where they are placed in a storage register. If the status of the U/W controlled function (e.g., wavelength filter wheel position, photomultiplier tube high voltage setting, chopper motor speed setting, or scale factor for depth measurement) is not in agreement with the command, a digital comparator senses this and initiates a sequence of changes until the status agrees with the command. The digital condition of the status generator associated with each controlled function is placed in the underwater shift register and sent to the surface where it may be displayed and recorded along with the data. If the command and status signals in the surface unit do not correspond, display and recording of data is inhibited.

Optical Design

Design Considerations

In order to obtain the smallest error in an instrument designed to measure the volume attenuation coefficient, α , it can be shown that the path lengths through the medium should be around $1/\alpha$ or one attenuation length. Thus in very clear oceanic water where α may be as large as $\alpha = 0.05 \text{ m}^{-1}$ a water path length of 20 meters is indicated. Such path lengths are usually impractical in field instruments without resorting to some system for multiple folding of the optical path. The multiplicity of optical surfaces which results, with the attendant requirement for knowing the exact reflectance or transmittance of each surface, quickly negates any gain resulting from the increased path length. Furthermore, the optimum length changes with wavelength and water mass, and the advantage of the long path rapidly decreases as α - attenuation length decreases. As an example, given an instrument having a path length of 20 meters and another with a path length of 2 meters - both having the same photometric accuracy - the "crossover attenuation coefficient," α_c , i.e., the coefficient where the errors in the measurement of α is the same for the two instruments, would be $\alpha_c = 0.128 \text{ m}^{-1}$. For a 2-meter instrument with a photometric error 0.2 percent, the error in the determination of $\alpha = 0.05 \text{ m}^{-1}$ due to this photometric error would be $\Delta\alpha = 0.0011 \text{ m}^{-1}$, and the relative error would be $\Delta\alpha/\alpha = 0.022$ or 2.2 percent. This should be acceptable for all but the most critical research purposes. The same instrument shortened to 1 meter and used in the same water would yield $\Delta\alpha = 0.0021 \text{ m}^{-1}$ and $\Delta\alpha/\alpha = 0.042$ or 4.2 percent - an error that would still be acceptable for most applications. Thus a 1 or 2-meter transmissometer with good photometric accuracy can provide satisfactory volume attenuation coefficient data for clear ocean waters. These shorter instruments are greatly to be preferred from the standpoint of ease of handling at sea to the longer instruments or to those having a large number of reflecting or transmitting surfaces having critical cleaning requirements as in some instrument designs with multiply-folded optical paths.

There was an additional and over-riding consideration forcing the design to shorter path lengths. That was the requirement to measure the small angle volume scattering function (VSF) using the same path as used for the beam transmittance measurement. Here the designer wishes to measure the scattering from a thin lamina so that the flux remains essentially constant throughout the measurement volume. The requirement for adequate receiver power places a lower limit on the measurement volume, and the cross-section of this volume, i.e., the beam diameter, finds practical limits in the size of the receiver optics. Optical requirements for the size of the transmissometer beam place further restrictions on the beam diameter.

The compromises then were (a) between long measurement path lengths for accuracy in clear water transmittance (hence α) measurements and short water path lengths for small-angle VSF measurements and for ease of handling at sea, and (b) between a large diameter beam for precision in measurement of VSF and small diameter to keep the size of the receiver optical system reasonable.

In this instrument the projector and receiver beams were collimated as opposed to the cylindrically limited design used in previous Visibility Laboratory instruments. The primary reason for this was to allow the precise specification of angular fields of view in both the VSF and the transmittance measurements. A corollary benefit is that the measurement path length may be changed without affecting the instrument calibration providing only that the receiver entrance aperture is of adequate diameter to accept all flux scattered at the maximum measured scattering angle for the longest measurement path.

Description of the Optical Design

The optical system consists of a projector which provides a small beam of highly collimated light and a collimated receiver whose optical axis is aligned with the axis of the projector. The field-of-view of the receiver is caused to change repetitively, by means of an indexing field stop wheel located at the focal point of the receiver objective lens. For the measurement of transmittance, the field-of-view is determined by the requirement to pass all flux leaving the projector which has been neither absorbed nor scattered. Thus if the power in the beam as it leaves the projector is P_0 and that remaining after traversing an instrument water path length l is P_l , then $T = P_l/P_0 = e^{-\alpha l}$.

For the measurement of the volume scattering function at angles close to the forward direction, the field-of-view of the receiver is such that it blocks the directly transmitted light and accepts flux which has been scattered by the water at a small range of angles around the desired median angle. Those portions of the optical system that are illuminated by the projector beam can also contribute to scattered flux which is indistinguishable from that scattered by the water. To reduce this unwanted signal to a minimum, the design emphasized reducing the number of optical surfaces and amount of glass to a minimum and specifying the highest quality materials and surfaces in the optics used.

The volume scattering function, $\sigma(\theta)$, at angle θ from the direction of propagation may be determined from the expression:

$$\sigma(\theta) = \frac{1}{\omega_g \ell} \cdot \frac{P_\ell(\theta)}{P_\ell(0)} \quad (2)$$

where $P_\ell(0)$ = the on-axis power leaving the measurement volume,
 $P_\ell(\theta)$ = the received power scattered at a mean angle, θ , into a solid angle ω_g ,
 ω_g = the solid angle of acceptance of the receiver about the measurement angle θ ,
and ℓ = the path length through the measurement volume.

This relationship may be derived as follows: The volume scattering function is defined by the differential relationship.

$$dJ(\theta) = \sigma(\theta) \cdot H \cdot dV \quad (3)$$

where $dJ(\theta)$ is the radiant intensity scattered in the direction θ by an elemental volume, dV , of the scattering medium. H is the irradiance incident on the elemental sample volume. In an instrumental determination of $\sigma(\theta)$, a sample volume of finite size is, of course, required in order to obtain measurable quantities of power. The size of the volume and of the receiver solid angle of acceptance, ω_g , are determined by the sensitivity of the receiver, the power in the projector beam, the spectral bandwidth, and the range of $\sigma(\theta)$ values to be measured. In ALSAAT the sample path length is sufficient so that losses along the path cannot be neglected in the derivation. The measurement path is shown schematically in Figure 1.

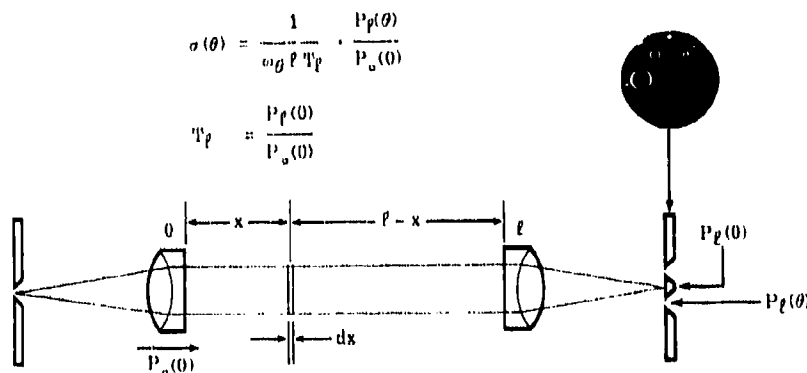


Fig. 1

Let $P_o(0)$ = the power in the beam emitted by the projector into the water,
 A_p = the area of the projector beam,
 ℓ = the length of the measurement volume,
 T_x = the transmittance of the water path to x
and T_ℓ = $P_\ell(0)/P_o(0)$ = the transmittance of the total water path.

Then, since power in the beam at x is given by

$$H_x A_x = P_x = P_o(0) \cdot T_x$$

and

$$dP_x(\theta) = \omega_g dJ_x(\theta),$$

represents the power scattered in direction θ by the element of path dx at x , Eq. (3) may be rewritten as

$$dP_x(\theta) = \sigma(\theta) \cdot T_x \cdot P_o(0) \omega_g dx \quad (3a)$$

Now the amount of this power reaching the receiver at ℓ will be

$$dP_{\ell, \omega}(\theta) = \sigma(\theta) T_{\omega} \cdot T_{\ell-\omega} \cdot P_{\omega}(0) \omega g dx \quad (4)$$

and since $T_{\omega} \cdot T_{\ell-\omega} = T_{\ell}$, Eq. (4) becomes

$$dP_{\ell, \omega}(\theta) = \sigma(\theta) T_{\ell} P_{\omega}(0) \omega g dx \quad (4a)$$

Solving for the total scattered power received from the entire measurement volume, we obtain

$$P_{\ell}(\theta) = \sigma(\theta) T_{\ell} P_{\omega}(0) \omega g \ell \quad (5)$$

from which we obtain

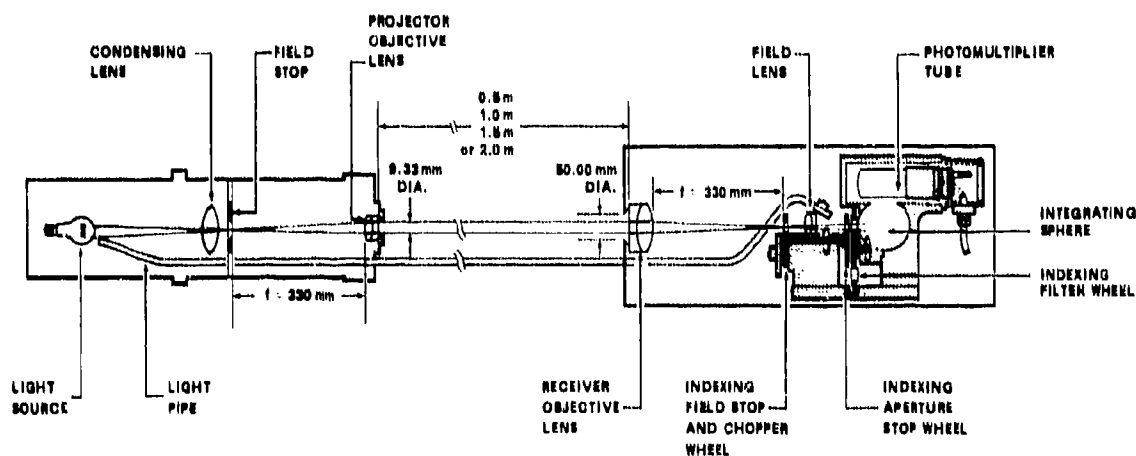
$$\sigma(\theta) = \frac{1}{\omega g \ell} \cdot \frac{P_{\ell}(\theta)}{P_{\omega}(0)} \quad (6)$$

or since $P_{\ell}(0) = T_{\ell} \cdot P_{\omega}(0)$

$$\sigma(\theta) = \frac{1}{\omega g \ell} \cdot \frac{P_{\ell}(\theta)}{P_{\ell}(0)} \quad (7)$$

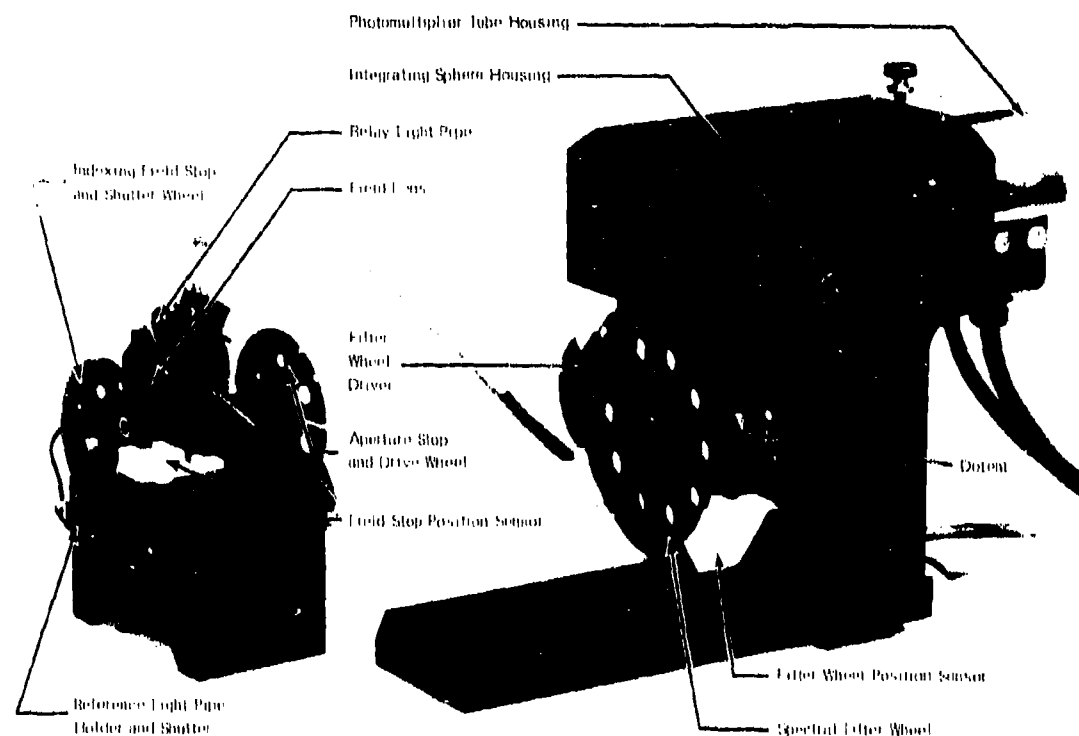
The above derivation assumes single scattering and that the path travelled by a scattered photon is not significantly longer, in terms of attenuation losses, than that travelled by an unscattered photon.

Projector. The projector source is a 15-watt, 6-volt projection lamp with a 1.5 x 1.9 mm "flat core" filament (Osram 8018). The lamp illuminates a field stop 0.44 millimeters in diameter placed at the focal distance from the projector objective lens (see Fig. 2). This lens is a 330-millimeter focal length 30 millimeter diameter plano-convex achromat with the plane surface in contact with the water. A condensing lens images the filament in the projector aperture stop. The projector clear aperture is 9.33 millimeters in diameter; however, since the diagonal of the filament image at this plane is slightly smaller than the aperture diameter, the projector beam as it enters the water is rectangular. The projector beam divergence is 0.87 milliradians in air and 0.5 milliradians in water.



OPTICAL SCHEMATIC - ALSCAT
(Not Drawn to Scale)

Fig. 2



Receiver Optical Subassembly, as mounted

Fig. 3

Receiver. The receiver also has a plano-convex achromatic lens of similar design but having an overall diameter of 75 millimeters. A disk containing four field stops is located in the focal plane of the lens. This disk rotates about a shaft through its center and is caused to index to six precisely determined positions by a mechanical intermittent drive (see Figs. 2 and 3). The four field stops are thus caused to stop, in sequence, at the required location on the receiver optical axis, while each of the four optical measurements are performed, i.e., transmittance, and the volume scattering function at each of three angles. As the field stop wheel assumes the remaining two of its six positions, the receiver, (a) samples light flux carried from the lamp by a fiber optic light pipe for systems gain adjustment and then, (b) is shuttered to place it in the dark for systems zero-set.

The four receiver field stops consist of: (1) a clear stop 1.3 millimeters in diameter which provides a 1.5 milliradian (half angle) field-of-view for the transmittance measurement, and (2) three clear annular stops which provide for volume scattering function measurements at the nominal angles of 3, 6, and 12 milliradians, as shown in the table below. When these annular field stops are in place, the image of the projector field stop falls on the opaque central spot of the stop preventing direct flux from the projector from reaching the receiver. In this situation only that flux from the projector which has been scattered by angles within the limits θ_{min} and θ_{max} (shown in the table) can be measured.

	Nominal Angle (mrad)	θ_{min} (mrad)	θ_{max} (mrad)	$\theta_{max-min}$ (mrad)	ω (sr)
θ_1	3	1.76	4.43	3.09	5.18×10^{-5}
θ_2	6	1.57	7.63	6.10	11.72×10^{-5}
θ_3	12	10.46	13.94	12.20	20.72×10^{-5}
θ_4	1.5		1.49		0.70×10^{-5}

The optimum size of the receiver aperture stop changes for the four measurements. For the transmittance measurement, the aperture needs to be large enough to accept all unscattered rays from the projector in air, for the longest path length. To accommodate for slight mechanical misalignment in the course of field use, a small increase in the receiver aperture diameter has been provided. For the VSF measurements, the size of the receiver aperture must be such that flux scattered by an angle θ_{max} from the perimeter

of the projector beam as it enters the water can be accepted. Thus if the projector aperture stop diameter is ϕ_p and the path length is l , the minimum receiver aperture stop must be

$$\phi_r = \phi_p + 2l\theta_{max}$$

To reduce the errors introduced by the inclusion of scattered light in the transmittance measurement and by the unwanted inclusion of secondary scattered light in the VSF measurement, it is desirable to limit the size of the aperture stop to that required for each measurement. In this instrument the receiver aperture stop is determined by the size of the image of a circular stop in the "indexing aperture stop wheel" formed by the field lens (see Figs. 2 and 3). This image is formed at the water surface of the receiver objective lens. The field stop wheel and the aperture stop wheel are on the same shaft and index together. Thus each of the four optical measurements are performed with an appropriate aperture stop size. A slight compromise was necessary in the interest of keeping the size of receiver lens and its mounting to within what were felt to be reasonable limits. Thus the maximum receiver stop diameter was kept to 50 millimeters which precludes measuring the VSF for $\theta = 12$ milliradians in the 1.5 or 2.0 meter path length configurations.

The stop wheel mechanism indexing speed can be controlled from the surface up to a maximum of 3 complete cycles of the wheel per second (18 indexing actions per second).

Spectral Filtering. A wheel carrying 10 narrow-band interference filters is located between the aperture stop wheel and the entrance port of the integrating sphere (see Figs. 2 and 3). The operator may select the filter required by a command from the surface control unit. The filter characteristics are shown in Fig. 4.

CHARACTERISTICS OF SPECTRAL FILTERS IN ALSCAT
(SECOND SET, DITRIC 3 CAVITY)

NOMINAL WAVELENGTH (nm)	CHARTOID λ (nm)	MAXIMUM λ (nm)	HALF BANDWIDTH (nm)	$\int T(\lambda) d\lambda$	T_{equiv}
400	400.7	402	8.4	4.120	0.492
430	430.3	431	7.0	3.402	0.486
460	459.8	459	5.9	2.903	0.492
490	489.5	489	7.4	4.097	0.554
520	520.1	521	6.7	4.600	0.687
550	548.3	549	7.6	4.840	0.637
580	580.0	579	9.4	6.284	0.669
610	608.4	604	11.3	6.427	0.604
640	641.0	638	11.2	6.666	0.595
670	669.3	668	12.3	7.519	0.611

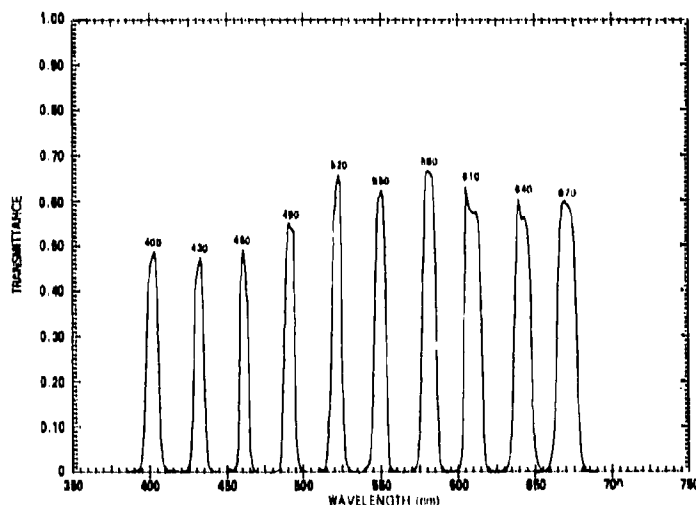


Fig. 4

Photodetector Unit. An integrating sphere has been used to ensure that the same portion of the photocathode of the photomultiplier tube (RCA 1P28AV1) is used for all measurements. This was particularly important since the distribution of flux in the beam exiting the filter wheel changes markedly for the five measurements (including the fiber optic "reference" measurement). Such changes in distribution can cause the output of the photomultiplier tube to be non-proportional to the total flux, if different areas of the photocathode are used.

Underwater Lenses

The amount of glass and the number of surfaces in the optical paths of the instrument was kept to a minimum in the interest of reducing the residual instrumental scattering. To this end plano-convex lenses with their plane side in contact with the water were used in lieu of the usual combination of lenses and plane-parallel optical glass windows. The requirements for strength, low scattering and achromatization dictated lens requirements that could be met only by special lens design and fabrication. Consequently, two-element cemented achromats were designed by one of the authors, (TJP), and manufactured to strict tolerances with respect to surface finish, bubbles, inclusions, strain and striae. The following table lists the major specifications of the lenses:

ALSCAT OBJECTIVE LENSES

Diameter	{ Receiver Projector	75 mm 30 mm
Focal Length (587.56 nm, He d-line)		330 mm \pm 1%
Axial Color Correction: 400 to 670 nm		\pm 0.2% of focal length
Front Surface		Flat
Rear Surface: Radius of Curvature		143.69 mm
All Surfaces: Conformity to Above		Within 1 fringe per 12 mm
Surface Quality per MIL-0-13830		80 - 40
	{ Central 14 mm (Receiver) Central 10 mm (Projector)	20 - 10 or better
Maximum Deviation Between Optical and Mechanical Axes		6 minutes
Lens Thickness	{ Receiver Projector	35 mm 10 mm

Mechanical Design

The mechanical design was predicated on providing a rugged, in-line instrument that could take the normal shipboard abuse and maintain its optical alignment. The projector and receiver assemblies are mounted in cylindrical pressure vessels that are accurately positioned with respect to each other by heavy aluminum cylindrical spacers. Figure 5 shows the instrument assembled in its 1-meter configuration at the top, and the sketches at the bottom of the figure show how various combinations of the spacers can be used to vary the water path length from 0.5 to 2.0 meters. The elongated holes in the cylinder walls of the spacers are provided to facilitate rapid exchange of water in the measurement path. The spacers are held together by split clamp rings which allow rapid and accurate changes in path length. All optical references are made to the large face plate to which the receiver pressure housing and the first spacer (B in Fig. 5) are attached. The plate was carefully machined to receive the curved surface of the receiver objective lens, and the plane water-contact surface of this lens is parallel to the plane of the outer surface of the plate. The optical components for the receiver are mounted on an optical bench fastened to the inner surface of this face plate and held rigid by the addition of two large rods and an end plate brace. The projector unit is centered and aligned to the receiver by means of two sets of three adjustment screws in the wall of the spacer tube.

Access to the receiver optics and electronics is obtained by removal of the cylindrical pressure housing. Access to the lamp is obtained by removing first the protective guard (unit E in Fig. 5), and second, the rear half of the projector pressure housing. The optical alignment is not affected by this procedure. Lamp replacement or adjustment are quickly and simply effected.

The fiber optic light pipe and wires from the receiver to the projector are carried through aluminum tubing attached to the respective face plates by conventional tubing compression fittings. A separate tubing length is required for each of the four measurement path lengths.

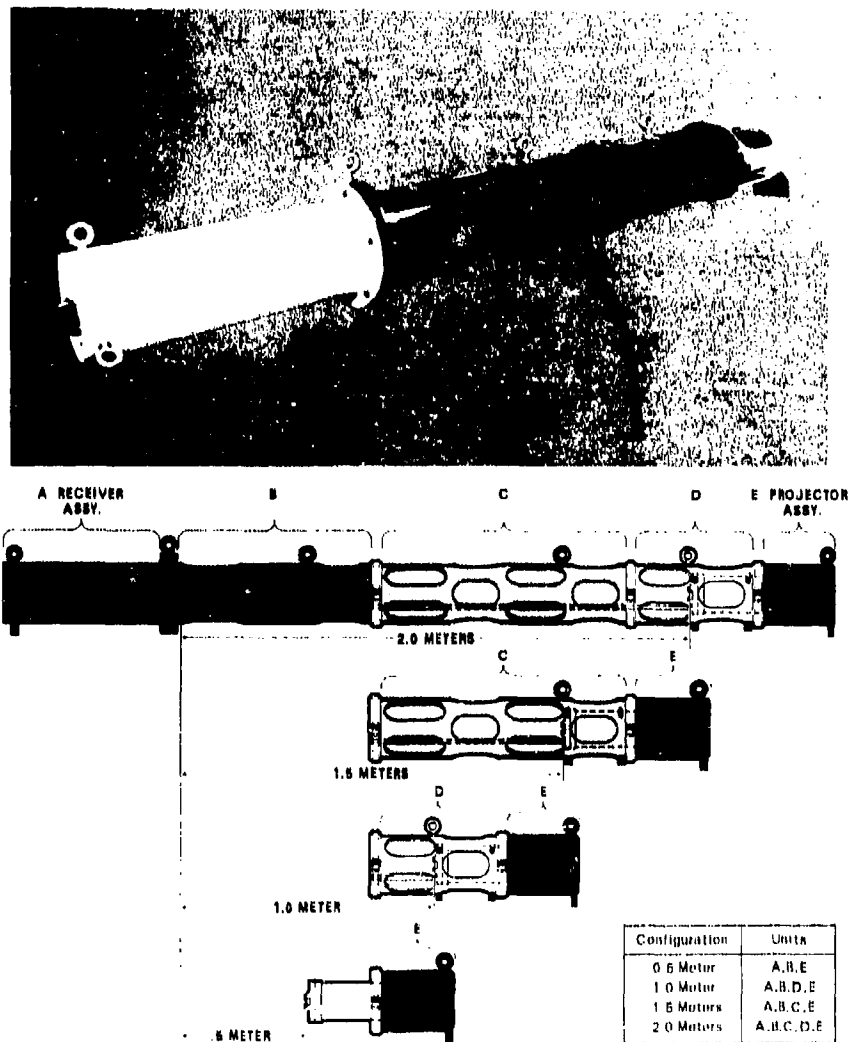


Fig. 5

Electronic Design

The electronics may be divided into two distinct parts: (1) the analog signal detection and processing circuits, and (2) the Digital Data And Command Transmission System (DIDACTS). Figure 6 is an abridged block diagram of the underwater unit. The multiplexer/analog-to-digital converter is the essential interface between the analog and digital circuits.

Underwater Analog Circuitry

An optoelectric coupler (LED/photodiode unit) senses the position of the indexing stop wheel and provides timing signals for the signal detection process. The primary photodetector is a 9-stage photomultiplier tube (RCA 1P28AV1). The gain of this tube is adjusted by controlling the high voltage applied to its dynodes in a manner described later. The output signal from the tube consists of a series of six discrete current levels corresponding to the six positions of the stop wheel. The current is converted to a voltage signal by an operational amplifier, and this voltage is, in turn, applied to the inputs of six sample-and-hold circuits. These circuits are switched by the timing signal generated by the stop wheel location. Thus the D.C. outputs of these S&H circuits correspond to the average value of the photomultiplier tube output during the sampling aperture. These signals are the voltage analogs of the light flux entering the integrating sphere and are updated once per revolution of the stop wheel. The output signals, corresponding to VSF (σ_1 , σ_2 , and σ_3) and transmittance, are applied directly to the analog multiplexer. In addition, the transmittance signal is applied to a logarithmic circuit which provides an output voltage analog of the volume attenuation coefficient α , i.e., $\alpha = -1/l \ln T$.

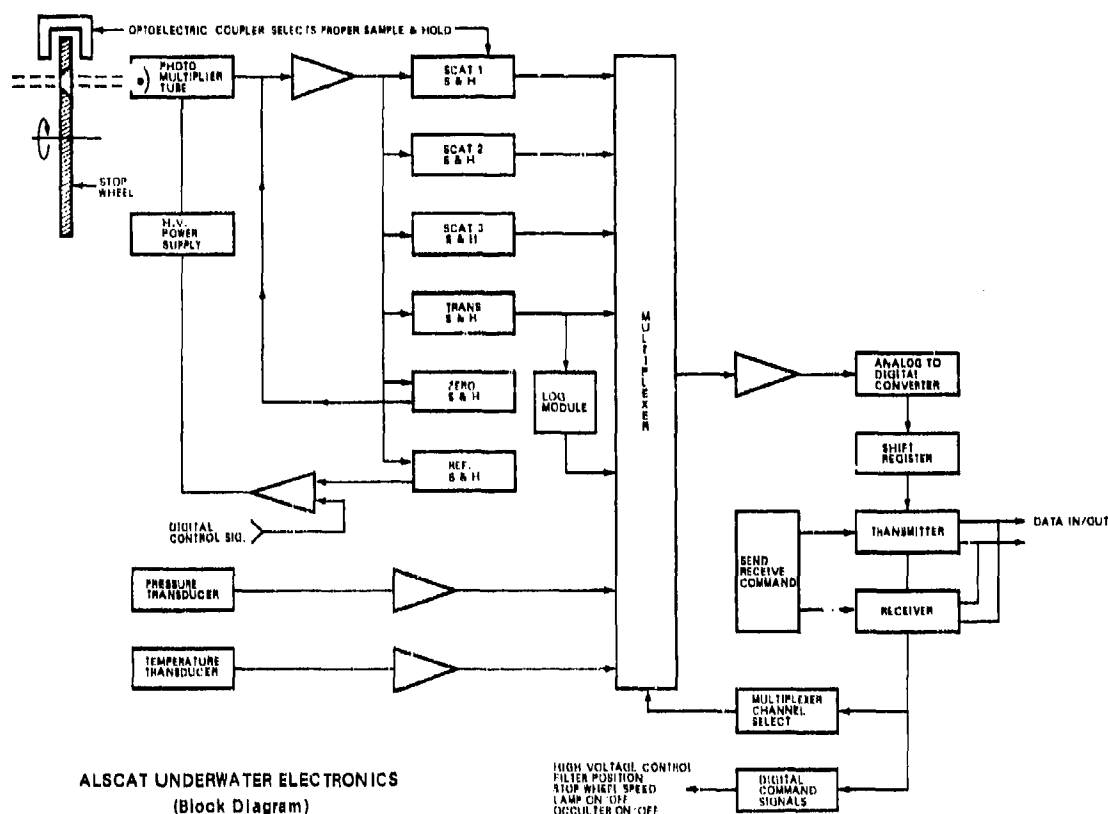


Fig. 6

The output from the "zero" S&H circuit provides an indication of the dark current in the photomultiplier tube and zero drift in the current-to-voltage connected operational amplifier. The "zero" signal is fed back to a summing junction at the input to this amplifier and forces the amplifier output to zero, thus compensating for the zero offsets generated at this point.

The output from the "reference" S&H is proportional to the signal arriving at the phototube through the fiber optic light pipe. As this signal is independent of the water path, its value should remain constant. Any variation in this signal is attributable to variations in the lamp output or in the overall response of the photomultiplier tube (PMT). Regardless of the cause, changing the gain of the PMT can restore the reference signal to a preset value. This value is determined with the instrument in air by adjusting the high voltage applied to the PMT dynodes until the indicated transmittance is 0.925. This value represents the transmittance change caused by the increase in losses at the two exterior surfaces of the lens/windows when these interfaces are in air as opposed to water. The high voltage is adjusted as follows: The output from the reference S&H is electronically compared to a reference signal generated by a digital-to-analog converter (DAC). The DAC output is adjusted from the surface by the setting of digital switches. The difference signal between the DAC output and the reference S&H controls the high voltage applied to the PMT. Thus once this adjustment has been made in air (after careful cleaning of the windows) the magnitude of this difference signal is established. With adequate loop gain small changes in the reference S&H output will provide sufficient compensating PMT gain change to hold the overall system response constant to within the desired ± 0.1 percent.

The pressure and temperature transducer outputs are processed, and voltage analogs of the depth (0 - 200.0 or 0 - 500 meters) and temperature (0 - 40.0°C) are applied to the analog multiplexer. Changes in the full scale range in depth and a measurement are effected by digital commands transmitted from the surface.

Digital Circuits

The seven underwater analog channels are multiplexed into an analog-to-digital converter (ADC) in accordance with address signals transmitted from the surface. The output of the ADC is fed to a shift register along with the address and status information from the seven channels. The underwater transmitter then sends this serialized digital information up a balanced digital data transmission cable. At the surface the data is shifted into five data registers that latch the data in accordance with the channel addresses (see Fig. 7). The information in the latched registers is provided to the digital displays, printer, magnetic tape recorder,

* The five are Transmittance, Alpha, Depth, Temperature, and one of the three VSF channels as selected by the operator.

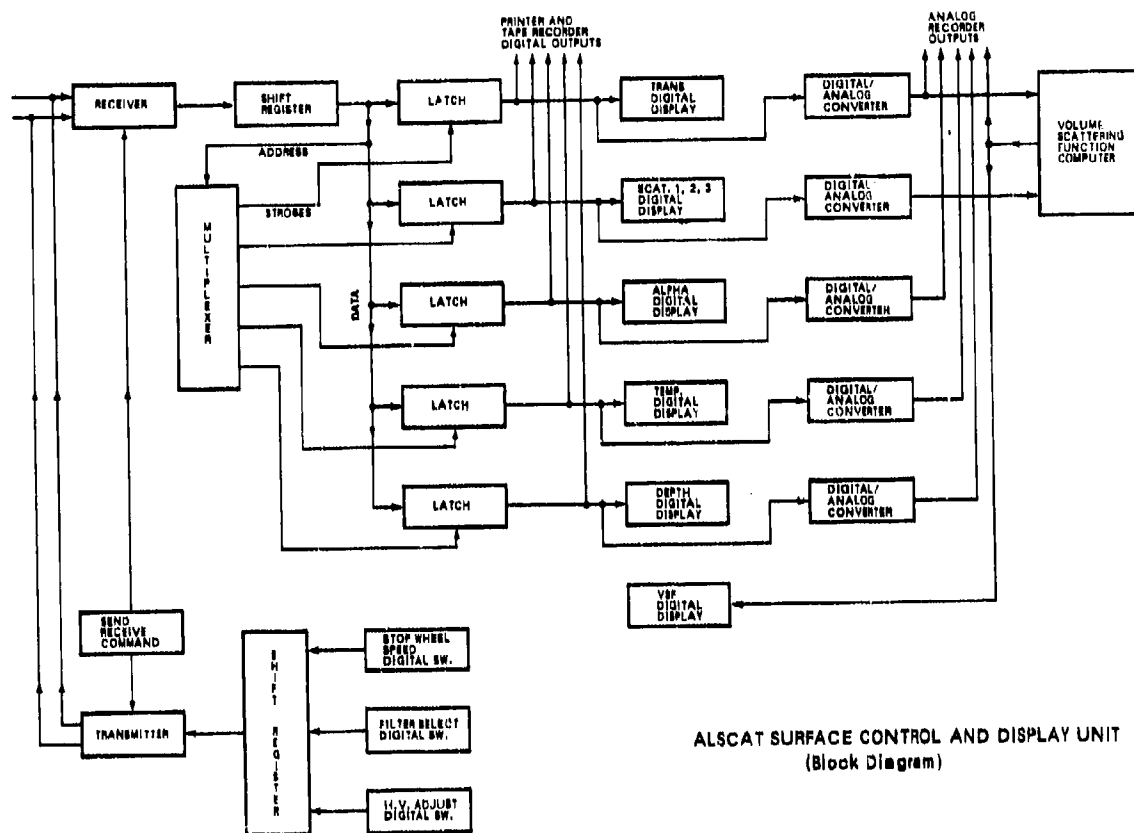


Fig. 7

and digital-to-analog converters (DAC). The analog outputs from the DAC are available for recording on an x, y, z flatbed recorder. The analog scattering signal is fed to a computation circuit where appropriate gains and offsets are applied, and the result is divided by the path transmittance in accordance with Eq. (6). The output of this computation is also fed to the x, y, z plotter and to a digital voltmeter for display and conversion to BCD output.

The surface unit provides digital addresses and commands to the individual channels in the underwater unit. These digital signals are placed in a shift register and transmitted to the underwater unit via the same twisted pair, data cable used for the up-link transmission. The timing of the send/receive cycle is determined by the number of bits required for the up and down link portions of the cycle and the basic clocking frequency, 8.0 kilohertz. The beginning of each channel's interrogation, command, data and status cycle is determined by a unique word of seven consecutive pulses. Each channel data cycle requires sending a total of 47 bits of information requiring 7.83 milliseconds. Thus for the seven channels, a total of 54.8 milliseconds are required, and the total data cycle rate is 18.24 hertz.

The timing is controlled by individual crystal oscillator clocks in the underwater and surface units. The surface clock is synchronized with the underwater clock once per channel data cycle.

Power Supply

The power for the underwater electronics and lamp is provided by transmitting 60 hertz current through two additional twisted pairs in the underwater cable. Although this requires using rather high voltages (ca. 200 volts) at the surface end of the cable, no problems in electrical leakage or from noise coupling into the digital circuits have been encountered. The advantage of this method was that of being able to use conventional line-powered power supplies.

Data Output

Two samples of the type of data which can be obtained with the instrument are presented. These samples are plots from the two-pen $x-y$ plotter. Figure 8 shows the temperature and transmittance profile in water having an unusually pronounced turbid layer from 10 to 30 meters below the surface. In Fig. 9 we present vertical profiles showing the volume attenuation coefficient and the volume scattering function for 12 milliradians. These curves were obtained at the same location 28 minutes later.

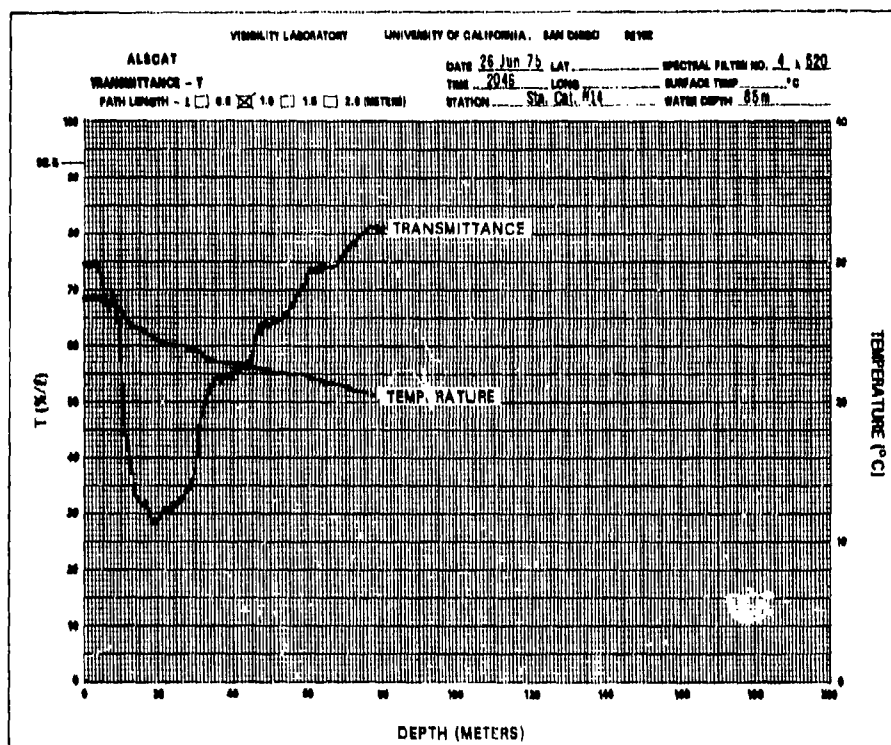


Fig. 8

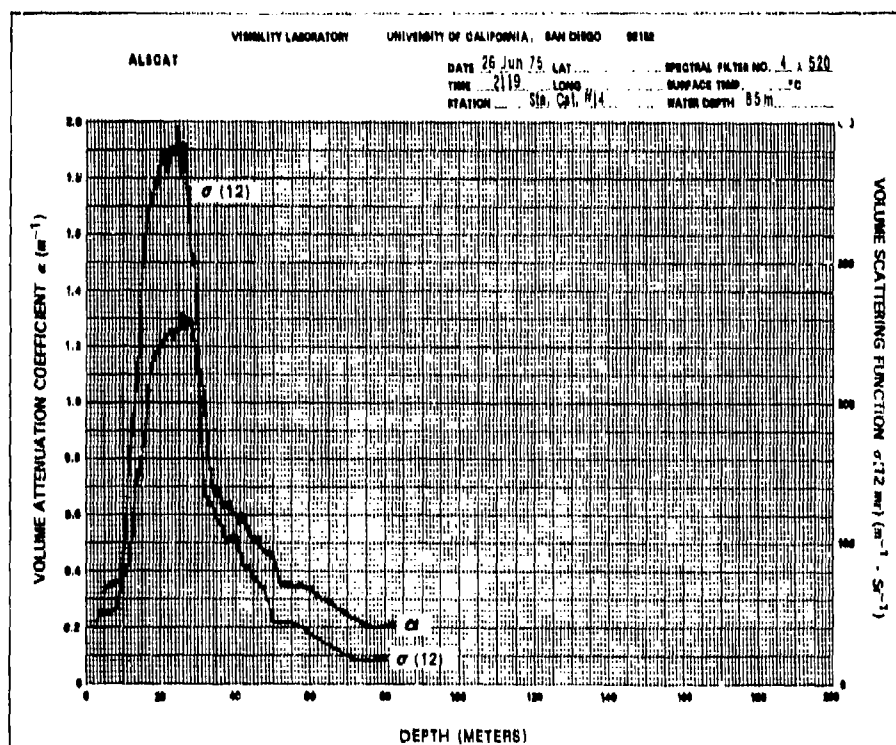


Fig. 9

SECTION 6 SURFACE SUPPORT PLATFORM

INTRODUCTION

The purpose of this appendix is to describe the Surface Support Platform and appendages used to provide sea-surface support including power, instrumentation, and control of underwater devices for the Optical Satellite Communications Program BLUE-GREEN experiment. The objectives of the platform-assembly task included the following:

- (1) Providing a platform which, when deployed, would be sufficiently stable to conduct the experiments under a variety of ocean conditions. It was necessary that the platform be sufficiently large to provide a work area for up to 7 people and be sufficiently equipped to support the necessary electrical, mechanical, and electronic equipments;
- (2) Providing vertical access to depths of approximately 50 metres in the form of an assembly which would be raised, lowered, and rotated and upon which various instruments could be mounted. The assembly position was required to be fixable to within 3 degrees (an allowable swing of 2.5 metres at the 50-metre depth);
- (3) Providing a method to traverse an optical detector along a horizontal path slightly below the surface of the water. It was necessary that orientation of the horizontal path and the pointing of the detector with respect to the vertical elements (described in 2 above) be well defined;
- (4) Providing support to personnel of the Scripps Institution of Oceanography Visibility Laboratory for the deployment and operation of the monitoring instruments for optical properties; and
- (5) Providing mooring, deployment, upkeep, support, watchstander personnel, small-boat platform-to-shore transportation, and correction of equipment breakdowns.

GENERAL DESCRIPTION

The objectives were required to be met within 5 months and construction was scheduled to begin in parallel with the development of experimental equipments which were only generally defined. Moreover, the task was to be accomplished within an extremely tight budget. For these reasons, some rather bizarre and unique designs were employed with flexibility as the primary guideline.

For example, to fit the budget constraints, it was determined that surveyed and excess equipment would have to be used, where possible, and this equipment would have to be augmented with rented accessories. This factor required that the platform be of sufficient size to fit the available equipment. The customary approach of designing equipment to fit the available space was not possible in this operation. Thus, for the base platform, a large barge (10.4 by 33.5 metres) was selected. The barge is described in detail in a later portion of this appendix.

Several techniques were considered for deploying stable equipment platforms to the desired depths. Common to all these techniques was excessive cost for boat and diver operations. To eliminate most of this cost factor, a technique was devised which would not require divers and which would cut boat operations to a minimum. This technique involved the fabrication of a single piece of pipe, 55 metres long and 0.2 metre (approximately 8 inches) in diameter into the form of a vertical guide assembly to which a platform could be fitted

and be raised and lowered. Deployment of the system to be accomplished without the use of divers, was reduced to the problem of fabricating, floating, and towing the pipe to the desired location. At the test location, it was only necessary to attach one end of the pipe to the barge and to sink the other end. (Fabrication of the pipe is described in a later section of this appendix.) It was found that the horizontal-path requirements could be met by suspending a guide rail along the side of the barge.

In summary, as depicted in figure 1, the overall design concept was to develop a platform (barge) and to attach a vertical and a horizontal optical bench to the platform in the form of a suspended pipe and an H-beam guide rail. With this arrangement, experiments could be conducted through an underwater path from equipment mounted on the vertical and horizontal optical benches. The vertical optical bench could also be used to deploy a laser and an underwater receiver for uplink and downlink measurements, respectively. Later on in this appendix, a section will be devoted to a description of the equipment selected to perform the remaining functions of the platform. Figure 2 illustrates the overall layout and points up the convenience of selecting the large barge as the first step in the operation. Through use of this procedure, it was possible to equip and test separate units at the Laboratory before transporting them to the barge for installation. In this way, planning and fabrication were accomplished in parallel. It was also found feasible to provide a fully self-contained maintenance and support activity aboard the barge. In addition, the large size and stability of the barge, when moored, provided comfort for system operators and, in particular, for watchstanders who manned the barge continuously.

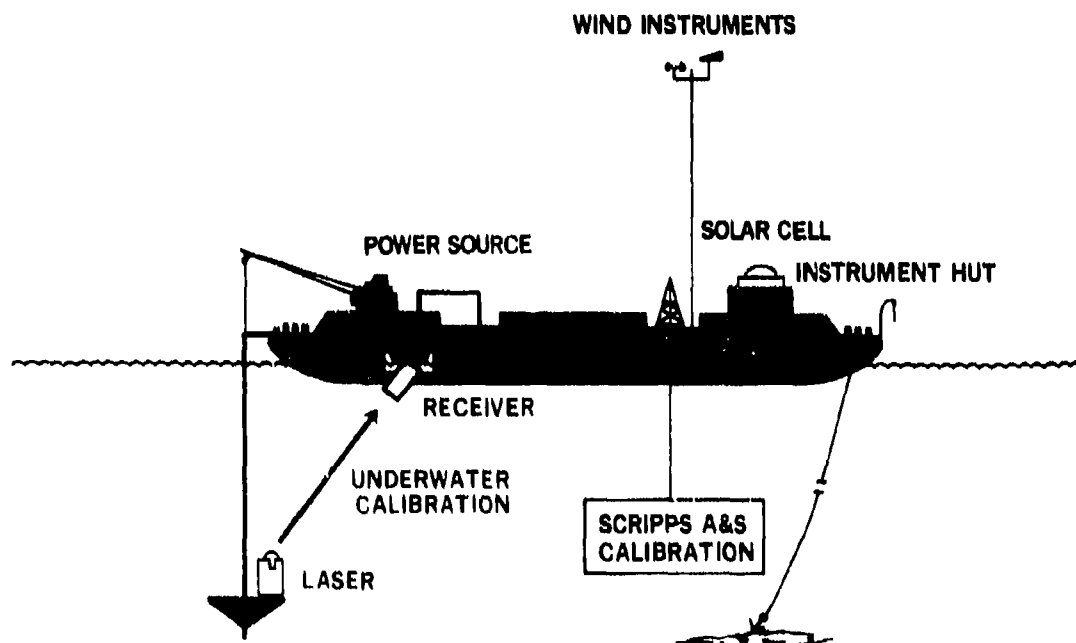


Figure 1. Surface platform design concept.

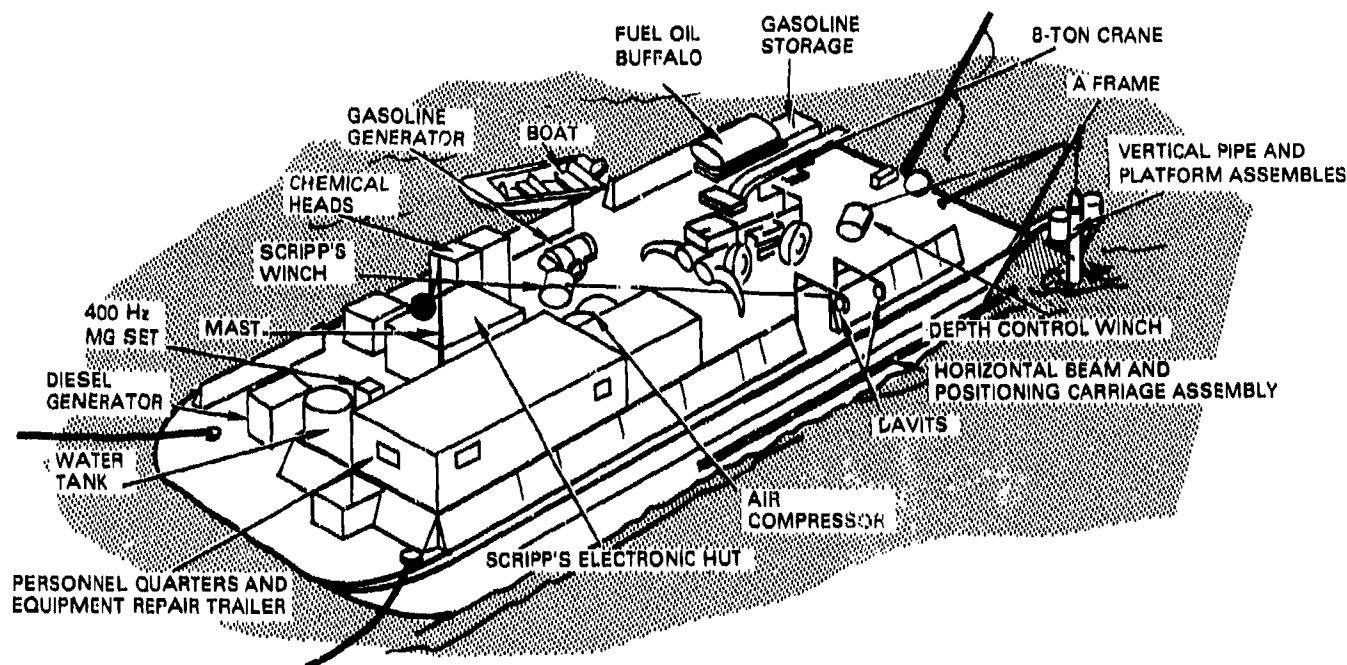


Figure 2. Aerial view of the surface support platform.

THE BARGE

For the surface platform, the YC-1087 barge was used. The principal dimensions of the YC-1087 are:

- Length of 33.5 metres,
- Width of 10.4 metres,
- Light draft (170 tons) of 0.56 metre,
- Full draft (670 tons) of 2.44 metres.

The YC-1087 has a 3.6-metre (from keel to deck height) molded deck and was built by the Soule Steel Company, San Francisco, in 1945. The deck is guarded by steel bulkheads 1.07 metres high with two 2.44-metre openings along both sides and a 3.36-metre opening at each end for deck-edge access. The deck area inside the bulkheads is 8.2 by 26.8 metres. The maximum displacement for open-ocean tow of the barge is 570 tons.

The interior (below decks) of the barge consists of 6 void spaces separated by athwartships bulkheads. Access to the voids is provided by hatches along both sides of the barge. In order to improve the stability of the barge during the tests, the 2 center voids were fitted with vents and were filled with fresh water. The resulting 2-metre draft also provided easy access to the water surface from the deck edge. The remaining 4 voids were fitted with external flooding alarms and were inspected at 4-hour intervals.

Three davits (3 metres high with 2-metre projections) were fabricated of 0.122-metre (4-inch) schedule-80 pipe and were fitted into bearing sleeves at port and starboard openings (fig 1). The davits were swung in and out by hand using a removable steel arm. The davits were fitted with sheaves and were used to lower the water-monitoring instruments over the side and clear of the platform.

The port after corner of the barge was fitted with a 6-metre A-frame guide which was fitted to pads welded to the deck. The A-frame was also fabricated of 0.122-metre schedule-80 pipe with sleeve bearings at the feet. Ladder rungs were welded up one leg of the frame to permit easy access to the top. The A-frame, designed to support a vertical load of 10 tons at an angle of 30 degrees from the vertical, was used to support the vertical pipe and test-instrument platform which represented a maximum load of approximately 3 tons.

Access to the waters edge for boarding small boats was provided by 2 ladders mounted at the edge of the deck. A 3-metre boom was rigged off the starboard side for stowing the small boat away from the side of the barge. Access to the test-instrument platform for instrument adjustments was provided by a hinged deck (2 metres by 1 metre) which could be lowered alongside the platform. The deck was fitted with hand rails and open deck grating for personnel safety.

Mooring for the barge was provided by 3 light-weight anchors (680 kilograms each) each equipped with one-half shot of 3.81-cm (1.5 in) chain to prevent bottom chaffing and 610 metres of 10.16-cm (4 in) braided nylon line. Excess line was stowed in cubical boxes 1.24 cubic metres in size. Each anchor was equipped with a nilspin retrieving wire and a marker buoy. The nilspin retrieving wire had a diameter of 1.6 centimeters.

The barge was towed to the test site at Santa Catalina Island and placed in a 3-point moor in 60 metres of water by the USS HITCHITI (ATF-103). Approximately 350 metres of line were used on each leg of the moor. The moor was set to point the after corner of the barge (the A-frame) due South. This was done so that the underwater receiver would have a maximum unobstructed view of the sun. After mooring, the position of the barge was checked periodically using relative bearings of landmarks taken with a mountain transit. The barge was subjected to maximum winds of 35 knots (broadside) and estimated maximum tidal currents of 5 knots.

Barge trim was recorded during the tests as 0.15 metre or a tilt of approximately 5 milliradians fore and aft. The position of the barge remained relatively stable during the tests. For this reason, positioning of instruments by sighting distant landmarks was expected to be accurate to ± 50 milliradians. This was true, for example, of the orientation of the camera axes or the aiming of the laser beam toward the aircraft.

Each side of the barge was fitted with a large wooden bumper (0.2 by 1 metre cross section) extending the full length of the barge. The barge draft was such that the bottom edge of the bumper was in contact with the surface of the water. An H-beam (0.15 metre), 18 metres long, was suspended 0.1 metre away from, and 0.1 metre up from the bottom of the beam using L-brackets and angle iron (fig 3). The supports were attached to the top flange of the H-beam leaving the bottom flange to support and guide a subsurface instrument-positioning carriage. The one-piece beam was installed in port and only minor adjustments to its configuration were made at the test site.

The positioning carriage (fig 4 and 5) consisted of a 1 by 0.7 metre section of channel iron fitted with nylon top runners to fit inside the flanges of the H-beam and a spring-loaded roller which pressed up against the bottom of the beam. A yoke assembly was fitted around the underwater instrument housing and was attached to bearings on each side of the positioning carriage. The outboard side of the yoke (fig 5) extended up to provide a control arm for pointing the instrument. A protractor was also fitted to the outboard side of the positioning carriage. Drilled holes in the protractor aligned with a pin in the control arm and allowed adjustments of the instrument pointing angle of ± 80 degrees in 5-degree increments. T-handled brakes were threaded into the outboard side of the positioning carriage to lock the unit in position and to minimize wave-induced sway in the suspended instrument. All assemblies were coated with anti-corrosion and anti-foul paint.

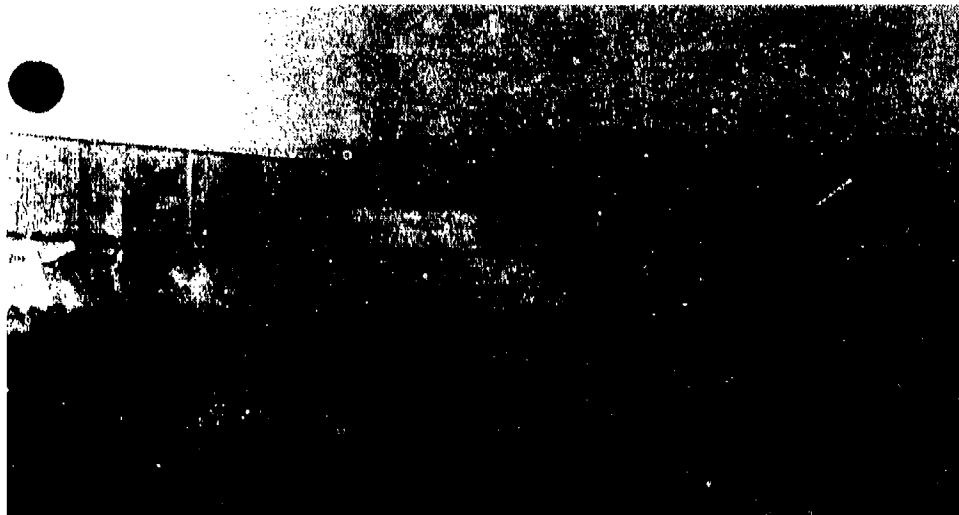


Figure 3. Side view of surface support platform showing the horizontal guide track.

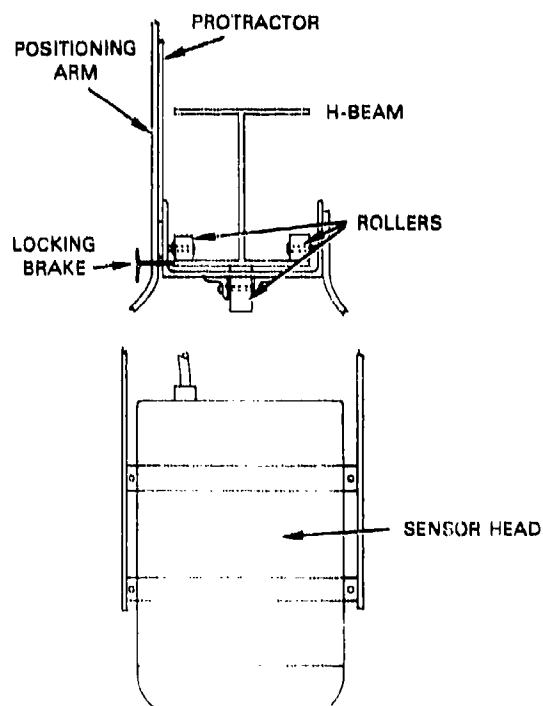


Figure 4. Positioning carriage subassembly (end view).

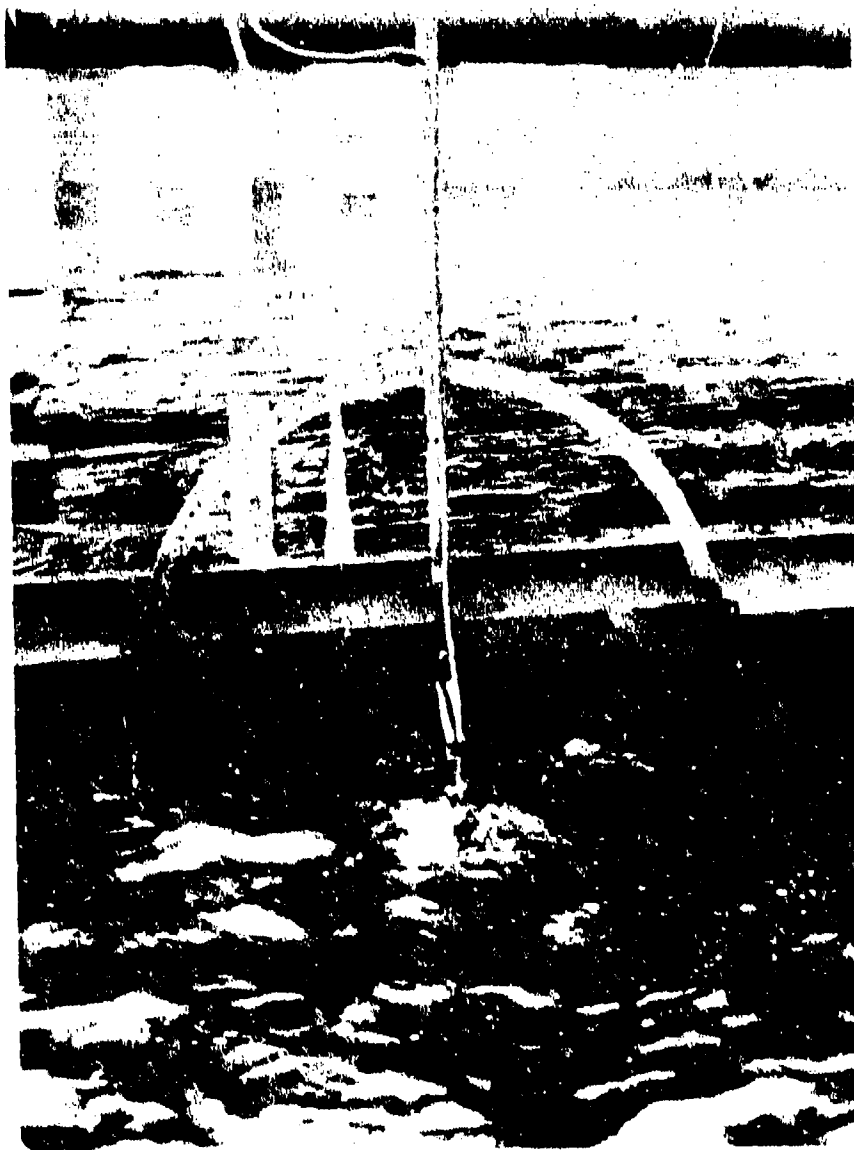


Figure 5. Positioning carriage subassembly (side view).

In operation, an instrument is walked to the desired beam location, the operator locks the positioning carriage in place, and tilts and pins the instrument at the desired angle. During the tests, angular positioning of the instrument was considered to be accurate to ± 50 milliradians and positioning along the beam, ± 0.15 metre.

VERTICAL GUIDE AND INSTRUMENT PLATFORM

The vertical guide for supporting the instrument platform at various depths consisted of a suspended, schedule-40, steel pipe, 56 metres long, and 0.2 metre in diameter, fitted with a guide rail down one side. The pipe was fabricated in one piece at San Diego and was later towed to the Santa Catalina test site. Lengths of pipe (nominally 7 metres) were welded together over 1-metre inserts (fabricated by turning down 0.2-metre (diameter) schedule-120 pipe sections) to manufacture the assembly. A tail assembly, fitted with a shackle mount and a 0.05-metre diameter flood and blow port, was welded to one end of the pipe, and a head or top assembly was fitted with a slotted flange, pin, and a D-ring for suspension support. A 0.15-metre fitting for a blow and vent port was welded to the top end of the pipe. The full length along one side of the pipe was drilled, tapped, and fitted with a 0.025 by 0.020 metre guide rail. The guide rail was segmented into sections, approximately 3 metres in length, to prevent fracture during normal pipe-bending modes. The threads of the bolts used to hold the guide rail in place were coated with elastic stop-leak material to prevent water leakage into the pipe during flotation periods. A tail stop was clamped to the pipe to prevent over-travel of the instrument platform when the assembly was placed in service.

To prepare the pipe for tow, both the vent and flood ports were sealed. Eighteen pairs of pontoons, each 2.9 metres long and constructed of capped segments of 0.1-metre diameter schedule-40 PVC pipe, were fitted. Each pair of pontoons was positioned and rigged to the pipe (fig 6) with 0.01-metre diameter braided nylon line. The rigging of the pontoon pairs provided 3 under-riding lines for each pair to support the pipe, and 3 over-riding lines to hold the pontoons next to the pipe. The front over-rider for each pair of pontoons was passed through a hole drilled in the guide rail and served to keep the pontoons from slipping back along the pipe while under tow. The rigging lines were adjusted so that the top edges of the pontoon pairs were in line with the top edge of the pipe. This was done to ensure that the pipe, when floated, could not roll over. The entire assembly, pipe and pontoons, was lifted by cranes and lowered into the water. In order not to bend the pipe, the lifting was accomplished using 3 cranes simultaneously, each lifting at two positions along the length of the pipe.

The design of the pontoon system was intended to provide continuous support along the length of the pipe and to provide a slightly positive buoyancy (approximately 3 pounds per metre of pipe length). Calculations had shown earlier that only about 7 metres of the pipe could be suspended safely without any support other than that provided by the pipe itself. In addition, it was determined that end-to-end flexing of approximately 3 metres, if encountered, would result in permanent deformation of the pipe. Since nominal sea conditions over the towing path from San Diego to Santa Catalina Island include swells in excess of 2 metres, it was apparent that destruction of the pipe would take place if the pipe were permitted to ride fully on the surface.

The dry weight of the pipe was approximately 4700 pounds. The pontoons were designed to provide approximately 1400 pounds of buoyancy. During the 5-knot tow (fig 7), the tail was seen to flex approximately 1 metre, side to side, as the pipe cleared each swell. (Note that a shark buoy was attached to a line at the tail of the pipe to warn small boats. The lift of the shark buoy added significantly to the lift of the pontoons causing

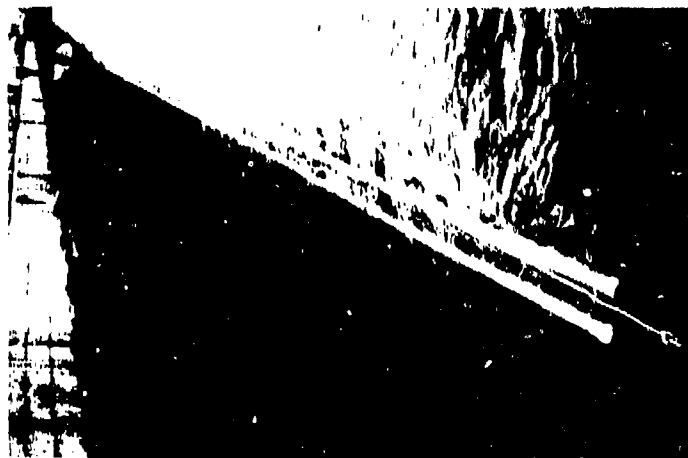


Figure 6. The arrangement of the support pontoons is shown. Note that the entire assembly has only slight positive buoyancy.



Figure 7. The pipe during tow.

the tail to lift up in a swell.) The design, however, proved sufficient to allow the principal portion of each swell to pass over the pipe. No damage to the pipe resulted during the 130-km trip.

Once in position alongside the barge, the tow line was removed from the pipe and a winch line was attached to the D-ring at the top. The winch line was passed through a sheave at the top of the A-frame and slack was taken out of the line. A tail line was attached to the pipe and secured to the barge. Next, the over-rider lines on the pontoons were cut leaving the pipe suspended in the cradle formed by the under-rider lines. The flood plug was removed from the tail of the pipe and the tail line was payed out simultaneously. As the pipe began to flood, it slowly lowered to the vertical position suspended by the winch line and the A-frame. Allowing the pipe to flood slowly and to swing down against the force of the pontoons was intended to help prevent bending of the pipe. Once the pipe was in the vertical position, the pontoons floated free.

The pipe was hoisted up on the A-frame until its top was approximately 0.5 metre above the barge deck. The pipe support was then transferred to a swivel and a 0.025-metre wire hung from the A-frame. A steel bar, 2 metres long, was inserted between the top flanges and rigged to prevent the pipe from rotating. (Later, the steel bar was used as a lever to rotate and point the pipe and instrument platform during the various phases of data acquisition.) The guy wires on the A-frame were adjusted to position the pipe in line with the horizontal guide rail. Finally, the vent line was opened and the pipe was allowed to fill with sea water to reduce its buoyancy. Recovery of the pipe was accomplished by performing the steps in reverse order, blowing the pipe dry and lifting with the tail line to the point where the pontoons could be refitted.

The instrument platform (fig 8) consisted of a 1.5-metre long tubular guide to which was welded a horizontal table or platform. The guide section was manufactured of 0.3-metre diameter, schedule-40 steel pipe and was fitted on its inside surface with a set of runners of a UHFM polymer designed to glide along the pipe and guide rail. The two sides of the horizontal platform table were arranged to accept both the laser and the radiance-scanner camera. The top of the platform was drilled to permit a rotational selection (intervals of 60 degrees) for orienting the instrument mounts. The platform was manufactured in one piece and then split in half for installation at the test site. Bolting brackets and guide keys were installed before splitting to ensure the alignment of the final assembly. Once reinstalled on the pipe at the test site, the half-ton assembly was fitted with wire straps leading to a winch hook configured to slide down the side of the pipe opposite the guide rail. The hook was wrapped with split fire-hose material to protect the pipe coatings. The platform assembly was raised and lowered through its 55-metre operating range by an automatic winch.

The laser mount (fig 8) was constructed so as to hold the laser securely in place and to permit it to be tilted in 10-degree intervals from zero to 50 degrees. The mount consists of a rubber-lined clamp which fits around the laser housing cylinder and to which a pair of pivot bearings are attached. One side of the pivot assembly is fitted with a tilt-control arm which can be pinned to a guide protractor drilled at 10-degree intervals. The camera mount is a rubber-lined assembly configured to hold the camera in an upright position at all times.

The platform was also fitted with a 2-axis tilt sensor to measure deviations in the platform position caused by pipe sway. During the conduct of the tests, no significant changes in the platform position were observed.

All metal components fabricated for the test were coated with anti-corrosion and anti-foul paints. The rubber liners were used to electrically isolate the instruments from the pipe and platform assemblies. A negligible amount of pitting of the platform in the area of the laser mount was noted after approximately 30 days of operation.



Figure 8. The vertical instrument platform is shown raised to a working access position. The laser mount (right) and the camera mount (left) are shown in the figure. The steel bar passing through the top flange of the pipe is used to fix the rotational orientation of the pipe and platform assembly.

Umbilical power and data cables leading to the laser, the camera, and the tilt sensor, were lashed together and to the platform to protect the connectors from parting forces. The umbilical cables were hand fed and retrieved from the deck of the barge as the platform was raised and lowered.

Platform depth was monitored by coding the winch cable with colored stripes at 1.5 metre intervals (approximately 5 feet). This technique was adequate to provide 0.3-metre accuracy at the maximum depth (52.5 metres). A mechanical level was used to check the orientation of the camera and the laser on the platform before lowering. The laser was found to be offset by +2.5 degrees. Hence, the laser position was recorded to be 2.5 to 52.5 degrees in increments of 10 degrees. Due to only slight variations in the platform orientation recorded on the tilt sensor, instrument vertical axes were assumed to be known to within ± 3 degrees.

It is important to observe, in support of the unusual techniques used to deploy the equipment, that the entire system was placed into full operation within 1 week of which 3 days were required for towing the pipe and barge into position. Particularly noteworthy is the fact that no divers were used to perform any part of the deployment operations, a fact which resulted in considerable savings in dollars and manhours.

BARGE EQUIPMENT

In addition to the many fabricated elements deployed with the barge, a large number of accessories were also installed. For example (fig 2), the most eye-catching piece of equipment is the crane. This unit had a rated lifting capacity of 8 tons and was selected because it provided a 14-metre hydraulic boom which, from its tied-down position, could service most of the lifting requirements on the barge. The crane was used as a utility machine for lifting heavy equipment, loading and off-loading stores and fuel supplies, lifting and positioning the vertical platform for installation on the pipe, and lifting the small boat and motor aboard for cleaning and maintenance.

The small boat had a 4.7-metre Fibreglas hull and was equipped with a 55-horsepower outboard engine. The boat was equipped with steering, shift, and speed controls and was fitted with a compass and night lights for night transits to the barge.

The quarters and maintenance housing unit was a 3 by 10 metre house trailer with the wheel and towing assemblies removed. The trailer had been remodeled previously as a temporary housing unit and was divided into two staterooms. For use in the tests, the forward stateroom was converted into a storage and maintenance facility and the after stateroom was fitted with bunks and emergency radio equipment for onboard watchstanding personnel.

The fresh-water storage tank contained 893 litres (500 gallons) of nonpotable fresh water and was used only for washing down instruments, cleaning the barge, and mixing chemicals for the chemical heads. Drinking water was provided from rented bottled-water supplies.

Two electronic huts were used to house recording and control equipment and the power-distribution system. Each measured approximately 3 by 4 metres and weighed approximately 2 tons. Both huts with their installed instruments were tested at the Laboratory before they were transported to the barge.

The Scripps winch was used to raise and lower the monitoring instruments for optical properties. The winch operated from 400-volt, 3-phase, 60-hertz power and was equipped with a friction clutch to control the rate of change of depth. A smaller winch (gasoline powered) was also provided for use by Scripps personnel in raising and lowering their smaller instruments.

The platform winch was a fully enclosed cable winch equipped with 63 metres of stainless-steel wire and powered by 28 volts (dc). The winch had a lift rating of 10 tons and operated at 2 speeds (5 and 10 feet per minute). Control of the winch was through a remote-control box which allowed the operator to be as much as 15 metres away from the unit if required for safety reasons. This winch was used to raise the pipe into position during its initial installation and later to control raising and lowering of the vertical instrument platform.

Miscellaneous equipment included an arc welder, a $0.06 \text{ m}^3/\text{m}$ (2-cfm), 7182-pascal (150-psi) air compressor, a hailing and fog-horn system, a 946-litres-per-minute (250-gpm) gasoline-powered pump for flood and fire control, 7 carbon-dioxide and 6 PKP fire extinguishers, mast-head lights, running lights, a black diamond and a black ball for towing and mooring requirements, flood lights for night lighting, and a refrigerator.

Prime power was provided by a 450-volt, 3-phase, 60-hertz, 50-kilowatt diesel generator. Transformers were used to step down to the necessary 200- and 110-volt supplies. A 400-hertz motor-generator set was installed to provide power for the laser. Direct-current power for the platform winch was obtained by passing a 220-volt supply through a rectifier. A second generator, a gasoline-powered 215/110-volt, single phase, 60-hertz, 2-kilowatt unit was used as an emergency supply and to conserve fuel during periods when full system operations were secured.

Gasoline and diesel fuel were stored on the barge. Gasoline was stored in 208-litre (55-gallon) drums stowed outboard of the large bulkheads for safety. Refueling of the gasoline supplies was accomplished by transporting the drums to shore facilities. Diesel fuel was stored in a 1500-litre (400-gallon) fuel buffalo. Refueling of the barge with diesel fuel (required only once during the experiment) was accomplished by transporting a second buffalo to the barge, hoisting it above the onboard buffalo (fig 9) and allowing the latter to fill by gravity.

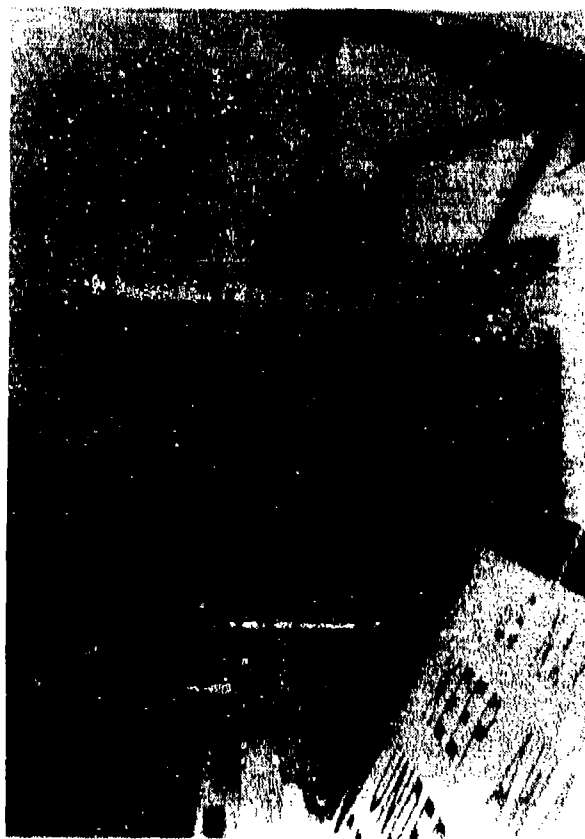


Figure 9. Replenishing the barge diesel oil supplies.

SECTION 7 ATMOSPHERICAL AND OPTICAL BACKGROUND MONITORING SYSTEM

BACKGROUND

The solar radiance distribution in the sea depends on several uncontrolled variables occurring on or above the surface. The most important in terms of magnitude of effect are:

- (1) Temporal and spatial fluctuations in sea surface irradiance.
- (2) The fraction of the total surface irradiance contributed by the sky.
- (3) Wind speed and direction.

Since these variables are uncontrolled they must be monitored, preferably in real time. Their effects on the underwater light field may then be corrected for in the radiance data. The recognition of this requirement led to the development of the Atmospheric and Optical Background Monitoring System (AOBMS).

SYSTEM DESCRIPTION

The AOBMS is composed of three functional units as shown in figure 1. They are the:

- (1) Sensors
- (2) Signal conditioners
- (3) Processor

Direct monitoring of the sun is accomplished by the solar monitor, while the deck cell covers the upper hemisphere; i.e., sun plus sky. The pyrheliometer covers the same field as the deck cell and functions as check on and backup for the deck cell. Wind speed and direction are determined by an anemometer and a vane wind direction indicator.

The sensors output a variety of analog signals that are routed to the Interface Panel located in the instrument hut housing the Nova computer. The single exception is the pyrheliometer which comes with its own strip chart recorder.

The first stages of signal conditioning occur at the Interface Panel. This unit takes the sensor outputs and transforms them into DC voltages in the range 0 to 10 volts thereby making them compatible with the input format of the Analog to Digital converter (A-D).

In the A-D the final stages of signal conditioning take place. The DC output of the Interface Panel is digitized for entry into the Nova 800. Twelve bits (2^{12}) of resolution are available so that a full scale reading from one of the sensors is equivalent to ± 2048 digital units.

The digitized background data is now available for entry into the Nova. Entry occurs during radiance scanner operation by command from the Nova unless directly accessed by the operator. Updated background data is interrogated each time a data set is taken by the radiance scanner. Both are then stored on magnetic tape and accessed via teletype. A sample printout is shown in figure 2.

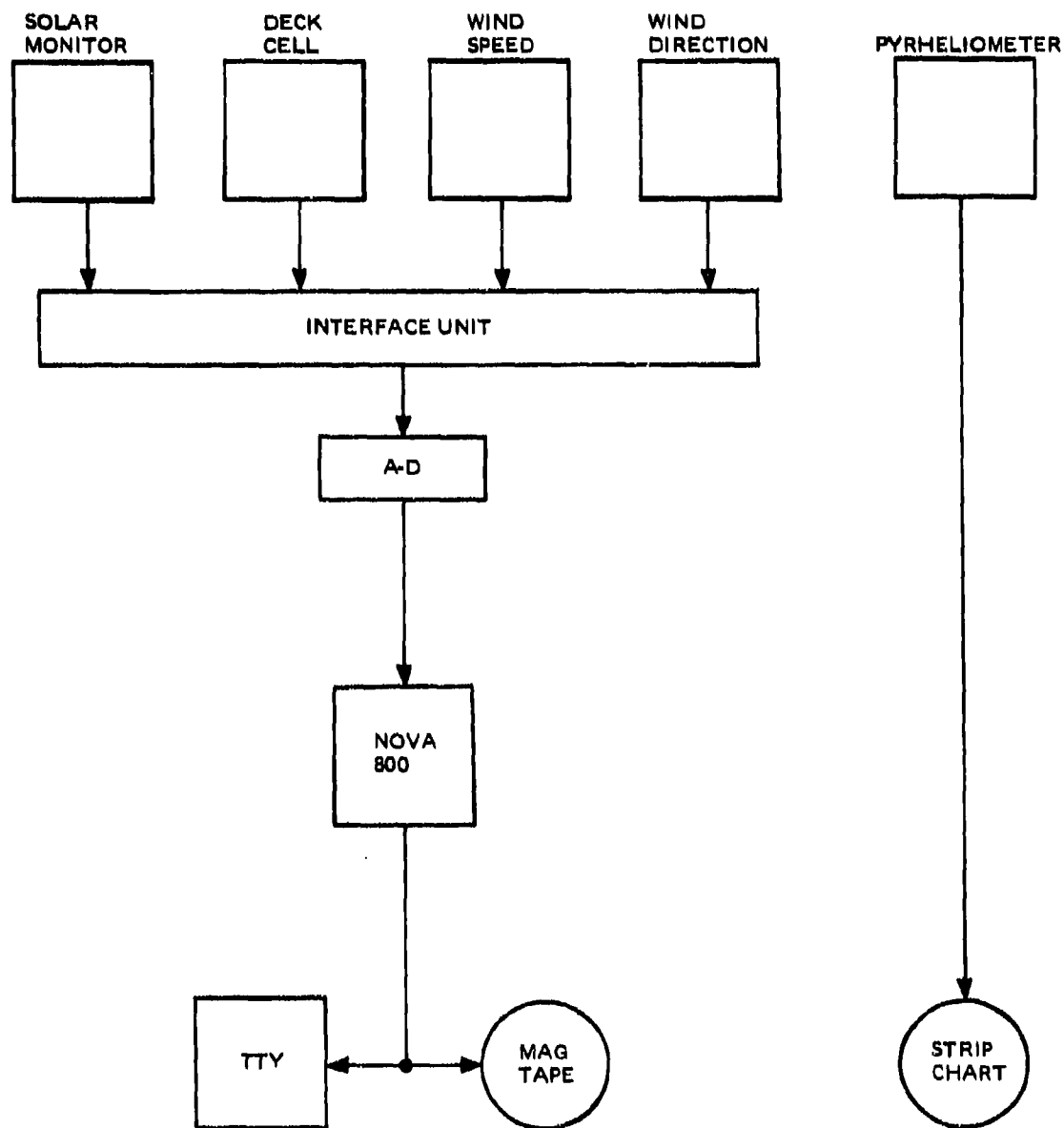


Figure 1. Atmospheric and optical background monitoring system.

X(CTR) = 0 Y(CTR) = 0 RES = 64 FILE # = 12 RECORD # = 0

Figure 2. Sample printout.

EQUIPMENT DESCRIPTION

The sensors used in the Atmospherical and Optical Background Monitoring systems are as follows:

- (1) **Solar Monitor:** This instrument consists of a silicon photodiode (EG&G 444-4) behind a 100 Å interference filter centered at 5200 Å (Pomfret 5200-100) which is identical to the filter in the radiance scanner. The spectral response is shown in figure 3. The narrow field (7 deg.) is provided by a Gershun tube within which the detector and filter are located. A panel meter is provided for maximizing detector input to insure that the instrument is pointed at the sun. Construction is of aluminum and was accomplished in-house. Unit is shown in figure 4.
- (2) **Deck Cell:** This device, shown in figure 5, is a commercial unit (Bendix, Model C1) consisting of a selenium photovoltaic detector, a Wratten 57A absorption filter and a diffuser. The field of view is approximately 180 degrees with a cosine response from the diffuser. The spectral response shown in figure 6 is peaked at 5220 Å with an 820 Å bandwidth.
- (3) **Pyrheliometer:** This instrument consists of a fifty-junction thermopile hermetically sealed in a spherical glass bulb manufactured by Eppley Laboratories, and a Minneapolis Honeywell chart recorder. The detector responds equally across the visible spectrum and has a cosine response over its field of 180 degrees. The complete unit is shown in figure 7.
- (4) **Wind Speed Indicator:** A Climet Instruments Model 011-4 (figure 8) was used to measure wind speed. The instrument uses three plastic cups to rotate a drive shaft at a rate proportional to wind speed. To the end of the drive shaft is attached a chopper disc. A small lamp is mounted directly above the chopper disc and the light directed through the disc to a photodiode mounted directly beneath the disc. Rotation of the disc alternately masks and exposes the photodiode to the lamp producing pulses of a frequency proportional to the rotation rate of the cups. The unit has a range of 0 to 90 miles per hour.
- (5) **Wind Direction Indicator:** A rotating vane linked to a 10K potentiometer make up the wind direction indicator (figure 8). Full scale output is 10 VDC representing 360 degrees.

The signal conditioning portion of the AOBMS is comprised of two units, the Interface Panel and the Analog to Digital Converter (A-D).

- (1) **Interface Panel**
 - (a) The interface panel is essentially a panel mounted card cage located in one of the instrument hat racks. Also included in the panel are reference power supplies for the deck cell and the wind direction pots, front panel analog outputs for operator monitoring of the various sensors, and the adjustments (gain, zero, etc.) necessary for set up. The unit was designed and built in-house. Function and signal flow is shown in the block diagram in figure 9. Referring to the block diagram, we first consider the solar monitor interface.

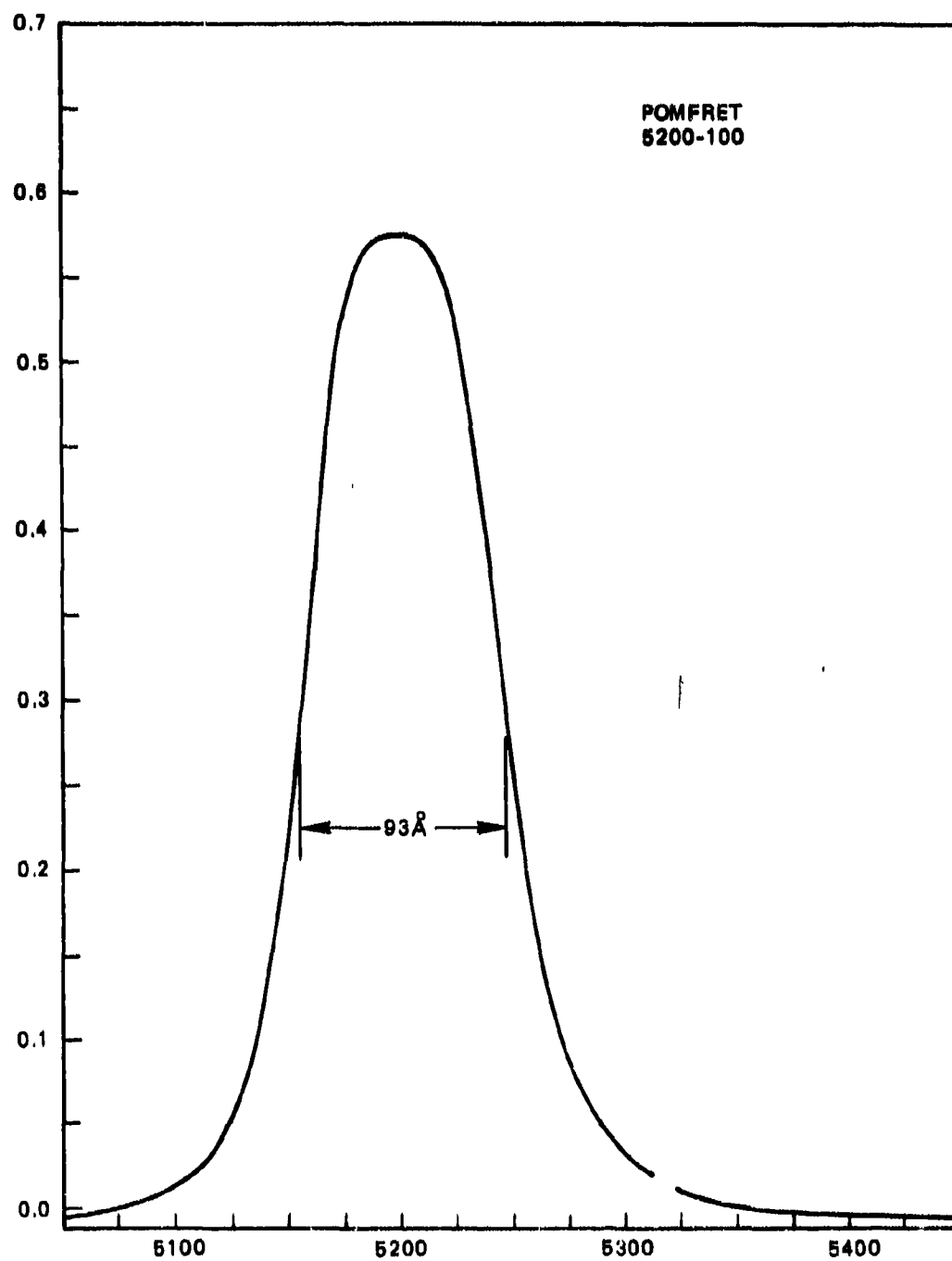


Figure 3. Spectral response, optical filter.

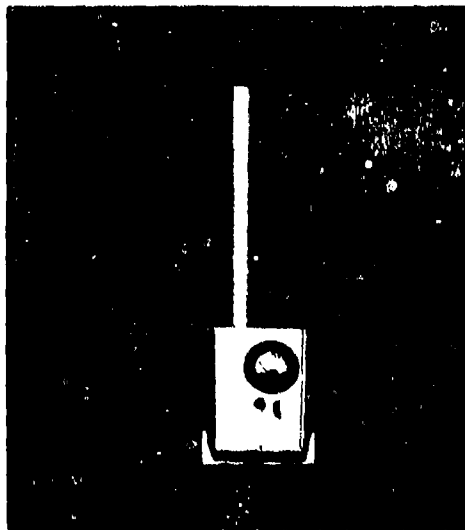


Figure 4. Solar monitor.



Figure 5. Deck cell.

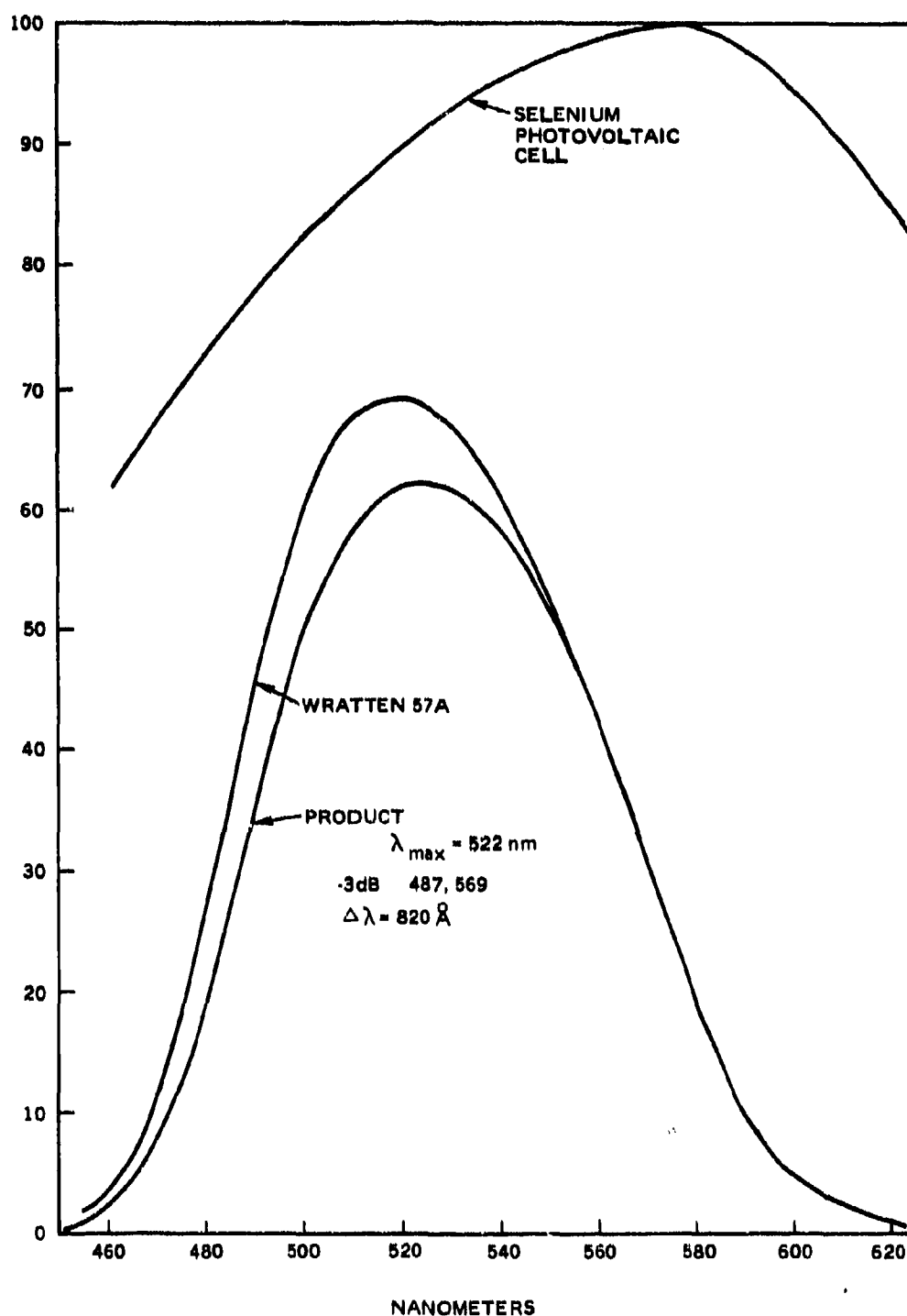


Figure 6. Spectral response (deck cell).

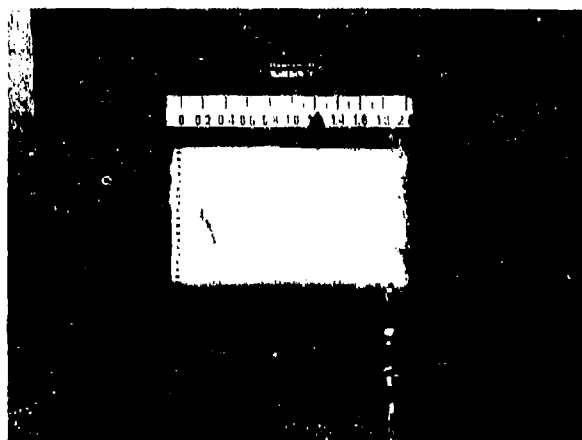


Figure 7. Pyrheliometer.

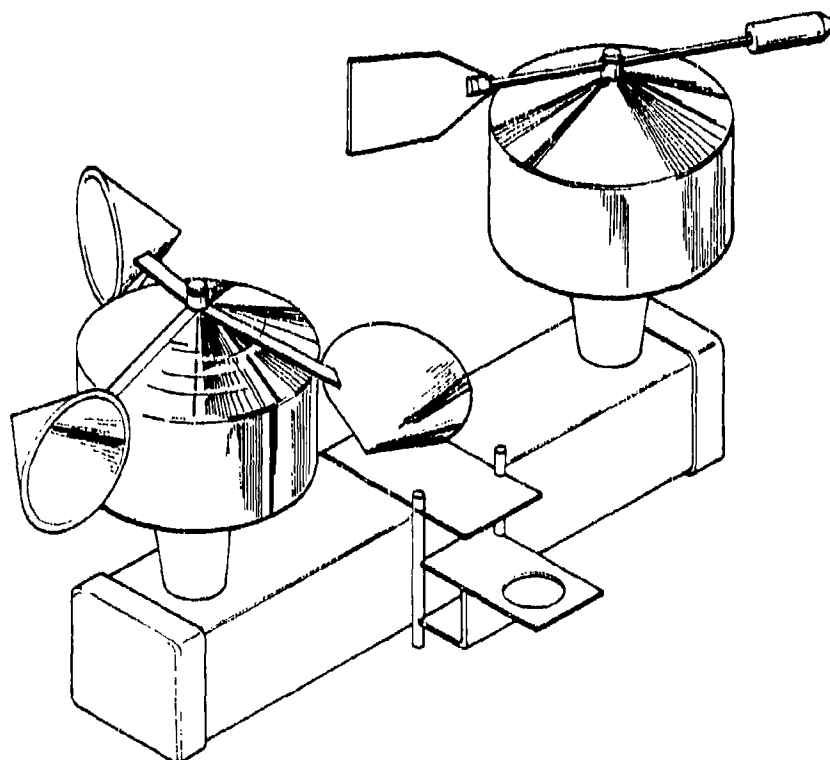


Figure 8. Wind speed and direction sensors.

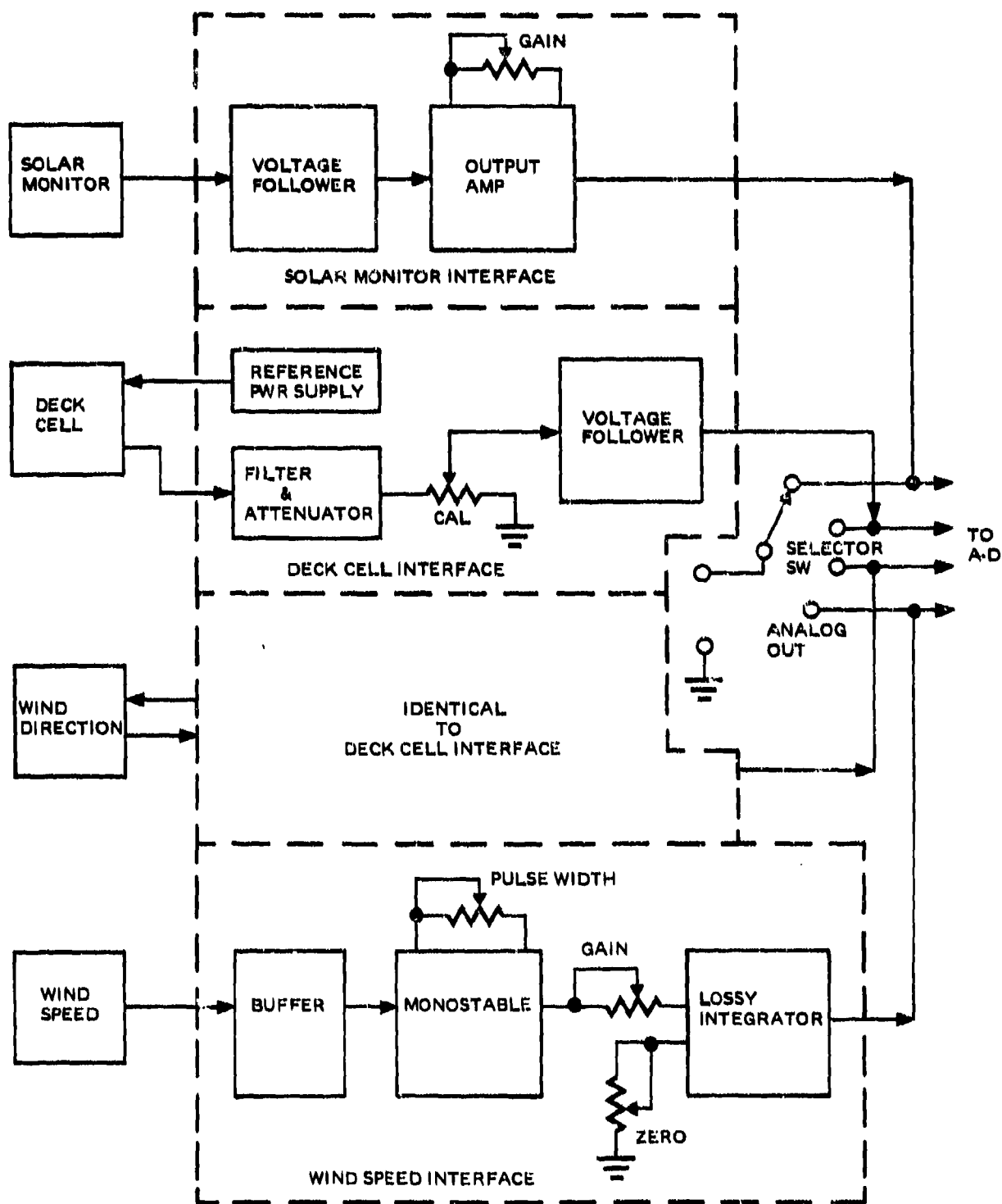


Figure 9. Interface panel block diagram.

The output of the solar monitor is fed to a circuit consisting of a high input impedance (100K) voltage follower and an output level amplifier. The output amplifier has gain adjustable from 1/2 to 2.

- (b) The deck cell and wind direction indicator have identical interface circuits. A 10.9 VDC power supply, consisting of two Zener diodes and a voltage follower, supplies the reference voltage for the sensor's pots. A value greater than 10 volts was chosen to allow for some lossess. The returned signal from the sensor is filtered and attenuated to yield a full scale value of 10.0 volts. With the level properly set via the Cal adjustment, the signal is fed to a voltage follower for isolation and impedance matching.
 - (c) The wind speed interface converts an input square wave to an analog voltage proportional to the input frequency. The input square wave drives a buffer transistor which fires a monostable multivibrator. The outputs of the monostable are fixed pulse width, fixed amplitude pulses with frequency proportional to the wind speed. These pulses are fed to a lossy integrator which takes a running average of the monostable pulses. A capacitor across an op amp stores voltage proportional to the number of pulses per unit time. The smoothed output of the integrator is then presented to the A-D. Provision is made to adjust the monostable pulse width and pulse amplitude as well as zero the integrator.
 - (d) All analog outputs of the interface circuits are made available through a selector switch for direct monitoring on the front panel.
- (2) Digital to Analog Converter: The A-D unit is a commercial unit manufactured by Analogic Corporation (Model AN5800). Figure 10 is a block diagram of the unit. The inputs are multiplexed one at a time into a high input impedance buffer amplifier, then supplied to a sample and hold amplifier. The buffered analog signals are converted to digital data via a high speed successive-approximation analog to digital converter. Digital data is then right hand justified and brought out to the digital interface connector for submission to the computer.

Processor: The processing of the digital output of the A-D is accomplished by the Nova 800 computer. This unit is described elsewhere in this report.

CALIBRATION

With the exception of the solar monitor, the atmospherical and optical sensors in the AOBMS are commercial units and calibration was performed by the manufacturer. Manufacturer supplied calibration documentation is included as an Appendix and the results summarized in table 1.

The solar monitor was calibrated in-house. The calibration was accomplished by simultaneous sampling of the solar irradiance with the solar monitor and a commercial irradiance meter (UDT-21A). The measurement was repeated six times with no detectable variation.

Both the solar monitor and the UDT-21A were fitted with identical interference filters to insure matching spectral response. A Gershen tube was affixed to the UDT to restrict the field of view to solar, not sky, radiation.

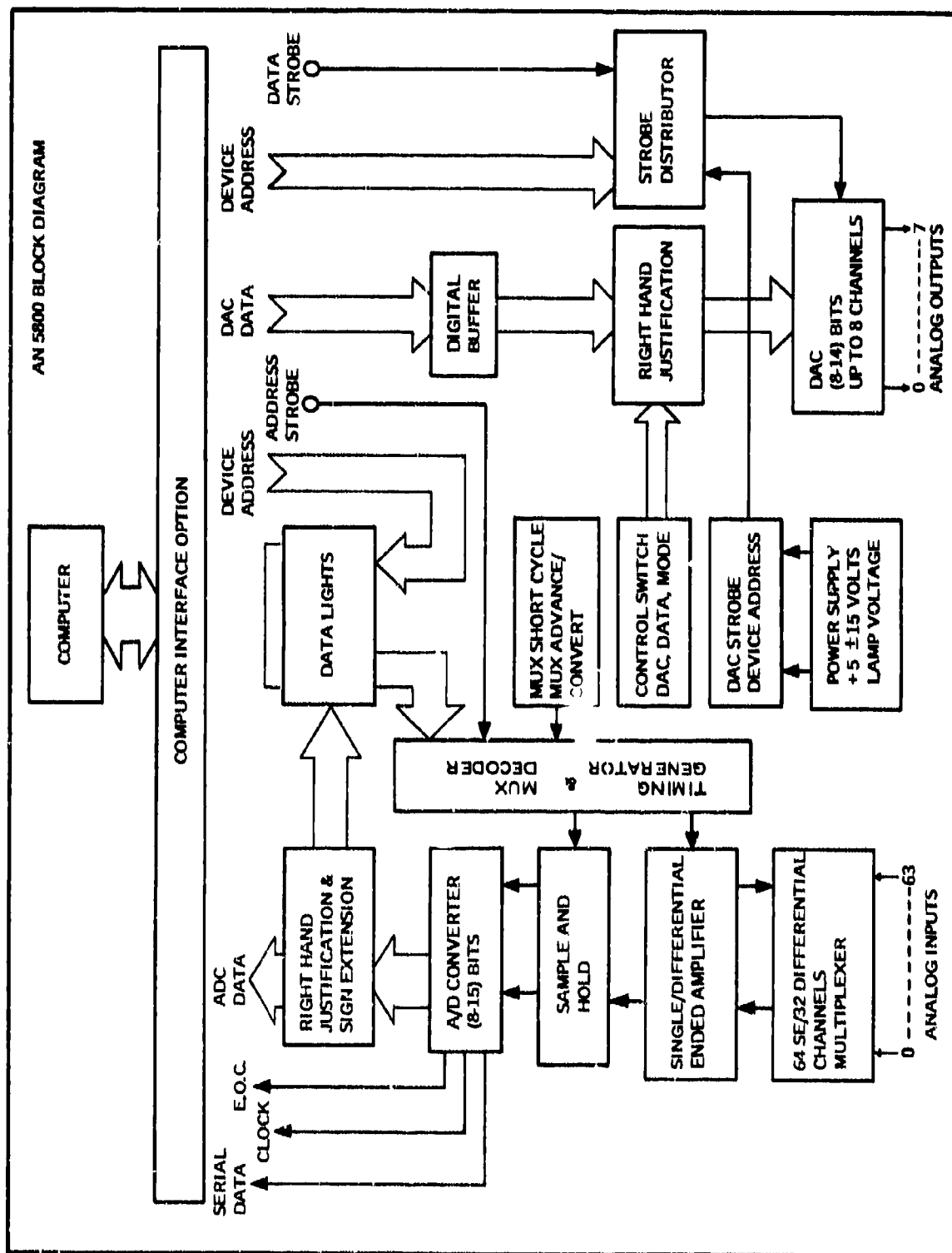


Figure 10. Digital to analog converter.

TABLE 1

Equipment	Calibration Constant	Accuracy/Linearity
Climet Model 014-5 anemometer	$S = F / .3187 + .52$ where S = speed (mph) and F = frequency (rps)	1% of true windspeed or ± 0.15 mph, whichever is greater for 0-90 mph
Eppley Model 50 junction pyrheliometer	$8.85 \text{ millivolts cal. cm}^{-2} \text{ min}^{-1}$	$\pm 1\%$ over intensity range 0.1 to $1.5 \text{ cal. cm}^{-2} \text{ min}^{-1}$
Bendix Model S-1 irradiance meter readout	$9.8 \times 10^{-7} \text{ watts cm}^{-2}$ per digit	<u>Accuracy</u> : standard deviation .06 or 6.1% of mean. <u>Linearity</u> : $\pm 3\%$ full scale.
Climet wind direction indicator	None	<u>Linearity</u> : $\pm 0.5\%$ full scale
Narrow angle/bandwidth solar monitor	$3.81 \times 10^{-5} \text{ watts cm}^{-2}$ per division	<u>Linearity</u> : $\pm 1\%$ 17 to 50 (full scale). <u>Accuracy</u> : $\pm 5\%$ meter movement.

The solar monitor's response linearity shown in figure 11 was determined by attenuation of the solar irradiance with neutral density filters. Deviation from linearity becomes more pronounced at lower irradiances due to a dark current of one to two meter divisions. This was not considered a problem as the instrument was not used at low irradiances.

To facilitate data handling, the sensor outputs were recorded on magnetic tape as integers in the range -2048 to 2047. To reconstruct the original values from the stored integer values, a number of multipliers, shown in table 2, were determined.

TABLE 2

Equipment	Multiply Mag Tape Output By:
Anemometer	$\frac{-1}{20.47}$ miles/hour
Deck cell	$4.79 \times 10^{-7} \frac{\text{watts}}{\text{cm}^2}$ through a Wratten 57A filter
Wind direction indicator	$\frac{1}{5.685}$ degrees
Solar monitor	$\frac{-1}{615} \frac{\text{mw}}{\text{cm}^2}$ for $5154 \text{ \AA} < \lambda < 5247 \text{ \AA}$

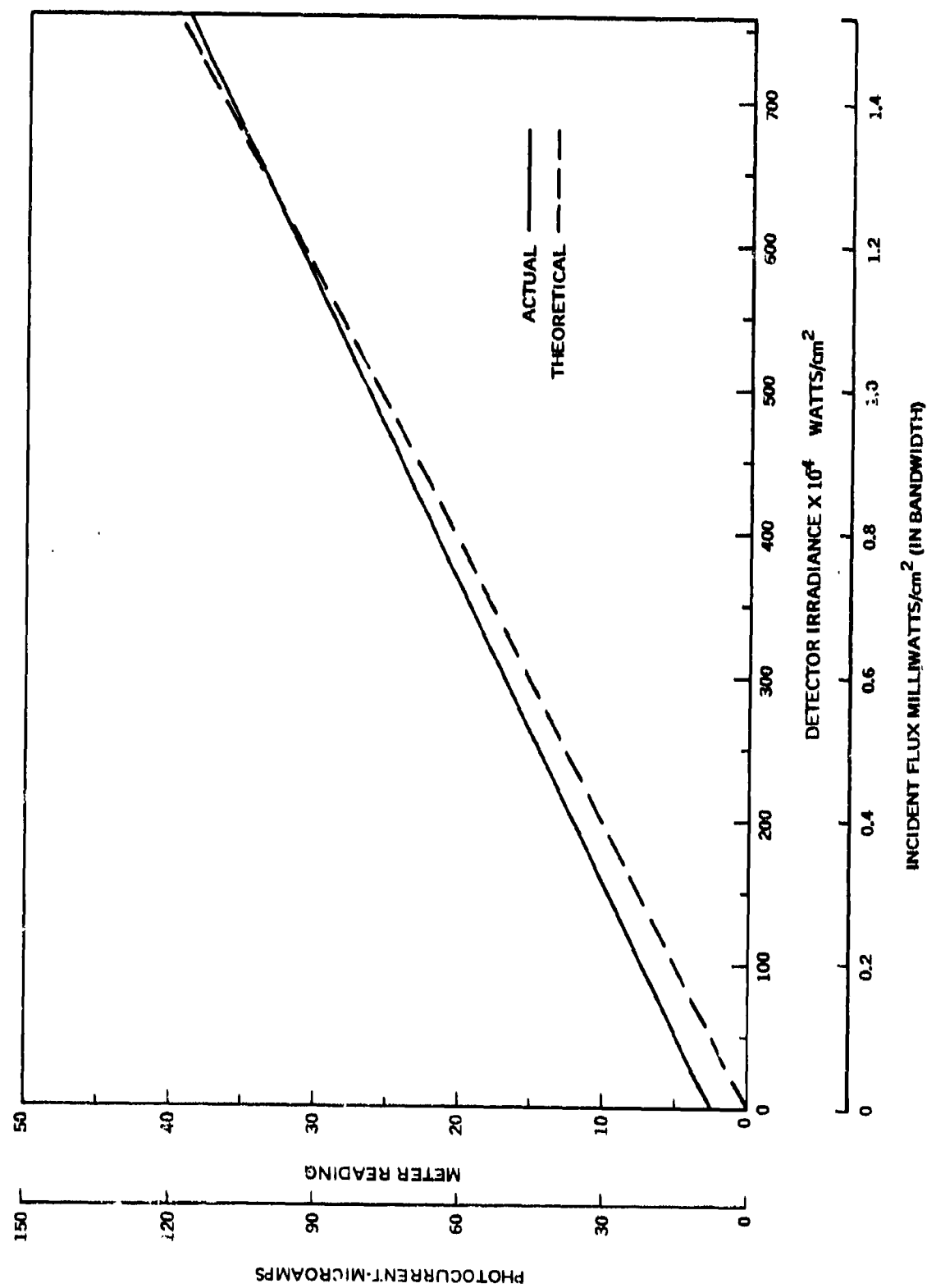


Figure 11. Solar monitor response linearity.

INITIAL DISTRIBUTION LIST

DEFENSE ADVANCED RESEARCH PROJECTS AGENCY
TECHNICAL LIBRARY (3)
OFFICE OF THE DIRECTOR OF DEFENSE
RESEARCH & ENGINEERING (3)
INFORMATION OFFICE, LIBRARY BRANCH
T. NYMAN (2)
DEFENSE TELECOMMUNICATIONS & COMMAND &
CONTROL SYSTEMS
DR. N. BURCH
DEFENSE COMMUNICATIONS AGENCY
CODE 101C
CODE 800 (DR. PARVIN JAIN)
DEFENSE DOCUMENTATION CENTER (12)
CHIEF OF NAVAL MATERIAL
NMAT-031 (LCDR J. DIETZLER) (6)
NAVAL ELECTRONIC SYSTEMS COMMAND
NELEX-031031 (T. B. HUGHES) (3)
NELEX-3102 (M. PARKER) (3)
PME 106-4 (CHARLES GOOD) (3)
PME 117 (DR. J. DON CARLOS) (6)
OFFICE OF NAVAL RESEARCH
PHYSICAL SCIENCES DIVISION
CODE 421 (DR. W. J. CONDELL) (3)
DIRECTOR OF TECHNOLOGY
CODE 201 (DR. L. E. LARMORE) (3)
(DR. D. LEWIS) (6)
(T. HORWATH) (1)
OFFICE OF NAVAL RESEARCH
BRANCH OFFICE
CHICAGO
PASADENA
BOSTON
SAN FRANCISCO AREA OFFICE
OFFICE OF NAVAL RESEARCH SCIENTIFIC DEPARTMENT
NEW YORK, NY
IRVING ROWE
NAVAL RESEARCH LABORATORY
CODE 7903 (E. DIX) (5)
CODE 6503 (DR. JOHN MAC CULLUM) (6)
CODE 7044 (DR. S. MELLMAN) (1)
NAVAL SHIP ENGINEERING CENTER
CODE 8113c (CDR ED VEAZY)
PEARL HARBOR NAVAL SHIPYARD
LCDR R. DRISCOLL
NAVAL AIR DEVELOPMENT CENTER
TECHNICAL LIBRARY
NAVAL WEAPONS CENTER
CHINA LAKE
TECHNICAL LIBRARY
NAVAL POSTGRADUATE SCHOOL
TECHNICAL LIBRARY
(CODE 0212)
PACIFIC MISSILE TEST CENTER
CODE 4253-3 (TECH LIBRARY)
POINT MUGU, CA 93042
NAVAL OCEANOGRAPHIC OFFICE
CODE 1640 (TECHNICAL LIBRARY)
NAVAL SURFACE WEAPONS CENTER, WHITE OAK
TECHNICAL LIBRARY
NAVAL UNDERSEA CENTER
TECHNICAL LIBRARY
NAVAL SHIP RESEARCH AND DEVELOPMENT CENTER
CENTRAL LIBRARY
US ARMY ENGINEERING RESEARCH AND DEVELOPMENT
LABORATORIES
TECHNICAL DOCUMENTS CENTER

AF SPACE & MISSILE SYSTEMS ORGANIZATION
SKX (DR. J. D. BARRY) (3)
P.O. BOX 92960
WORLDWAY POSTAL CENTER
LOS ANGELES, CA 90009
AIR FORCE CAMBRIDGE RESEARCH CENTER
TECHNICAL LIBRARY
NATIONAL AERONAUTICS AND SPACE ADMINISTRATION
GODDARD SPACE FLIGHT CENTER
JOHN McELROY (3)
NATIONAL BUREAU OF STANDARDS
TECHNICAL LIBRARY
RAND CORP
S. KATZ
1700 MAIN STREET
SANTA MONICA, CA 90496
UNIVERSITY OF CALIFORNIA, SAN DIEGO
VISIBILITY LABORATORY
R. AUSTIN (6)
VIA MARINE PHYSICAL LABORATORY (MPL 106)
SAN DIEGO, CA 92093
McDONNELL-DOUGLAS
G. LEE
P.O. BOX 516
ST. LOUIS, MO 63166
LINCOLN LABORATORY
MASSACHUSETTS INSTITUTE OF TECHNOLOGY
H. HEGGESTAD
J. WARD
P.O. BOX 73
LEXINGTON, MA 02173
McDONNELL-DOUGLAS
S. SPINAK
5301 BOLSA AVE
HUNTINGTON BEACH, CA 92647
ITT/GILFILLAN
JOHN WARD
7821 ORION AVE
VAN NUYS, CA 91406
TETRA TECH
H. HODARA
630 NORTH ROSEMEAD
PASADENA, CA 91107
PACIFIC SIERRA RESEARCH CORP.
A. SHAPIRO
1454 CLOVERFIELD BLVD.
SANTA MONICA, CA 90404
STANFORD RESEARCH INSTITUTE
DR. RICHARD HONEY
333 RAVENSWOOD AVE.
MENLO PARK, CA 94025
UNIVERSITY OF SOUTHERN CALIFORNIA
PROFESSOR R. M. GAGLIARDI
LOS ANGELES, CA 90007
UNIVERSITY OF CALIFORNIA
LAWRENCE LIVERMORE LABORATORY
DR. LOWELL WOOD
BOX 808
LIVERMORE, CA 94550